Unraveling the mechanisms of dengue virus non-structural protein 1 (NS1)-mediated pathogenesis

By

Dustin Robert Glasner

A dissertation submitted in partial satisfaction of the

requirements for the degree of

Doctor of Philosophy

in

Infectious Diseases and Immunity

in the

Graduate Division

of the

University of California, Berkeley

Committee in charge:

Professor Eva Harris, Chair
Professor Suzanne M.J. Fleiszig
Professor Laurent Coscoy
Doctor Lu Chen

Summer 2018

Abstract

Unraveling the mechanisms of dengue virus non-structural protein 1 (NS1)-mediated pathogenesis

by

Dustin Robert Glasner

Doctor of Philosophy in Infectious Diseases and Immunity

University of California, Berkeley

Professor Eva Harris, Chair

Dengue virus (DENV) is the most medically-important arbovirus worldwide, and infection with any of the four serotypes of the virus (DENV1-4) can lead to a range of outcomes, from inapparent infection to classical dengue fever (DF) to dengue hemorrhagic fever/dengue shock syndrome (DHF/DSS), severe disease manifestations characterized by endothelial barrier dysfunction and vascular leak. Non-structural protein 1 (NS1) is the only protein secreted from DENV-infected cells and is produced as a monomer, is found in association with cell membranes as a dimer, and is secreted as a hexamer. NS1 is a key component of the viral replication complex and has been implicated in immune evasion and pathogenesis. Recently, we and others described novel roles for NS1 in directly triggering endothelial barrier dysfunction and inducing inflammatory cytokine production from human immune cells, contributing to vascular leak *in vivo*. In this dissertation, the mechanisms behind NS1-induced pathogenesis of the endothelium are explored.

Using *in vitro* techniques, we found that NS1 from all four DENV serotypes can induce endothelial hyperpermeability of human pulmonary microvascular endothelial cells (HPMEC) and showed that this effect is mediated by endothelial sialidases, cathepsin L, and heparanase. These enzymes contribute to degradation of the endothelial glycocalyx-like layer (EGL), an important determinant of endothelial barrier function, and inhibition of sialidases, cathepsin L, and heparanase prevented NS1-induced endothelial hyperpermeability. Next, we found that NS1 does not trigger the production of inflammatory cytokines from human dermal microvascular endothelial cells (HMEC-1) *in vitro* and showed that neither TLR4 nor TNF-α signaling contribute to NS1-mediated vascular leak in the dermis of mice *in vivo*. Further, we demonstrated that inhibition of sialidases, cathepsin L, and heparanase prevents NS1-induced hyperpermeability and EGL degradation of HMEC-1 *in vitro* and vascular leak in the mouse dermis *in vivo*. We then sought to elucidate the early events that occur immediately following NS1 binding to endothelial cells. Using a glycosylation mutant of NS1, N207Q, we found that the N207 glycosylation site is not required for binding of NS1 to HPMEC but is required for NS1-induced hyperpermeability and EGL degradation. Further, we observed that wild-type NS1 is internalized by endothelial cells via clathrin-mediated endocytosis and is trafficked

to the endosome. While the N207Q mutant is internalized, it is not as efficient as wild-type, is not dependent on clathrin, and does not lead to endosomal localization.

We then broadened our studies to include NS1 proteins from other flaviviruses, including Zika (ZIKV), West Nile (WNV), Japanese encephalitis (JEV), and yellow fever (YFV) viruses. We found that these proteins selectively bind to and alter the permeability of human endothelial cell monolayers from the lung, dermis, umbilical vein, brain, and liver *in vitro* and, remarkably, cause vascular leakage upon inoculation into mice in a tissue-dependent manner, reflecting the pathophysiology of each flavivirus. Mechanistically, each flavivirus NS1 protein leads to differential disruption of key endothelial glycocalyx components after activation of sialidases, cathepsin L, and heparanase.

Finally, we sought to determine whether sera from individuals vaccinated with Takeda's live-attenuated Tetravalent Dengue Vaccine candidate (TDV) could protect against NS1-induced hyperpermeability of HPMEC *in vitro*. We found that sera from DENV-naïve individuals at day 0 pre-vaccination did not protect against DENV2 NS1-induced hyperpermeability, while day 0 sera from DENV-pre-immune subjects provided varying levels of protection. However, all day 120 post-vaccination samples from both DENV-naïve and pre-immune subjects abrogated DENV2 NS1-induced endothelial hyperpermeability, and, across all serum samples, the magnitude of protection correlated with the respective anti-NS1 antibody concentration. We observed a similar pattern when evaluating protection against DENV2 NS1-induced EGL degradation. Lastly, we found that serum from vaccinees could cross-protect against NS1 from DENV1, DENV3, and DENV4, and this protection also correlated with anti-NS1 antibody concentration.

Taken together, the work included in this dissertation represents a substantial advancement of the field's understanding of NS1 and its pathogenesis and further supports a key role for NS1 in dengue disease. Although a number of novel findings are described here, additional important questions remain unanswered, specifically regarding the molecular pathways and players involved in NS1-mediated pathogenesis as well as broader topics such as the relative contributions of NS1 in the greater context of the pathogenesis of dengue and other flaviviral diseases. Nonetheless, this work provides considerable mechanistic insight into NS1 pathogenesis and establishes NS1 as a key target for therapeutic intervention and important component of dengue vaccines.

Dedication

To my parents, Donald & Gail Glasner,
my sister, Alexandra Glasner,
and my wife, Charlotte Roh,
for all of their support and all of their sacrifices
that have allowed me to be the person and scientist I am today.

Table of Contents

List of Figures and Tables

Acknowledgements

I would like to first thank my advisor, Dr. Eva Harris, for accepting me into her lab and giving me the chance to learn and grow as a scientist. The past five years have been unequivocally amazing, and I cannot imagine having learned how to be a scientist – in every sense of the word – from a more supportive and brilliant individual. I have thoroughly enjoyed my time as a member of your group, and I am so thankful for all you have done for me. Dr. Robert Beatty has also been an unwavering supporter of my journey through my PhD, and I would not be here without the long writing sessions in his office, his excellent advice, and his tough love over the years. I also must thank my undergraduate mentor, Dr. Kurt E. Williamson at the College of William & Mary. You were the one to begin my scientific career and kindle my love for research and viruses, and your belief in me a decade ago and your continued support ever since has meant the world to me. I truly would not have accomplished this without you.

The Harris Lab itself has been such a perfect place for me to spend my PhD career. I have been supported by a collection of awesome post-docs, and I would not be where I am today without them. I need to particularly acknowledge Drs. Henry Puerta-Guardo and Micha Schmid for their tireless, thoughtful, and careful mentorship of me since I first joined the Harris Lab. Not only are you both two of the smartest, most gifted scientists I have ever met, you are also two of the kindest, brightest people I know. I am a better person for having known you, and I am the scientist I am today because of you. Special thanks to Drs. Diego Espinosa, Chunling Wang, Daniela Michlmayr, and Kaycie Hopkins as well: these individuals helped teach me the technical intricacies of molecular virology and taught me how to better think about science, and their mentorship and support have been absolutely crucial to my success as an early career researcher. Major thanks to the other PhD students in the lab – future Drs. Daniela Valente, Paulina Andrade, and Milena Dimitrova. You have provided me with such outstanding friendship, and the Harris Lab was far more fun because we were all together in it. To the countless others – techs, undergraduates, work-study students, visiting scholars, post-docs – my experience at Berkeley would not have been the same without you all. There are too many to acknowledge by name, but please know that your impact on my life and career has not gone unnoticed and is greatly appreciated. I would, however, like to specifically mention Kalani Ratnasiri and Trent Gomberg, my two undergraduate mentees. You are both such promising young scientists who have bright careers ahead of you, no matter what you choose to pursue. You have taught me to be a better teacher and mentor and have also helped me see science and our research in new and exciting ways, and your contributions to the work in this dissertation and the lab as a whole cannot be understated.

I am truly blessed to have spent my career as a PhD student in such a unique environment. The Harris Lab offered me a place where the importance of global health was never lost on those of us performing molecular research. Each day offered new and exciting challenges and the opportunity to work with a diverse group of wonderful, caring, and selfless individuals who were always willing to share a meal and some laughs or to lend a hand. I am lucky to have worked in a truly collaborative and multi-disciplinary environment, and the years spent here have broadened my focus and mindset, helping me to see science and the world in ways I had not previously considered. I will always be

grateful for the time I have spent in the Harris Lab, and these experiences will undoubtedly continue to shape all aspects of my career.

I am thankful for the Infectious Diseases & Immunity program that gave me a chance to pursue my PhD. It was my top choice program from the outset, and the experience did not disappoint. I must thank Teresa Liu for all of her work to keep the program running smoothly as well as Dr. Richard Stephens, the former chair of IDI, for his willingness to take a chance on me back in 2013 and for his influence over the early stages of my PhD career. I would also like to acknowledge Drs. Suzi Fleiszig, Laurent Coscoy, Sarah Stanley, Lu Chen, and John Marshall. These faculty members served on my thesis and/or qualifying exam committee and always challenged me to be a better scientist and helped me approach my research from different perspectives, and I have grown considerably because of their advice. And of course, a huge acknowledgement to all of the IDI students who have come and gone over the years. You have been a much-needed and beyond fun support system. From meetings in Barker to post-retreat outings at Spats to summer softball games, you have all made this experience more enjoyable and often less painful than it probably would have been otherwise. Every single one of you has left a mark on my life, and I have fond memories with each of you. I am excited to see where life takes you all after IDI.

Living in Berkeley and being part of the UC Berkeley community has afforded me the opportunity to grow outside of my PhD program as well. As someone who has been a rock climber for the past 8 years, I would be lying if I said the amazing climbing community in Berkeley did not play a small role in my decision to apply to and attend Cal, and I am thankful to have spent the past five years as a member and sometimes-officer of Cal Climbing. I have met some of my best friends through the club and spent many amazing weekends and trips exploring California through the lens of climbing. A special shout-out to the Old Man Crew – Evan Urton, Mark Patana, and Brian Estey – for being a group of people I could always count on to be there for me. You are some of my closest friends, and my life would not be the same without you. I also had the extremely unique chance to play collegiate sports and represent Cal with the club roller hockey team. I did not anticipate reviving my hockey career at Berkeley as a 26-30 year old grad student, but I am so happy to have had that chance. I will be forever grateful for having known everyone on those teams, especially Micah Chang and Mitch Robinson for believing in me those first few years and Alec Lang for his friendship and support as we made our way through our hockey and Berkeley lives. Most of all, though, I am grateful for Brendan “Walt” Samuel’s friendship over the past four years and all of the memories we have made manning the crease together. You have been a fantastic concert buddy, a loyal drinking companion, and a fierce friend, and you’ve helped me survive my PhD more than you know.

There are so many other people – from the Bay Area, Washington, D.C., William & Mary, Park Ridge, and beyond – who have impacted my life and career who I cannot acknowledge here. To all my friends, near and far, you have helped make me the person I am today, and I am constantly thankful for your love and friendship. I appreciate all you have done for me over the years, and I hope I have been as good of a friend to you as you have been to me.

I would not be where I am today – or the person I am today – without the support of my family. To my mother and father, Gail and Don Glasner, thank you for all that you've done for me, especially since moving to California. I know it is challenging to be 3000 miles apart, and I hope my journey has made you proud. You have been so supportive of my pursuit of my career, and I am forever grateful for that and for your belief that it is all worth it for me personally and professionally. To the rest of my family – my loving sister Ali, my amazing group of cousins, the sweetest grandparents in the world, and all of the wonderful aunts and uncles – you motivate and inspire me every day, and I'm always thinking about and missing you.

And of course, for my wife, Charlotte. There is no way to properly thank you for or acknowledge everything you have done for me over the past few years, but your support has meant the absolute world to me. You have brought newfound joy and happiness to my life and given it a new sense of purpose and meaning. I am excited to continue walking together with you into our future, and I hope to be as much of a cornerstone in your life as you have been in mine.

The experience of completing my PhD has been the most rewarding challenge I have ever faced, and receiving my degree is my proudest achievement to date. This would not have been possible without the amazing support structure I have in place – from family to friends to the academic community of which I am a member. Once again, to everyone who has made this journey possible: you have my sincerest thanks and eternal gratitude.

Curriculum Vitae

Education

Doctor of Philosophy, Infectious Diseases and Immunity

School of Public Health, University of California, Berkeley, Berkeley, CA

Dissertation Adviser: Dr. Eva Harris

Dissertation Title: Unraveling the mechanisms of dengue virus non-structural protein 1 (NS1)-mediated pathogenesis

GPA: 3.942

Master of Science, Biohazardous Threat Agents & Emerging Infectious Diseases – completed May 2011

Georgetown University, Washington, D.C.

GPA: 3.85

Bachelor of Science, Biology (Departmental Honors) – completed May 2010

The College of William & Mary, Williamsburg, VA

Thesis Adviser: Dr. Kurt E. Williamson

Honors Thesis: The Optimization of Pulsed Field Gel Electrophoresis for Use with Profiling the Freshwater Viral Community

Awards: Dean's List (Fall 2007, Fall 2010)

GPA: 3.23

Research Experience

2014 – 2018 Graduate Student Researcher, Lab of Dr. Eva Harris

School of Public Health, University of California, Berkeley, Berkeley, CA

- Investigated the mechanisms driving dengue virus non-structural protein 1 (NS1)-mediated pathogenesis, particularly vascular leak and endothelial barrier dysfunction during severe dengue disease as well as the role of NS1 in other flavivirus infections, such as Zika, West Nile, and yellow fever viruses

2013 – 2014 Doctoral Rotation Student, Lab of Dr. Charles Y. Chiu

Viral Diagnostics and Discovery Center, University of California, San Francisco, San Francisco, CA

- Developed qRT-PCR to detect hantavirus RNA in rodent

samples for the California Department of Public Health

2011 – 2013 ORISE Fellow, Laboratory of Retroviruses, Division of Viral Products, Office of Vaccine Research & Review, Center for Biologics Evaluation & Research

U.S. Food & Drug Administration, Bethesda, MD

- Characterized cell lines with novel application in vaccine production, particularly to identify adventitious agents, such as retroviruses, which may emerge during manufacturing and contaminate final vaccine products

2008 – 2010 Undergraduate Research, Lab of Dr. Kurt E. Williamson

Department of Biology, The College of William & Mary, Williamsburg, VA

- Performed honors research challenging the accepted efficacy of pulsed field gel electrophoresis in profiling viral assemblages in freshwater communities
- Investigated temporal and spatial variability of viral and bacterial abundance in a freshwater lake on campus

Teaching Experience

Fall 2017 Instructor for Splash at Berkeley, University of California, Berkeley, Berkeley, CA

Courses Taught:

- Intro to Infectious Diseases
- Zombies! (And Why They Matter for Public Health)

Spring 2016 Graduate Student Instructor, Molecular Cell Biology 50 – The Immune System and Disease

Department of Molecular & Cell Biology, University of California, Berkeley, Berkeley, CA

Instructor of Record: Dr. P. Robert Beatty

Fall 2014 Graduate Student Instructor, Public Health 162A – Public Health Microbiology

School of Public Health, University of California, Berkeley, Berkeley, CA

Instructor of Record: Dr. Gertrude Buehring

Publications

1. **Glasner, D.R.**, Puerta-Guardo, H., Beatty, P.R., Harris, E. The Good, the Bad,

and the Shocking: The Multiple Roles of Dengue Virus Nonstructural Protein 1 in Protection and Pathogenesis. *Annu Rev Virol*. 2018 Jul 25. doi: 10.1146/annurev-virology-101416-041848.

2. **Glasner, D.R.**, Ratnasiri, K., Puerta-Guardo, H., Espinosa, D.A., Beatty, P.R., and Harris, E. Dengue virus NS1 cytokine-independent vascular leak is dependent on endothelial glycocalyx integrity. *PLoS Pathog*. 2017 Nov 9;13(11):e1006673. doi: 10.1371/journal.ppat.1006673.

3. Puerta-Guardo, H., **Glasner, D.R.**, and Harris, E. 2016. Dengue Virus NS1 Disrupts the Endothelial Glycocalyx, Leading to Hyperpermeability. *PLoS Pathog*. 2016 Jul 14;12(7):e1005738. doi: 10.1371/journal.ppat.1005738.

4. Schmid, M.A., **Glasner, D.R.**, Shah, S., Michlmayr, D., Kramer, L.D., and Harris, E. Mosquito Saliva Increases Endothelial Permeability in the Skin, Immune Cell Migration, and Dengue Pathogenesis during Antibody-Dependent Enhancement. *PLoS Pathog.* 2016 Jun 16;12(6):e1005676. doi: 10.1371/journal.ppat.1005676.

5. Beatty, P.R., Killingbeck S., Puerta-Guardo, H., **Glasner, D.R.**, Hopkins, K.C., and Harris, E. 2015. Dengue virus NS1 triggers endothelial permeability and vascular leak that is prevented by NS1 vaccination. *Sci Transl Med*. 2015 Sep 9;7(304):304ra141. doi: 10.1126/scitranslmed.aaa3787.

6. Taliaferro, L.P., Galvin, T.A., Ma, H., Shaheduzzaman, S., Williams, D.K., **Glasner, D.R.,** and Khan, A.S. 2014. Evaluation of the broad-range PCR-electrospray ionization mass spectrometry (PCR/ES-MS) system and virus microarrays for virus detection. *Viruses*. 2014 Apr 25;6(5):1876-96. doi: 10.3390/v6051876. Erratum in: *Viruses*. 2014 Nov;6(11):4464-5.

7. Ma, H., Galvin, T.A., **Glasner, D.R.**, Shaheduzzaman, S., and Khan, A.S. 2014. Identification of a novel rhabdovirus in *Spodoptera frugiperda* cell lines. *J Virol*. 2014 Jun;88(12):6576-85. doi: 10.1128/JVI.00780-14.

8. Williams, D.K., Galvin, T.A., Gao, Y., O'Neill, C.M., **Glasner, D.R.**, and Khan, A.S. 2013. No evidence of xenotropic murine leukemia virus-related virus (XMRV) transmission by blood transfusion from infected rhesus macaques. *J Virol*. 2013 Feb;87(4):2278-86. doi: 10.1128/JVI.02326-12.

9. Hardbower, D.M., Dolman, J.L., **Glasner, D.R.**, and Williamson, K.E. 2012. Optimization of viral profiling approaches reveals strong links between viral and bacterial communities in a eutrophic freshwater lake. *AME, 67:*59-76. doi: 10.3354/ame01582.

Publications in Submission, Revision, or Preparation (* denotes equal author contributions)

1. Puerta-Guardo, H. (*), **Glasner, D.R. (*)**, Espinosa, D.A., Ratnasiri, K., Beatty, P.R., and Harris, E. Flavivirus nonstructural protein 1 triggers tissue-specific endothelial hyperpermeability and vascular leak that reflects disease tropism.

Cell Rep. In revision, July 23, 2018.

2. Wang, C., Puerta-Guardo, H., **Glasner, D.R.**, Biering, S., Patana, M., Tran, E.B., Malvar, C., Gomberg, T.A., Espinosa, D.A., Harris, E. Endocytosis of flavivirus NS1 by human endothelial cells is required for NS1-mediated barrier dysfunction and is abolished by a single N-glycosylation site mutation. In submission, August 17, 2018.

Presentations

1. Glasner, D.R., Ratnasiri, K., Puerta-Guardo, H., Espinosa, D.A., Beatty, P.R., and Harris, E. November 2017. Dengue virus NS1 cytokine-independent vascular leak is dependent on endothelial glycocalyx integrity. Oral presentation at the 66th Annual Meeting of the American Society of Tropical Medicine and Hygiene, Baltimore, MD

2. Glasner, D.R., Ratnasiri, K., Puerta-Guardo, H., Beatty, P.R., and Harris, E. May 2017. Dengue virus NS1 cytokine-independent vascular leak is dependent on endothelial glycocalyx integrity. Poster presentation at the 7th annual Bay Area Viruses Symposium, University of California, Berkeley, Berkeley, CA

3. Glasner, D.R. February 2017. Unraveling the role of flavivirus non-structural 1 protein in viral pathogenesis and disease. Invited speaker for the Spring 2017 Biology Seminar Series at the College of William & Mary, Williamsburg, VA

4. Glasner, D.R., Schmid, M.A., Shah, S., Kramer, L.D., Harris, E. June 2016. *Aedes aegypti* salivary gland extract-induced endothelial hyperpermeability in dermal microvasculature. Oral presentation at the 35th Annual Meeting of the American Society for Virology, Virginia Tech, Blacksburg, VA

5. Glasner, D.R., Schmid, M.A., Shah, S., Kramer, L.D., Harris, E. April 2016. *Aedes aegypti* salivary gland extract-induced endothelial hyperpermeability in dermal microvasculature. Oral presentation at the 5th annual Pan-American Dengue Research Network Meeting, Panama City, Panama

6. Glasner, D.R. April 2015. The Effect of Dengue Virus NS1 Protein and Mosquito Salivary Gland Extract on Endothelial Cells *in vitro*. Oral presentation for the Spring 2015 Infectious Diseases & Immunity Seminar Series at the University of California, Berkeley, Berkeley, CA

7. Glasner, D.R., Hardbower, D.M., Kendra, J.A., Kiernan, D.C., Javier, K.A., and Williamson, K.E. June 2010. Temporal and spatial variability of viral and bacterial abundance in a freshwater lake (Lake Matoaka, Williamsburg, VA). Poster presentation at the 110th General Meeting of the American Society for Microbiology, San Diego, CA

8. Glasner, D.R. May 2010. The optimization of pulsed field gel electrophoresis for use with profiling the freshwater viral community. Honors Thesis Seminar, Williamsburg, VA

9. Glasner, D.R. February 2010. The optimization of pulsed field gel

electrophoresis for use in freshwater environments. Oral presentation at the 11th Annual Charles Center Honors Colloquium, Williamsburg, VA

Science Communication and Engagement

1. “Dengue Virus Pathogenesis & Disease”. Speaker for the bi-annual Piedmont High School Biotechnology class visit to UC Berkeley, April 2018
2. Skype-A-Scientist participant with Kimberly White’s 6th grade science classes at San Marcos Unified School District, San Marcos, CA, February 2018
3. Invited panelist for panel discussion in PH162A Public Health Microbiology, University of California, Berkeley, Berkeley, CA, November 2017
4. “Dengue Virus Pathogenesis & Disease”. Speaker for the bi-annual Piedmont High School Biotechnology class visit to UC Berkeley, April 2017
5. “Dengue Virus Pathogenesis & Disease”. Guest lecturer for BIOL 356/357 General Microbiology, University of San Francisco, March 2017
6. Invited speaker for the University of California, Berkeley One Health Student Initiative at Berkeley Annual Speaker Event, November 2016
7. “The Spread of Flaviviruses Across the Globe”. Speaker for the bi-annual Piedmont High School Biotechnology class visit to UC Berkeley, November 2016
8. “How dengue virus NS1 protein triggers endothelial permeability and vascular leak”. Speaker for the bi-annual Piedmont High School Biotechnology class visit to UC Berkeley, May 2016
9. Invited panelist for the University of California, Berkeley Cal Undergraduate Public Health Coalition's Grad/Undergrad Mixer, February 2016
10. Invited panelist for the University of California, Berkeley Minority Health and Health Disparities International Training (MHIRT) Graduate Student Panel, April 2015
11. “Zombies & Public Health”. Guest lecturer for the University of California, Berkeley DeCal Sociocalypse: The Sociological Perspectives of Societal Breakdown, April 2014

Conferences Attended

1. 10th Annual Center for Emerging Neglected Diseases Symposium, January 2018, University of California, Berkeley, Berkeley, CA
2. 66th Annual Meeting of the American Society of Tropical Medicine and Hygiene, November 2017, Baltimore, MD
3. 7th Annual Bay Area Viruses Symposium, May 2017, University of California, Berkeley, Berkeley, CA

4. Kinks in the Armor: Bypassing the Immune Barriers of the Skin, September 2016, National Institute of Allergy and Infectious Diseases, Bethesda, MD
5. 35th Annual Meeting of the American Society for Virology, June 2016, Virginia Tech, Blacksburg, VA
6. 6th Annual Bay Area Viruses Symposium, May 2016, University of California, Berkeley, Berkeley, CA
7. 5th Annual Pan-American Dengue Research Network Meeting, April 2016, Panama City, Panama
8. 5th Annual Bay Area Viruses Symposium, May 2015, University of California, Berkeley, Berkeley, CA
9. 4th Annual Bay Area Viruses Symposium, May 2014, University of California, Berkeley, Berkeley, CA
10. 110th General Meeting of the American Society for Microbiology, June 2010, San Diego, CA

Honors, Awards, and Fellowships

2018	Ridpath Memorial Award for Excellence in the Final Seminar Presentation of Doctoral Dissertation Research, University of California, Berkeley
2017	Berkeley Graduate Division Conference Travel Grant, University of California, Berkeley
2016 – 2017	The Eki & Nobuta and Seiko Baba Brodbeck Fellowship, School of Public Health, University of California, Berkeley
2015	Outstanding Graduate Student Instructor, School of Public Health, University of California, Berkeley
2013 – 2014	The Dr. Richard T. Spath and Linda S. Spath Endowed Fund, School of Public Health, University of California, Berkeley
2011 – 2013	ORISE Fellowship, U.S. Food & Drug Administration
2009	DeFontes Fellowship, the College of William & Mary

Leadership and Service Experience

Spring 2018	Volunteer Judge, Molecular & Cell Biology Undergraduate Honors Poster Session, University of California, Berkeley
Spring 2017	Volunteer Judge, Molecular & Cell Biology Undergraduate Honors Poster Session, University of California, Berkeley
2016 – 2017	President, Infectious Diseases & Immunity Doctoral Student Group, School of Public Health, University of California, Berkeley

2015 – 2016 Admissions Committee, Infectious Diseases & Immunity PhD Program, School of Public Health, University of California, Berkeley

2014 – 2015 Admissions Committee, Infectious Diseases & Immunity PhD Program, School of Public Health, University of California, Berkeley

Chapter 1: Introduction to dengue virus non-structural protein 1 (NS1)-mediated pathogenesis

Background

Epidemiology

Dengue is the most prevalent mosquito-borne viral disease of humans worldwide, with up to an estimated 396 million dengue virus (DENV) infections and 96 million cases annually (1). Approximately half of the world's population is at risk of infection, with the majority of cases occurring in tropical and sub-tropical regions, including Latin America, Southeast Asia, and India (1). The four serotypes of DENV (DENV1-4) are transmitted by infected female *Aedes aegypti* and *Aedes albopictus* mosquitoes and are members of the *Flavivirus* genus in the *Flaviviridae* family, which also contains the medically important Zika (ZIKV), West Nile (WNV), Japanese encephalitis (JEV), St. Louis encephalitis (SLEV), yellow fever (YFV), and tick-borne encephalitis (TBEV) viruses (2).

Dengue is a major public health problem and causes substantial economic burden (3), and its geographic distribution has increased greatly over the past 50 years, with a 30-fold increase in global disease incidence (4). In 2010, it was estimated that the direct and indirect costs of dengue, including mosquito control, surveillance, and medical care, were $39 billion (5).

Life cycle

DENV is a positive-sense single-stranded RNA virus whose ~10.7-kb genome encodes for three structural proteins (capsid, C; pre-membrane/membrane, prM/M; envelope, E) and seven non-structural proteins (NS1, NS2A, NS2B, NS3, NS4A, NS4B, NS5) (6). DENV primarily infects myeloid lineage immune cells in humans, including monocytes, macrophages, and dendritic cells (DCs) (7-9). Upon receptor-mediated entry into host cells, a conformational change in the E protein is triggered by acidification of the endosome, releasing the viral capsid into the cytoplasm, where uncoating of the genome occurs (6, 10). The genome is translated into a single polyprotein and cleaved into ten proteins by viral and host proteases. Following synthesis of the NS5 RNA-dependent RNA polymerase and the NS3 helicase, RNA replication begins, and viral particle assembly occurs in the endoplasmic reticulum (ER). Particles pass through the ER and Golgi, where post-translational modifications and maturation occurs before particles are secreted from the host cell (6, 10).

Clinical characteristics of dengue disease

Following an incubation period of 2-7 days, DENV infection can result in a wide range of outcomes, with ~75% of infections leading to asymptomatic or inapparent disease (1). Most patients who are symptomatic suffer from classical dengue fever (DF), a self-limiting but debilitating disease characterized by high fever, muscle, joint, and bone pain, and rash (11). However, some patients progress to severe disease, initially designated dengue hemorrhagic fever/dengue shock syndrome (DHF/DSS), characterized by vascular leakage, thrombocytopenia, and bleeding, potentially resulting in shock and organ failure (11). Viremia peaks in the early acute phase (days 1-4), whereas vascular leak and shock occur during the critical phase (days 4-6). In 2009, a new classification

scheme of disease severity was introduced by the World Health Organization to facilitate clinical management, consisting of Dengue without Warning Signs, Dengue with Warning Signs, and Severe Dengue (12).

Immunopathogenesis of dengue disease

One of the primary hypotheses for severe dengue disease is immunopathogenesis, where a secondary infection with a different DENV serotype from the first can lead to more severe disease (13, 14). This is thought to occur in part because of antibody-dependent enhancement (ADE), whereby cross-reactive but sub-neutralizing antibodies facilitate viral uptake and infection of Fcγ receptor (FcγR)-bearing cells, leading to increased viremia and activation of target immune cells (15-17). *In vitro* experiments have shown that sub-neutralizing antibodies increase infection of FcγR-bearing cells, and passive transfer of heterologous, poorly-neutralizing antibodies results in antibody-enhanced lethal disease in mouse models (16, 18, 19). A recent study in a large, well-characterized pediatric cohort in Nicaragua demonstrated that a narrow range of pre-existing low antibody titers predicted increased disease severity while high titers were protective, demonstrating that ADE occurs in humans and contributes to DHF/DSS (20).

In addition to antibodies, serotype cross-reactive T cells may play a role in both the pathogenesis of severe dengue disease and protection (21, 22), and activation of $CD4^+$ and $CD8^+$ T cells has been shown to occur in human patients (23, 24). During secondary infection, memory T cells are activated, leading to production of interferon-γ and tumor necrosis factor (TNF)-α, further activating macrophages and monocytes, which in turn produce inflammatory cytokines (e.g., TNF-α, interleukin (IL)-6 and IL-8) that can increase vascular permeability (23, 25, 26). This dysregulated production of cytokines by T cells, macrophages, and monocytes, sometimes referred to as a “cytokine storm,” is thought to contribute to severe dengue disease (27, 28). In addition to cytokines, other inflammatory mediators such as histamine, platelet-activating factor, and leukotrienes are produced by mast cells, platelets, and other cell types during DENV infection and have been shown to be associated with DHF (29-31).

Determinants of endothelial barrier function

The two primary determinants of endothelial barrier function are the endothelial glycocalyx and intercellular junctional complexes, including tight and adherens junctions (32, 33). When the endothelial barrier is disrupted, hyperpermeability occurs, and fluids and molecules leak across the endothelium, extravasating from the vasculature and accumulating in tissues (34, 35). The endothelial glycocalyx is a complex, membrane-bound structure of carbohydrates, proteoglycans, and glycoproteins (GPs) that lines the luminal surface of the endothelium. This dense, forest-like matrix protects the underlying endothelial cells from shear forces generated by blood flow and creates a physical barrier that blocks molecules and fluids from reaching the endothelial surface. The glycocalyx contributes to hemostasis, molecular signaling, and interactions of blood cells with endothelial cells (36). Sialic acid residues and glycosaminoglycans, such as heparan sulfate, chondroitin sulfate, and hyaluronic acid, are the major constituents of the glycocalyx that contribute to the maintenance of the endothelial barrier. Intercellular

junctions are key complexes involved in endothelial cell adhesion, communication, and barrier function (33). Specifically, tight and adherens junctions regulate paracellular permeability, or the passage of molecules between cells (37). Occludin, claudin, and cadherin proteins, anchored by zona occludens (ZO) and catenin proteins, connect neighboring endothelial cells to one another and prevent molecules and cells in the blood from accessing the underlying tissue (38). Upon disruption of the glycocalyx and intercellular junctions, fluid and molecules are able to extravasate from the bloodstream more freely, leading to the hallmark characteristics of vascular leak observed in severe dengue disease (39).

NS1 biology

NS1 is synthesized by DENV-infected cells as a monomer, which then dimerizes in the ER. NS1 is glycosylated in both the ER and the trans-Golgi network. NS1 forms part of the replication complex and can be found on intracellular membranes and the cell surface. NS1 is also secreted into the extracellular milieu as a hexamer and circulates in the blood during acute illness, where its presence is useful as a diagnostic biomarker. NS1 is a key factor during infection, with roles in viral RNA replication, virion production, immune evasion, and multiple aspects of pathogenesis {Muller, 2013 #30}.

Structure and morphology of a multimeric viral protein

The NS1 gene in all flaviviruses is approximately 1,056 nucleotides in length and encodes a 352-amino acid (aa) protein with a molecular weight of 46-55 kDa, depending on its glycosylation status (40, 41). Phylogenetic analyses of NS1 amino acid sequences from different flaviviruses, including DENV1-4, ZIKV, WNV, JEV, SLEV, YFV, Murray Valley encephalitis virus (MVEV), and TBEV, revealed variable conservation that ranges from 50% to ~80% (42, 43). This analysis suggests that different flavivirus NS1 proteins have conserved functions as well as unique features leading to group-specific NS1 clusters (42).

After translation of the flavivirus polyprotein in the ER, newly synthesized NS1 monomers undergo post-translational modifications in the trans-Golgi network, such as glycosylation at asparagine (Asn)-130 (complex glycan), Asn-207 (high-mannose glycan), and, in some flaviviruses, Asn-175 (complex glycan) (41, 44, 45). Following glycosylation, NS1 monomers dimerize, facilitating membrane association of the protein. The dimeric form associates with intracellular membranes as well as the plasma membrane at the cell surface. Subsequent oligomerization of flavivirus NS1 dimers leads to formation of different multimeric species (e.g., tetramers, hexamers) (41, 46). The hexameric form is secreted from infected cells, and glycosylation at Asn-130 and Asn-207 stabilizes the hexamer and facilitates its secretion (47) **(Figure 1.1)**.

DENV NS1 is secreted at high levels into the extracellular environment during DENV infection, predominantly as a soluble hexamer that is a barrel-shaped, high-density lipoprotein containing a hydrophobic core that interacts tightly with lipids such as triglycerides, cholesteryl esters, and phospholipids (41, 48, 49) **(Figure 1.1)**. Recently, the macromolecular organization of NS1 was finally solved at high resolution (3.0 Å) (50,

51). The crystal structure of NS1 reveals three distinct domains that constitute each NS1 monomer. A small dimerization domain known as the central β-roll domain (aa 1-29) forms the inner-facing hydrophobic face that interacts with lipids (50). A second, protruding domain designated the wing domain (aa 30-180) contains two glycosylation sites (Asn-130 and Asn-175), an internal disulfide bond (Cysteine (Cys)-55 – Cys-143), and two discrete subdomains: the α/β subdomain (aa 38-151) and a discontinuous connector subdomain (aa 30-37 and 152-180) that links the wing domain to the central β-roll domain. The hydrophobic protrusion (greasy finger) between the β-roll and the wing domains facilitates NS1 interaction with the membrane of the ER and viral proteins, such as NS4A and NS4B, that are essential for viral replication (50). Finally, a third domain, known as the β-ladder (aa 181-352), is formed by a continuous β-sheet that forms half of the C-terminus of NS1 (50). As the extracellular NS1 hexamer is a target of humoral immune system recognition, the C-terminal tip of the β-ladder along with the wing domain are the most antigenic regions and contain the most frequently identified epitopes of the NS1 hexamer (52-54).

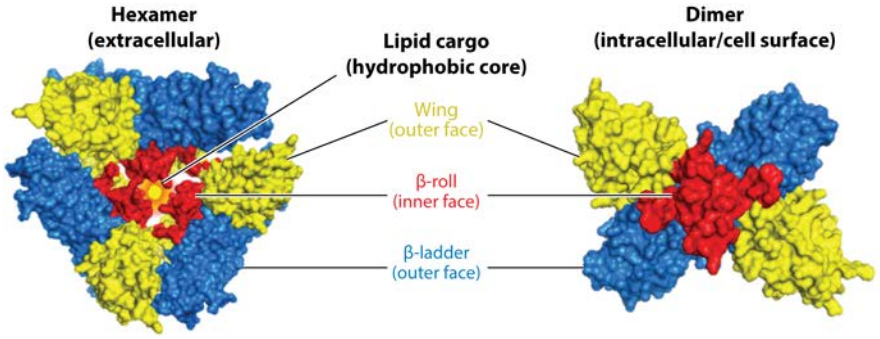

Figure 1.1. Model of the 3D organization of the DENV NS1 hexamer and dimer.
Three NS1 dimers bind together to form a barrel-shaped hexamer structure. Each dimer contains three domains: β-roll (red), wing (yellow), and β-ladder (blue). The lipid cargo-containing hydrophobic core (orange) inside the hexamer is also shown. Structure based on the DENV NS1 protein crystal structure deposited in the Protein Data Bank (PDB4O6B) (50). Molecular graphics were performed using the PyMOL Molecular Graphics system v1.3r1.

Viral cofactor in flavivirus replication

Intracellular expression of NS1 in the lumen of the ER colocalizes with double-stranded RNA (dsRNA) and other components of the viral replication complex in membranous compartments known as vesicle packets (55, 56). This finding suggests that NS1 plays a role in viral replication and negative-strand viral RNA synthesis (57-59), and deletion of NS1 prevents viral replication and infection (58). Substitution of DENV sequences into WNV NS1 at RQ10NK, a site previously identified to play a role in cell membrane association, enhanced WNV NS1 secretion but also reduced viral replication (55). NS1 has also been shown to interact with multiple host proteins and the transmembrane viral replicase proteins NS4A and NS4B (55, 59). More recently, physical interactions between NS1 and the structural proteins E and prM were reported (60). Together, these data

suggest that NS1, along with other viral proteins, may fulfill a structural role, helping to anchor the replication complex to membranes and inducing formation of membrane compartments that facilitate viral RNA replication, virus assembly, and release.

Another important feature of secreted NS1 that may influence its role in viral replication is the two N-glycosylation sites at Asn-130 and Asn-207. Removal of either one or both glycosylation sites in DENV, WNV, or YFV results in decreased NS1 secretion and virus yield, as well as reduced invasion of the central nervous system and neuropathology in mice (40, 44, 47, 61). Recently, a global proteomic analysis of human host factors interacting with NS1 combined with a functional RNA-interference screen identified many host cellular pathways, including those related to glycosylation of NS1 and NS4B, that may facilitate or restrict DENV infection (62). Additionally, the flavivirus replication cycle induces intracellular lipid redistribution that results in extensive membrane rearrangements (63, 64). Given that NS1 dimers have been found to localize with cholesterol-associated molecules on cell membranes (65) and present a markedly hydrophobic surface that promotes interactions with the ER membrane (50), NS1 may contribute to the modulation of cellular lipid dynamics during flavivirus infection and/or lead to recruitment of cholesterol and triglycerides to the replication complex. Together, these results indicate that NS1 glycosylation as well as the lipid composition of the hydrophobic core of NS1 may represent important factors not only for protein secretion, but also for viral RNA replication and possibly membrane rearrangement.

Diagnostic antigen and potential biomarker for clinical prognosis

Laboratory diagnostic methods for confirming DENV infection involve different molecular and serological approaches, such as reverse transcription-polymerase chain reaction (RT-PCR), virus isolation, and detection of increased levels of IgM and IgG antibodies, especially against E. Currently, the detection of NS1 circulating in the serum/plasma of infected patients constitutes a commonly used approach for the early diagnosis of flavivirus infection, particularly DENV, although sensitivity varies by serotype and is greater in primary than secondary infection (66, 67). Further, the duration of NS1 antigenemia is significantly longer in primary than in secondary infections (68). Different generations of commercially available kits and in-house enzyme-linked immunosorbent assays (ELISA) as well as rapid immunochromatographic assays are widely available (67). NS1 antigenemia in DENV-infected patients has been shown to correlate with disease severity (68-70). Circulating levels of NS1 have been described to vary from 0.1 to 2 µg/ml, with reports of up to 50 µg/ml, and persist for up to 14 days from the onset of fever (69, 71-75). These data are based on NS1 levels measured in the bloodstream of infected patients. However, NS1 may exit the bloodstream into tissues, leading to an apparent clearance of NS1 from the blood and increased presence in tissues.

With the recent emergence of new flaviviruses, such as ZIKV (76), and the potential re-emergence of flaviviruses such as YFV (77), the differential diagnosis of flavivirus infection is challenging, especially in regions of the world where multiple flaviviruses co-circulate (78, 79). The limited window to detect viral RNA in body fluids, as well as the highly cross-reactive antibody responses generated during different flavivirus infections such as DENV and ZIKV, especially during the acute phase, represent a significant

obstacle for the efficient, accurate, and specific diagnosis of these infections using either molecular techniques or serological assays. Recently, two studies reported NS1-based assays for differential diagnosis and surveillance of ZIKV and DENV infections (80, 81). One assay detects the circulation of anti-NS1 antibodies, the other detects soluble NS1, and both distinguish between DENV and ZIKV infections with high sensitivity and specificity (80-82). An NS1-based assay was also recently used to distinguish natural infection from vaccination with Sanofi Pasteur's Dengvaxia®, a chimeric dengue vaccine built on a YFV backbone, enabling determination of pre-immune status (83). Thus, NS1 can serve as a diagnostic and prognostic biomarker and can differentiate between flavivirus infections.

DENV NS1-mediated pathogenesis

Because NS1 antigenemia levels correlate with disease severity, it was hypothesized that NS1 may directly influence pathogenesis. However, NS1 had not been shown to play a direct pathogenic role during DENV infection until recently. Researchers from two different groups showed that DENV NS1 alone is capable of inducing endothelial hyperpermeability of human pulmonary, dermal, and umbilical vein endothelial cells *in vitro* (84, 85). DENV NS1 also induced lethality in a mouse model when administered with a sublethal dose of virus, and NS1 alone triggered vascular leak in the lung, liver, and small intestine of mice (84). The specific mechanisms of NS1-mediated pathogenesis identified to date are described below.

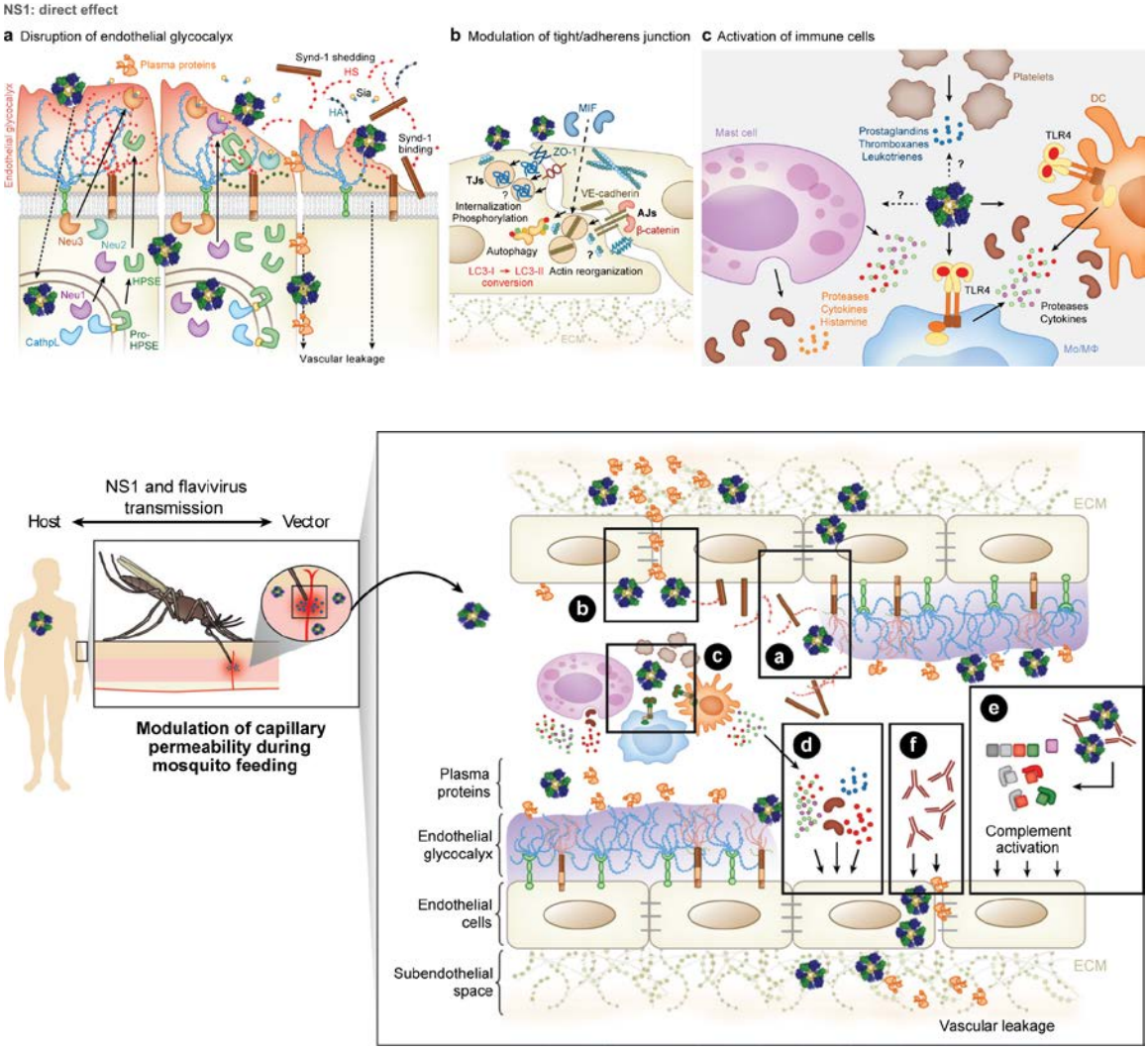
NS1: direct effect
a Disruption of endothelial glycocalyx
Plasma proteins
Synd-1 shedding
HS
Sia
HA
Synd-1 binding
Endothelial glycocalyx
Neu3
Neu2
HPSE
Neu1
CathpL
Pro-HPSE
Vascular leakage
b Modulation of tight/adherens junction
MIF
ZO-1
TJs
Internalization
Phosphorylation
VE-cadherin
AJs
β-catenin
Autophagy
LC3-I → LC3-II conversion
Actin reorganization
ECM
c Activation of immune cells
Platelets
DC
Mast cell
Prostaglandins
Thromboxanes
Leukotrienes
TLR4
Proteases
Cytokines
Histamine
Mo/MΦ
NS1 and flavivirus transmission
Host
Vector
Modulation of capillary permeability during mosquito feeding
ECM
Plasma proteins
Endothelial glycocalyx
Endothelial cells
Subendothelial space
Complement activation
Vascular leakage
NS1: indirect effect
d Induction of vasoactive molecules
Other vasoactive molecules
Prostaglandins
Thromboxanes
Leukotrienes
Pro-inflammatory cytokines
TNF-α
IL-1β
IL-6
IFN-γ
VEGF
MIF
Proteases and enzymes
MMPs
HPSE
PGE2
TXA2
Modulation of cell-to-cell contacts
Degradation of the endothelial glycocalyx layer
TJs
Mislocalization
Degradation
AJs
Actin reorganization
ECM
e Modulation of complement pathways
Inhibition
LP
CP
C1s
C2
C4
C3
C5
Cleavage
C2a
C4a
C3a
C2b
C4b
C3b
AP
C5b-9 (MAC)
Activation
Inactivation
Vitronectin
Interaction
C4BP
DHF > DF
Factor D
Factor H
C3 convertase
Activity
DHF
Inactivation
C4b deposition
Vascular leakage
TJs
AJs
ECM
f EC-cross-reactive anti-NS1 antibodies
Blood vessel
Cytokines
Clotting cascade
Auto-reactive antibodies
Nitric oxide
Plasminogen
Thrombin
Platelets
TJs
eNOS
p53
Caspase-3 activity
Cytochromec
AJs
Vascular leakage
ECM

Figure 1.2. Mechanisms of DENV NS1 pathogenesis leading to disease during DENV infection. DENV NS1 mediates pathogenesis through multiple pathways in the host. Secreted DENV NS1 circulating in the blood of infected humans influences virus transmission from human to mosquito by helping DENV to overcome the midgut barrier in the vector, and NS1 in the saliva of infected mosquitoes may modulate capillary permeability in the dermis of the host and impact viral dissemination in humans. **(a)** Direct DENV NS1 interaction with endothelial cells leads to increased expression and/or activation of cathepsin L; heparanase; and the endothelial sialidases Neu1, Neu2, and Neu3, leading to disruption and shedding of key glycocalyx components (heparan sulfate (HS), syndecan-1 (Synd-1), sialic acid (Sia)). **(b)** NS1 also modulates intercellular junction proteins, resulting in endothelial hyperpermeability. **(c,d)** NS1 can directly activate TLR4-expressing immune cells to trigger the secretion of proinflammatory cytokines that cause endothelial dysfunction. NS1 may also stimulate secretion of other soluble molecules with vasoactive and proteolytic activities that can affect endothelial barrier integrity. **(e)** NS1 contributes to immune evasion via interaction with components of the complement pathway, leading to their activation (e.g., C3 convertase; Factor D, Factor H, C5b-9) or degradation (e.g., C4b, C5b-9). Hence, NS1 protects DENV from complement-mediated clearance and DENV-infected cells from complement-mediated lysis, leading to more viral replication and potentially contributing to endothelial injury resulting in vascular leakage. **(f)** Cross-reactive anti-NS1 antibodies may also contribute to DENV pathogenesis by binding to platelets and components of the clotting cascade (e.g., plasminogen, thrombin) and may recognize autoreactive epitopes expressed on the surface of endothelial cells, potentially leading to endothelial cell damage via apoptosis. Mosquito graphic modified with permission from Chisenhall et al. (86).

Endothelial-intrinsic pathogenesis

Endothelial glycocalyx

After being secreted by infected cells, DENV NS1 circulates in the blood of patients and can bind to the surface of microvascular endothelial cells in capillary beds (87). Recent studies have shown that NS1 from all four DENV serotypes induces endothelial hyperpermeability in multiple human endothelial cell lines as measured by transendothelial electrical resistance (88). NS1 upregulates expression of the sialidases Neu1, Neu2, and Neu3, leading to cleavage of sialic acid on the surface of endothelial cells. NS1 also triggers increased activation of cathepsin L, which leads to increased expression and activation of heparanase that then cleaves heparan sulfate and heparan sulfate proteoglycans, such as syndecan-1, from the surface of the endothelium. Altogether, the ensuing degradation of the endothelial glycocalyx-like layer (EGL) results in barrier dysfunction. Cathepsin L activation, heparanase expression, sialic acid shedding, and hyperpermeability can all be blocked *in vitro* using inhibitors of sialidases (Zanamivir), cathepsin L (Cathepsin L Inhibitor), and heparanase (OGT 2115) (88, 89). These results were recently supported in an animal model of localized vascular leak, where NS1-induced vascular leak in the dorsal dermis of wild-type mice was prevented using a cocktail of Zanamivir, Cathepsin L Inhibitor, and OGT 2115, suggesting that the glycocalyx and its components are key mediators of NS1-induced pathogenesis *in vivo* (89) **(Figure 1.2a)**.

The glycocalyx was originally hypothesized to play a role in severe dengue after increased levels of heparan sulfate were detected in the urine of children with DSS (39, 90). A later study investigating the molecular sieving properties of the microvasculature in Vietnamese dengue patients further implicated the glycocalyx (91). Because dextran

fractional clearance studies showed no difference between dengue patients with evidence of vascular leak and healthy controls, it was hypothesized that administration of dextran may have contributed to stabilization of the glycocalyx after loss of plasma proteins during DENV infection, leading to restoration of endothelial glycocalyx integrity and normal barrier function (91). Further, recent studies have evaluated patient sera during acute DENV infection and found that levels of key endothelial glycocalyx molecules, such as hyaluronic acid, heparan sulfate, chondroitin sulfate, and syndecan-1, are all elevated to a greater degree in patients with severe disease (92, 93). This suggests that disruption of the glycocalyx occurs during DENV infection, potentially as a result of NS1 interactions with the vascular endothelium, and is associated with disease severity in humans.

Intercellular junction complexes

No lasting structural damage to the endothelium has been observed in human DHF/DSS cases (9, 94). Therefore, it is likely that transient disruption of intercellular junctions that, along with the glycocalyx, control vascular homeostasis may be one of the mechanisms responsible for vascular leak. DENV NS1 has been shown to stimulate production of macrophage migration inhibitory factor (MIF) from dermal endothelial cells *in vitro*, and MIF can induce endothelial hyperpermeability through autophagy of intercellular junction proteins in dermal endothelial cells (95). Both NS1-induced endothelial hyperpermeability and autophagy were prevented using a specific inhibitor of MIF, and hyperpermeability was prevented by blocking autophagy. Further, loss of the normal distribution of the adherens junction protein vascular endothelial cadherin (VE-cadherin) was blocked by MIF and autophagy inhibitors, suggesting its involvement in increased permeability (95). Additionally, studies using human endothelial cells from different tissues including lung, brain, and umbilical vein also showed that NS1 induces disruption of both tight and adherens junction proteins in a cytokine-independent manner. Using confocal microscopy analyses, investigators found that NS1 induces mobilization of intercellular junction proteins (e.g., ZO-1, VE-cadherin, and β-catenin) via clathrin-mediated internalization and/or phosphorylation, which may compromise the integrity of cell-to-cell contacts (H. Puerta-Guardo & E. Harris, unpublished data). Further, in a study of dengue patients in Indonesia, increased levels of the tight junction protein claudin-5 circulating in the blood were associated with vascular leak in patients with severe plasma leakage, suggesting a role for the disruption of intercellular junctions during severe dengue (92). Together, these data suggest an additional mechanism for NS1-mediated vascular leak via disruption of endothelial intercellular junctions **(Figure 1.2b)**.

Cytokine-mediated pathogenesis

Inflammatory cytokines are thought to play an important role in the pathogenesis of severe dengue. Dysregulated production of cytokines has been hypothesized as a mechanism for vascular leak in DHF/DSS, and several cytokines, including TNF-α, IL-10, IL-6, and IFN-γ, have been proposed as potential predictors of disease severity (96-100). In human studies, levels of TNF-α were elevated in DHF/DSS cases (97), and levels of IL-6 were elevated in patients with fatal dengue compared with survivors of severe or mild disease (101, 102). In a mouse model, intravenous administration of DENV2 NS1 resulted in significantly higher levels of both TNF-α and IL-6 in the blood 3 days post-injection

compared with injection of the control protein ovalbumin, supporting a role for NS1 in inducing secretion of inflammatory cytokines that may contribute to vascular leak during severe disease (84) **(Figure 1.2c,d)**.

DENV NS1 has been shown to activate both murine bone marrow-derived macrophages and human peripheral blood mononuclear cells (PBMCs) via Toll-like receptor 4 (TLR4), leading to secretion of the inflammatory cytokine IL-6 and transcription of the TNF-α, IL-1β, and IL-8 genes (85). Further, vascular leak in the small intestine and liver of mice infected with DENV2 was reduced in the presence of lipopolysaccharide from Rhodobacter sphaeroides (LPS-RS), a TLR4 antagonist (85). Treatment of human pulmonary endothelial cells with LPS-RS also partially reduced loss of sialic acid on the cell surface following treatment with NS1, an effect that may be mediated by TLR4-dependent translocation of Neu1 to the cell surface (88). Another group has reported that NS1 may induce secretion of inflammatory cytokines from PBMCs via TLR2 and TLR6 (103); however, these data are controversial (104).

Monocyte-derived dendritic cells (mo-DCs) are one of the primary targets of DENV infection, and they have been shown to take up NS1 *in vitro* (105). Internalization of NS1 increased infection and early viral replication in mo-DCs by DENV1, and this led to an increase of IL-6 production during infection; however, NS1 did not affect expression of DC maturation markers, such as DC-SIGN, HLA-DR, CD80, or CD86 in uninfected mo-DCs (105). Though it is unclear if NS1, virus infection, or a synergistic effect leads to the increase of IL-6 production, these data suggest that NS1 may mediate the production of IL-6 by DCs, contributing to the “cytokine storm” observed in DHF/DSS.

In addition to inflammatory cytokines, levels of IL-10, an immunoregulatory cytokine, have been shown to be elevated in patients with severe dengue disease (106, 107). NS1 stimulates high levels of IL-10 production from monocytes, and this effect was blocked with NS1-specific monoclonal antibodies (mAbs) (108). Though the precise role of IL-10 in dengue disease has yet to be defined, these results support a role for NS1 in increasing the levels of IL-10 in DHF/DSS patients.

Collectively, these studies demonstrate that NS1 can interact with innate immune cells, potentially through TLR4, leading to the secretion of cytokines and other mediators that contribute to vascular leak and viral pathogenesis. Though it has yet to be demonstrated, NS1 may also interact with other immune cells that have been described to actively participate in DENV pathogenesis, including mast cells and platelets (31, 109-112), leading to their activation and secretion of non-cytokine mediators such as eicosanoids, leukotrienes, or proteases that also may contribute to inflammation and vascular leak during DHF/DSS **(Figure 1.2c,d)**.

NS1 and complement

Early literature identified DENV NS1 as a soluble complement-fixing protein (113-115). Complement proteins are primarily serine proteases found throughout the blood and in tissues that, when activated, can lead to inflammation, opsonization, or cell lysis via formation of the C5b-9 membrane attack complex **(Figure 1.2e)**.

Anti-NS1 antibodies and complement activation

Anti-NS1 antibodies have been demonstrated to activate complement (C'), presumably to lyse virus-infected cells (116), and recent work has identified an anti-NS1 mAb that triggers complement-mediated lysis of DENV-infected cells (117). Soluble NS1 was shown to activate serum C', but cell surface-associated NS1 may cause antibody-dependent C' lysis, which could be a mechanism to eliminate DENV-infected cells (118). However, if soluble NS1 binds non-specifically to cells, it could trigger antibody-mediated C' activation and lysis of uninfected cells and, thus, potentially enhance viral pathogenesis (87).

Immune evasion

DENV NS1 has been shown to bind to the complement protein C4 and to recruit and activate the protease C1s, leading to cleavage of C4 to C4b and reducing both the deposition of C4b on the surface of cells and C3 convertase activity, thereby protecting DENV from complement-mediated neutralization and protecting DENV-infected cells from lysis (119) **(Figure 1.2e)**. A second mechanism was identified wherein NS1 binds to C4b binding protein (C4BP), a protein that attenuates the classical and lectin pathways of complement, leading to inactivation of C4b in solution and on the cell surface (120). More recently, NS1 has been shown to bind to vitronectin, a complement regulator, and this interaction was demonstrated *in vitro* and in DENV-infected patients (121). In the same study, NS1 inhibited the membrane attack complex and polymerization of the complement protein C9. NS1 also binds to mannose-binding lectin, a key component in complement activation, thereby protecting DENV from the lectin pathway of complement (122). Taken together, evidence supports a role for NS1 in binding complement components, thus protecting the virus from complement-mediated neutralization and preventing the killing of infected cells.

Pathogenesis

Clinically, dysregulated complement activation has been demonstrated in DHF patients, with higher levels of complement Factor D and lower levels of Factor H observed in DHF versus DF patients, suggesting formation of the C3 convertase and activation of complement (123). Further, C3a, C5a, and soluble C5b-9 were present at higher levels in the plasma of DHF patients starting 3 days before signs of plasma leakage, suggesting a role for complement activation in severe dengue disease (118). Additionally, NS1 may lead to generation of higher levels of C5a, resulting in increased vascular leak and pathogenesis **(Figure 1.2e)**.

Cross-reactive pathogenic anti-NS1 antibodies

Murine anti-NS1 antibodies bind to human platelets, thrombin, plasminogen, and endothelial cells *in vitro* (124-126), and data from mouse models suggested that cross-reactive antibodies to NS1 may contribute to pathogenesis (127-131). Initial studies tested the cross-reactivity of mAbs and polyclonal antibodies from mice (124, 132); subsequent studies examined human anti-DENV sera for binding to endothelial cells

(133) and plasminogen (134). Another study showed that anti-NS1 antibodies could trigger endothelial cell apoptosis via nitric oxide production by glycogen synthase kinase-3b-induced NF-kB activation and inducible nitric oxide synthase (iNOS) expression (132, 135); however, whether DENV infection leads to endothelial cell apoptosis in humans has not been established. The ability of anti-NS1 antibodies to bind to self-molecules and trigger increased production of nitric oxide provides evidence of indirect pathogenesis triggered by NS1 **(Figure 1.2f)**. Host cross-reactive NS1 epitopes have been mapped to various regions of NS1, with the cross-reactivity to endothelial cells thought to target epitopes in the C terminus of NS1 (aa 300-352). In a vaccine mouse model, deleting this region of NS1 reduced the production of host cross-reactive antibodies (136-139). Though a role for NS1-derived autoantibodies has been implicated in DENV infection and NS1 immunization models, it has been difficult to demonstrate a direct role for these antibodies in human dengue disease, and there is no indication of autoimmune manifestations during DENV infections or post-infection sequelae.

NS1 and the mosquito vector

Beyond its demonstrated functions during human infection, NS1 has also been shown to enhance mosquito acquisition of flaviviruses, including DENV. When mosquitoes feed on DENV-infected humans, they acquire virus along with soluble NS1 in the blood meal. NS1 was found to help the virus overcome the midgut barrier in mosquitoes – a key step in the flavivirus life cycle in the vector – through the inhibition of reactive oxygen species production and the JAK-STAT pathway, thus helping the virus establish infection in the mosquito (140). Additionally, soluble NS1 has been detected in the saliva of infected *Aedes aegypti* mosquitoes, suggesting that NS1 may be inoculated along with virus during blood feeding (122). Combined with proteins in mosquito saliva that impact viral replication and pathogenesis (141-143), soluble NS1 may play a role in early immune evasion, viral infection, and induction of endothelial hyperpermeability in the human dermis, possibly contributing to further virus dissemination **(Figure 1.2)**.

Conclusions

Taken together, recent research advances have further demonstrated the multifactorial role of NS1 during dengue disease. Beyond its described functions in immune evasion and viral replication, recent literature supports a key role for NS1 in the pathogenesis of severe dengue disease. Researchers have identified multiple pathways that contribute to NS1-mediated vascular leak, including degradation of the endothelial glycocalyx and secretion of inflammatory cytokines following NS1 stimulation of innate immune cells. There remain several significant unanswered questions, including the molecular determinants of pathogenesis, the binding partner(s) for NS1 on endothelial and immune cells, and the full mechanism of action of NS1 in its various functions. NS1 offers a potential target for both therapeutics and vaccine design, and further research into the mechanisms that drive pathogenesis and the nuances of the immune response to the protein may lead to substantial advances in the treatment and prevention of severe dengue disease.

Dissertation Overview

Given the novel role for NS1 in pathogenesis described by our group and others in 2015, the work in this dissertation represents recent efforts to further elucidate the mechanisms underlying NS1-induced barrier dysfunction. In Chapter 2, I describe the identification of key endothelial cell enzymes, including cathepsin L, heparanase, and the Neu family of sialidases, and their role in degrading the endothelial glycocalyx-like layer. In Chapter 3, we developed a model of local vascular leak in the dermis of mice and show that TLR4 and TNF-α signaling are not required for NS1-mediated barrier dysfunction *in vivo*, whereas the endothelial cell-intrinsic pathway and endothelial glycocalyx components are necessary. In Chapter 4, I discuss the importance of the N207 glycosylation site for NS1-mediated pathogenesis and show that internalization of NS1 by endothelial cells via clathrin-mediated endocytosis is required for downstream pathogenic functions of NS1. In Chapter 5, we demonstrate a striking pattern of differential induction of flavivirus NS1- and tissue-specific endothelial barrier dysfunction that parallels the pathophysiology of the respective flaviviruses both *in vitro* and *in vivo*. In Chapter 6, we describe for the first time the functionality of an anti-NS1 antibody response elicited by vaccination with a dengue vaccine, Takeda's live-attenuated Tetravalent Dengue Vaccine candidate. Taken together, this work contributes substantially to the field's understanding of NS1 pathogenesis and opens doors for additional mechanistic studies as well as NS1-based interventions.

Chapter 2: Dengue virus NS1 disrupts the endothelial glycocalyx, leading to hyperpermeability

This chapter was published in:

Puerta-Guardo, H., Glasner, D.R., Harris, E. Dengue Virus NS1 Disrupts the Endothelial Glycocalyx, Leading to Hyperpermeability. *PLoS Pathog*. 2016 Jul 14;12(7):e1005738. doi: 10.1371/journal.ppat.1005738. eCollection 2016 Jul.

Summary

Dengue is the most prevalent arboviral disease in humans and a major public health problem worldwide. Systemic plasma leakage, leading to hypovolemic shock and potentially fatal complications, is a critical determinant of dengue severity. Recently, we and others described a novel pathogenic effect of secreted dengue virus (DENV) non-structural protein 1 (NS1) in triggering hyperpermeability of human endothelial cells *in vitro* and systemic vascular leakage *in vivo*. NS1 was shown to activate toll-like receptor 4 signaling in primary human myeloid cells, leading to secretion of pro-inflammatory cytokines and vascular leakage. However, distinct endothelial cell-intrinsic mechanisms of NS1-induced hyperpermeability remain to be defined. The endothelial glycocalyx layer (EGL) is a network of membrane-bound proteoglycans and glycoproteins lining the vascular endothelium that plays a key role in regulating endothelial barrier function. Here, we demonstrate that DENV NS1 disrupts the EGL on human pulmonary microvascular endothelial cells, inducing degradation of sialic acid and shedding of heparan sulfate proteoglycans. This effect is mediated by NS1-induced expression of sialidases and heparanase, respectively. NS1 also activates cathepsin L, a lysosomal cysteine proteinase, in endothelial cells, which activates heparanase via enzymatic cleavage. Specific inhibitors of sialidases, heparanase, and cathepsin L prevent DENV NS1-induced EGL disruption and endothelial hyperpermeability. All of these effects are specific to NS1 from DENV1-4 and are not induced by NS1 from West Nile virus, a related flavivirus. Together, our data suggest an important role for EGL disruption in DENV NS1-mediated endothelial dysfunction during severe dengue disease.

Introduction

The four dengue virus serotypes (DENV1-4) are mosquito-borne flaviviruses that are responsible for ~390 million infections per year worldwide (1). Of these, up to 96 million manifest in clinical disease. The majority of these cases are dengue fever (DF), the uncomplicated form of disease. However, a subset develop severe dengue disease, including dengue hemorrhagic fever (DHF) and dengue shock syndrome (DSS), characterized by increased vascular leak, leading to shock and potentially death (12). Pleural effusion resulting in respiratory distress is one of the most common signs of plasma leakage in DHF/DSS cases (144).

Vascular hyperpermeability arises as a result of endothelial barrier dysfunction, leading to increased passage of fluids and macromolecules across the endothelium. Traditionally, tight and adherens junctions have been considered to be the primary determinants of endothelial barrier function (33). Over the past few years, however, the endothelial glycocalyx layer (EGL) has been recognized as a key regulator of vascular permeability (32). The EGL is a network of glycoproteins bearing acidic oligosaccharides and terminal sialic acid (*N*-acetyl-neuraminic acid, Sia), as well as membrane-bound proteoglycans associated with glycosaminoglycan (GAG) side chains including heparan sulfate (HS), hyaluronic acid, and chondroitin sulfate (36). The EGL extends along the endothelial layer coating the luminal surface of blood vessels.

Secondary DENV infection with a serotype distinct from the first DENV infection is a known risk factor for severe dengue disease. Several hypotheses have been proposed to explain severe dengue disease, including poorly neutralizing, cross-reactive antibodies and exacerbated T cell responses that together lead to production of vasoactive cytokines, causing vascular leakage that can result in shock (145). Another potential component is DENV non-structural protein 1 (NS1), a glycosylated 48 kDa protein that is the only viral protein secreted from infected cells, with high concentrations circulating in the blood of patients with severe dengue disease. NS1 plays a role in viral replication, immune evasion, and pathogenesis via activation of complement pathways (146). More recently, we and others demonstrated that DENV NS1 alone can trigger endothelial hyperpermeability, resulting in vascular leakage (84, 85). Modhiran et al. (85) showed that NS1 acts as a pathogen-associated molecular pattern (PAMP), activating mouse macrophages and human peripheral blood mononuclear cells (PBMCs) via toll-like receptor 4 (TLR4) to secrete pro-inflammatory cytokines such as tumor necrosis factor-α (TNF-α), interleukin-6 (IL-6), interferon-β (IFN-β), IL-1β, and IL-12. This effect was inhibited by a TLR4 antagonist (LPS-RS) and an anti-TLR4 antibody (85). Further, we found that inoculation of mice with NS1 alone causes increased vascular leakage and induction of pro-inflammatory cytokines (TNF-α, IL-6), while NS1 combined with a sub-lethal DENV inoculum results in a lethal vascular leak syndrome (84). Our *in vitro* experiments showed that NS1 also increases the permeability of human endothelial cells (84). The increased permeability *in vitro*, as well as mortality in mice, was prevented by administration of NS1-immune polyclonal mouse sera or anti-NS1 monoclonal antibodies (84). Likewise, immunization with recombinant NS1 from each of the four DENV serotypes protected against lethal challenge in the vascular leak model (84).

However, the mechanism by which DENV NS1 stimulates endothelial cells to induce vascular leak is poorly understood. NS1 has been proposed to bind to heparan sulfate on the surface of endothelial cells (87), but how this interaction leads to an increase in endothelial permeability has not been described. Therefore, we evaluated whether NS1 triggers disruption of the EGL and defined the mechanism through which this occurs.

Results

Binding of DENV2 NS1 to endothelial cells induces endothelial hyperpermeability

Soluble DENV2 NS1 attaches to the surface of human endothelial cells, especially pulmonary microvascular endothelial cells (87). In severe dengue disease, major accumulation of fluids occurs in the pleura (pleural effusion), a thin membrane that lines the surface of the lungs (147). This suggests that the lung represents an important site of endothelial barrier dysfunction characteristic of severe dengue. In this study, we used an *in vitro* model of endothelial permeability to initially examine the ability of soluble NS1 from DENV serotype 2 and West Nile virus (WNV NS1) to interact with cultured human pulmonary microvascular endothelial cells (HPMEC). In the first experiment, we found that DENV2 NS1 showed dose-dependent binding (1.25-10 µg/ml) to HPMEC monolayers at one hour post-treatment (hpt) **(Figure 2.1a,c)**. In contrast, WNV NS1 (2.5-10 µg/ml), from a closely-related member of the *Flavivirus* genus, displayed significantly less binding **(Figure 2.1b,c)**. A time course for DENV2 NS1 (5 µg/ml) attachment to the surface of HPMEC showed a maximum peak for NS1 staining between 3 and 12 hpt; no NS1 could be detected on the surface of HPMEC after 24 hpt **(Figure 2.S1a,b).** This NS1 binding pattern reflected decreased transendothelial electrical resistance (TEER) observed in HPMEC and other endothelial cell lines **(Figure 2.1d,e)**. Increased endothelial permeability is induced by NS1 from DENV1-4 (84) after 3 hpt in a dose-dependent manner, and the effect persists for more than 12 hours **(Figure 2.1e)**.

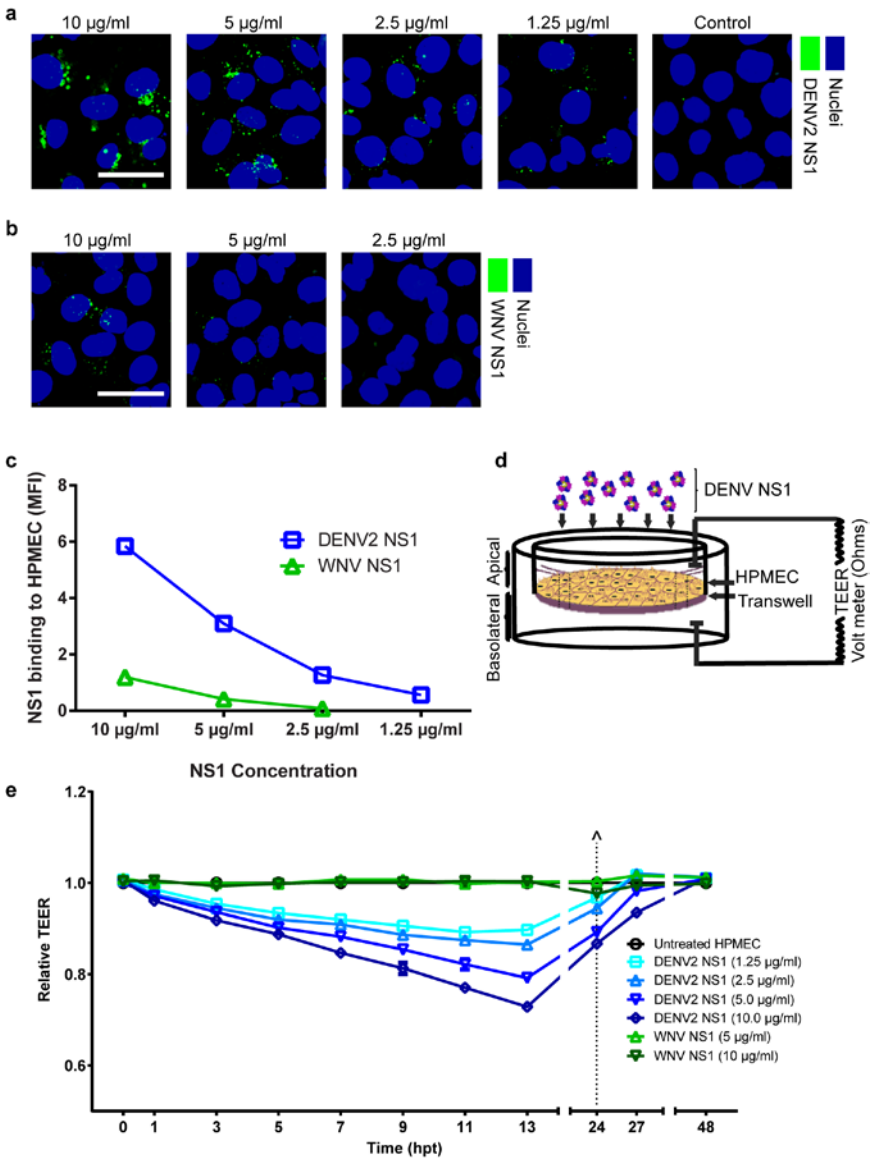

Figure 2.1. DENV2 but not WNV NS1 binding to endothelial cells induces endothelial barrier dysfunction.
(a,b) Binding of DENV2 NS1 **(a)** and WNV NS1 **(b)** proteins, examined by confocal microscopy. NS1 is stained in green, and nuclei are stained with Hoechst (blue). Images (20X) are representative of three individual experiments. Scale bars, 10 µm. **(c)** The amount of NS1 bound to HPMEC monolayers in **(a)** and **(b)** is quantified and expressed as mean fluorescence intensity (MFI). Graph shows average of quantification from three independent experiments. DENV2 NS1 binding to HPMEC monolayers is significantly higher than WNV NS1 binding at all concentrations ($P < 0.0001$). **(d)** Experimental schematic of transendothelial electrical resistance (TEER) experiments. **(e)** TEER assay to evaluate the effect of DENV2 and WNV NS1 proteins on HPMEC endothelial permeability at indicated concentrations. All DENV2 NS1 concentrations induce statistically significant decreases in TEER ($P < 0.0001$). (^) represents change of medium. Relative TEER values from three independent experiments performed in duplicate are plotted at the indicated time points. Error bars indicate standard error of the mean (SEM). Confocal microscopy images acquired and analyzed by Dr. Henry Puerta-Guardo.

DENV2 NS1 induces degradation of sialic acid in the EGL of endothelial cells

The EGL on the surface of the endothelium plays an important role in several cellular functions, including cell-to-cell communication, cell-matrix interaction, and vascular homeostasis (32), and a mature EGL has been shown to exist on cultured HPMEC *in vitro* (148). To examine the effect of flavivirus NS1 proteins on the integrity of the EGL, HPMEC monolayers were exposed to DENV2 or WNV NS1 (5 μg/ml), in the range of NS1 concentrations seen in severe dengue in humans (69, 72). The expression of Sia, a major component of the EGL (149), was visualized using the lectin wheat germ agglutinin (WGA) conjugated to Alexa 647 (150, 151). The homogenous distribution of Sia observed in untreated HPMEC was significantly disrupted in a dose-dependent manner 3-12 hours after addition of DENV2 NS1 but not WNV NS1 (**Figure 2.2a-c**). Normal distribution of Sia was re-established by 24 hpt (**Figure 2.2a,b**). Binding of DENV2 NS1 to HPMEC appeared to colocalize with the WGA staining of Sia residues in the EGL, suggesting that DENV2 NS1 may use Sia-linked glycans as adhesion molecules to mediate NS1-endothelial cell surface interaction (**Figures 2.2c, 2.S1c**). Next, to examine whether Sia was degraded or released from the surface of HPMEC exposed to DENV2 NS1, we assessed the presence of free Sia in cultured HPMEC supernatant using a specific Sia immunoassay. Supernatant collected from endothelial monolayers treated with DENV2 NS1 showed a significant time-dependent decrease in Sia levels compared with supernatant from untreated cells and WNV NS1-treated monolayers (**Figure 2.2d**), indicating Sia is not released into the medium of DENV2 NS1-treated HPMEC. Interestingly, expression of Neu1, Neu2, and Neu3, three mammalian sialidases found in endothelial cells, was strongly increased in HPMEC monolayers treated with DENV2 NS1 but not WNV NS1 at 3 hpt, potentially contributing to Sia degradation (**Figure 2.2e**). To determine the functional significance of DENV2 NS1-triggered disruption of Sia in the EGL, sialidase activity was inhibited using Zanamivir, an influenza neuraminidase inhibitor that has been shown to significantly inhibit Neu2 and Neu3 (152), and 2-deoxy-2,3-didehydro-N-acetyl-neuraminic acid (DANA), a transition state analog inhibitor of influenza virus neuraminidase found to be active against mammalian Neu3 (153). Both Zanamivir (50, 100 μM) and DANA (25 μg/ml) partially protected HPMEC monolayers from DENV2 NS1-mediated endothelial hyperpermeability as measured by TEER (**Figure 2.2f**), indicating that alteration of Sia distribution on the surface of HPMEC induced by DENV2 NS1 contributes to increased permeability.

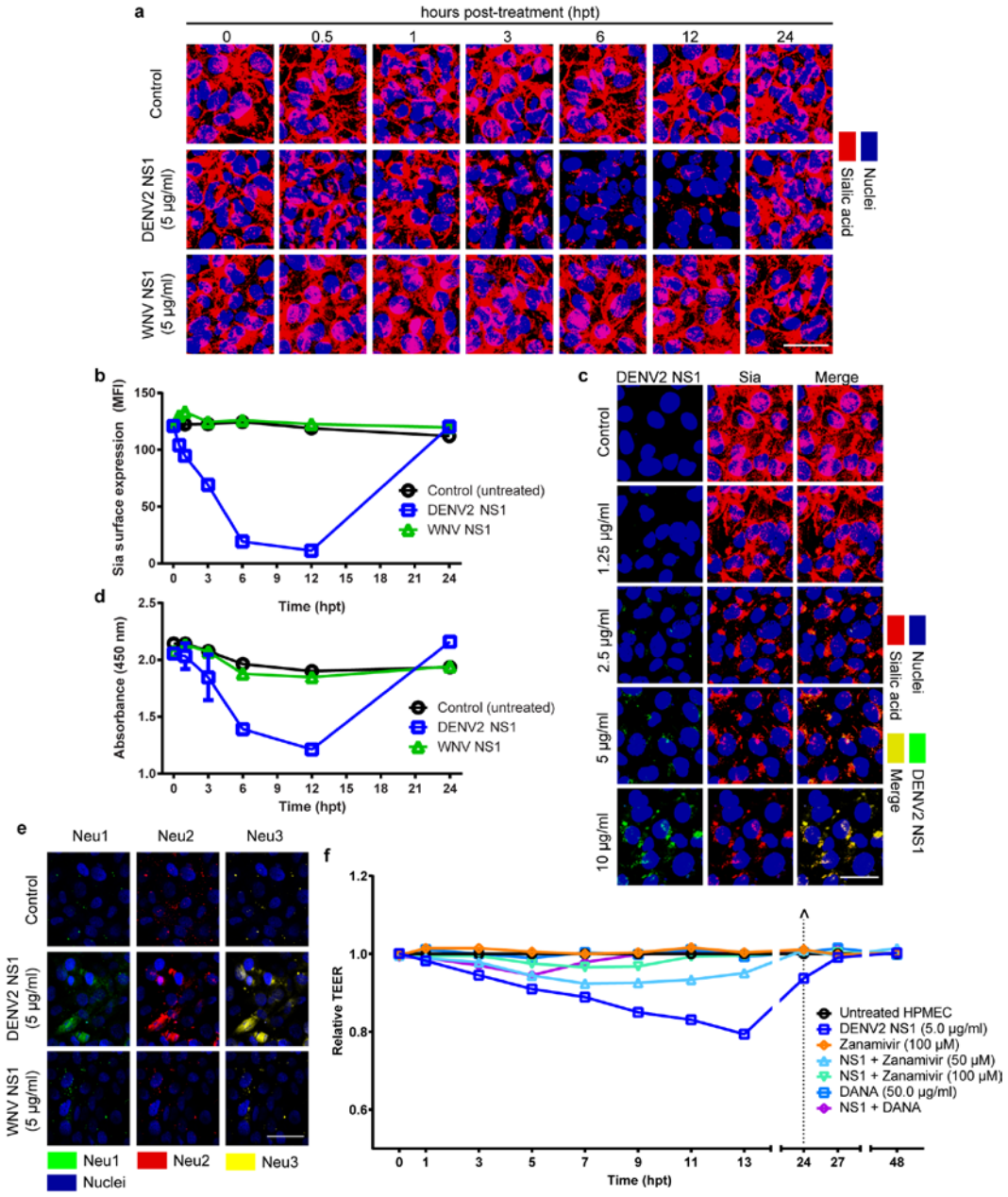

Figure 2.2. DENV2 but not WNV NS1 modulates the expression of Sia in the EGL of HPMEC.
(a) Sia expression on HPMEC monolayers after treatment with DENV2 or WNV NS1 (5 µg/ml), examined by confocal microscopy. Sia was stained with WGA-A647 (red) at indicated time points (hpt). Nuclei stained with Hoechst (blue). Images (20X) and MFI values are representative of three independent experiments. Scale bar, 10 µm. **(b)** Quantification of MFI in **(a)** from three independent experiments. Sia expression in DENV2 NS1-treated monolayers is significantly different from WNV-treated and untreated controls from 0.5 to 12 hpt ($P < 0.0001$). **(c)** DENV2 NS1 (green) induces dose-dependent reduction of Sia staining (red) on HPMEC after 3 hpt. Untreated cells were used as a positive control for Sia expression. **(d)** ELISA to detect free Sia released into culture supernatant of HPMEC over time (hpt) under indicated experimental conditions. DENV2 NS1 shedding of Sia is significantly lower than WNV-treated and untreated controls at 6 and 12 hpt ($P < 0.0005$). **(e)** Endothelial sialidase (Neu1, Neu2, Neu3) expression in HPMEC monolayers after treatment with DENV2 or WNV NS1 (5 µg/ml) at 3 hpt. Neu1,

Neu2, and Neu3 are stained in green, red, and yellow, respectively. **(f)** Effect of Zanamivir and 2,3-didehydro-2-deoxy-N-acetylneuraminic acid (DANA) on DENV2 NS1-mediated endothelial hyperpermeability (TEER) in HPMEC monolayers. TEER values for monolayers treated with DENV2 NS1 combined with Zanamivir (50, 100 µM) or DANA (50 µg/ml) are significantly different from monolayers treated with DENV2 NS1 alone ($P < 0.0001$). (^) represents change of medium. Relative TEER values from three independent experiments performed in duplicate are plotted at indicated time points (hpt). Error bars indicate SEM throughout. Confocal microscopy images acquired and analyzed by Dr. Henry Puerta-Guardo.

DENV2 NS1 induces shedding of heparan sulfate proteoglycans from the EGL

In addition to Sia, the EGL contains a large variety of heparan sulfate proteoglycans (HSPGs) (154, 155), including syndecans, which consist of a core protein modified by HS chains (156). Syndecan-1 is considered the primary syndecan of endothelial cells, including the vascular endothelium (157); thus, alteration of its expression or distribution can affect the integrity of the EGL as well as endothelial barrier function (158). The expression and distribution of syndecan-1 was evaluated on HPMEC stimulated with DENV2 NS1 or WNV NS1. WNV NS1 did not modify the distribution of syndecan-1 on HPMEC monolayers, but treatment with DENV2 NS1 resulted in increased staining of syndecan-1 starting 30 min post-treatment and persisting for more than 12 hours **(Figures 2.3a, 2.S2a)**. Similar results were observed for the extracellular matrix (ECM) HSPG perlecan **(Figure 2.S2b)**. However, syndecan-1 levels were similar in HPMEC treated with DENV2 NS1 or WNV NS1 compared to untreated controls, as detected by Western blot (**Figure 2.3a,c**). At 24 hpt, a small increase of syndecan-1 protein levels was detected by confocal microscopy and Western blot in DENV2 NS1-treated cells compared to control and WNV NS1-treated cells. Using an immunoassay for detection of soluble syndecan-1 ectodomain, increased levels of syndecan-1 ectodomain were found in conditioned media from DENV2 NS1-stimulated HPMEC at 1-24 hpt compared to untreated and WNV NS1-treated HPMEC (**Figure 2.3d**). Notably, recombinant syndecan-1 alone was able to increase the permeability of HPMEC monolayers in a dose-dependent manner (**Figure 2.3e**), suggesting that syndecan-1 shed from HPMEC after DENV2 NS1 stimulation may be involved in modulating endothelial barrier function.

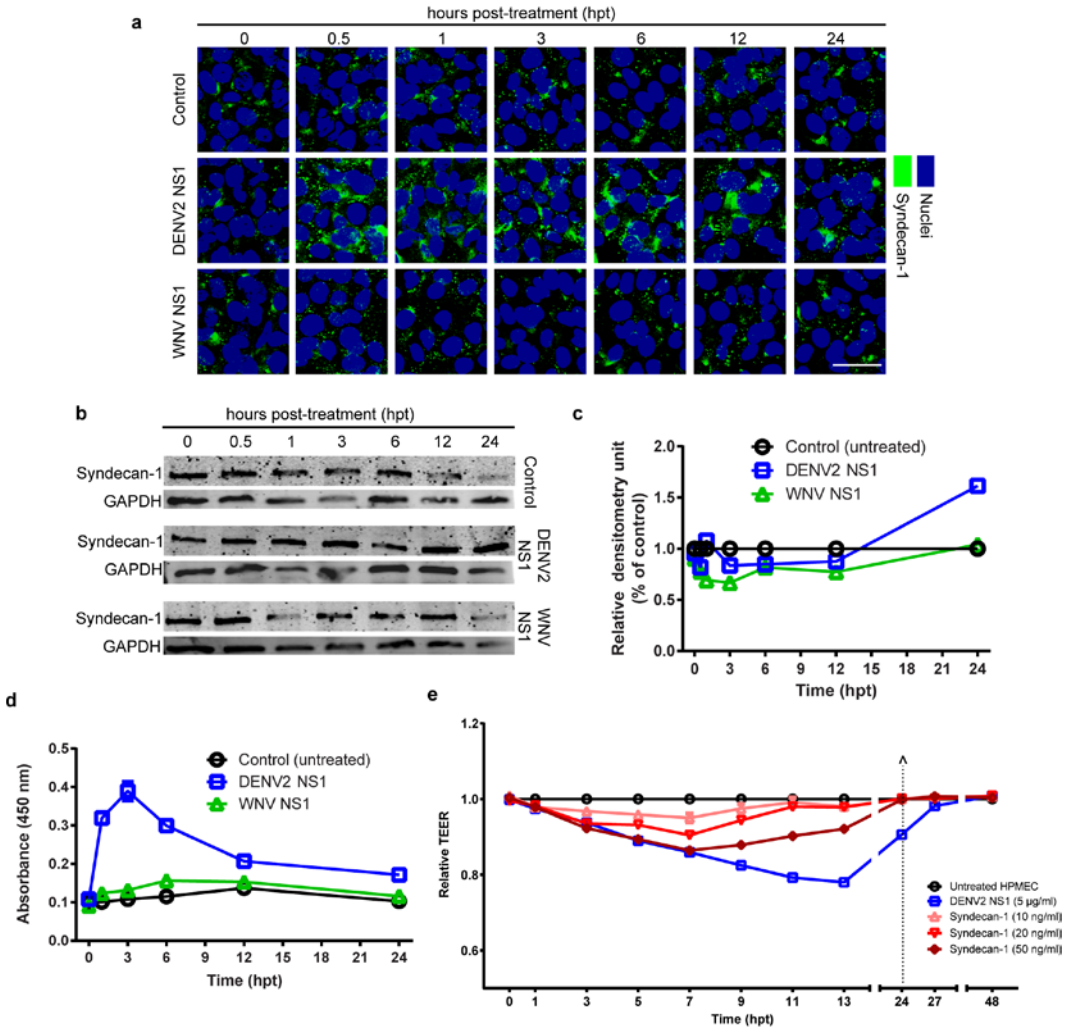

Figure 2.3. DENV2 NS1 increases the surface staining of syndecan-1 in the EGL of HPMEC.
(a) Staining of syndecan-1 (green) on the surface of HPMEC monolayers over time (hpt) after treatment with DENV2 or WNV NS1 proteins (5 µg/ml), examined by confocal microscopy. Untreated cells were used as a control for basal syndecan-1 detection. Nuclei are stained with Hoechst (blue). Images are representative of three individual experiments (20X). Scale bar, 10 µm. **(b)** Expression of syndecan-1 in total protein extracts at indicated time points (hpt) in the presence of DENV2 or WNV NS1 proteins (5 µg/ml), as measured by Western blot. 10 µg/ml of total protein was loaded, and GAPDH expression was used as protein loading control. **(c)** Densitometry data normalized to control untreated cells. **(d)** Levels of syndecan-1 shed from the surface of HPMEC after treatment with DENV2 or WNV NS1 proteins (5 µg/ml) as measured by ELISA from three independent experiments. Surface staining of syndecan-1 is significantly higher in monolayers treated with DENV2 NS1 than in WNV-treated and untreated controls ($P < 0.0005$). **(e)** Effect of recombinant syndecan-1 on TEER of HPMEC monolayers. All concentrations of syndecan-1 induce significant decreases in TEER value (10 ng/ml: $P < 0.05$; 20 ng/ml, 50 ng/ml: $P < 0.0001$). (^) represents change of medium. Relative TEER values from three independent experiments performed in duplicate are plotted at indicated time points. Error bars indicate SEM throughout. Confocal microscopy images acquired and analyzed by Dr. Henry Puerta-Guardo.

DENV2 NS1 increases activity of cathepsin L and its activation of heparanase in endothelial cells

As a result of the dynamic equilibrium between biosynthesis and shedding of various HSPG components, perturbation of the EGL upon shearing stress or increased enzymatic activity (i.e., metalloproteinases or heparanase) results in the alteration of distinct EGL functions, including vascular permeability (36, 150). Heparanase, an endo-β-D-glucuronidase that cleaves GAGs such as HS, is involved in structural remodeling of the ECM and EGL (159, 160). Analyses of the expression/activation of human heparanase in HPMEC demonstrated that DENV2 NS1 increases the expression of heparanase starting 30 min post-treatment, with a maximum peak expression detected at 6 hpt (**Figure 2.4a,b**). Heparanase levels induced by DENV2 NS1 were significantly greater than expression levels in untreated control and WNV NS1-treated monolayers. Human heparanase is produced as an inactive precursor (65 kDa) whose activation involves excision of an internal linker segment, yielding the active heterodimer composed of 8 and 50 kDa subunits (161). Along with the augmented expression of heparanase, increased proteolytic processing of pro-heparanase into an active form (~50 kDa) was detected in HPMEC stimulated with DENV2 NS1 to a much greater degree than WNV NS1-treated and untreated controls **(Figure 2.4c,d)**. Increased enzymatic activity of heparanase has been shown to enhance remodeling of the EGL and ECM, particularly by increasing levels of soluble syndecan-1 on endothelial cells (162, 163). Immunolocalization of heparanase and syndecan-1 in DENV2 NS1-treated HPMEC showed a temporal pattern of expression and colocalization on the surface of endothelial monolayers (**Figure 2.4e**), suggesting that heparanase may induce increased shedding of syndecan-1 in DENV2 NS1-exposed endothelial cells.

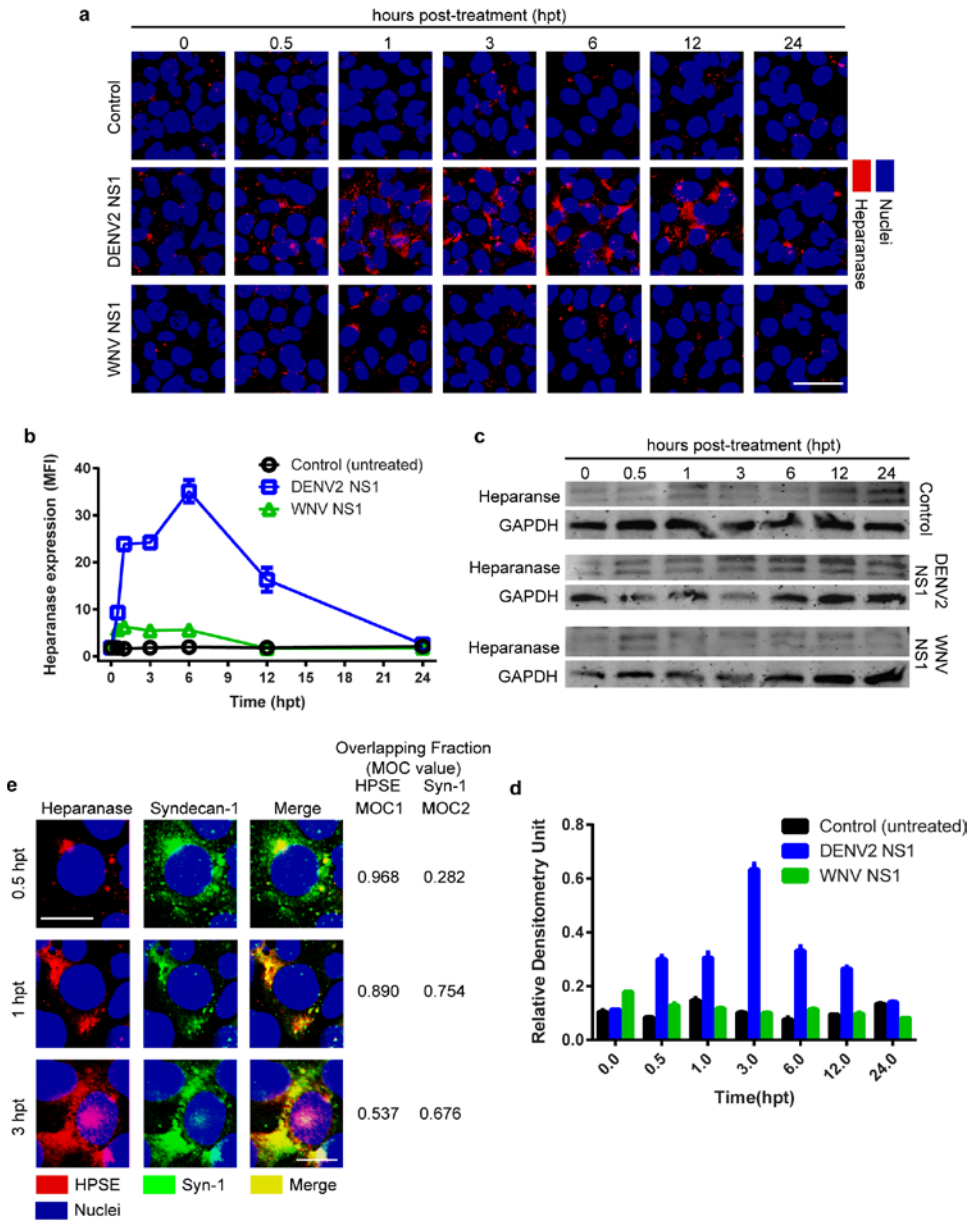

Figure 2.4. DENV2 NS1 triggers the activation/increased expression of endothelial heparanase. **(a)** Heparanase expression (red) in HPMEC monolayers over time (hpt) after treatment with DENV2 or WNV NS1 proteins (5 µg/ml), examined by confocal microscopy. Untreated cells were used as a control for basal heparanase expression. Nuclei stained with Hoechst (blue). Images are representative of three individual experiments (20X). Scale bar, 10 µm. **(b)** Quantification of MFI in **(a)** from three independent experiments. Staining of heparanase in monolayers treated with DENV2 NS1 is significantly different from WNV-treated and untreated controls from 0.5-12 hpt ($P < 0.0001$). **(c)** Heparanase activation in HPMEC monolayers at indicated time points (hpt) after interaction with DENV2 and WNV NS1 proteins (5 µg/ml) via Western blot. Ten µg/ml of total protein was loaded, and GAPDH expression was used as a protein loading control. Upper (~60 kDa) and lower bands (~50 kDa) correspond to inactive and active forms of human heparanase I, respectively. **(d)** Densitometry of Western blot from **(c)**. Graph shows lower band densitometries corresponding to active heparanase (~50 kDa), normalized to GAPDH at each time-point. Heparanase activation is significantly higher in monolayers treated with DENV2 NS1 than in

WNV-treated and untreated controls from 0.5-12 hpt ($P < 0.0001$). **(e)** Co-staining of human heparanase I (red) and syndecan-1 (green) in HPMEC treated with DENV2 NS1 (5 µg/ml) after 30 min, 1 and 3 hpt. Manders' Overlapping Coefficient (MOC) value for the overlapping fraction (merge) is listed to the right of each time point. Confocal microscopy images acquired and analyzed by Dr. Henry Puerta-Guardo.

Activation of heparanase occurs after proteolytic processing by cathepsin L, a ubiquitously expressed endosomal/lysosomal cysteine endopeptidase that is involved in degradation of the ECM (164, 165). Assessment of cathepsin L activity levels demonstrated that DENV2 NS1 increases the proteolytic activity of intracellular cathepsin L in a time-dependent manner (30 min-12 hpt) in cultured HPMEC to a significantly greater degree than WNV NS1 (**Figures 2.5a** rows 2 and 3**, 2.5b**). The activation of cathepsin L by DENV2 NS1 was blocked by a cathepsin L inhibitor but not a cathepsin B inhibitor (**Figures 2.5a** rows 4 and 5**, 2.5b**).

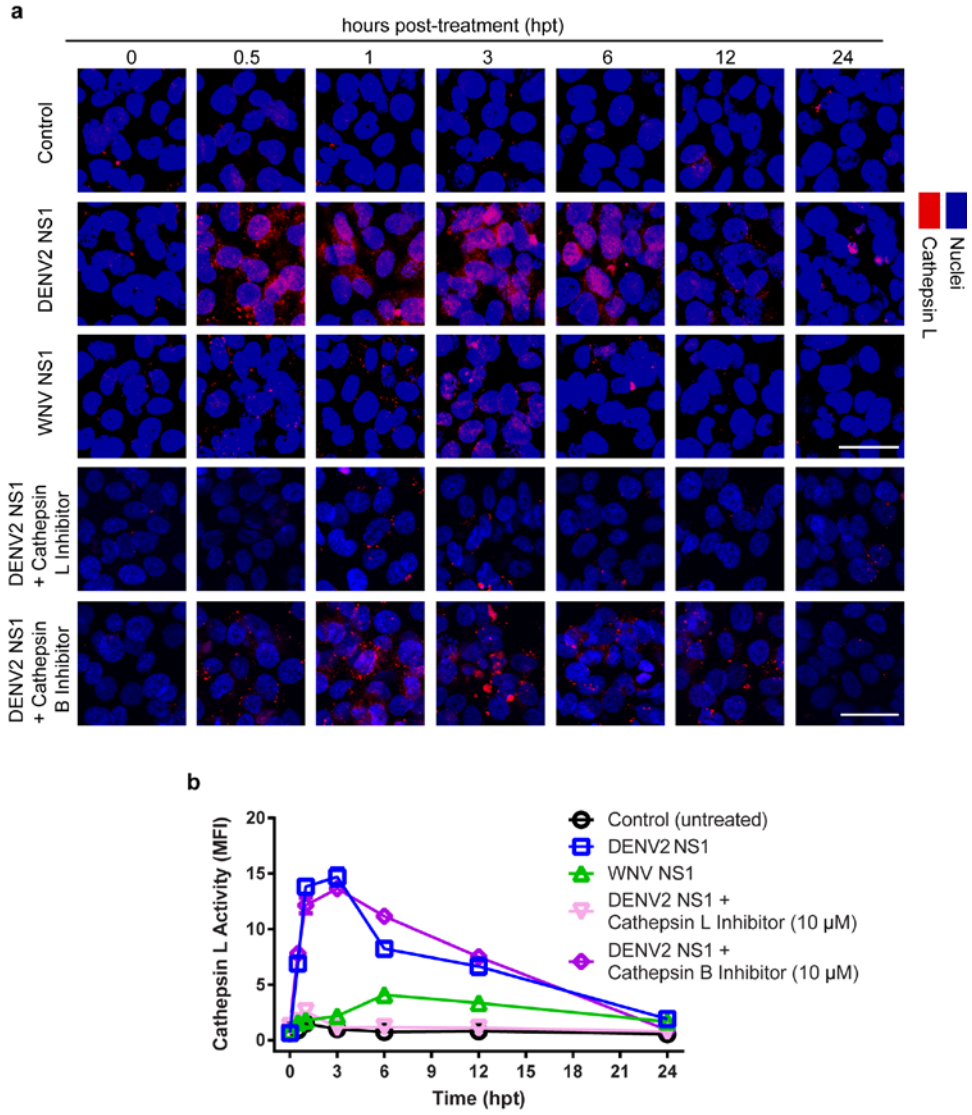

Figure 2.5. DENV2 NS1 increases the activity of cathepsin L protease.
(a) Cathepsin L proteolytic activity (Magic Red assay, in red) in HPMEC monolayers over time (hpt) after treatment with DENV2 or WNV NS1 (5 µg/ml) and cathepsin L or B inhibitors (10 µM). Nuclei are stained with Hoechst (blue). Untreated cells were used as control for basal cathepsin L expression. Images are representative of three individual experiments (20X). Scale bars, 10 µm. **(b)** Quantification of MFI in **(a)** from three independent experiments. Staining for cathepsin L activity is significantly higher in monolayers treated with DENV2 NS1 than in WNV-treated and untreated controls at 0.5-12 hpt ($P < 0.0001$). Staining for cathepsin L is significantly lower in monolayers treated with DENV2 NS1 and Cathepsin L Inhibitor compared to monolayers treated with DENV2 NS1 alone at 0.5-12 hpt ($P < 0.0001$). Error bars indicate SEM throughout. Confocal microscopy images acquired and analyzed by Dr. Henry Puerta-Guardo.

Heparanase and cathepsin L inhibition blocks DENV2 NS1-triggered EGL disruption and endothelial hyperpermeability

To confirm the role of cathepsin L in DENV2 NS1-mediated disruption of the EGL, a cathepsin L inhibitor (10 µM), alongside a cathepsin B inhibitor as a control for specificity, was tested in HPMEC monolayers. Alterations of the HPMEC EGL induced by DENV2 NS1, including degradation of sialic acid, shedding of syndecan-1, and increased expression of heparanase, were prevented in the presence of cathepsin L but not cathepsin B inhibitors (**Figure 2.6a**). Next, the effect of blocking cathepsin L and/or heparanase, using Cathepsin L Inhibitor and the heparanase inhibitor OGT 2115 (1.0 µM) (166), respectively, on syndecan-1 and Sia shedding in supernatants of NS1-treated HPMEC was examined by ELISA. The decrease in Sia as well as the increase in syndecan-1 observed in HPMEC supernatants in response to NS1 treatment were both reversed by cathepsin L and/or heparanase inhibitors (**Figure 2.6b,c**). Both OGT 2115 and cathepsin L inhibitor were used at concentrations that do not affect endothelial cell viability as determined by CellTox Green Cytotoxicity Assay (Promega).

Finally, to characterize the role of endothelial heparanase and cathepsin L in DENV2 NS1-mediated endothelial permeability, Cathepsin L Inhibitor and OGT 2115 were tested in HPMEC monolayers treated with DENV2 NS1. OGT 2115 induced substantial protection against DENV2 NS1-induced hyperpermeability in HPMEC at 3-7 hpt (**Figure 2.6d**), as measured by TEER. HPMEC monolayers exposed to Cathepsin L Inhibitor were also protected in a dose-dependent manner from DENV2 NS1-induced endothelial hyperpermeability (**Figure 2.6e**). In contrast, DENV2 NS1 still increased permeability of HPMEC monolayers in the presence of a cathepsin B-specific inhibitor **(Figure 2.6e**). Further, the use of an inhibitor cocktail containing DANA (50 µg/ml), OGT 2115 (1.0 µM), and Cathepsin L Inhibitor (10 µM) completely prevented DENV2 NS1-induced endothelial hyperpermeability in HPMEC **(Figure 2.S3)**. Together, these data demonstrate the functional significance of the cathepsin L-heparanase pathway, in that the inhibition of either enzyme prevented both the disruption of the EGL and the hyperpermeability of HPMEC triggered by DENV2 but not WNV NS1.

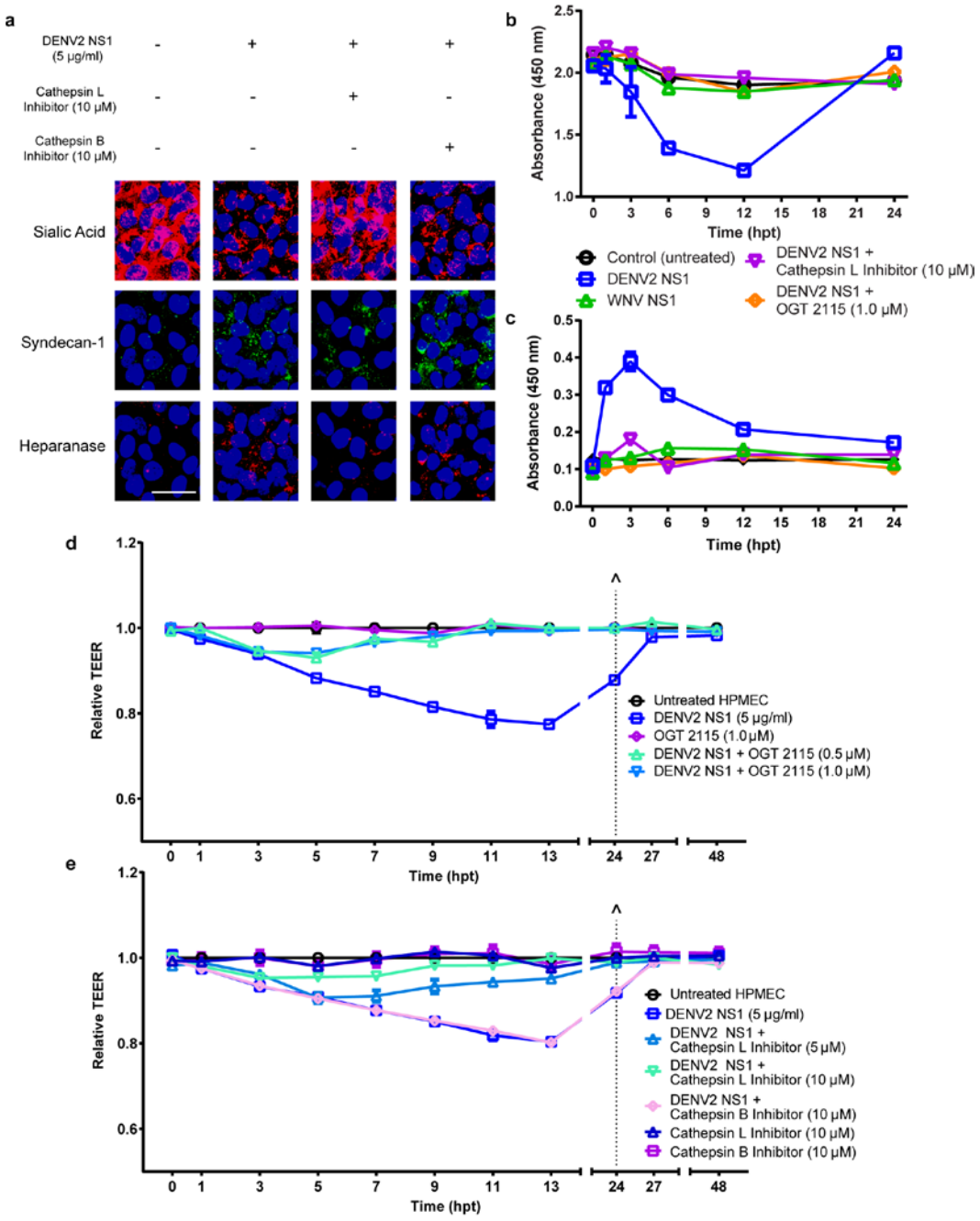

Figure 2.6. DENV2 NS1-mediated endothelial dysfunction is blocked by inhibition of heparanase activation and cathepsin L activity.
(a) Effect of Cathepsin L Inhibitor (10 µM) on DENV2 NS1-mediated disruption of the EGL components Sia (red, upper panels) and syndecan-1 (green, middle panels), and on DENV2 NS1-induced increase of heparanase expression (red, lower panels). Nuclei stained with Hoechst (blue). Untreated cells were used as a control for basal expression of EGL components and heparanase. Cathepsin B inhibitor (10 µM) is used as a negative control. Images are representative of three individual experiments (20X). Scale bar, 10 µm. **(b)** Effect of Cathepsin L Inhibitor and OGT 2115 (human heparanase I inhibitor) on DENV2 NS1-induced release of Sia into the supernatant, as measured by ELISA from three independent experiments. Shedding of Sia is significantly different in monolayers treated with DENV2 NS1 and

cathepsin L inhibitor or OGT 2115 than in monolayers treated with DENV2 NS1 alone at 6 and 12 hpt ($P < 0.0001$). **(c)** Effect of cathepsin L inhibitor on DENV2 NS1-induced shedding of syndecan-1, as measured by ELISA from three independent experiments. Shedding of syndecan-1 is significantly lower in monolayers treated with DENV2 NS1 and cathepsin L inhibitor compared to monolayers treated with DENV2 NS1 alone at 1-12 hpt ($P < 0.0001$). **(d)** Effect of OGT 2115 (heparanase I inhibitor) on DENV2 NS1-triggered endothelial hyperpermeability (TEER) in HPMEC monolayers. TEER values of monolayers treated with DENV2 NS1 and OGT 2115 (0.5, 1.0 µM) are significantly different than values of monolayers treated with DENV2 NS1 alone ($P < 0.0001$). **(e)** Effect of cathepsin L inhibitor on DENV2 NS1-induced endothelial hyperpermeability (TEER) in HPMEC monolayers. TEER values of monolayers treated with DENV2 NS1 and cathepsin L inhibitor (5, 10 µM) are significantly different than values of monolayers treated with DENV2 NS1 alone ($P < 0.0001$). In **(c)** and **(d)**, (^) represents change of medium, and relative TEER values from three independent experiments performed in duplicate are plotted at indicated time points. In **(a)** and **(c)**, Cathepsin B inhibitor (CA-074, 10 µM) was included as a control for specific cysteine protease inhibition. Error bars indicate SEM throughout. Confocal microscopy images acquired and analyzed by Dr. Henry Puerta-Guardo.

TLR4 plays a role in disruption of sialic acid but in not activation of the cathepsin L-heparanase pathway

Because TLR4 has been implicated as a component of DENV2 NS1-induced vascular leak, we investigated the impact of LPS-RS, a TLR4 antagonist, on NS1-induced effects in HPMEC monolayers. We first evaluated Sia expression and found that treatment with DENV2 NS1 in the presence of LPS-RS (50 µg/ml) significantly increased the staining of Sia on the surface of HPMEC by 68-98% compared to DENV2 NS1 alone, suggesting that TLR4 is somehow involved in the disruption of Sia in the EGL **(Figure 2.7a,c)**. LPS-RS also increased the surface staining of syndecan-1 by 14-36% **(Figure 2.7b,d)** but slightly decreased the activity of cathepsin L by 8-19% in HPMEC **(Figure 2.8a,c)**; the expression of heparanase was unaffected **(Figure 2.8b,d)**. However, monolayers treated with LPS-RS and DENV2 NS1 still showed significant differences in syndecan-1 surface staining (5-fold) and cathepsin L activity (10-fold) compared to untreated controls. Overall, these data suggest that TLR4 may play a role in Sia disruption in the EGL of HPMEC but only minimally affects the cathepsin L-heparanase pathway following binding of DENV2 NS1 to HPMEC, as this pathway is still strongly activated even with inhibition of TLR4.

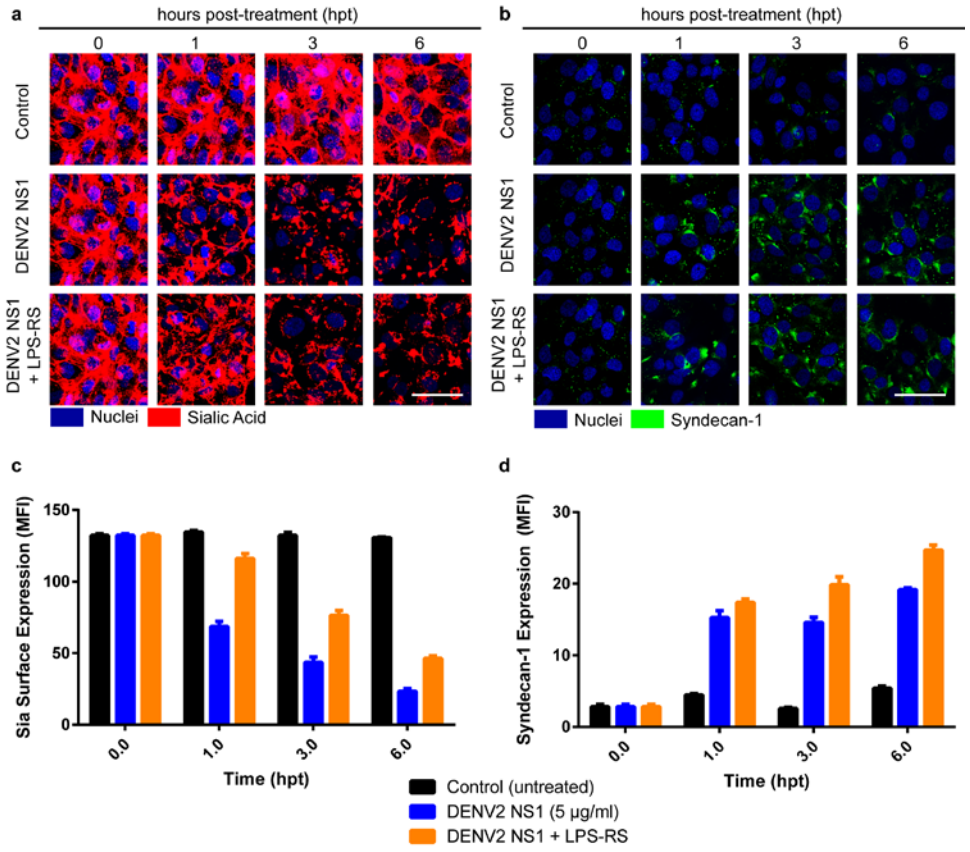

Figure 2.7. LPS-RS, an LPS antagonist, partially prevents DENV2 NS1-induced modulation of Sia expression and further increases surface staining of syndecan-1 in the EGL of HPMEC.
(a) Sia expression on HPMEC monolayers after treatment with DENV2 NS1 (5 µg/ml) and LPS-RS (50 µg/ml), examined by confocal microscopy. Sia was stained with WGA-A647 (red) at indicated time points (hpt). Untreated cells were used as a control for basal Sia expression. Nuclei stained with Hoechst (blue). Images (20X) are representative of three independent experiments. Scale bar, 10 µm. **(b)** Staining of syndecan-1 (green) on the surface of HPMEC monolayers over time (hpt) after treatment with DENV2 NS1 (5 µg/ml) and LPS-RS (50 µg/ml), examined by confocal microscopy. Untreated cells were used as a control for basal syndecan-1 expression. Nuclei are stained with Hoechst (blue). Images are representative of three individual experiments (20X). Scale bar, 10 µm. **(c)** Quantification of MFI in **(a)** from three independent experiments. Sia expression in monolayers treated with DENV2 NS1 and LPS-RS is significantly higher than in monolayers treated with only DENV2 NS1 at 1, 3, and 6 hpt ($P < 0.0001$). **(d)** Quantification of MFI in **(b)** from three independent experiments. Syndecan-1 expression in monolayers treated with DENV2 NS1 and LPS-RS is significantly higher than in monolayers treated with only DENV2 NS1 at 3 and 6 hpt ($P < 0.0001$). Confocal microscopy images acquired and analyzed by Dr. Henry Puerta-Guardo.

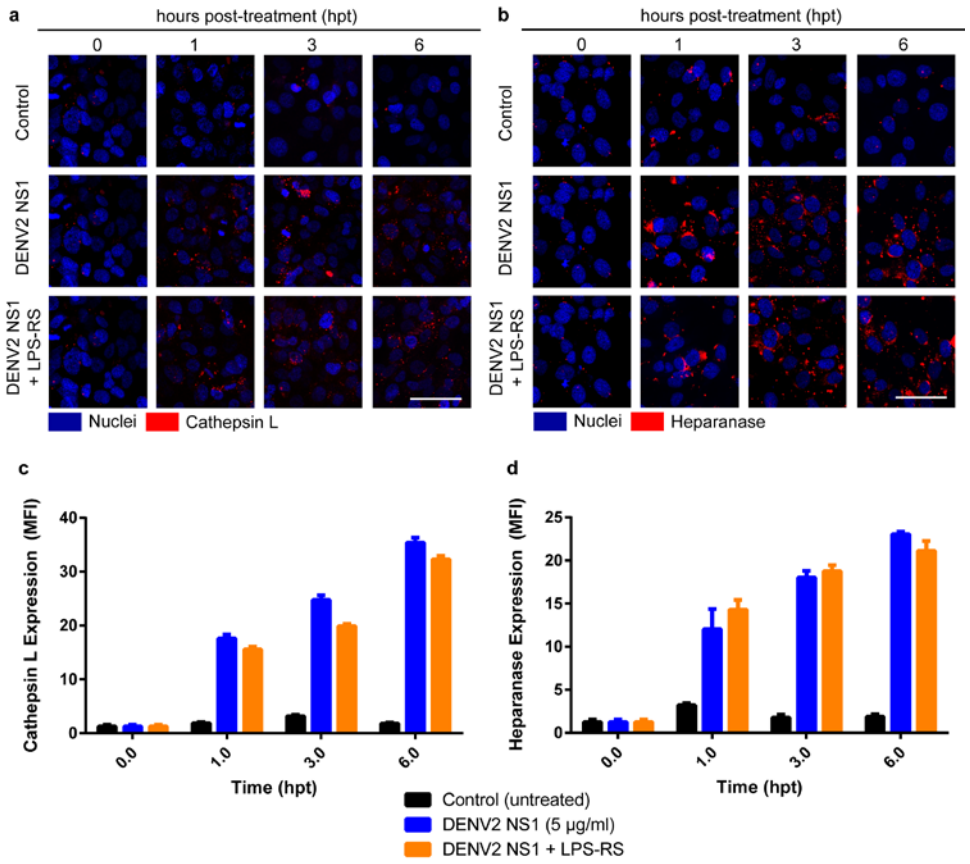

Figure 2.8. LPS-RS, an LPS antagonist, partially prevents DENV2 NS1-induced increase of cathepsin L activity in HPMEC.
(a) Cathepsin L proteolytic activity (Magic Red assay, in red) in HPMEC monolayers over time (hpt) after treatment with DENV2 NS1 (5 µg/ml) and LPS-RS, examined by confocal microscopy. Nuclei are stained with Hoechst (blue). Untreated cells were used as control for basal cathepsin L expression. Images are representative of three individual experiments (20X). **(b)** Heparanase expression (red) in HPMEC monolayers over time (hpt) after treatment with DENV2 NS1 (5 µg/ml) and LPS-RS, examined by confocal microscopy. Untreated cells were used as a control for basal heparanase expression. Nuclei stained with Hoechst (blue). Images are representative of three individual experiments (20X). Scale bar, 10 µm. **(c)** Quantification of MFI in **(a)** from three independent experiments. Cathepsin L activity in monolayers treated with DENV2 NS1 and LPS-RS is significantly lower than in monolayers treated with only DENV2 NS1 at 3 and 6 hpt (3 hpt, $P < 0.0001$; 6 hpt, $P < 0.005$). **(d)** Quantification of MFI in **(b)** from three independent experiments. Heparanase expression in monolayers treated with DENV2 NS1 and LPS-RS is not significantly different than in monolayers treated with only DENV2 NS1. Confocal microscopy images acquired and analyzed by Dr. Henry Puerta-Guardo.

NS1 from DENV1, DENV3, and DENV4 induces effects similar to DENV2 NS1 in endothelial cells

To determine whether the effects observed in endothelial cells were specific to DENV2 NS1, NS1 from DENV1, DENV3, and DENV4 was evaluated using the same experimental setup as previously described. As we have shown previously (84), endothelial

permeability of HPMEC was significantly increased following addition of DENV1-4 NS1, as measured by TEER **(Figure 2.9a)**. Staining for Sia on the surface of HPMEC was significantly decreased 1-12 hpt after treatment with DENV1 and DENV2 NS1 and 2-12 hpt after treatment with DENV3 and DENV4 NS1 **(Figure 2.9b)**. Increased expression of Neu1 was observed in HPMEC monolayers 1-12 hpt following treatment with DENV1-4 NS1 when compared to untreated controls and WNV NS1-treated cells **(Figure 2.9c)**. Expression of Neu2 was significantly increased 1-12 hpt following treatment with NS1 from DENV1, DENV2, and DENV4 and 3-12 hpt following treatment with DENV3 NS1 when compared to untreated and WNV-treated HPMEC **(Figure 2.9d)**. Neu3 expression was similarly increased 1-12 hpt following treatment with DENV1, DENV2, and DENV3 NS1 and 6-12 hpt following treatment with DENV4 NS1 when compared to untreated and WNV NS1-treated controls **(Figure 2.9e)**. Significantly increased staining of syndecan-1 on the surface of HPMEC monolayers was observed following DENV1-4 NS1 treatment, although the kinetics varied depending on serotype (DENV1-2: 1-12 hpt; DENV3: 3-12 hpt; DENV4: 3-6 hpt) **(Figure 2.9f)**. Expression of heparanase was also significantly increased following treatment with NS1 from all four DENV serotypes, though the effect was slightly delayed in DENV3-4 (3-12 hpt) compared to DENV1-2 (1-12 hpt) **(Figure 2.9g)**. Further, cathepsin L activity was significantly increased from 1-12 hpt following treatment with DENV1-4 NS1 **(Figure 2.9h)**. Taken together, these data demonstrate that NS1 from all four DENV serotypes induces hyperpermeability in endothelial cells using similar molecular mechanisms. For all source confocal microscopy images, see Puerta-Guardo et al. (88).

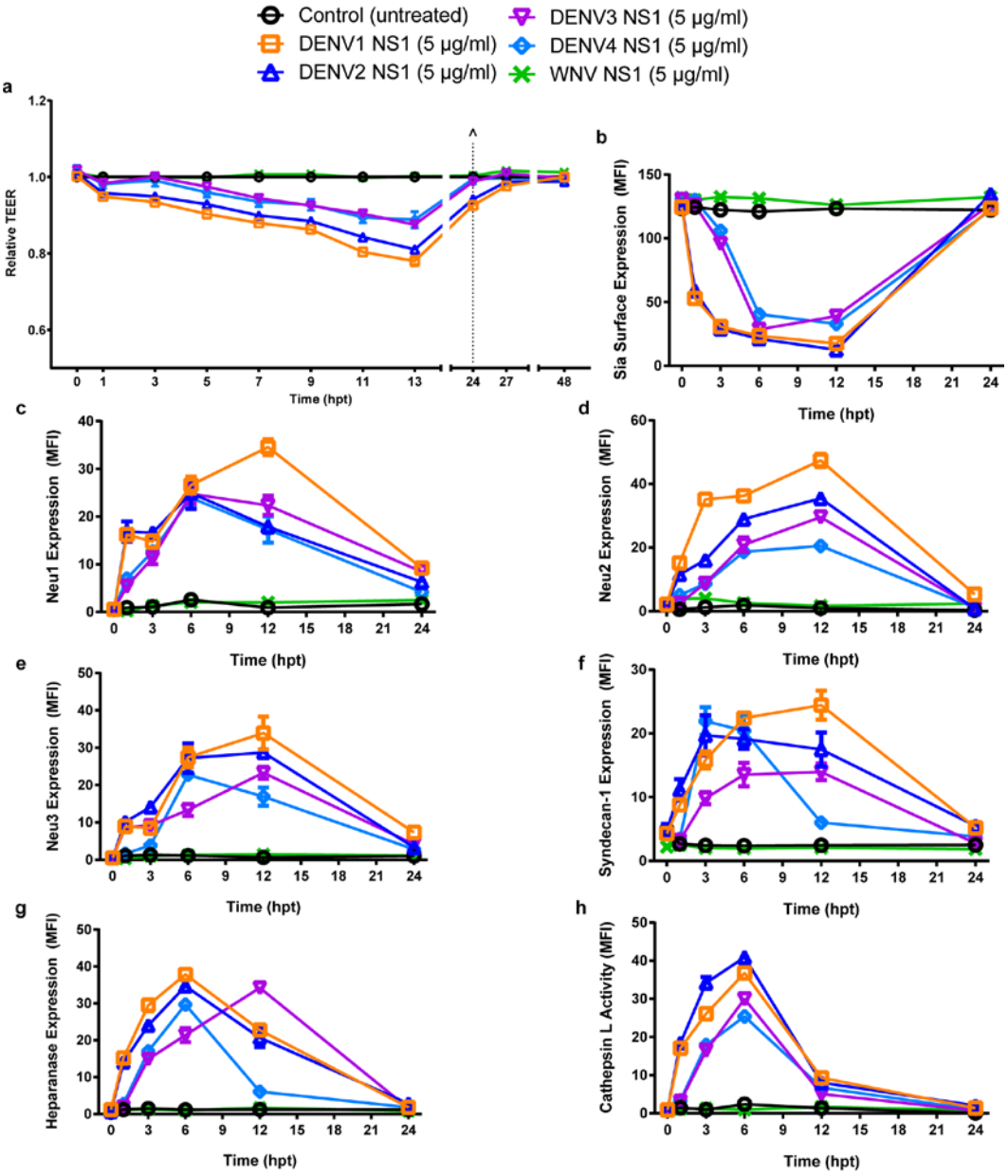

Figure 2.9. DENV NS1-induced effects on the EGL leading to endothelial hyperpermeability are similar across all four DENV serotypes.
(a) TEER assay to evaluate the effect of NS1 proteins from DENV1-4 and WNV (5 µg/ml) on HPMEC endothelial permeability. (^) represents change of medium. Relative TEER values from three independent experiments performed in duplicate are plotted at the indicated time points. Error bars indicate standard error of the mean (SEM). NS1 from all DENV serotypes induces statistically significant decreases in TEER ($P < 0.0001$), while NS1 from WNV does not. **(b)** Quantification of MFI in **Figure S9** (88) from three independent experiments. Sia expression in DENV1 and DENV2 NS1-treated monolayers is significantly different from WNV NS1-treated and untreated controls from 1 to 12 hpt ($P < 0.0001$), and Sia expression in DENV3 and DENV4 NS1-treated monolayers is significantly different from WNV NS1-treated and untreated controls from 3-12 hpt ($P < 0.0001$). **(c)** Quantification of MFI in **Figure S10** (88) from three independent experiments. Neu1 expression in DENV1, DENV2, DENV3, and DENV4 NS1-treated monolayers is significantly different from WNV NS1-treated and untreated controls from 1

to 12 hpt ($P < 0.0001$). **(d)** Quantification of MFI in **Figure S11** (88) from three independent experiments. Neu2 expression in DENV1, DENV2, and DENV4 NS1-treated monolayers is significantly different from WNV NS1-treated and untreated controls from 1 to 12 hpt ($P < 0.0001$), and Neu2 expression in DENV3 NS1-treated monolayers is significantly different from WNV NS1-treated and untreated controls from 3-12 hpt ($P < 0.0001$). **(e)** Quantification of MFI in **Figure S12** (88) from three independent experiments. Neu3 expression in DENV1, DENV2, and DENV3 NS1-treated monolayers is significantly different from WNV NS1-treated and untreated controls from 1 to 12 hpt ($P < 0.0001$), and Neu3 expression in DENV4 NS1-treated monolayers is significantly different from WNV NS1-treated and untreated controls from 6-12 hpt ($P < 0.0001$). **(f)** Quantification of MFI in **Figure S13** (88) from three independent experiments. Syndecan-1 expression in DENV1 and DENV2 NS1-treated monolayers is significantly different from WNV NS1-treated and untreated controls from 1 to 12 hpt ($P < 0.0001$); syndecan-1 expression in DENV3 NS1-treated monolayers is significantly different from WNV NS1-treated and untreated controls from 3-12 hpt ($P < 0.0001$); syndecan-1 expression in DENV4 NS1-treated monolayers is significantly different from WNV NS1-treated and untreated controls from 3-6 hpt ($P < 0.0001$). **(g)** Quantification of MFI in **Figure S14** (88) from three independent experiments. Heparanase expression in DENV1 and DENV2 NS1-treated monolayers is significantly different from WNV NS1-treated and untreated controls from 1 to 12 hpt ($P < 0.0001$), and heparanase expression in DENV3 and DENV4 NS1-treated monolayers is significantly different from WNV NS1-treated and untreated controls from 3-12 hpt ($P < 0.0001$). **(h)** Quantification of MFI in **Figure S15** (88) from three independent experiments. Cathepsin L activity in DENV1, DENV2, DENV3, and DENV4 NS1-treated monolayers is significantly different from WNV NS1-treated and untreated controls from 1 to 12 hpt ($P < 0.0001$). For all original confocal microscopy images, see Puerta-Guardo et al. (88).

Discussion

Secondary DENV infection with a serotype different from primary infection is considered an epidemiological risk factor for severe disease. Immune responses after primary DENV infection lead to protective immunity against homologous re-infection but may either protect against or cause increased disease severity in a subsequent DENV infection with a different serotype (167). The latter is thought to be mediated by serotype cross-reactive T cells or antibody-dependent enhancement that triggers an exaggerated and skewed immune response to a previously infecting serotype, resulting in a “cytokine storm”, including TNF-α and IL-6, that leads to endothelial permeability and vascular leak (145). New evidence has demonstrated the ability of DENV NS1 to directly induce release of vasoactive cytokines via TLR4 stimulation of PBMCs, leading to the disruption of endothelial barrier function *in vitro* and increased vascular leakage *in vivo* (84, 85). However, NS1-mediated mechanisms specific to the endothelial barrier itself have yet to be defined. Here, we show that binding of DENV NS1 to endothelial cells triggers endothelial barrier dysfunction through alterations to the EGL. DENV NS1 induces the degradation of Sia, a major constituent of the EGL, an effect that is mediated by cellular sialidases. Further, DENV NS1 increases the activity of cathepsin L, which subsequently increases expression and activation of heparanase in endothelial cells, leading to shedding of heparan sulfate proteoglycans from the EGL, thus altering its integrity. Inhibition of sialidases or the cathepsin L-heparanase pathway prevents DENV NS1-mediated disruption of the EGL as well as endothelial hyperpermeability. These results were observed during treatment with amounts of DENV NS1 similar to levels reported in DHF/DSS patients (69, 72) and suggest a novel mechanism whereby soluble NS1 directly interacts with endothelial cells, inducing the activation of endothelial cell-intrinsic pathways that lead to hyperpermeability. A model summarizing these findings is shown in **Figure 2.10**.

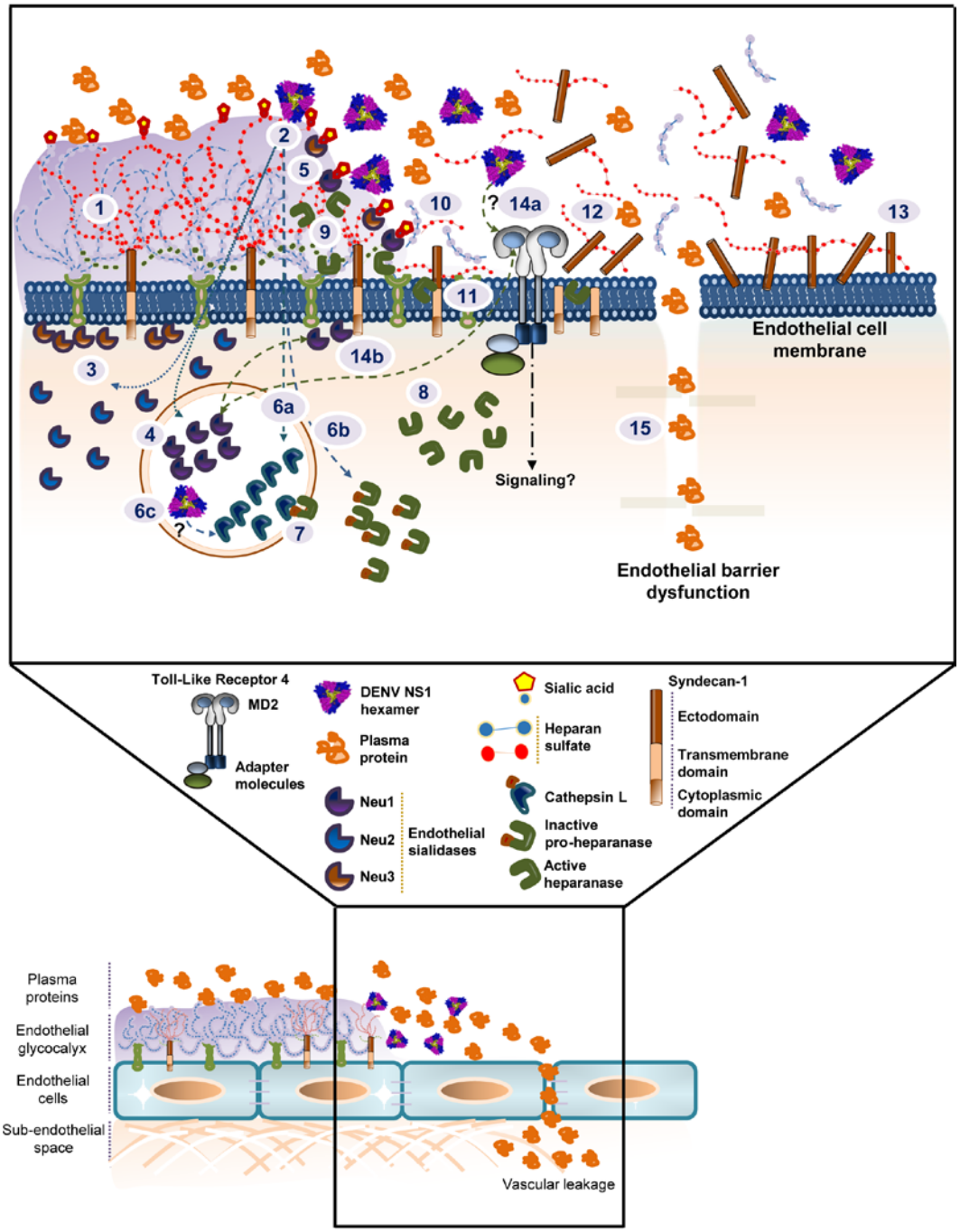

Figure 2.10. Model of DENV NS1-induced endothelial hyperpermeability of human pulmonary microvascular endothelial cells (HPMEC).
(1) The endothelial glycocalyx layer (EGL), a network of membrane-bound proteoglycans and glycoproteins, lines the endothelium on the luminal side. Both endothelium- and plasma-derived soluble molecules interact with this mesh. **(2)** Hexameric NS1 protein secreted from flavivirus-infected cells binds to the surface of uninfected cells, including human pulmonary microvascular endothelial cells (HPMEC), upregulating the expression of lysosomal, cytosolic, and cell membrane endothelial sialidases **(3,4)** that

translocate to the cell membrane, initiating trimming of terminal sialic acid residues expressed on EGL **(5)**. In addition, DENV NS1 enhances the expression of the inactive precursor of the endoglycosidase (pro-heparanase) **(6a)** and the activity of the lysosomal cysteine protease cathepsin L **(6b)**, which processes pro-heparanase into an active/mature form **(7,8),** leading to cleavage of heparan sulfate chains on the EGL **(9,10)**. This results in shedding of syndecan-1, a main component of the EGL **(11,12)**, and its accumulation after binding back to the cell surface **(13)**. Additionally, DENV NS1 may trigger TLR4 signaling **(14a)**, leading to the translocation of Neu1 to the cell membrane and further disruption of sialic acid in the EGL **(14b)**. Together, these processes lead to EGL disruption on the surface of endothelial cells, resulting in endothelial barrier dysfunction and fluid extravasation (hyperpermeability) that occurs in severe dengue disease **(15)**.

Endothelial cells are the most important cellular component of the vasculature, separating blood from underlying tissue (168). In severe dengue disease, plasma leakage occurs in multiple organs around the time of defervescence; however, profuse accumulation of fluids usually takes place in organs such as the lung, where pleural effusion can lead to respiratory distress and shock (144). Secreted hexameric DENV NS1 has been shown to bind to the surface of cultured human dermal and pulmonary microvascular endothelial cells *in vitro* (87), and NS1 binds to lung and liver tissues *in vivo* (87). *In vitro*, we had shown that NS1 from all four DENV serotypes triggers increased permeability of HPMEC monolayers (84). Our results here demonstrate that NS1 from DENV2 but not from WNV, a closely related flavivirus, binds in a dose-dependent fashion to the surface of HPMEC, and this binding pattern is reflected in the dose-dependent decrease of TEER following the addition of NS1 from DENV2. These results support previous observations where inoculation of DENV NS1 alone increased vascular leakage *in vivo* (84) and also suggest that DENV NS1 can modulate endothelial barrier function in different microvascular beds and organs, thereby contributing to the systemic vascular leakage observed in patients experiencing severe dengue disease.

Over the last several decades, the EGL has emerged as a potential regulator of vascular permeability (36). The negative charge provided by glycoproteins bearing terminal monosaccharides, such as Sia residues, and proteoglycans bearing GAGs, such as HS, chondroitin sulfate, and hyaluronic acid (32, 169, 170), contributes to the barrier function of the EGL. To examine the integrity of the EGL, we initially evaluated the distribution of Sia by staining with the lectin WGA and found that NS1 from all four DENV serotypes significantly reduces Sia staining on the surface of HPMEC monolayers. This effect does not occur in the presence of WNV NS1. Due to its prominent position as the outermost monosaccharide unit on the glycan chains of glycolipids and glycoproteins in the EGL as well as its negative charge, Sia is involved in a variety of functions, including regulation of vascular permeability (32, 149, 169-172). Therefore, removal of Sia from the EGL may result in reduction of the net negative charge and hydrophilicity of the endothelial surface (32, 169). Accordingly, disruption of Sia on the EGL may play a key role in DENV NS1-induced endothelial barrier dysfunction observed in HPMEC.

In eukaryotic systems, Sia can be metabolized via enzymatic release or degradation by sialidases/neuraminidases or Sia-specific pyruvate lyases (149). As such, reduced Sia expression in HPMEC exposed to DENV NS1 may be a consequence of enzymatic trimming by endothelial sialidases. Our data demonstrate that free Sia levels in conditioned media were significantly reduced in DENV NS1-treated HPMEC compared

to untreated or WNV NS1-treated monolayers, indicating that DENV NS1 may trigger degradation rather than release of Sia from the cell surface. Furthermore, no endothelial sialidase activity was found in supernatant collected from DENV NS1-treated HPMEC, indicating that Sia on endothelial cells is removed by the action of specific membrane-associated sialidases and/or metabolized by intracellular lyases. Analyses by confocal microscopy identified that Neu1, Neu2, and Neu3 sialidases were selectively upregulated in HPMEC in the presence of all DENV NS1 proteins but not WNV NS1. Neu1 is mainly localized in lysosomes but is also capable of translocation to the cell surface (173). Neu2, also known as the soluble sialidase, is a cytosolic enzyme that cleaves a variety of substrates, including oligosaccharides, glycoproteins, and gangliosides (Sia-containing glycolipids) (174). Neu3 is found on the cell membrane, acting specifically on the sialic acids of gangliosides (172). Thus, increased expression of endothelial sialidases triggered by DENV NS1 may lead to trimming of Sia on the surface of HPMEC, resulting in initial degradation of the EGL and increased endothelial permeability. Additionally, we found that treatment of HPMEC monolayers with Zanamivir or DANA, influenza neuraminidase inhibitors that have also been shown to significantly inhibit human sialidases (152), substantially protects endothelial monolayers from DENV NS1-induced hyperpermeability. These data suggest that removal of Sia from the EGL by human sialidases contributes to increased permeability of human endothelial cell monolayers following binding of DENV NS1.

In vertebrates, mammalian sialidases and their target substrates have been implicated in crucial biological processes, including the regulation of cell proliferation/differentiation, clearance of plasma proteins, control of cell adhesion, metabolism of gangliosides and glycoproteins, immunocyte function, and modification of receptors (172). More recently, a novel role for Neu1 in controlling the activation of TLR4 signaling pathways was described (175, 176). Briefly, Neu1 activity has been shown to influence receptor desialylation and disruption of TLR4:Siglec-E interaction, which subsequently activates TLR4 signaling, leading to the production of nitric oxide and pro-inflammatory cytokines in dendritic and macrophage cells (175-179). Further, TLR4 signaling has been shown to be required for translocation of Neu1 to the cell membrane (177). Thus, DENV NS1 stimulation of Neu1 may lead to TLR4 signaling, in turn contributing to the translocation of Neu1 to the cell membrane and subsequent disruption of Sia in the EGL of HPMEC. Interestingly, we found that when HPMEC monolayers are treated with LPS-RS, a TLR4 antagonist that binds MD-2 in the TLR4 complex, DENV NS1-induced disruption of Sia is significantly decreased. This suggests that treatment with LPS-RS may prevent TLR4 signaling and ensuing translocation of Neu1 to the cell membrane, thereby partially preventing the disruption of Sia that occurs after treatment with DENV NS1 alone.

In addition to Sia residues, cell surface proteoglycans and their associated GAG side chains help to preserve the stability and function of the EGL. Transmembrane syndecans, membrane-bound glypicans, and basement matrix-associated perlecans are the three major protein core families of HSPGs found on endothelial cells (36, 156). Structurally, syndecans are composed of an N-terminal signal peptide, an extracellular domain containing several consensus sequences for GAG attachment, a single transmembrane domain, and a short C-terminal cytoplasmic domain (180). Syndecan ectodomains can be shed intact by proteolytic cleavage of their core proteins (181, 182). Due to its HS

chains, syndecan-1 can function as a co-receptor on the cell surface and also as a soluble HSPG that binds to a wide variety of extracellular ligands, including matrix proteins, cytokines, and chemokines. In this study, a specific immunoassay to detect soluble syndecan-1 from conditioned HPMEC media demonstrated that DENV NS1 induces enhanced shedding of the syndecan-1 ectodomain from the EGL. Since the *in vitro* HPMEC monolayer system is static, this shedding may lead to increased deposition and accumulation of syndecan-1 on the surface of HPMEC, thereby explaining the increased signal for syndecan-1 detected by confocal microscopy. The shedding of syndecan-1 can then result in increased stimulation of inflammatory signaling pathways in the endothelium. Elevated levels of syndecan-1 ectodomains have been implicated in adhesion, migration, cytoskeleton organization, cell differentiation, and vascular permeability (180). Here, we showed that recombinant syndecan-1 increases permeability when added to HPMEC, suggesting that altered expression, distribution, and release of HSPGs (e.g., syndecan-1) from the surface of HPMEC after stimulation with DENV NS1 may result in the activation of inflammatory processes that contribute to endothelial barrier dysfunction.

Accelerated shedding of syndecan-1 has been shown to result from direct proteolytic cleavage by matrix metalloproteinases (MMP) (181, 182). However, syndecan shedding has also been found to be enhanced by enzymatic degradation of HS chains, indicating that non-MMP mechanisms are also involved in this process (162, 183). Heparanase is a β-D-endoglucuronidase that cleaves HS, facilitating degradation of the EGL and the ECM and resulting in release of proteoglycans bearing HS, such as syndecan-1 (160, 162, 163). Remodeling of the EGL and ECM by heparanase is important for various physiological and pathological processes, including inflammation, wound healing, tumor angiogenesis, and metastasis (184). Human pro-heparanase is produced as an inactive precursor protein (~543 amino acids) whose activation involves excision of an internal linker segment (Ser110 – Gln157), yielding the active heterodimer composed of 8 and 50 kDa subunits (160). Processing and activation of pro-heparanase requires cathepsin L, a papain-like lysosomal cysteine proteinase that is ubiquitously expressed in human tissues and is involved in normal cellular protein degradation and turnover (165). Here, analyses of HPMEC monolayers by confocal microscopy demonstrated an increase of heparanase staining and cathepsin L protease activity, detected as early as 30 min after endothelial cell stimulation with DENV but not WNV NS1. Increased expression of the active form of heparanase (~50 kDa) was also shown, indicating that the DENV NS1-induced endothelial hyperpermeability may result from enhanced processing and activation of heparanase by intracellularly expressed cathepsin L. Cathepsin L and heparanase may thus play a critical role in NS1-induced disruption of HS and HSPG components of the EGL, such as syndecan-1. Though MMPs are primarily responsible for the homeostasis of the ECM, cysteine proteases can significantly contribute to its destruction under disease conditions (165). Increased cathepsin L activity has been found to promote disease pathogenesis by creating an inflammatory environment associated with degradation of the ECM in cardiovascular disease, cancer, and rheumatoid arthritis (165). Further, heparanase is upregulated in numerous human diseases such as cancer, diabetes, renal disease, and Alzheimer disease (184, 185). Therefore, overexpression of endothelial heparanase and its increased processing by lysosomal cathepsin L may constitute a key component of the intrinsic endothelial mechanisms initially triggered by

DENV NS1, leading to the disruption of EGL integrity that contributes endothelial barrier dysfunction in endothelial cell monolayers.

The mechanism by which DENV NS1 induces increased activity of cathepsin L is still unclear. Cathepsins are lysosomal cysteine proteases mainly responsible for the remodeling of the extracellular matrix (ECM) (165). They are optimally active at a slightly acidic pH; however, the mechanism of their activation is not fully understood. We have obtained preliminary results that indicate that DENV NS1 is not only able to interact with the surface of the endothelium but also may be internalized and subsequently transported through endothelial monolayers via unidentified endocytic pathways, leading to its accumulation in basolateral compartments. It is possible that this NS1 internalization process leads to the activation of cathepsin L in endosomes of HPMEC, thus contributing to subsequent degradation of the ECM and NS1-induced endothelial hyperpermeability. Alternatively, it is possible that cathepsin L is activated via a sequence of molecular signals following DENV NS1 binding to the surface of endothelial cells.

Our data suggest that DENV NS1 induces endothelial hyperpermeability through significant disruption of the EGL, a phenomenon that may be primarily regulated by the activation the cathepsin L-heparanase pathway. This conclusion was further tested through the use of specific inhibitors of both heparanase (OGT 2115) and cathepsin L (Cathepsin L Inhibitor). Endothelial hyperpermeability induced by DENV NS1 in HPMEC monolayers was significantly reversed in the presence of OGT 2115 and Cathepsin L Inhibitor and was completely reversed in the presence of an inhibitor cocktail containing DANA, OGT 2115, and cathepsin L inhibitor. Further, disruption of Sia, increased surface staining of syndecan-1, and increased activation of heparanase were prevented after inhibition of cathepsin L activity. Notably, when an inhibitor for cathepsin B, a related cysteine protease (165), was used, neither increased endothelial permeability nor EGL disruption was inhibited in DENV NS1-treated HPMEC monolayers. These data support our conclusion that activation of EGL remodeling pathways play a significant role in the endothelial barrier dysfunction induced by DENV NS1.

This work provides insight into endothelial cell-intrinsic mechanisms that contribute to endothelial hyperpermeability triggered by DENV NS1 protein. We have identified multiple pathways that were previously not known to play a role in severe DENV disease, including disruption of the EGL through endothelial sialidases and the cathepsin L-heparanase pathway. The full story is still incomplete, as the precise timing and signaling cascades remain to be defined, and future work will need to further elucidate the kinetics. More comprehensive studies are underway to understand the relative contribution of these endothelial-intrinsic mechanisms in the context of dengue disease, as other factors, including vasoactive cytokines triggered by NS1 (84, 85) and immunopathogenic mechanisms (186), are known to play an important role in DHF/DSS. Overall, these findings add to the novel functions of DENV NS1 and the discovery of new potential pathways contributing to endothelial dysfunction and vascular leak during severe dengue disease, and they may contribute to future advancements in dengue treatment and diagnostics.

Experimental Procedures

Cell culture. The human pulmonary microvascular endothelial cell line HPMEC-ST1.6R was kindly donated by Dr. J.C. Kirkpatrick (Institute of Pathology, Johannes Gutenberg University, Germany) and propagated (passages 5-8) and maintained at 37°C in humidified air with 5% CO_2 in endothelial cell basal medium-2 supplemented with growth factors, antibiotics, and fetal bovine serum as per the manufacturer's specifications (Clonetics, Lonza).

Antibodies, recombinant proteins, and inhibitors. For staining of EGL components, the following monoclonal antibodies (mAbs) and lectins were used: Wheat germ agglutinin (WGA) lectin conjugated to Alexa 647 (WGA-A647, Molecular Probes) to stain N-acetyl neuraminic acid (Sia); anti-human heparanase 1 (HPA1, Santa Cruz Biotech); anti-human cathepsin L (eBioscience); anti-heparan sulfate proteoglycan 2 for perlecan (Abcam), anti-human CD138 for syndecan-1 (eBioscience); Neu1 antibody (H-300): sc-32936 (Santa Cruz Biotech); Neu2 antibody PA5-35114 (Thermo Scientific); Ganglioside sialidase antibody (N-18): sc-55826 for Neu3 (Santa Cruz Biotech). Recombinant NS1 proteins from DENV1 (strain Nauru/Western Pacific/1974), DENV2 (strain Thailand/16681/84), DENV3 (strain Sri Lanka D3/H/IMTSSA-SRI/2000/1266), DENV4 (strain Dominica/814669/1981) and WNV (New York NY99 strain) used in all experiments were produced by Native Antigen (Oxfordshire, United Kingdom) in HEK 293 cells and were shown to be >95% pure and oligomeric, as demonstrated by native PAGE and Western blot analyses (84). In addition, the NS1 proteins were tested and shown to be free of endotoxin contaminants, as determined using the Endpoint Chromogenic Limulus Amebocyte Lysate (LAL) QCL-1000TM kit (Lonza) (<0.1 EU/ml) and as certified by the manufacturer. Recombinant syndecan-1/CD138 used in TEER assays was >95% pure and <1.0 EU/µg endotoxin by LAL assay according to the manufacturer's indications (R&D Systems). Recombinant neuraminidase from *Clostridium perfringens* was obtained from Sigma. Selective inhibitors of human heparanase (OGT 2115, Tocris), cathepsin L (Cathepsin L inhibitor I, Calbiochem), cathepsin B (CA-074, Tocris Bioscience), neuraminidase (Zanamivir and *N*-Acetyl-2,3-dehydro-2-deoxyneuraminic acid (Sigma)) were used in TEER assays at concentrations that do not affect cell viability. Cell viability was determined by the Promega CellTox Green Cytotoxicity Assay following manufacturer's instructions.

Flavivirus NS1 protein binding assay. Confluent HPMEC monolayers grown on gelatin-coated coverslips (0.2%, Sigma) were exposed to different concentrations of DENV2 NS1 (1.25-10 µg/ml) and WNV NS1 (5-10 µg/ml) and incubated for one hour at 37°C. NS1 protein bound to the cell surface was then detected using the anti-NS1 mAb 9NS1 conjugated to Alexa 488 (cross-reactive to WNV and DENV2 NS1; gift from Dr. M.S. Diamond, Washington University in St. Louis) (187) and the anti-NS1 mAb 7E11 conjugated to Alexa 568 (gift from Dr. R. Putnik, Walter Reed Army Institute of Research). For the time course of DENV2 NS1 binding, 5 µg/ml of NS1 was used, and cell monolayers were incubated as described above and fixed (PFA 2%) at 1, 3, 6, 12 and 24 hpt. Images were acquired using a Zeiss LSM 710 AxioObserver-34-channel spectral detector confocal microscope and processed using ImageJ software (188). A

quantification of NS1 protein bound to the cell surface was expressed as mean fluorescence intensity (MFI) compared to untreated cells used as a negative control.

Transendothelial Electrical Resistance (TEER). The effect of recombinant NS1 proteins on endothelial permeability was evaluated by measuring TEER [Ohms (Ω)] in HPMEC monolayers grown on a 24-well Transwell polycarbonate membrane system (Transwell permeable support, 0.4 µm, 6.5 mm insert; Corning Inc.) as previously described (84). Untreated HPMEC grown on Transwell inserts were used as negative untreated controls, and inserts with medium alone were used for blank resistance measurements. Relative TEER represents a ratio of resistance values (Ω) obtained at sequential 2 hour time points following the addition of test proteins as follows: (Ω experimental condition - Ω medium alone)/(Ω non-treated endothelial cells - Ω medium alone). After 24 hours of treatment, 50% of upper and lower chamber media were replaced by fresh endothelial cell medium. An Epithelial Volt Ohm Meter (EVOM) with "chopstick" electrodes (World Precision Instruments) was used to measure TEER values.

Fluorescence microscopy. For imaging experiments, HPMEC were grown on coverslips and imaged on a Zeiss LSM 710 Axio Observer inverted fluorescence microscope equipped with a 34-channel spectral detector. Images acquired using the Zen 2010 software (Zeiss) were processed and analyzed with ImageJ software (188). All RGB images were converted to grayscale, then mean grayscale values and integrated density from selected areas were taken along with adjacent background readings and plotted as mean fluorescence intensity (MFI). To assess the effect of flavivirus NS1 on integrity of the endothelial architecture, the distribution of EGL components was examined on confluent HPMEC monolayers treated with DENV or WNV NS1 proteins (5 µg/ml) and fixed with 2% paraformaldehyde (PFA) and ethanol-methanol (1:1) at different time points (0, 30 min, 1, 3, 6, 12 and 24 hpt). Primary antibodies were incubated overnight at 4°C, and detection was performed using secondary species-specific anti-IgG antibodies conjugated to Alexa fluorophores (488, 568 and 647).

Western blot. For protein expression, confluent HPMEC monolayers (~$1x10^6$ cells/well, 6-well tissue culture-treated plates) were treated with DENV and WNV NS1 proteins (5 µg/ml), and at different time points (0, 30 min, 1, 3, 6, 12 and 24 hpt), cell monolayers were scraped on ice using RIPA lysis buffer (50 mM Tris [pH 7.4], 150 mM NaCl, 1% [v/v] Nonidet-P40, 2 mM EDTA, 0.1% [w/v] SDS, 0.5% Na-deoxycholate and 50 mM NaF) supplemented with complete protease inhibitor cocktail (Roche). After total protein quantification using a bicinchoninic acid (BCA)-based colorimetric assay (Pierce BCA Protein Assay Kit, Thermo Scientific), 10 µg of total protein per sample was boiled and placed in reducing Laemmeli buffer and separated by 4-20% gradient SDS-PAGE. After immunoblotting using specific primary antibodies for syndecan-1, human heparanase, human cathepsin L, and GAPDH (used as housekeeping protein control) and secondary species-specific anti-IgG antibody conjugated to Alexa 680 or Alexa 750, protein detection and quantification was carried out using the Odyssey CLx Infrared Imaging System (LI-COR). Relative densitometry represents a ratio of the values obtained from each experimental protein band over the values obtained from loading controls (GAPDH) after subtracting background from both using Image Studio Lite V 5.2 (LI-COR Biosciences).

ELISA. ELISAs for human syndecan-1 (CD138), Sia (NANA), and human cathepsin L were performed following the manufacturer's instructions (Abcam).

Enzymatic activity assays. Cathepsin L activity in living cells was monitored using the Magic Red Cathepsin L detection kit (Immunochemistry Technologies, Inc.). Briefly, confluent HPMEC monolayers grown on coverslips were exposed to DENV and WNV NS1 proteins (5 µg/ml), and at different time points, a cell membrane-permeant fluorogenic substrate MR-$(Phe\text{-}Arg)_2$, which contains the cresyl violet (CV) fluorophore branded as Magic Red (MR), was added. Cultured cell monolayers expressing active cathepsin L catalyze the hydrolysis of the two Phe-Arg target sequences, generating a red fluorescent species that can be detected by immunofluorescence microscopy. Magic Red excites at 540-590 nm (590 nm optimal) and emits at >610nm (630 nm optimal). For neuraminidase detection, culture supernatants from NS1-exposed HPMEC monolayers were collected at different time points and processed for neuraminidase activity using the Amplex Red reagent-based assay and fluorescence detection following recommended procedures (Molecular Probes).

Statistical analysis. Statistical analysis was performed using GraphPad Prism 6 software, and all graphs were generated using Prism 6. Comparison between MFI, ELISA, and densitometry data was conducted using multiple t-tests with a False Discovery Rate of 1%. For TEER experiments, statistical significance was determined using a two-way analysis of variance (ANOVA).

Supplementary Material

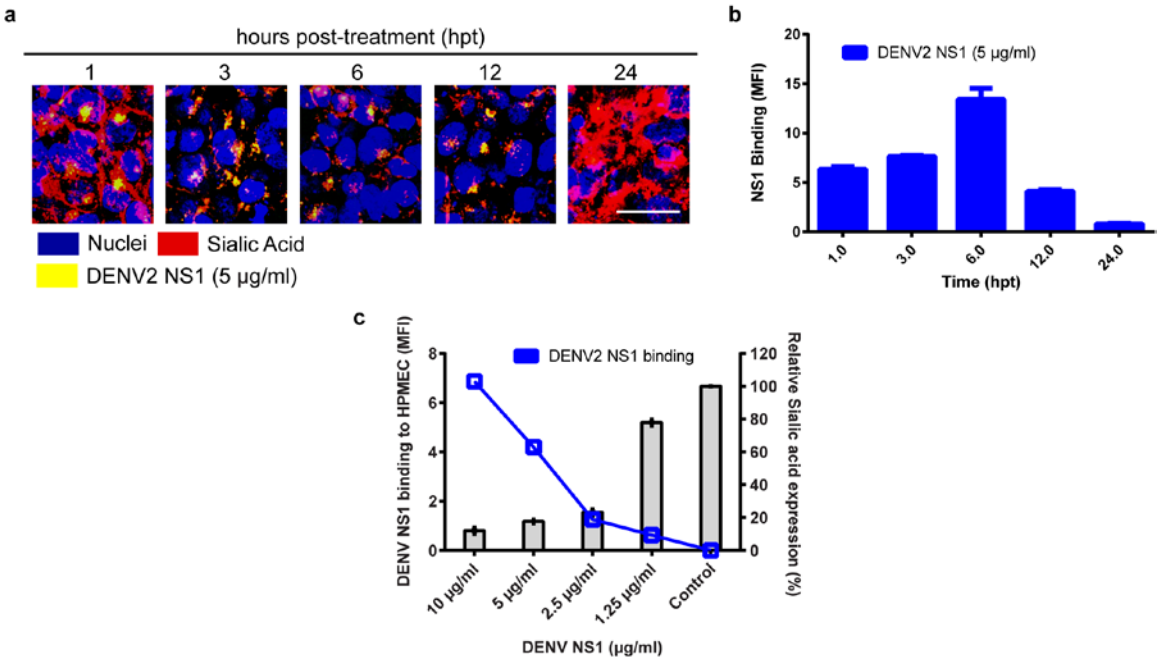

Figure 2.S1. Related to Figures 2.1, 2.2C. Binding of DENV2 NS1 to endothelial cells is both a dose- and time-dependent effect.
(a) Binding of DENV2 NS1 to HPMEC monolayers, examined by confocal microscopy. DENV2 NS1 was stained with a specific monoclonal antibody (9NS1 conjugated to Alexa 488), and Sia was stained with WGA-A647 (red) at indicated time points (hpt). Nuclei stained with Hoechst (blue). Images (20X) are representative of three independent experiments. Scale bar, 10 µm. **(b)** Quantification of MFI of DENV2 NS1 staining in **(a)** from three independent experiments. **(c)** DENV2 NS1 disrupts Sia on the EGL of HPMEC in a dose-dependent manner. Quantification of Sia expression on cell surface and DENV2 NS1 binding to HPMEC monolayers in the presence of different concentrations of DENV2 NS1 (1.25, 2.5, 5, and 10 µg/ml) in **Figure 2.2c**. Results represent mean fluorescence intensity (MFI) values from three independent experiments. Grey bars represent relative sialic acid expression, calculated by normalizing each condition to untreated control cells (relative sialic acid expression = sialic acid expression in DENV2 NS1-treated monolayers/sialic acid expression in untreated control monolayers). The blue line represents DENV2 NS1 binding. Confocal microscopy images acquired and analyzed by Dr. Henry Puerta-Guardo.

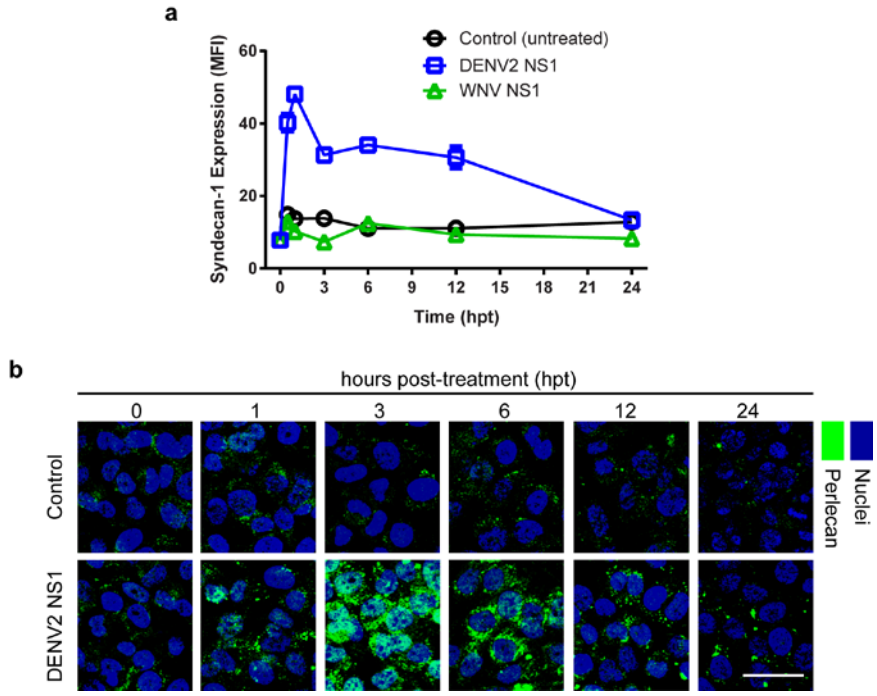

Figure 2.S2. Related to Figure 2.3. DENV2 NS1 increases the surface staining of syndecan-1 and perlecan in the EGL of HPMEC.
(a) Quantification of syndecan-1 MFI in **Figure 2.3a**. Staining is significantly higher with DENV2 NS1 compared to controls at 0.5-12 hpt ($P < 0.0001$). Error bars indicate SEM. **(b)** Expression of perlecan (green) on the surface of HPMEC monolayers over time (hpt) after treatment with DENV2 or WNV NS1 proteins (5 µg/ml), examined by confocal microscopy. Untreated cells were used as a control for basal perlecan expression. Nuclei are stained with Hoechst (blue). Images are representative of three individual experiments (20X). Scale bar, 10 µm. Confocal microscopy images acquired and analyzed by Dr. Henry Puerta-Guardo.

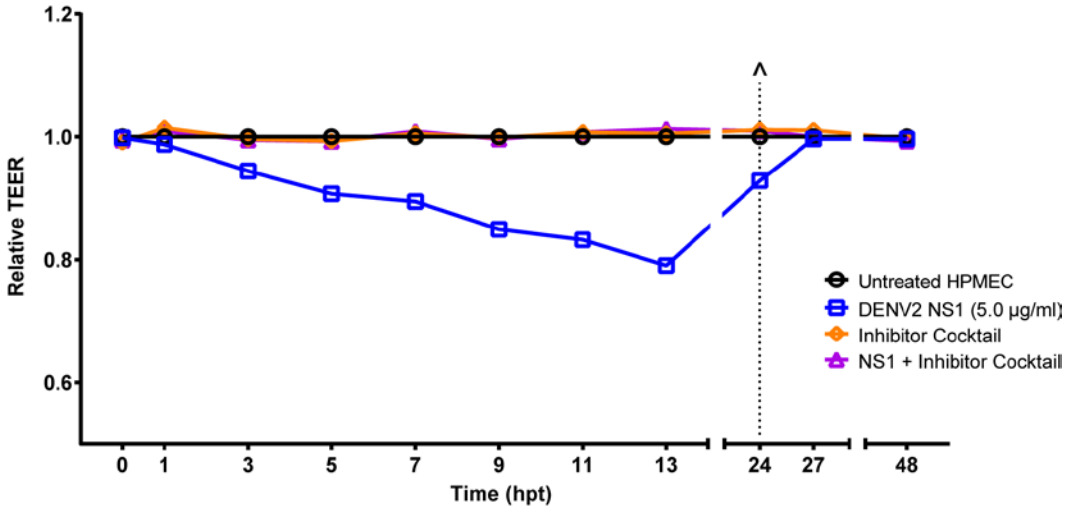

Figure 2.S3. Related to Figure 2.6. DENV2 NS1-induced endothelial hyperpermeability is blocked by an inhibitor cocktail of DANA, OGT 2115, and cathepsin L inhibitor.
Effect of an inhibitor cocktail (DANA, 50 µg/ml; OGT 2115, 1.0 µM; Cathepsin L Inhibitor, 10 µM) on DENV2 NS1-triggered endothelial hyperpermeability (TEER) in HPMEC monolayers. TEER values of monolayers treated with DENV2 NS1 plus the inhibitor cocktail are significantly different than values of monolayers treated with DENV2 NS1 alone ($P < 0.0001$) and not significant compared to untreated control monolayers. (^) represents change of medium.

Chapter 3: Dengue virus NS1 cytokine-independent vascular leak is dependent on endothelial glycocalyx components

This chapter was published in:

Glasner, D.R., Ratnasiri, K., Puerta-Guardo, H., Espinosa, D.A., Beatty, P.R., Harris, E. Dengue virus NS1 cytokine-independent vascular leak is dependent on endothelial glycocalyx components. *PLoS Pathog*. 2017 Nov 9;13(11):e1006673. doi: 10.1371/journal.ppat.1006673. eCollection 2017 Nov.

Summary

Dengue virus (DENV) is the most prevalent, medically important mosquito-borne virus. Disease ranges from uncomplicated dengue to life-threatening disease, characterized by endothelial dysfunction and vascular leakage. Previously, we demonstrated that DENV non-structural protein 1 (NS1) induces endothelial hyperpermeability in a systemic mouse model and human pulmonary endothelial cells, where NS1 disrupts the endothelial glycocalyx-like layer. NS1 also triggers release of inflammatory cytokines from PBMCs via TLR4. Here, we examined the relative contributions of inflammatory mediators and endothelial cell-intrinsic pathways. *In vivo*, we demonstrated that DENV NS1 but not the closely-related West Nile virus NS1 triggers localized vascular leak in the dorsal dermis of wild-type C57BL/6 mice. *In vitro*, we showed that human dermal endothelial cells exposed to DENV NS1 do not produce inflammatory cytokines (TNF-α, IL-6, IL-8) and that blocking these cytokines does not affect DENV NS1-induced endothelial hyperpermeability. Further, we demonstrated that DENV NS1 induces vascular leak in TLR4- or TNF-α receptor-deficient mice at similar levels to wild-type animals. Finally, we blocked DENV NS1-induced vascular leak *in vivo* using inhibitors targeting molecules involved in glycocalyx disruption. Taken together, these data indicate that DENV NS1-induced endothelial cell-intrinsic vascular leak is independent of inflammatory cytokines but dependent on endothelial glycocalyx components.

Introduction

Dengue (DENV) is a mosquito-borne flavivirus that causes up to 390 million infections, 96 million cases of dengue, and ~500,000 hospitalizations annually. Infection with any of the 4 DENV serotypes (DENV1-4) results in a spectrum of disease from inapparent infection to classic dengue fever (DF) to dengue hemorrhagic fever/dengue shock syndrome (DHF/DSS), characterized by vascular leakage and shock. The DENV positive-strand 10.7-kb RNA genome encodes a polyprotein that is cleaved into 3 structural proteins and 7 non-structural proteins. DENV non-structural protein 1 (NS1) is synthesized by infected cells as a monomer (48 kDa), glycosylated in the ER, and released into the extracellular milieu as a hexamer (~310 kDa) (41, 47, 48). Secreted DENV NS1 circulates in the blood during acute illness, and serum NS1 levels correlate with dengue disease severity, as does viral load (i.e., viremia) (69).

Under normal physiological conditions, the microvascular endothelium maintains a low permeability to fluids and molecules (34). Disruption of the endothelial barrier can result in excessive leak across the endothelium, a phenomenon known as hyperpermeability. Clinically, this manifests as vascular leakage, where fluid accumulates in tissues after extravasating from the vasculature (34, 35). Two of the primary determinants of endothelial barrier function are the endothelial glycocalyx and intercellular junctional complexes, such as tight and adherens junctions (32, 33). The glycocalyx lines the luminal surface of the endothelium, protecting the underlying endothelial cells from shear forces and contributing to hemostasis, signaling, and blood cell-endothelial cell interactions (36). Disruption of the glycocalyx has been shown to lead to vascular pathology and has been previously hypothesized to play a role in the pathogenesis of severe dengue disease (91), and modulation of the glycocalyx under inflammatory conditions is thought to contribute to various diseases (158).

DENV NS1 has been shown to play a role in viral replication (57, 60) and immune evasion (118, 120). We recently showed that DENV NS1 can directly induce endothelial hyperpermeability *in vitro* and vascular leak *in vivo* in the absence of DENV infection, as well as lethally exacerbate an otherwise sublethal DENV infection (84). We also demonstrated that DENV NS1 can disrupt the endothelial glycocalyx-like layer (EGL) *in vitro* through the activation of endothelial sialidases and the cathepsin L/heparanase pathway (88). Further, glycocalyx components, such as heparan sulfate and chondroitin sulfate, have been shown to circulate at higher levels in the sera of DENV-infected patients than healthy controls (92, 93). Others recently showed that NS1 can also act through Toll-like receptor 4 (TLR4) on mononuclear cells to induce secretion of vasoactive cytokines, and systemic inoculation of NS1 alone leads to significant increases in circulating levels of inflammatory cytokines in our mouse model (84).

In this study, we sought to evaluate the relative contributions of cytokine-driven inflammatory mechanisms and NS1-induced EGL degradation to NS1 pathogenesis of the endothelium. Using an *in vitro* model of endothelial permeability, we found that DENV NS1 triggers hyperpermeability independently of the pro-inflammatory cytokines TNF-α and IL-6. *In vivo*, we demonstrated that DENV NS1 induces localized vascular leak in the dermis of wild-type mice and that this effect is specific to DENV NS1 and independent of

TLR4 and TNF-α signaling. Finally, we showed that DENV NS1-induced endothelial dysfunction is dependent on endothelial sialidases, cathepsin L, and heparanase both *in vitro* and *in vivo*. Taken together, our results indicate that DENV NS1 acts directly on the endothelium to induce vascular leak *in vivo* that is dependent on components of the glycocalyx.

Results

DENV2 NS1 triggers localized vascular leak in the dorsal dermis of mice

In vivo, vascular permeability is often assessed by intravenous (IV) injection of small-molecule dyes, such as the albumin-binding Evans Blue dye (EBD); extravasation into tissues is then quantified by extracting dye in formamide and measuring absorbance at 620 nm. To measure the induction of vascular leak by DENV NS1 in the dermal endothelium, we removed hair from the dorsal side of wild-type C57BL/6 (B6) mice and administered a retro-orbital (RO) injection of EBD and four intradermal (ID) injections: phosphate-buffered saline (PBS) as a vehicle control, vascular endothelial growth factor (VEGF, 200 ng) as a positive control, and DENV2 NS1 (7.5 µg and 15 µg) **(Figure 3.1a).** Two hours post-injection, the dorsal dermis of the mice was removed, and equal areas of tissue were excised for EBD quantification. We found that VEGF and 15 µg of DENV2 NS1 induced vascular leak at levels significantly higher than PBS ($P \leq 0.0001$, $P = 0.0085$, respectively) **(Figure 3.1c)**. These data demonstrate that DENV2 NS1 can induce vascular leak in the dermis of wild-type B6 mice.

To improve the sensitivity of the assay, we established a novel measure of vascular leak using IV injection of dextran molecules labeled with a fluorophore (Alexa Fluor 680), which can be quantified via fluorescent scanning. Similar to the traditional Evans Blue model, hair was removed from the dorsal side of wild-type B6 mice, fluorescent dextran was delivered RO, and the same four ID injections were administered as above **(Figure 3.1b)**. Using this model, we found that VEGF and both 7.5 µg and 15 µg of DENV2 NS1 induced vascular leak at levels significantly higher than PBS ($P \leq 0.0001$, $P = 0.0230$, $P \leq 0.0001$, respectively) **(Figure 3.1d)**. However, 15 µg of NS1 from West Nile Virus (WNV), a closely related flavivirus that causes encephalitis, did not trigger vascular leak in the dermis of wild-type B6 mice **(Figure 3.1d)**. NS1 from DENV1, 3, and 4 also induced vascular leak in our dermal model **(Figure 3.S1)**. Additionally, DENV2 NS1 was shown to induce vascular leak in the dermal endothelium of mouse ears using both Evans Blue and fluorescent dextran **(Figure 3.S2)**. Therefore, these data confirm our observations using Evans Blue dye and demonstrate a more sensitive method for detecting local vascular leak *in vivo*.

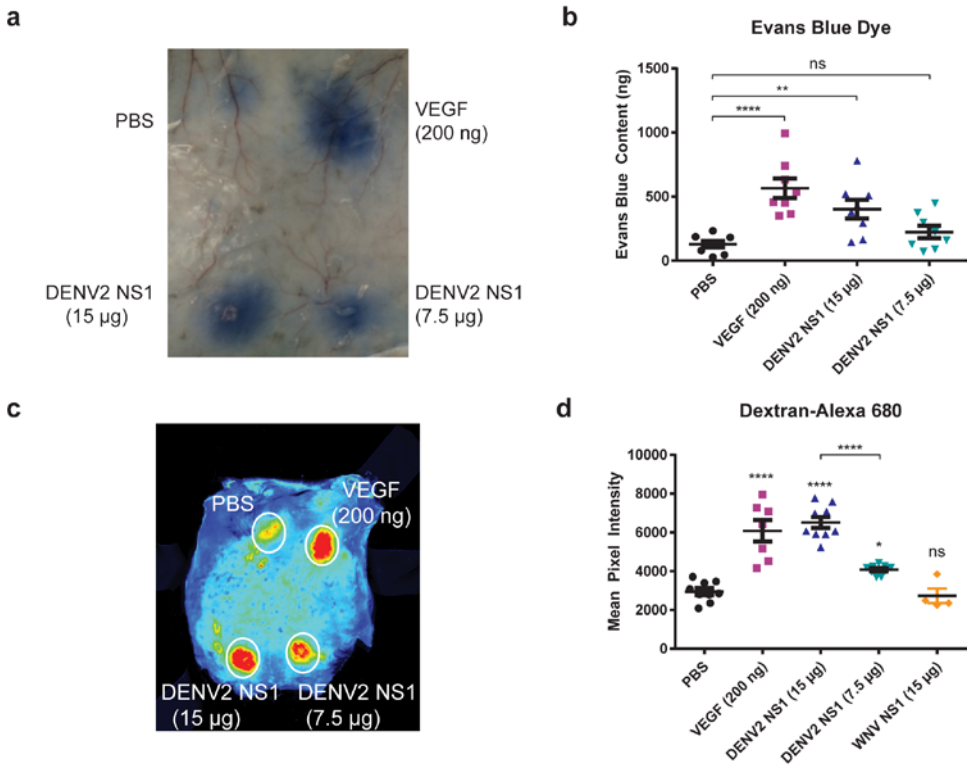

Figure 3.1. DENV2 NS1 triggers localized vascular leak in the dorsal dermis of mice.
(a-d) Hair was removed from the dorsal dermis of mice, and mice were allowed to recover for 3 days. On the day of the assay, retro-orbital injections of **(a,b)** Evans Blue dye (EBD) or **(c,d)** Alexa Fluor 680-conjugated dextran were administered, followed by intradermal injections of PBS (black circles), 200 ng VEGF (purple squares), 15 µg DENV2 NS1 (blue triangles), 7.5 µg DENV2 NS1 (green triangles), and 15 µg WNV NS1 (orange diamonds). The dermis from each mouse was collected and processed two hours post-injection. **(a)** Representative image of mouse dorsal dermis following Evans Blue assay. **(b)** EBD was extracted from tissue in formamide for 24 hours at 56˚C and quantified using a standard curve of EBD (30.5 to 500,000 ng/ml) using linear regression analysis. Data represent quantified EBD from 8 animals. **(c)** Representative image of mouse dorsal dermis following fluorescent dextran assay. **(d)** Dermises were scanned using a fluorescent detection system (LI-COR Odyssey CLx Imaging System) at a wavelength of 700 nm, and extravasated fluorescent dextran was quantified in tissue using Image Studio software (LI-COR Biosciences). Data represent the quantification of mean fluorescent intensity from mice in **(c)**: PBS (n = 9); VEGF (n = 7); DENV2 NS1 – 15 µg (n = 9); DENV2 NS1 – 7.5 µg (n = 9); WNV NS1 (n = 4). Data in **(b)** and **(d)** represent mean +/- SEM and were collected from 3 independent experiments. An ordinary one-way ANOVA with multiple comparisons to the PBS group using Dunnett's multiple comparison test was used to determine significance of VEGF, DENV2 NS1, and WNV NS1. An unpaired, parametric, two-tailed t-test was used to determine significance between 15 µg of DENV2 NS1 and 7.5 µg of DENV2 NS1. ns = not significant; *, $P < 0.05$; **, $P < 0.01$; ****, $P < 0.0001$.

Inflammatory cytokines TNF-α and IL-6 are not involved in DENV2 NS1-induced endothelial hyperpermeability *in vitro*

In addition to the direct NS1-mediated hyperpermeability we showed in endothelial cells that is due in part to disruption of the EGL (88), Modhiran et al. reported that DENV NS1 can trigger release of vasoactive cytokines from peripheral blood mononuclear cells

(PBMCs) via activation of TLR4 (85). To determine whether inflammatory cytokines are involved in DENV2 NS1-mediated endothelial hyperpermeability *in vitro*, we first determined whether human dermal endothelial cells produce specific cytokines in response to DENV2 NS1. We stimulated the human dermal microvascular endothelial cell line HMEC-1 with 5 µg/ml and 10 µg/ml of DENV2 NS1 and collected supernatant at 0, 1, 3, 6, 12, and 24 hours post-treatment. Untreated HMEC-1 were used as a steady-state control, and HMEC-1 treated with 10 ng/ml or 100 ng/ml of lipopolysaccharide (LPS) were used as a positive control. We found that HMEC-1 did not produce IL-6 in response to DENV2 NS1 but did in response to both concentrations of LPS in a dose-dependent manner **(Figure 3.2a)**. HMEC-1 did not produce detectable levels of TNF-α in response to either DENV2 NS1 or LPS **(Figure 3.2b)**; LPS only stimulates production of TNF-α from endothelial cells in the presence of a secondary inflammatory signal (189). Additionally, IL-8, a chemokine known to play a role in the inflammatory response, was only produced in response to LPS and not DENV2 NS1 in HMEC-1 (**Figure 3.2c)**. Similar results for IL-6, TNF-α, and IL-8 were obtained when human pulmonary microvascular endothelial cells (HPMEC) were studied **(Figure 3.S3)**. This suggests that endothelial cells do not produce inflammatory cytokines in response to DENV2 NS1 *in vitro*.

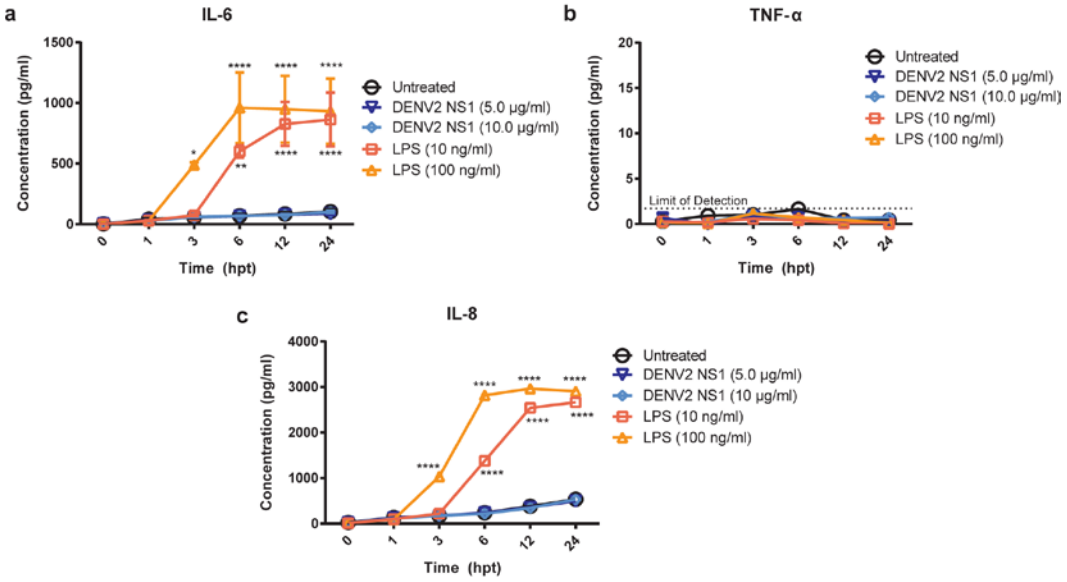

Figure 3.2. HMEC-1 do not produce the inflammatory cytokines IL-6, TNF-α, or IL-8 in response to DENV2 NS1 stimulation *in vitro*.
(a-c) HMEC-1 were stimulated with LPS (10 or 100 ng/ml; red squares and orange triangles, respectively) or DENV2 NS1 (5 or 10 µg/ml; dark blue triangles and light blue diamonds, respectively), and supernatant was collected at 0, 1, 3, 6, 12, and 24 hours post-treatment. Untreated HMEC-1 monolayers were used as a control (black circles). ELISAs for **(a)** IL-6, **(b)** TNF-α, and **(c)** IL-8 were performed on all samples. All data shown represent the mean +/- SEM and were collected from two independent experiments. A repeated measure two-way ANOVA with multiple comparisons to the untreated group using Dunnett's multiple comparison test was used to determine significance of treatment with LPS (10 and 100 ng/ml) or DENV2 NS1 (5 and 10 µg/ml). *, $P < 0.05$; **, $P < 0.01$; ****, $P < 0.0001$.

To further confirm that IL-6 and TNF-α are not involved in DENV2 NS1-induced endothelial cell-intrinsic mechanisms of endothelial hyperpermeability, we used a Transwell model that measures transendothelial electrical resistance (TEER) to evaluate the effect of anti-cytokine monoclonal antibodies (mAbs) on DENV2 NS1-induced endothelial hyperpermeability in HMEC-1 monolayers. We found that both recombinant human IL-6 and TNF-α significantly induced endothelial hyperpermeability ($P \leq 0.0001$) and that addition of anti-IL-6 and anti-TNF-α mAbs blocked this effect ($P \leq 0.0001$); however, anti-IL-6 and anti-TNF-α mAbs did not affect DENV2 NS1-induced endothelial hyperpermeability ($P = 0.1845$, $P = 0.1879$, respectively) **(Figure 3.3a,b)**. Similar results were obtained when evaluating HPMEC as well **(Figure 3.S4)**. Taken together, these results suggest that IL-6 and TNF-α are not involved in the direct action of DENV2 NS1 on the human endothelium *in vitro*.

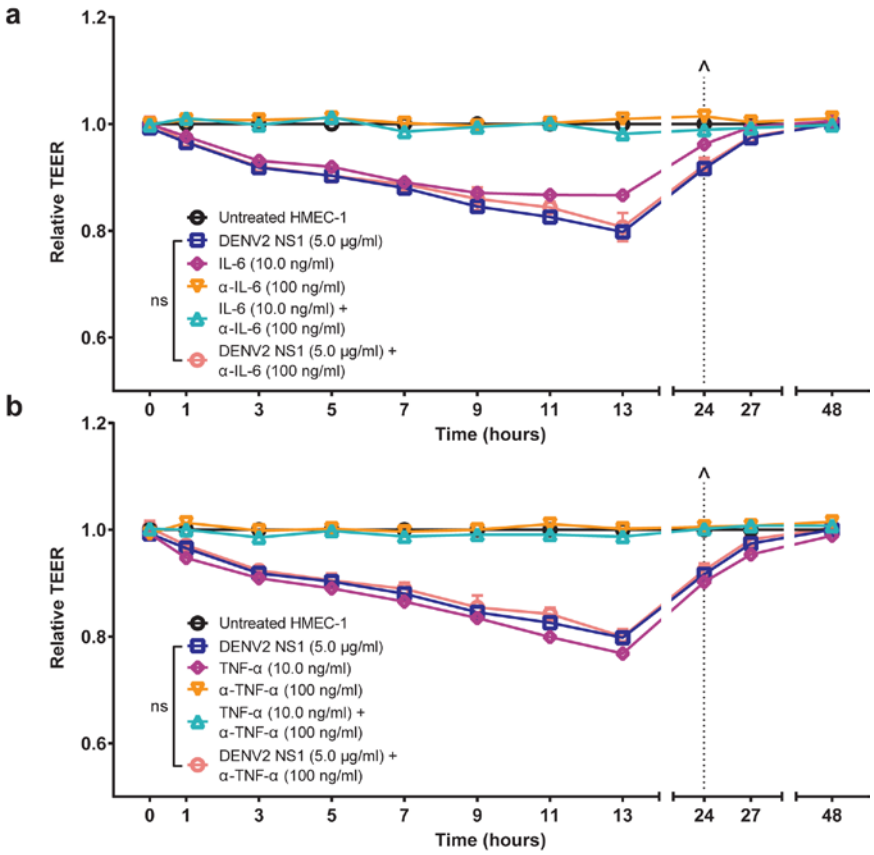

Figure 3.3. Inflammatory cytokines TNF-α and IL-6 are not involved in DENV2 NS1-induced endothelial hyperpermeability *in vitro*.
(a,b) Transendothelial electrical resistance (TEER) of HMEC-1 monolayers incubated with 5 µg/ml DENV2 NS1 (blue squares), 10 ng/ml recombinant cytokine (**(a)** IL-6, **(b)** TNF-α; purple diamonds), 100 ng/ml anti-cytokine mAbs (**(a)** IL-6, **(b)** TNF-α; orange triangles), recombinant cytokine + specific mAb (**(a)** IL-6, **(b)** TNF-α; green diamonds), or DENV2 NS1 + specific mAb (**(a)** IL-6, **(b)** TNF-α; red circles). The background signal was subtracted (using TEER values from a blank Transwell), and data were normalized to untreated HMEC-1. (^) represents change of medium. All data shown represent the mean +/- SEM and were collected from two independent experiments. Data represent two replicate Transwells

per condition. A repeated measure two-way ANOVA was used to determine the significance of anti-cytokine mAbs on DENV2 NS1-induced hyperpermeability in HMEC-1. ns = not significant.

DENV2 NS1-induced vascular leak is independent of TLR4 and TNF-α signaling *in vivo*.

To follow up on our *in vitro* results and to assess the role of TLR4 *in vivo*, we used our murine fluorescent dextran model of dermal vascular leak to evaluate the contributions of TLR4 and TNF-α signaling to DENV2 NS1-induced vascular leak. In both TLR4- and TNF-α receptor (TNF-αR)-deficient B6 mice, we found that both 7.5 µg and 15 µg of DENV2 NS1 triggered vascular leak at similar levels as observed in wild-type B6 mice, though knockout mice demonstrated slightly higher levels of leak than wild-type mice across all conditions **(Figure 3.4a,b)**. To further investigate the role of TLR4 in DENV NS1 pathogenesis, we utilized a model of systemic vascular leak in wild-type and TLR4-deficient B6 mice. Briefly, mice were injected IV with 10 mg/kg of DENV2 NS1 or 10 mg/kg of ovalbumin as a protein control. Three days post-injection, EBD was administered RO and allowed to circulate for 3 hours. Mice were then euthanized, and tissues were harvested for EBD extraction. We found that similar amounts of EBD extravasated into the lungs and liver of TLR4-deficient mice and wild-type B6 mice, though the levels were slightly lower in *Tlr4*$^{-/-}$ mice, suggesting comparable levels of NS1-induced vascular leak **(Figure 3.S5)**. Further, when mice deficient in both TLR4 and interferon-α/β receptor (IFNAR) were infected with DENV2, no significant differences were observed in either morbidity or mortality when compared with IFNAR-deficient B6 mice, though a slight delay in both morbidity and mortality were observed in doubly deficient mice **(Figure 3.S6)**. These data indicate that TLR4 and TNF-α are not substantially involved in the endothelial cell-specific mechanism of DENV2 NS1-induced vascular leak *in vivo*.

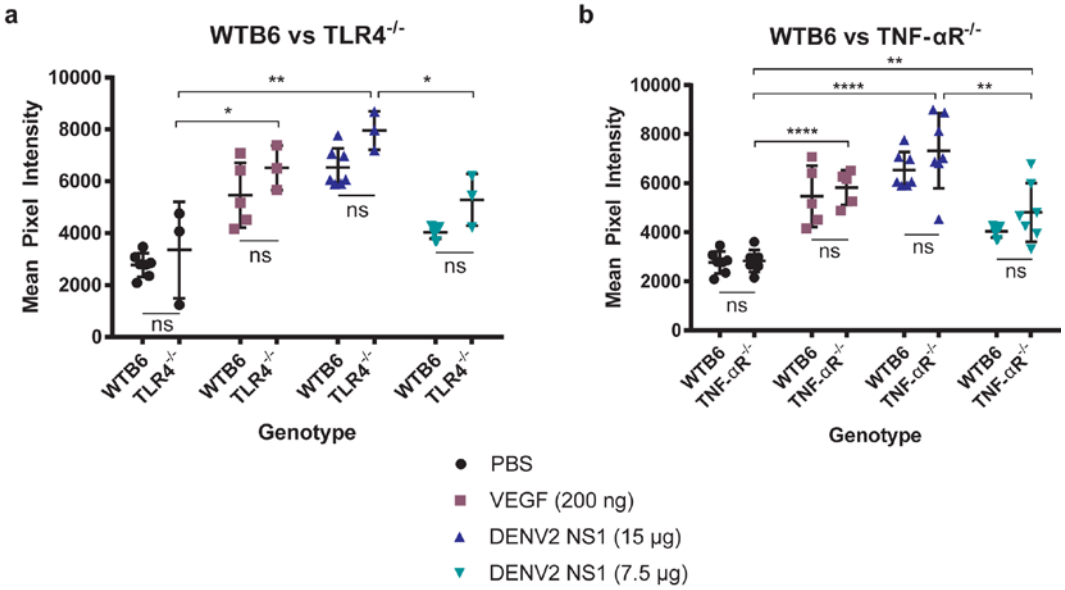

Figure 3.4. DENV2 NS1-induced vascular leak is independent of TLR4 and TNF-α signaling *in vivo*. **(a,b)** Hair was removed from the dorsal dermis of **(a,b)** wild-type (n = 7), **(a)** *Tlr4*$^{-/-}$ (n = 3) and **(b)** *TNF-αR*$^{-/-}$ (n = 7) B6 mice, and mice were allowed to recover for 3 days. On the day of the assay, retro-orbital injections of Alexa Fluor 680-conjugated dextran were administered, followed by intradermal injections of PBS (black circles), 200 ng VEGF (purple squares), 15 µg DENV2 NS1 (blue triangles), and 7.5 µg DENV2 NS1 (green triangles). The dermis from each mouse was collected and processed two hours post-injection. Data represent quantification of mean fluorescent intensity from the dermis +/- SEM and were collected from 2-3 independent experiments. The same wild-type B6 mice are used for comparison in both **(a)** and **(b)**. An ordinary one-way ANOVA with multiple comparisons to the PBS group using Dunnett's multiple comparison test was used to determine significance of VEGF and DENV2 NS1. An unpaired, parametric, two-tailed t-test was used to determine significance between wild-type and knockout mice for each treatment group. ns = not significant; *, P < 0.05; **, P < 0.01; ****, P < 0.0001.

Inhibition of sialidases, cathepsin L, and heparanase prevents DENV2 NS1-induced vascular leak

We previously demonstrated that the EGL is an important determinant of endothelial dysfunction triggered by DENV2 NS1 in HPMEC. Specifically, human sialidases, cathepsin L, and heparanase were implicated as enzymes responsible for degrading the EGL and whose expression and activation were triggered by DENV NS1. Further, we showed that sialic acid was degraded and cathepsin L activity was increased following DENV2 NS1 treatment of HMEC-1 (88). Here, we utilized the TEER system to evaluate the effect of specific inhibitors that target sialidase (Zanamivir), cathepsin L (Cathepsin L Inhibitor), and heparanase (OGT 2115), on DENV2 NS1-induced endothelial hyperpermeability of HMEC-1 *in vitro*. We found that all three inhibitors partially abrogated the increased permeability observed following treatment with DENV2 NS1 ($P \leq 0.0001$) (**Figure 3.5a-c**). Further, a cocktail of all three inhibitors completely eliminated hyperpermeability *in vitro* ($P \leq 0.0001$) (**Figure 3.5d**), reflecting our previous work with HPMEC (88). These findings demonstrate that endothelial cell-intrinsic enzymes contribute importantly to DENV2 NS1-induced endothelial hyperpermeability *in vitro*.

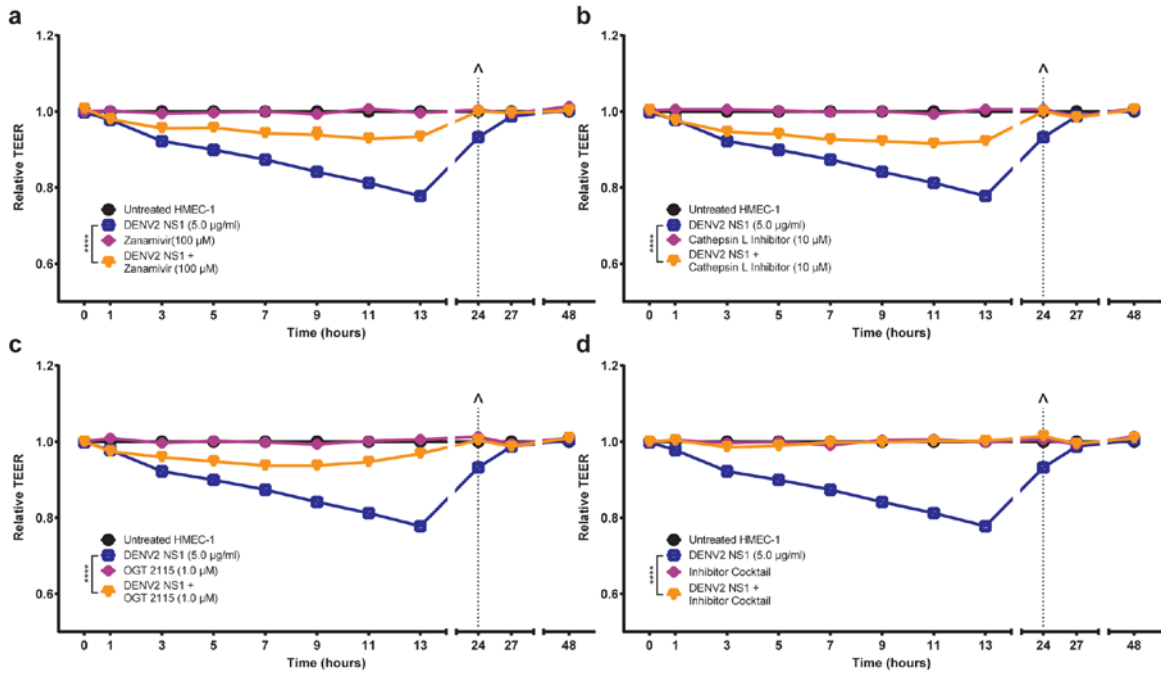

Figure 3.5. Inhibition of sialidases, cathepsin L, and heparanase prevents DENV2 NS1-induced endothelial hyperpermeability *in vitro*.
(a-d) Transendothelial electrical resistance (TEER) of HMEC-1 monolayers incubated with 5 µg/ml DENV2 NS1 (blue squares), specific inhibitor alone (**(a)** Zanamivir, 100 µM, **(b)** Cathepsin L inhibitor, 10 µM, **(c)** OGT 2115, 1.0 µM, **(d)** inhibitor cocktail; purple diamonds), or DENV2 NS1 + specific inhibitors (**(a)** Zanamivir, 100 µM, **(b)** Cathepsin L inhibitor, 10 µM, **(c)** OGT 2115, 1.0 µM, **(d)** inhibitor cocktail; orange triangles). The background signal was subtracted (using TEER values from a blank Transwell), and data were normalized to untreated HMEC-1. (^) represents change of medium. All data shown represent the mean +/- SEM and were collected from two independent experiments with two replicate Transwells per condition. A repeated measure two-way ANOVA was used to determine the significance of anti-cytokine mAbs on DENV2 NS1-induced hyperpermeability in HMEC-1. ****, $P < 0.0001$.

Additionally, we performed confocal microscopy on HMEC-1 monolayers to assess the presence of glycocalyx components, including sialic acid, chondroitin sulfate, heparan sulfate, and hyaluronic acid, and found that all components were expressed at high levels on the surface of HMEC-1 **(Figure 3.S7)**. Further, we found that DENV2 NS1 induced the degradation of sialic acid, the upregulation of cathepsin L activity, and the shedding of heparan sulfate in HMEC-1 at 6 hours post-treatment, and these effects could be prevented through the use of the previously-mentioned inhibitor cocktail **(Figure 3.6)**. These data provide additional support that HMEC-1 express an EGL composed of known glycocalyx components.

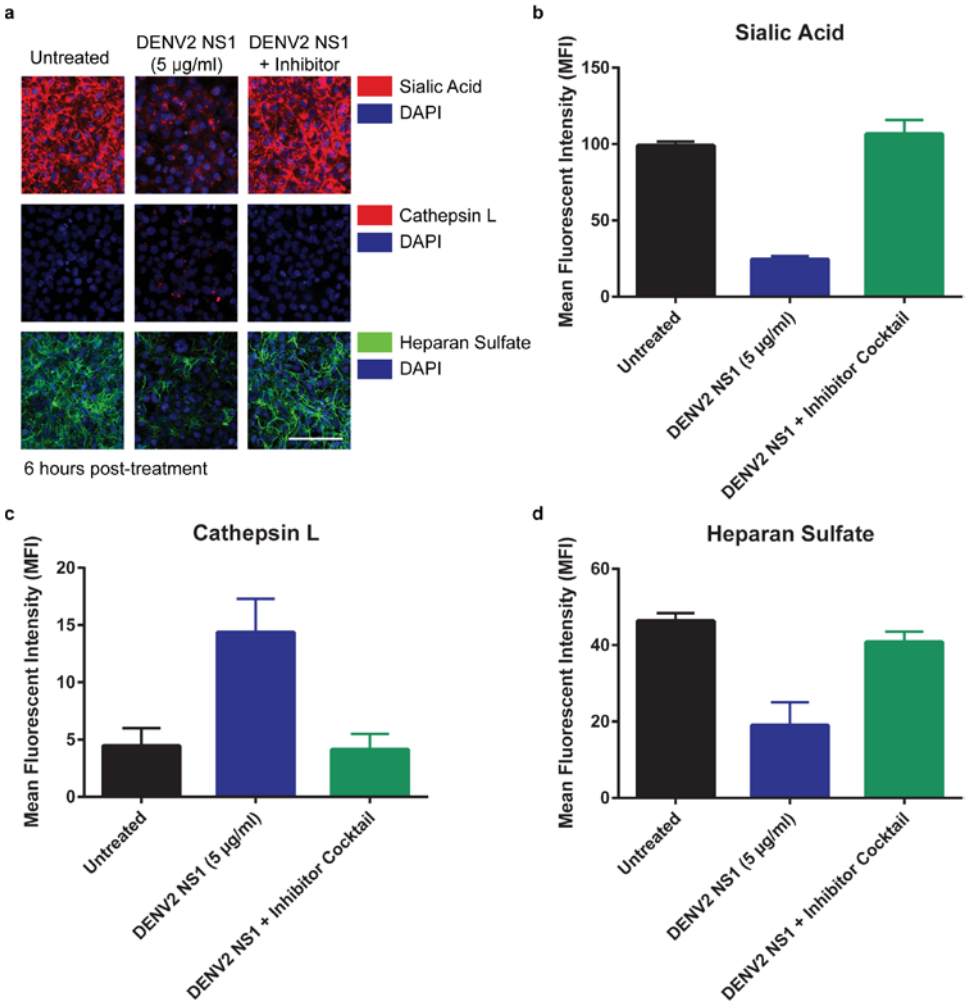

Figure 3.6. DENV2 NS1 induces degradation of sialic acid, activation of cathepsin L, and shedding of heparan sulfate in HMEC-1 *in vitro*.
(a-d) HMEC-1 monolayers treated with 5 µg/ml of DENV2 NS1 (middle column) or 5 µg/ml of DENV2 NS1 and an inhibitor cocktail (Zanamivir, 100 µM; Cathepsin L Inhibitor, 10 µM; OGT 2115, 1.0 µM; right column). Untreated monolayers were used as a control (left column). Six hours post-treatment, cells were stained for **(b)** sialic acid (WGA-A647, red; top row images), **(c)** cathepsin L activity (Magic Red Cathepsin L detection kit, red; middle row images), or **(d)** heparan sulfate (Heparan Sulfate mAb clone F58-10E4, green; bottom row images) and imaged on a Zeiss LSM 710 Axio Observer inverted fluorescence microscope equipped with a 34-channel spectral detector at 20x magnification. **(a)** Images were acquired using the Zen 2010 software (Zeiss). Nuclei were stained with Hoechst (blue). Images shown at 20X; scale bar, 10 µm. Representative images shown. **(b-d)** Quantification of MFI in **Figure 3.6a**.

Next, we sought to determine the relative contribution of glycocalyx components to vascular leak *in vivo*. Wild-type B6 mice were administered an intraperitoneal (IP) dose of a cocktail containing the same sialidase, cathepsin L, and heparanase inhibitors used *in vitro* 6 hours before and immediately preceding ID injections of DENV2 NS1. Experiments were then performed as previously detailed. A separate group of mice was

administered a combination of DMSO, PBS, and water as a vehicle control. We found that mice receiving the inhibitor cocktail as opposed to the vehicle control demonstrated a significantly lower fold-change in vascular leak as compared to PBS when exposed to 15 µg of DENV2 NS1 (inhibitor cocktail: 0.917; vehicle control: 2.08; P = 0.0038), and the data trended towards a decrease in fold-change when exposed to 7.5 µg of NS1 (inhibitor cocktail: 0.848; vehicle control: 1.12) (**Figure 3.7**). VEGF-induced vascular leak was also decreased with the inhibitor cocktail but not as strongly as DENV2 NS1 (inhibitor cocktail: 1.57; vehicle control: 2.20; P = 0.0156). Taken together, these data demonstrate that endothelial sialidases, cathepsin L, and heparanase strongly contribute to the local vascular leak induced by DENV2 NS1 in the dermis of wild-type B6 mice.

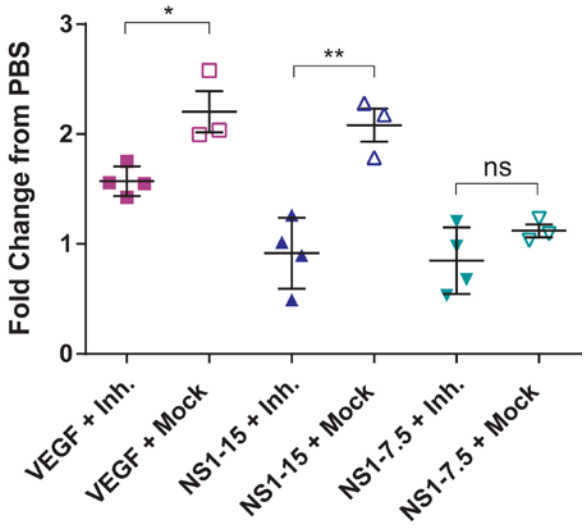

Figure 3.7. Inhibition of sialidases, cathepsin L, and heparanase prevents DENV2 NS1-induced vascular leak *in vivo*.
Hair was removed from the dorsal dermis of wild-type B6 mice, and mice were allowed to recover for 3 days. On the day of the assay, mice received an intraperitoneal dose of inhibitor cocktail (Zanamivir, Cathepsin L Inhibitor, and OGT 2115; 1 mg/ml of each inhibitor) 6 hours pre-assay and then immediately preceding the start of the assay (n = 4; closed symbols). Control mice received injections of DMSO, PBS, and water as a vehicle control (n = 3; open symbols). Retro-orbital injections of Alexa Fluor 680-conjugated dextran were then administered, followed by intradermal injections of PBS (black circles), 200 ng VEGF (purple squares), 15 µg DENV2 NS1 (blue triangles), and 7.5 µg DENV2 NS1 (green triangles). The dermis from each mouse was collected and processed two hours post-injection. Data represent the fold change of mean fluorescent intensity from VEGF and DENV2 NS1 injections to PBS injections. Data represent mean +/- SEM and were collected from 2 independent experiments. Unpaired, parametric, two-tailed t-tests were used to determine significance between inhibitor-treated and mock-treated groups. ns = not significant; *, P < 0.05; **, P < 0.01.

Discussion

In this study, we demonstrate that DENV2 NS1 can directly trigger vascular leak in the dermis of wild-type B6 mice in the absence of viral infection and that this effect is specific to DENV2 NS1 and was not observed with WNV NS1. *In vivo*, TLR4 and TNF-α did not contribute to NS1-induced vascular leak in our dermal model, which reflects endothelial cell-intrinsic NS1-triggered leak. Consistent with this observation, human dermal endothelial cells did not produce TNF-α or IL-6 in response to DENV2 NS1 stimulation *in vitro*, nor was NS1-induced endothelial hyperpermeability mediated by these cytokines. Finally, we show that inhibition of endothelial sialidases, cathepsin L, and heparanase is sufficient to prevent vascular leak induction by DENV2 NS1 both *in vitro* and *in vivo*.

Endothelial glycocalyx components have not previously been experimentally shown to play a role in dengue pathogenesis *in vivo*. Here, we showed that disruption of glycocalyx components is responsible for the induction of vascular leak observed in the murine dermis by DENV2 NS1. We were able to protect mice from local vascular leak using a combination of Zanamivir, Cathepsin L Inhibitor, and OGT 2115, demonstrating that the activity of endothelial sialidases, cathepsin L, and heparanase mediate the disruption of endothelial barrier function by DENV2 NS1 *in vivo*. These enzymes contribute to glycocalyx disruption via degradation of sialic acid and trimming of heparan sulfate proteoglycans. Using our *in vitro* HMEC-1 model of endothelial permeability, we demonstrated that inhibition of each enzyme alone partially abrogated NS1-induced hyperpermeability, while the combination of all three inhibitors completely protected endothelial monolayers. Our results are consistent with previous findings that demonstrated that NS1 induces endothelial hyperpermeability by increasing expression of sialidases, cathepsin L, and heparanase in human pulmonary endothelial cells *in vitro* (88). These results suggest potential targets for novel therapeutics that inhibit enzymes that contribute to degradation of glycocalyx components for the treatment of severe dengue disease.

It has previously been shown that TLR4 is an important mediator of DENV NS1 pathogenesis, as NS1 activation of TLR4 on PBMCs leads to production of IL-6 and IL-8, cytokines that have been shown to contribute to endothelial barrier dysfunction (85). Therefore, we evaluated the effect of DENV2 NS1 on local and systemic vascular leak in TLR4-deficient B6 mice and found no significant differences in the levels of EBD and dextran extravasation in TLR4-deficient and wild-type mice following NS1 inoculation, suggesting that NS1 induces acute vascular leak that is not dependent on TLR4. In addition, infection of mice doubly deficient in TLR4 and IFNAR with a lethal dose of DENV2 did not result in significant differences in morbidity or mortality compared to IFNAR-deficient mice. However, slight differences were observed between wild-type and TLR4-deficient mice in all assays. In our model of localized vascular leak, levels of leak were marginally higher in *Tlr4*$^{-/-}$ mice, whereas levels were slightly lower in our systemic vascular leak model. In our DENV infection model, morbidity and mortality were both somewhat delayed in *Ifnar*$^{-/-}$ *x Tlr4*$^{-/-}$ B6 mice, though mice succumbed to infection at the same rates. Modhiran et al. found that LPS-RS, a potent antagonist of TLR4, and an anti-TLR4 antibody both protected HMEC-1 monolayers from DENV2 NS1-induced endothelial hyperpermeability as measured by TEER (85). These observations suggest

that TLR4 does play a contributing role to NS1-induced vascular leak, but because substantial vascular leak, morbidity, and mortality are still observed in the absence of TLR4, we conclude there are additional, more critical drivers of NS1 pathogenesis.

Previously, we demonstrated that systemic administration of DENV2 NS1 resulted in significantly elevated levels of IL-6 and TNF-α 72 hours post-injection (84). We sought to evaluate whether endothelial cells produce these inflammatory cytokines in response to DENV2 NS1 in the absence of PBMCs. We demonstrated that HMEC-1 did not produce IL-6, TNF-α, or IL-8 in response to DENV2 NS1, although HMEC-1 produced high levels of IL-6 and IL-8 in response to the positive control, the TLR4 ligand LPS. Further, to evaluate the role of these cytokines in our HMEC-1 model of endothelial permeability, we measured TEER in the presence of both DENV2 NS1 and IL-6- and TNF-α-specific mAbs. We demonstrated that DENV2 NS1-induced endothelial hyperpermeability is independent of both IL-6 and TNF-α, although HMEC-1 can respond to both cytokines, an effect that is prevented with blocking antibodies. We then sought to determine the contribution of TNF-α to NS1-induced vascular leak *in vivo*. Using TNF-αR-deficient B6 mice, we found that DENV2 NS1 triggered similar levels of vascular leak in both knockout and wild-type mice. These results suggest that NS1 stimulation of endothelial cells does not result in the production of pro-inflammatory cytokines and that any directly pathogenic effects of NS1 on the endothelium occur independently of key endothelial cell-produced cytokines, further emphasizing the role of endothelial cell-specific mechanisms such as glycocalyx component disruption and mislocalization of intercellular junction proteins.

In humans, severe symptoms of vascular leak appear several days after the peak of NS1 antigenemia in blood has passed, suggesting a requirement for prolonged exposure to NS1 to cause severe leak and presumably reflecting the cumulative effects and accumulation of NS1 in target tissues. Our previous mouse model data, also requiring three days of exposure to NS1 delivered systemically before morbidity and mortality were observed (84), suggest that the induction of systemic vascular leak caused by NS1 is cumulative over time *in vivo*. The NS1 dose that we used here in our *in vivo* model of localized vascular leak was meant to reflect the cumulative effect of NS1 in tissues, allowing us to simulate the effects of NS1 on the endothelium in a shorter time span. Overall, the endothelial-intrinsic mechanisms we observe following NS1 inoculation in the dermis may be working in conjunction with NS1 activation of TLR4 on the surface of PBMCs and release of inflammatory cytokines to contribute to systemic vascular leak observed in both our previous findings and clinical manifestations of DHF and DSS.

Clinically, DHF and DSS are both characterized by vascular leak and endothelial dysfunction in multiple organs. The lungs are particularly affected, with pulmonary edema representing a common complication in severe dengue disease. We have previously published a study identifying the EGL as a required determinant of endothelial barrier function in human pulmonary microvascular endothelial cells *in vitro* (88), and our *in vitro* results here further support that DENV2 NS1 triggers endothelial hyperpermeability in HPMEC in a cytokine-independent manner in the absence of virus and non-endothelial cell types. Further, petechiae are an additional sign of capillary fragility and leak in dengue disease in humans, and previous reports have shown that DENV is absent at the site of rash and petechiae in dengue fever patients (190), though DENV antigens have been

found in skin biopsies (191). Here, we demonstrated the ability of DENV2 NS1 to trigger localized vascular leak in the absence of virus in the mouse dermis, suggesting a potential link between DENV NS1 and formation of petechiae. Combined with our results in HPMEC, our findings suggest that NS1 may be an important contributor to vascular leak in various tissue sites during DENV disease.

The glycocalyx has been previously implicated in plasma leakage in DENV-infected patients. Nguyen-Pouplin et al. performed dextran fractional clearance studies in a group of Vietnamese dengue patients with evidence of vascular leak and in healthy controls and found that there was no difference in dextran clearance between infected and healthy patients, seemingly contradictory results. However, their data suggest that the dextran administered for the study may have helped stabilize the glycocalyx following loss of plasma proteins during DENV infection, thereby restoring glycocalyx integrity and normal endothelial barrier function (91). More recent studies have evaluated different glycocalyx components in patient sera during acute DENV infection and found that serum levels of hyaluronic acid, heparan sulfate, chondroitin sulfate, and syndecan-1 are all elevated, suggesting disruption of the endothelial glycocalyx by DENV infection (92, 93).

Ascertainment that disruption of the endothelial glycocalyx is mediated by DENV NS1 entails direct visualization of the glycocalyx layer *in vivo*. As the glycocalyx is a delicate and complex structure, this direct visualization requires challenging techniques, such as intravital microscopy, two-photon microscopy, and electron microscopy, which have previously been used to image the glycocalyx in live mice and in fixed murine tissues (151, 192-194). Further, though cultured endothelial cells express key components of the glycocalyx on their surface, they do not necessarily express a true glycocalyx structure *in vitro*. Thus, drawing definitive conclusions regarding the glycocalyx and its role in dengue disease is difficult; however, we believe our results support a critical role for glycocalyx components and thus implicitly for the glycocalyx in vascular leak, though further validation *in vivo* is necessary.

As we have previously speculated, we believe that DENV NS1 induces endothelial hyperpermeability following its internalization by endothelial cells (88). After NS1 binds to an as-yet unidentified receptor, internalization may then facilitate NS1 interaction with cathepsin L (which can then cleave heparanase into an active form) and the endothelial sialidase Neu1, both of which are localized in lysosomal compartments (164, 195). It is also possible that binding and downstream signaling triggers activation of these enzymes, specifically Neu3, which is localized to the plasma membrane (196). Preliminary data from our laboratory suggests that inhibition of endocytic pathways in endothelial cells may protect monolayers *in vitro* from DENV NS1-induced hyperpermeability. Further research is required to fully elucidate the mechanisms driving DENV NS1-related pathogenesis.

Finally, our model improves upon the existing Miles assay that uses Evans Blue dye as a tracer for vascular leak. By using dextran conjugated to Alexa Fluor 680, we were able to observe greater differences between groups in our model, as well as decreased variability as compared to using EBD. Additionally, we are able to evaluate positive and negative controls alongside experimental conditions in the same animal. These factors serve to decrease the total number of mice required to achieve statistical significance of

our data, saving on costs and contributing to the overall goal of limiting animal numbers used in experiments. Additionally, this method does not require excision of individual spots or extraction of dye but allows for direct imaging of the skin on a fluorescent scanner, thereby decreasing the time spent processing each animal and allowing for faster development and analysis of results. Compared to our systemic models of vascular leak (84), the modified Miles assay facilitates the evaluation of the direct and immediate effects of NS1 on the vascular endothelium, as ID injections deliver the protein to a localized spot. Additionally, this allows for usage of substantially lower quantities of NS1 protein. It is, however, possible that compounds delivered intradermally may interact with resident dermal immune cells or the abluminal surface of the endothelium following inoculation. Thus, results obtained in the intradermal assay should be validated using intravenous delivery of NS1 in a systemic model of leak, as we have done here.

Taken together, these results contribute to the growing body of literature demonstrating a critical role for NS1 in dengue pathogenesis, specifically in its contributions to directly pathogenic effects on the vascular endothelium. We show that DENV2 NS1-induced endothelial barrier dysfunction is not related to inflammatory cytokines in a mouse model of dermal vascular leak or in endothelial cells *in vitro* but that instead, specific endothelial enzymes that degrade components of the endothelial glycocalyx layer are required. Overall, these findings further illustrate the role of NS1 in the pathogenesis of severe dengue disease and highlight the importance of the endothelial glycocalyx in vascular leak, suggesting targets for novel therapeutics in the treatment of DHF and DSS.

Experimental Procedures

Ethics Statement. All *in vivo* experiments were performed strictly following the guidelines of the American Veterinary Medical Association and the Guide for the Care and Use of Laboratory Animals from the National Institutes of Health and were approved by the University of California (UC) Berkeley Animal Care and Use Committee (protocol AUP-2014-08-6638).

Mice. Six-to-eight-week-old wild-type C57BL/6 (B6) mice were obtained from the Jackson Laboratory. *Tlr4*$^{-/-}$ and *TNF-αR*$^{-/-}$ B6 mice were originally obtained from Dr. Greg Barton (UC Berkeley) and the Jackson Laboratory, respectively. *Ifnar*$^{-/-}$ B6 were originally obtained from the Jackson Laboratory. *Tlr4*$^{-/-}$ *x Ifnar*$^{-/-}$ B6 mice were generated at UC Berkeley by backcrossing *Tlr4*$^{-/-}$ onto an *Ifnar*$^{-/-}$ B6 background 10 times. All mice were bred and maintained in specific pathogen-free conditions at the animal facility at UC Berkeley. A mix of male and female six-to-eight-week-old mice were used in all experiments. Trained and certified laboratory personnel performed anesthesia of mice via isoflurane inhalation and euthanasia of mice using exposure to isoflurane followed by cervical dislocation.

Cell culture and viruses. The human dermal microvascular endothelial cell line HMEC-1 was kindly donated by Dr. Matthew Welch (UC Berkeley) and propagated (passages 18-25) and maintained at 37˚C in humidified air with 5% CO_2 in MCDB 131 medium (Sigma) supplemented with 1% penicillin/streptomycin (Life Technologies), 0.2% Epidermal Growth Factor (Life Technologies), 0.4% hydrocortisone (Sigma), and 5% Fetal Bovine Serum (Corning). The human pulmonary microvascular endothelial cell line HPMEC-ST1.6r (HPMEC) was kindly donated by Dr. J.C. Kirkpatrick (Institute of Pathology, Johannes Gutenberg University, Germany) and grown as previously described (88). DENV2 D220 was generated in our laboratory from the parental strain DENV2 PL046 (197). Virus was propagated in the *Aedes albopictus* C6/36 cell line (American Type Culture Collection; ATCC) and titered by plaque assay on baby hamster kidney cells (BHK21, clone 15).

Recombinant NS1 proteins. Recombinant DENV1 (Nauru/Western Pacific/1974), DENV2 (Thailand/16681/84), DENV3 (Sri Lanka D3/H/IMTSSA-SRI/2000/1266), DENV4 (Dominica/814669/1981), and WNV (NY99) NS1 proteins, greater than 95% purity and certified to be free of endotoxin contaminants, were produced by the Native Antigen Company (Oxfordshire, United Kingdom) in HEK293 cells at their facility and used in all experiments. NS1 preparations were also tested using the Endpoint Chromogenic Limulus Amebocyte Lysate (LAL) QCL-1000TM kit (Lonza) and confirmed to be free of bacterial endotoxins (88).

Recombinant proteins, monoclonal antibodies, and inhibitors. For staining of EGL components, the following monoclonal antibodies and lectins were used: Wheat germ agglutinin (WGA) lectin conjugated to Alexa Fluor 647 (WGA-A647, Molecular Probes) to stain N-acetyl neuraminic acid (sialic acid); Ab Heparan Sulfate, purified (clone F58-10E4, Amsbio); anti-Chondroitin Sulfate antibody (CS-56, Abcam); anti-Hyaluronic acid antibody (Abcam). Goat anti-mouse IgG conjugated to Alexa Fluor 647 (Abcam), donkey

anti-mouse IgM conjugated to Alexa Fluor 488 (Jackson), and donkey anti-sheep IgG conjugated to Alexa Fluor 568 (Abcam) were used as secondary detection antibodies in confocal microscopy experiments. Vascular endothelial growth factor (VEGF; Sigma) was used as a positive control in *in vivo* dermal Miles assay experiments. Ovalbumin (Life Technologies) was used as a negative control in *in vivo* systemic Miles assay experiments. Anti-Flavivirus group antigen against the DENV envelope (E) protein (4G2, clone number D1-4G2-4-15; Absolute Antibody) was used in antibody-dependent enhancement (ADE) infections *in vivo*. Recombinant human TNF-α and recombinant human IL-6 (eBiosciences) were used in transendothelial electrical resistance (TEER) assays. Anti-human TNF-α and anti-human IL-6 mAbs (eBiosciences; clones MAb1 and MQ2-13A5, respectively) were used in anti-cytokine and anti-NS1 TEER experiments. Selective inhibitors of sialidases (Zanamivir, Sigma), heparanase (OGT 2115, Tocris), and cathepsin L (Cathepsin L Inhibitor, Santa Cruz Biotechnology) were used in TEER assays and in mouse experiments at concentrations that do not affect cell viability, animal welfare, or vascular leakage. Cell viability was determined using the Promega CellTox Green Cytotoxicity Assay following the manufacturer's instructions.

Evans Blue dermal Miles assay. The effect of recombinant DENV2 NS1 protein on localized vascular leak *in vivo* was evaluated using the Miles assay adapted for mouse skin as previously described (198). Wild-type B6 mice were shaved 3-4 days prior to each experiment using Wahl Show Pro Plus clippers, and hair was further removed using Nair (Church & Dwight) and 70% ethanol. On the day of the assay, mice were anesthetized with isoflurane and injected RO with EBD (0.5% in PBS, 150 µl; Sigma). After 10 minutes, PBS (50 µl), VEGF (200 ng in 50 µl PBS), and DENV2 NS1 (15 µg or 7.5 µg in 50 µl PBS) were injected ID into distinct sites on the shaved dorsal skin of mice. Two hours post-injection, mice were euthanized using isoflurane, and the dorsal dermis was removed. A 13 mm diameter circular punch was used to mark the biopsy site surrounding the locations of Evans Blue leakage, and sites were removed using a surgical scalpel and placed in formamide for 24 hours at 56^{o}C. The absorbance of the extravasated dye was measured at 620 nm using a spectrophotometer. EBD concentration was calculated using a standard curve (30.5 to 500,000 ng/ml) using linear regression analysis. Representative images were obtained using an iPhone 5S (Apple).

Dextran-adapted dermal Miles assay. Dorsal hair was removed from mice as described above. On the day of the assay, mice were anesthetized with isoflurane and injected ID with PBS (50 µl), VEGF (200 ng in 50 µl PBS), and DENV2 NS1 (7.5 µg or 15 µg in 50 µl PBS) and/or WNV NS1 (15 µg in 50 µl PBS) into the shaved back skin of the mouse. Immediately following ID injections, 200 µl of 10 kDa dextran conjugated with Alexa Fluor 680 (5 mg/ml; Sigma) was delivered by RO injection. Two hours post-injection, mice were euthanized using isoflurane, and the dorsal dermis was removed and placed in Petri dishes. Tissues were scanned using a fluorescent detection system (LI-COR Odyssey CLx Imaging System) at a wavelength of 700 nm, and leakage in a 13 mm diameter circle surrounding the sites of injection was quantified using Image Studio software (LI-COR Biosciences). For experiments using inhibitors, compounds were administered IP in a total volume of 200 µl 6 hours before the start of the assay and then immediately before beginning the assay. All inhibitors were used at a final concentration of 1 mg/kg. A combination of DMSO, PBS, and water was used as a vehicle control.

Intradermal injection of murine ears. Vascular leak in murine ears was measured as previously described (143). Ears of isoflurane-anesthetized mice were immobilized using cover slip forceps. A sterilized needle (30-gauge, 25 mm length, and 10°-12° bevel), used with a 25 µl reusable glass microinjection syringe (Hamilton), was inserted ~3 mm into the ventral side of the ear skin at a flat angle with the bevel pointing up, and either 20 µl PBS or 7.5 µg DENV2 NS1 diluted in 20 µl PBS was slowly injected. EBD (0.5% in PBS, 150 µl) or 200 µl of 10 kDa dextran conjugated with Alexa Fluor 680 (5 mg/ml) was immediately delivered by RO injection. EBD and dextran were allowed to circulate for 30 minutes and 2 hours, respectively, and mice were then euthanized using isoflurane. For EBD assays, representative images were obtained using an iPhone 5S (Apple). For dextran assays, ears were removed and imaged using a fluorescent detection system (LI-COR Odyssey CLx Imaging System) at a wavelength of 700 nm.

Evans Blue systemic Miles assay. The effect of recombinant DENV2 NS1 protein on systemic vascular leak *in vivo* was evaluated using the Miles assay as previously described (84). Briefly, wild-type or *Tlr4*$^{-/-}$ B6 mice were anesthetized using isoflurane and injected IV with either 10 mg/kg of ovalbumin or DENV2 NS1. Three days post-injection, mice were administered 200 µl of 0.5% EBD, and dye was allowed to circulate for 3 hours before mice were euthanized and cardiac puncture was performed. Tissues were collected and thoroughly dried in pre-weighed tubes. One ml of formamide was then added and incubated at 56°C for 48 hours. The absorbance of the extravasated dye was measured at 620 nm using a spectrophotometer. EBD concentration was calculated using a standard curve (30.5 to 500,000 ng/ml) using linear regression analysis.

DENV2 infection of mice. Mice deficient in the interferon-α/β receptor (*Ifnar*$^{-/-}$) or *Tlr4*$^{-/-}$ *x Ifnar*$^{-/-}$ doubly deficient B6 mice were challenged IV with 10^7 plaque-forming units (PFU) of DENV2 D220 or 5 µg of 4G2 (anti-DENV E mAb) 20-24 hours prior to infection with 3 x 10^5 PFU of D220 (ADE). Animals were monitored daily and DENV-induced morbidity and mortality were scored using a standardized scale (199).

Transendothelial electrical resistance (TEER). The effect of recombinant DENV2 NS1 protein on endothelial permeability was evaluated by measuring TEER in HMEC-1 grown on a 24-well Transwell polycarbonate membrane system (Transwell permeable support, 0.4 µm, 6.5 mm insert; Corning Inc.) as previously described (84, 88). Briefly, TEER was measured in Ohms (Ω) at sequential 2-hour time-points following the addition of test proteins using an Epithelial Volt Ohm Meter (EVOM) with “chopstick” electrodes (World Precision Instruments). Untreated endothelial cells grown on Transwell inserts were used as negative untreated controls, and inserts with medium alone were used for blank resistance measurements. Relative TEER represents a ratio of resistance values (Ω) as follows: (Ω experimental condition - Ω medium alone) / (Ω non-treated endothelial cells - Ω medium alone). After 24 hours of treatment, 50% of upper and lower chamber media were replaced by fresh endothelial cell medium. For experiments using mAbs, antibodies were added immediately before the addition of test proteins. For experiments using inhibitors, compounds were added to the apical compartment of the Transwell 1 hour before the addition of DENV NS1 protein.

Fluorescence microscopy. Microscopy was performed as previously described (88). For imaging experiments, HMEC-1 were grown on coverslips coated with 0.2% gelatin (Sigma) and imaged on a Zeiss LSM 710 Axio Observer inverted fluorescence microscope equipped with a 34-channel spectral detector. Images acquired using the Zen 2010 software (Zeiss) were processed and analyzed with ImageJ software (188). All RGB images were converted to grayscale, then mean grayscale values and integrated density from selected areas were taken, along with adjacent background readings, and plotted as mean fluorescence intensity (MFI). To assess the effect of DENV2 NS1 on integrity of the EGL architecture, the distribution of sialic acid and heparan sulfate, as well as cathepsin L activity, was examined on untreated confluent HMEC-1 monolayers and on monolayers treated with DENV2 NS1 proteins (5 µg/ml) and fixed with 4% paraformaldehyde (PFA) at 6 hours post-treatment. Confluent untreated HMEC-1 monolayers were also fixed and stained for chondroitin sulfate and hyaluronic acid, normal constituents of the endothelial glycocalyx. Primary antibodies were incubated overnight at 4°C, and detection was performed using secondary species-specific anti-IgG or anti-IgM antibodies conjugated to Alexa fluorophores (488, 568 and 647).

Enzymatic activity assays. Cathepsin L activity in living cells was monitored using the Magic Red Cathepsin L detection kit (Immunochemistry Technologies, Inc.) as previously described (88). Briefly, confluent HMEC-1 monolayers grown on coverslips were exposed to DENV2 NS1 protein (5 µg/ml), and at 6 hours post-treatment, a cell membrane-permeant fluorogenic substrate MR-$(Phe\text{-}Arg)_2$, which contains the cresyl violet (CV) fluorophore branded as Magic Red (MR), was added. Cultured cell monolayers expressing active cathepsin L catalyze the hydrolysis of the two Phe-Arg target sequences, generating a red fluorescent species that can be detected by immunofluorescence microscopy. Magic Red excites at 540-590 nm (590 nm optimal) and emits at >610 nm (630 nm optimal).

ELISA. TNF-α, IL-6, and IL-8 levels were measured using ELISA assays following the manufacturer's instructions (Abcam).

Statistics. Statistical analyses were performed using GraphPad Prism 6 software, and all graphs were generated using Prism 6. For *in vivo* murine dermis experiments, an ordinary one-way ANOVA with multiple comparisons to the PBS group using Dunnett's multiple comparison test was used to determine significance of VEGF, DENV2 NS1, and WNV NS1. An unpaired, parametric, two-tailed t-test was used to determine significance between individual groups. For DENV infection experiments, comparison of survival rates was conducted using a nonparametric log-rank (Mantel-Cox) test and graphed as Kaplan-Meier survival curves. For ELISA experiments, a repeated measure two-way ANOVA with multiple comparisons to the untreated group using Dunnett's multiple comparison test was used to determine significance of treatment with LPS (10 and 100 ng/ml) or DENV2 NS1 (5 and 10 µg/ml). For TEER experiments, a repeated measure two-way ANOVA was used to determine the significance of treatments (i.e. anti-cytokine mAbs or inhibitors) on DENV2 NS1-induced hyperpermeability in HMEC-1. Significance was further confirmed using a repeated measure two-way ANOVA with multiple comparisons to the untreated group using Dunnett's multiple comparison test as well as an ordinary one-way ANOVA

with multiple comparisons to the PBS group using Dunnett's multiple comparison test of area under the curve values for each group.

Supplementary Material

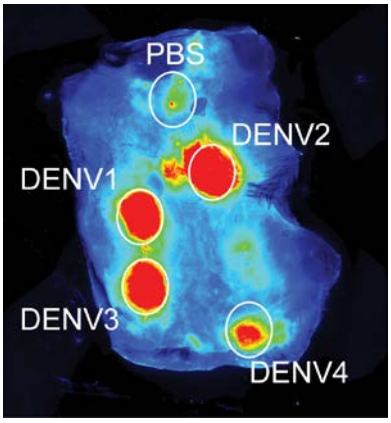

Figure 3.S1. Related to Figure 3.1. NS1 from DENV1-4 triggers localized vascular leak in the dorsal dermis of mice.
Representative image of mouse dorsal dermis following fluorescent dextran assay. Hair was removed from the dorsal dermis of mice, and mice were allowed to recover for 3 days. On the day of the assay, retro-orbital injections of Alexa Fluor 680-conjugated dextran were administered, followed by intradermal injections of PBS, 15 µg DENV1 NS1, 15 µg DENV2 NS1, 15 µg DENV3 NS1, and 15 µg DENV4 NS1. The dermis from each mouse was collected and processed two hours post-injection and scanned using a fluorescent detection system (LI-COR Odyssey CLx Imaging System) at a wavelength of 700 nm, and images were obtained using Image Studio software (LI-COR Biosciences).

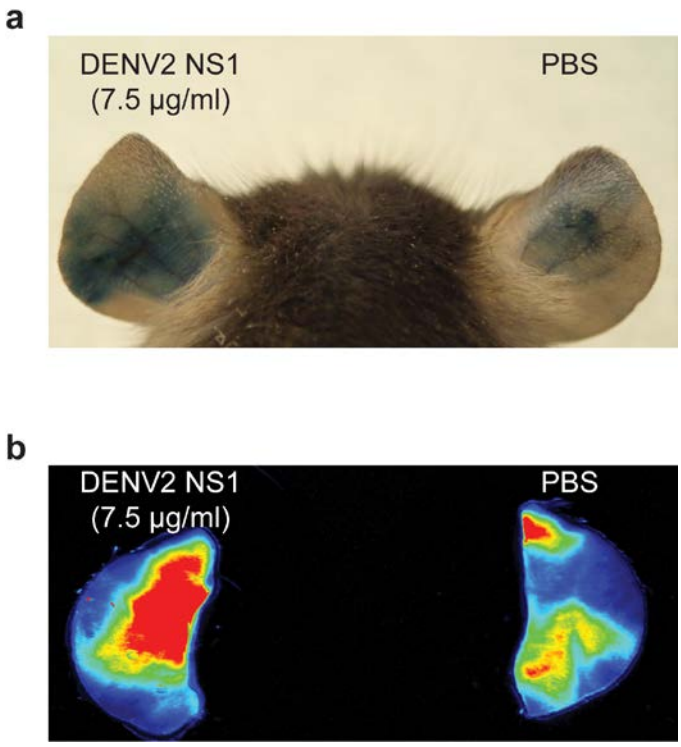

Figure 3.S2. Related to Figure 3.1. DENV2 NS1 triggers localized vascular leak in the dermis of mouse ears.
(a,b) Wild-type B6 mice received intradermal injections with either PBS (right ear) or 7.5 µg DENV2 NS1 (left ear) and, immediately after, intravenous injections of either **(a)** Evans Blue dye (EBD) or **(b)** Alexa Fluor 680-conjugated dextran. **(a)** EBD was allowed to circulate for 30 minutes and ears were photographed. **(b)** Dextran was allowed to circulate for 2 hours. Ears were removed and scanned using a fluorescent detection system (LI-COR Odyssey CLx Imaging System) at a wavelength of 700 nm, and images obtained using Image Studio software (LI-COR Biosciences).

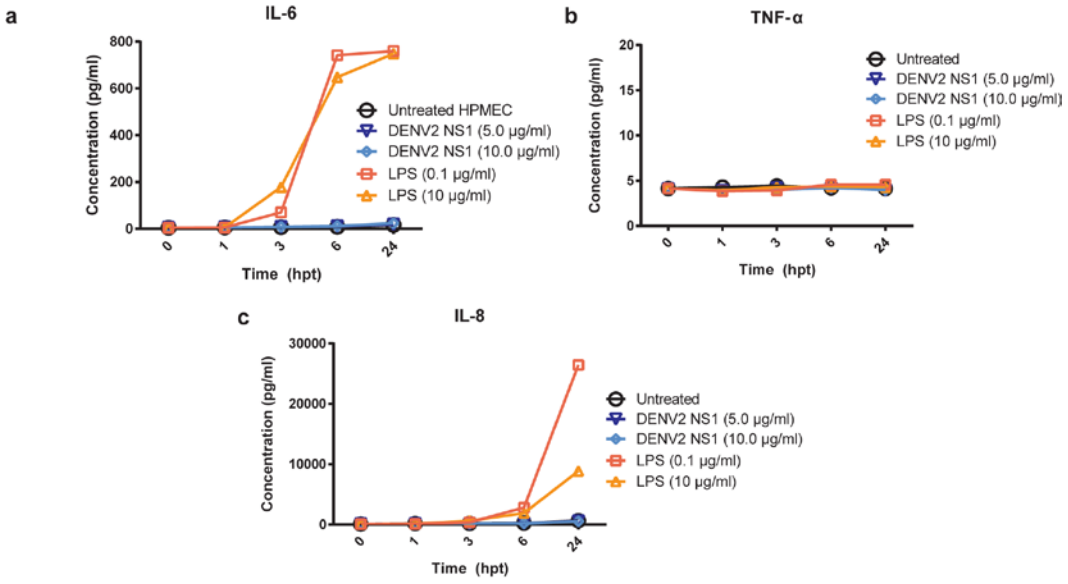

Figure 3.S3. Related to Figure 3.2. HPMEC do not produce the inflammatory cytokines IL-6, TNF-α, or IL-8 in response to DENV2 NS1 stimulation *in vitro*.
(a-c) HPMEC were stimulated with LPS (0.1 or 10 µg/ml; red squares and orange triangles, respectively) or DENV2 NS1 (5 or 10 µg/ml; dark blue triangles and light blue diamonds, respectively), and supernatant was collected at 0, 1, 3, 6, and 24 hours post-treatment. Untreated HPMEC monolayers were used as a control (black circles). ELISAs for **(a)** IL-6, **(b)** TNF-α, and **(c)** IL-8 were performed on all samples.

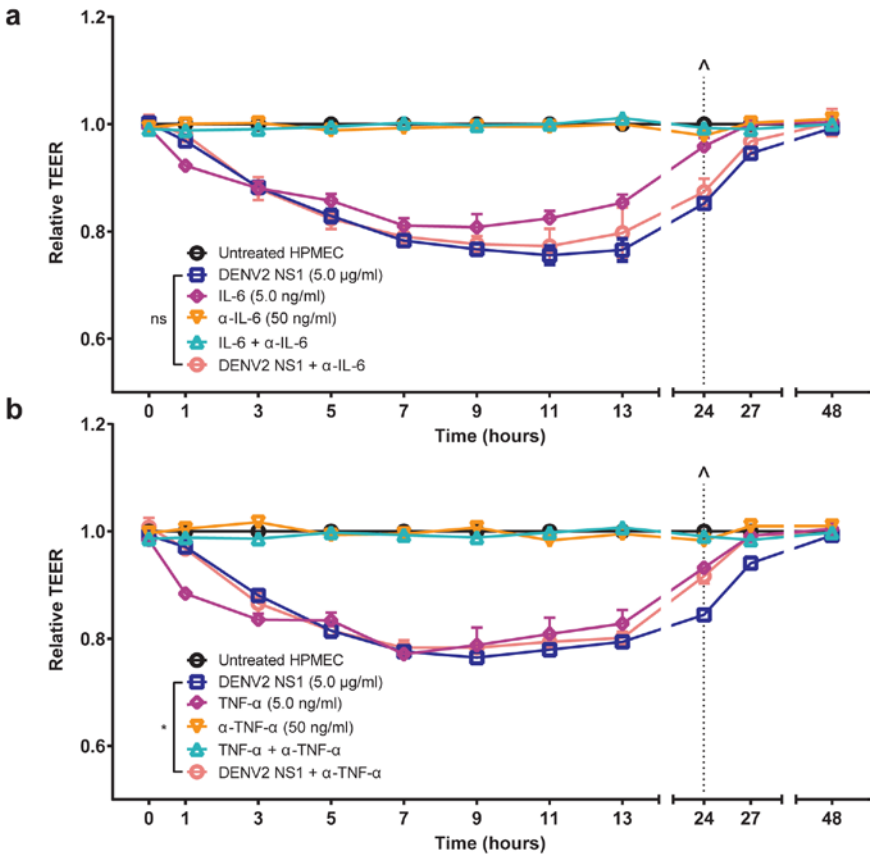

Figure 3.S4. Related to Figure 3.3. Inflammatory cytokines TNF-α and IL-6 are not involved in DENV2 NS1-induced endothelial hyperpermeability in HPMEC *in vitro*.
(a,b) Transendothelial electrical resistance (TEER) of HPMEC monolayers incubated with 5 µg/ml DENV2 NS1 (blue squares), 5 ng/ml recombinant cytokine (**(a)** IL-6, **(b)** TNF-α; purple diamonds), 50 ng/ml anti-cytokine mAbs (**(a)** IL-6, **(b)** TNF-α; orange triangles), recombinant cytokine + specific mAb (**(a)** IL-6, **(b)** TNF-α; green diamonds), or DENV2 NS1 + specific mAb (**(a)** IL-6, **(b)** TNF-α; red circles). The background signal was subtracted (using TEER values from a blank Transwell), and data were normalized to untreated HPMEC. (^) represents change of medium. All data shown represent the mean +/- SEM and were collected from two independent experiments. Data represent two replicate Transwells per condition. A repeated measure two-way ANOVA was used to determine the significance of anti-cytokine mAbs on DENV2 NS1-induced hyperpermeability in HPMEC. ns = not significant; *, $P < 0.05$.

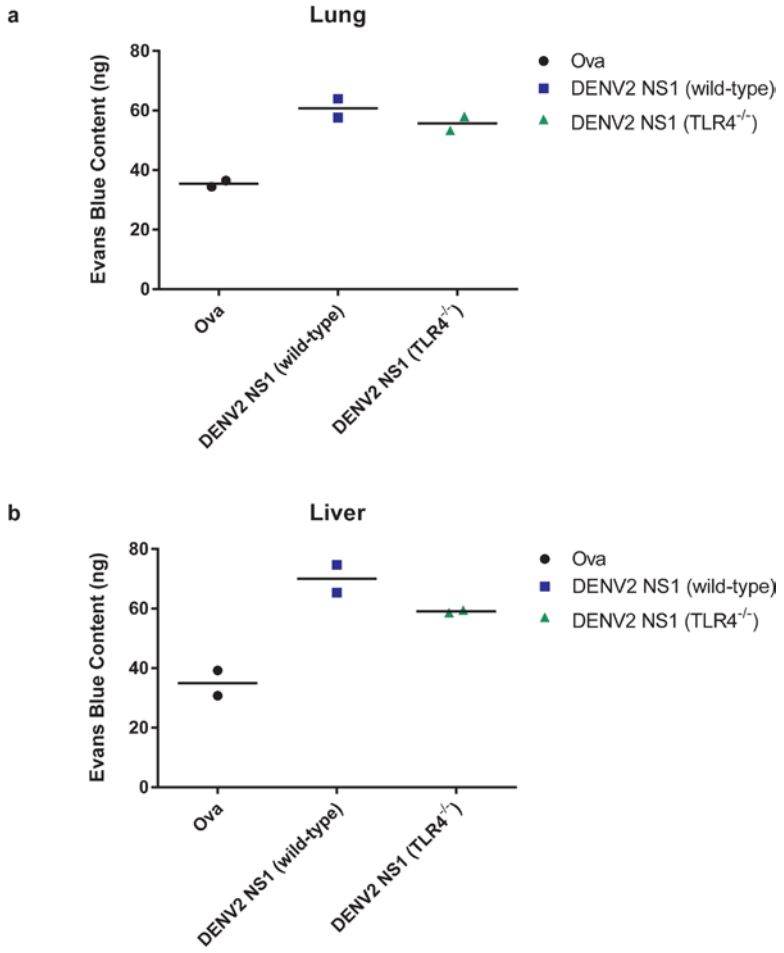

Figure 3.S5. Related to Figure 3.4. DENV2 NS1-induced systemic vascular leak *in vivo* is similar in wild-type and TLR4-deficient mice.
(a,b) Evans Blue dye (EBD) was injected intravenously into wild-type or *Tlr4*$^{-/-}$ B6 mice 3 days after intravenous injection of 10 mg/kg DENV2 NS1 (wild-type: blue squares; *Tlr4*$^{-/-}$: green triangles; n = 2 per genotype) or 10 mg/kg OVA (wild-type: black circles; n = 2). The dye was allowed to circulate for 3 hours before mice were euthanized. Tissues were harvested, and EBD was extracted in formamide and quantified in **(a)** lungs and **(b)** liver by measuring absorbance at 620 nm against a standard curve. Systemic vascular leak experiments performed and analyzed by Dr. Diego Espinosa.

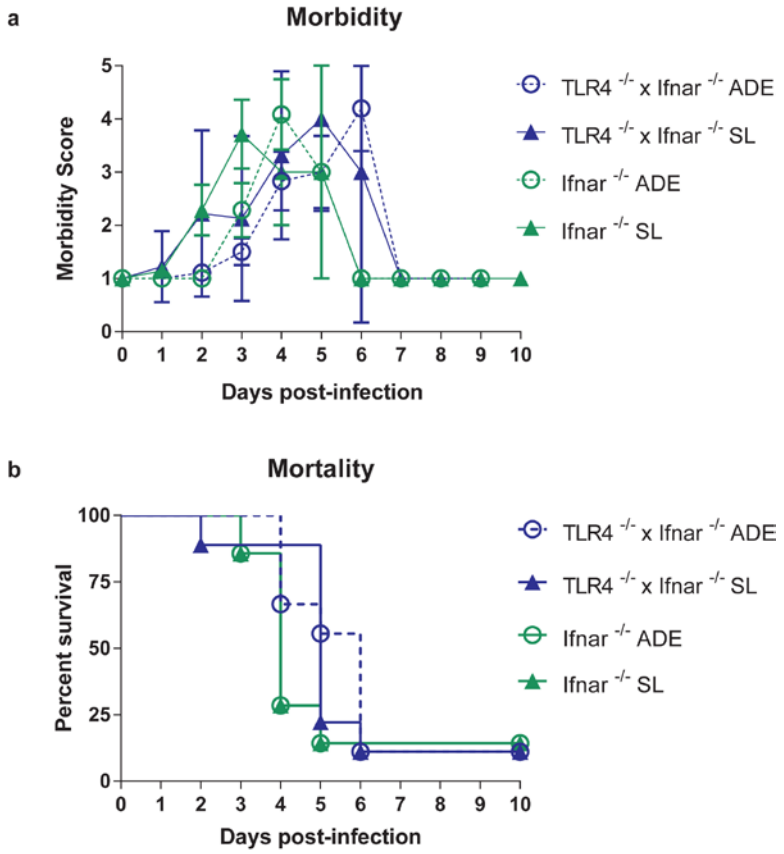

Figure 3.S6. Related to Figure 3.4. DENV2 infection leads to similar levels of morbidity and mortality in *Ifnar*$^{-/-}$ and *Tlr4*$^{-/-}$ *x Ifnar*$^{-/-}$ mice.
(a,b) *Ifnar*$^{-/-}$ and *Tlr4*$^{-/-}$ *x Ifnar*$^{-/-}$ B6 mice were injected intravenously with either 10^7 plaque-forming units (PFU) of DENV2 D220 (straight-lethal, SL; *Ifnar*$^{-/-}$: closed green triangles, n = 7; *Tlr4*$^{-/-}$ *x Ifnar*$^{-/-}$: closed blue triangles, n = 9) or 5 µg of 4G2 (anti-DENV Envelope mAb) 20-24 hours prior to infection with 3 x 10^5 PFU of D220 (antibody-enhanced, ADE; *Ifnar*$^{-/-}$: open green triangles, n = 7; *Tlr4*$^{-/-}$ *x Ifnar*$^{-/-}$: open blue triangles, n = 9). Mice were then monitored for **(a)** morbidity and **(b)** mortality for 10 days post-infection. **(a)** Mice were observed twice per day and scored for morbidity on a scale of 1 to 5, with 1 being healthy and 5 being moribund. **(b)** Kaplan-Meier survival curve, with data derived from 2 independent experiments. A nonparametric Mantel-Cox log rank test was used to determine significance between groups. Morbidity and mortality experiments performed and analyzed by Dr. Diego Espinosa.

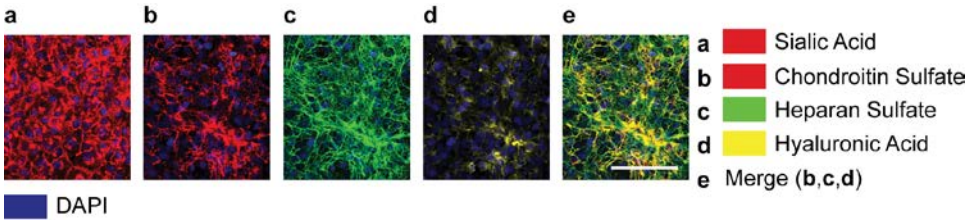

Figure 3.S7. Related to Figure 3.5. HMEC-1 express canonical glycocalyx components on the cell surface *in vitro*.
HMEC-1 monolayers were grown for 5 days until confluent on glass cover slips coated with 0.2% gelatin. Monolayers were stained for **(a)** sialic acid (stained with WGA-A647, red), **(b)** chondroitin sulfate (stained with anti-Chondroitin Sulfate mAb CS-56, red), **(c)** heparan sulfate (stained with Heparan Sulfate mAb clone F58-10E4, green), or **(d)** hyaluronic acid (stained with anti-Hyaluronic Acid polyclonal antibody, yellow), and imaged on a Zeiss LSM 710 Axio Observer inverted fluorescence microscope equipped with a 34-channel spectral detector at 20x magnification. **(e)** Merge of **(b-d)**. Images were acquired using the Zen 2010 software (Zeiss). Nuclei were stained with Hoechst (blue). Scale bar, 10 µm. Confocal microscopy images acquired and analyzed by Dr. Henry Puerta-Guardo.

Chapter 4: Internalization of DENV NS1 by human endothelial cells is required for NS1-mediated barrier dysfunction

Summary

Dengue virus (DENV) is the most prevalent arbovirus worldwide, and infection with any of the four serotypes leads to a range of outcomes, from inapparent infection to classic dengue fever to dengue hemorrhagic fever and dengue shock syndrome. Recently, we described a novel role for DENV non-structural protein 1 (NS1) in triggering hyperpermeability of human endothelial cells and systemic vascular leak *in vivo* via disruption of the endothelial glycocalyx-like layer (EGL). However, the molecular determinants of NS1-induced endothelial hyperpermeability have not yet been identified. Here, using *in vitro* model systems, we report that a glycosylation site (Asn-207) is required for DENV NS1 internalization by endothelial cells and activation of endothelial cell-intrinsic pathways characterized by degradation of EGL components. This mutation (N207Q) completely prevents NS1-induced hyperpermeability, as measured by transendothelial electrical resistance (TEER). It also prevents disruption of key EGL components, heparan sulfate and sialic acid, as well as activation of cathepsin L on human pulmonary microvascular endothelial cells (HPMEC), as measured by confocal microscopy. Mechanistically, we found that the DENV2 NS1 N207Q mutant is less efficiently internalized by HPMEC than wild-type NS1 at 37°C as determined by Western blot and colocalization with Rab5, an early endosome marker, as measured by confocal microscopy. However, similar binding levels were found for both proteins at 4°C, suggesting that the N207Q mutation does not affect NS1 interaction with the cell surface but abrogates its internalization by HPMEC. Finally, we show that NS1 is internalized by HPMEC via clathrin-mediated endocytosis (CME) and that Pitstop 2, a CME-specific inhibitor, prevents DENV NS1 internalization and NS1-induced hyperpermeability and EGL degradation. These results describe the molecular determinant of NS1 required for its internalization by endothelial cells via CME and its induction of endothelial hyperpermeability and EGL degradation in HPMEC. These findings further elucidate the pathways contributing to endothelial cell-intrinsic pathogenic processes activated by NS1 and provide more extensive insight into DENV pathogenesis overall.

Introduction

DENV is a mosquito-borne flavivirus, and infection with any of its four serotypes can result in inapparent infection, classic dengue fever, or dengue hemorrhagic fever/dengue shock syndrome – severe manifestations characterized by vascular leak that can lead to shock and death (200). The 10.7-kb RNA genome encodes three structural and seven non-structural (NS) proteins, including NS1. We and others previously described a novel role for DENV NS1 in increasing permeability of human endothelial cells and systemic vascular leak via two distinct mechanisms: a cytokine-independent, endothelial cell-intrinsic pathway via disruption of components of the endothelial glycocalyx-like layer (EGL) (84, 88, 89) and a cytokine-mediated, TLR4-dependent pathway involving activation of peripheral blood mononuclear cells (PBMCs) (85). However, the early interactions between NS1 and endothelial cells leading to barrier dysfunction have not yet been fully characterized.

All flavivirus NS1 genes are highly homologous and encode a 352-amino acid polypeptide with slight variation in glycosylation status that results in a molecular weight of 46-55 kDa (146). NS1 forms a dimer intracellularly that is also found on the cell surface, and NS1 is secreted from infected cells as a barrel-shaped hexamer containing lipid cargo (48). High-resolution structures of the C-terminal half (51) and full-length (50) DENV and the closely related West Nile virus (WNV) NS1 proteins provided the structural understanding of flavivirus NS1 assembly and antibody recognition. DENV NS1 contains two conserved N-linked glycans at Asn-130 (N130) and Asn-207 (N207), and NS1 proteins derived from different cells/species exhibit distinct types of N-glycosylation (122). In mammalian cell-derived DENV NS1, complex glycans are attached at Asn-130 and high-mannose glycans are attached at Asn-207 (44); the N-linked glycans are involved in NS1 dimer stability and secretion (44, 47). Further, when compared to wild-type (WT) virus, DENV2 (strain 16681) de-glycosylated at either site exhibited significant attenuation of neurovirulence in mice (61).

To examine the importance of NS1 glycosylation status on NS1-mediated pathogenesis, Dr. Chunling Wang, a postdoctoral fellow in the Harris Laboratory, generated four NS1 constructs targeting glycosylation sites in DENV2 NS1, including WT, single N-glycosylation mutants N130Q and N207Q, and double N-glycosylation mutant N130Q+N207Q. Recombinant NS1 proteins were produced in a mammalian expression system, and DENV WT and N207Q NS1 proteins were successfully secreted and purified as oligomers; the N130Q mutant and the double N130Q+N207Q mutant were not efficiently secreted and were not included in further analyses.

In this study, we sought to investigate whether the glycosylation status of NS1 may contribute to its binding to endothelial cells and/or its ability to induce endothelial hyperpermeability. Using both transendothelial electrical resistance (TEER) and confocal microscopy, we show that the N207Q mutant does not induce endothelial barrier dysfunction or degradation of the EGL of human pulmonary microvascular endothelial cells (HPMEC). Further, we demonstrate that there are no differences in binding between

WT DENV NS1 and the N207Q mutant, but the latter is not efficiently internalized by endothelial cells, indicating that internalization of NS1 is required for endothelial cell-intrinsic pathogenesis. Finally, we show that endothelial cells internalize NS1 via clathrin-mediated endocytosis (CME) and that inhibition of CME prevents NS1-induced hyperpermeability and EGL degradation. Taken together, our results suggest that the N207 glycosylation site is required for NS1 internalization by endothelial cells and that CME is a key step in the pathway leading to NS1-induced endothelial hyperpermeability and barrier dysfunction.

Results

DENV N207Q NS1 does not induce endothelial hyperpermeability or degrade the endothelial glycocalyx-like layer in human pulmonary endothelial cells *in vitro*

Previously, we demonstrated that NS1 from all four DENV serotypes induces endothelial hyperpermeability of HPMEC as measured by transendothelial electrical resistance (TEER). To investigate the functional role of NS1 glycosylation in pathogenesis, we first evaluated the effect of DENV N207Q NS1 on endothelial permeability. Using our TEER model, we found that DENV2 NS1 produced in-house induces endothelial hyperpermeability of HPMEC at similar levels to commercially purchased NS1 but that the DENV N207Q NS1 mutant is defective in increasing permeability **(Figure 4.1)**. These data demonstrate that mutation of N-glycosylation site 207 in DENV2 NS1 completely abrogates the ability of NS1 to induce endothelial hyperpermeability.

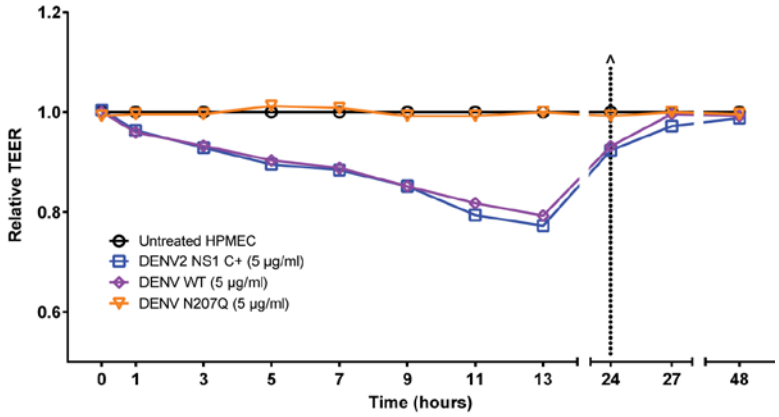

Figure 4.1. Mutation of the N-glycosylation site 207 (N207Q) completely abrogates NS1-induced hyperpermeability of HPMEC.
Human pulmonary microvascular endothelial cells were grown on Transwell semi-permeable membranes (0.4 µm pore size), and distinct flavivirus NS1 proteins (5 µg/ml) were added to the apical chamber (DENV2 NS1, commercially purchased, blue squares; DENV2 NS1, produced in-house, purple diamonds; DENV2 N207Q mutant NS1, orange triangles). A TEER assay was used to evaluate the effect of these NS1 proteins on endothelial permeability at indicated time-points over 48 hours. (^) represents change of medium. Relative TEER values from two independent experiments performed in duplicate are plotted. Error bars indicate standard error of the mean (SEM).

We have previously shown that DENV NS1 binds to endothelial cells and activates cathepsin L, which subsequently activates heparanase that cleaves heparan sulfate on the cell surface (88, 89). NS1 also activates the endothelial sialidases Neu1, Neu2, and Neu3, which cleave sialic acid on the cell surface. Together, these mechanisms contribute to NS1-induced degradation of the EGL, leading to endothelial barrier dysfunction (88, 89). To investigate whether DENV N207Q NS1 is able to trigger activation of these pathways, we performed confocal microscopy of NS1-treated HPMEC monolayers at 6 hours post-treatment. We found that while both WT preparations of NS1 activate cathepsin L and induce loss of heparan sulfate as well as sialic acid from the EGL, the N207Q mutant was unable to trigger these effects **(Figure 4.2)**. Taken together, these

results indicate that glycosylation status is a key molecular determinant of NS1-mediated pathogenesis.

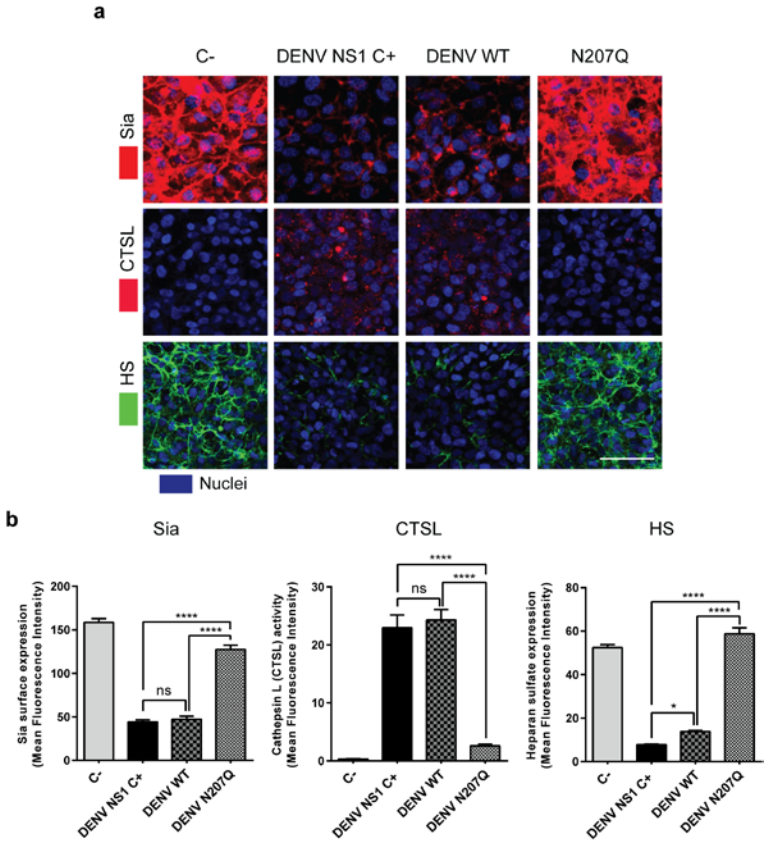

Figure 4.2. Mutation of the N-glycosylation site 207 prevents NS1-induced EGL disruption on pulmonary endothelial cells.
(a) The integrity of the EGL on HPMEC was assessed by the presence of sialic acid (Sia) surface expression, stained with WGA-A647 (red, top row), and heparan sulfate (HS) surface expression (green, bottom row), as well as cathepsin L (CTSL) activity (red, middle row), at 6 hpt with NS1 proteins at 37°C, as visualized via confocal microscopy. Nuclei were stained with Hoechst (blue). Images (20X; scale bars, 50 µm) are representative of 2 independent experiments performed in duplicate. **(b)** Quantification of MFI in **(a)** from two independent experiments. Error bars indicate standard deviation (SD). ns = not significant; *, P < 0.05; ***, P < 0.0005; ****, P < 0.0001. Confocal microscopy images acquired and analyzed by Dr. Henry Puerta-Guardo.

DENV N207Q NS1 binds to HPMEC but is retained on the surface of endothelial cells

Since DENV N207Q NS1 is unable to induce endothelial hyperpermeability or degradation of the EGL, we next investigated whether DENV N207Q NS1 is able to bind to the surface of HPMEC. Using confocal microscopy, we found that both commercial and in-house-produced WT DENV NS1 and the N207Q mutant all bind to endothelial cells at 1 hour post-treatment at 37˚C. Interestingly, the DENV N207Q mutant NS1 appeared to bind to the surface of HPMEC at substantially higher levels than both preparations of WT DENV NS1 **(Figure 4.3a, top row; 4.3b, left panel)**.

We next examined whether this apparent increase in binding was due to an increased inherent ability of the N207Q mutant to bind to endothelial cells by evaluating NS1 levels on the surface of HPMEC at 4°C, a temperature where endocytosis should be greatly reduced. We found that the N207Q mutant was able to bind HPMEC at similar levels to both commercial and in-house-produced WT DENV NS1 when NS1 proteins were incubated with HPMEC at 4°C for 1 hour **(Figure 4.3a, bottom row; 4.3b, right panel)**. These data suggest that the N207Q mutant binds to HPMEC at similar levels to WT NS1, but the mutant is retained on the surface of endothelial cells at higher levels than WT.

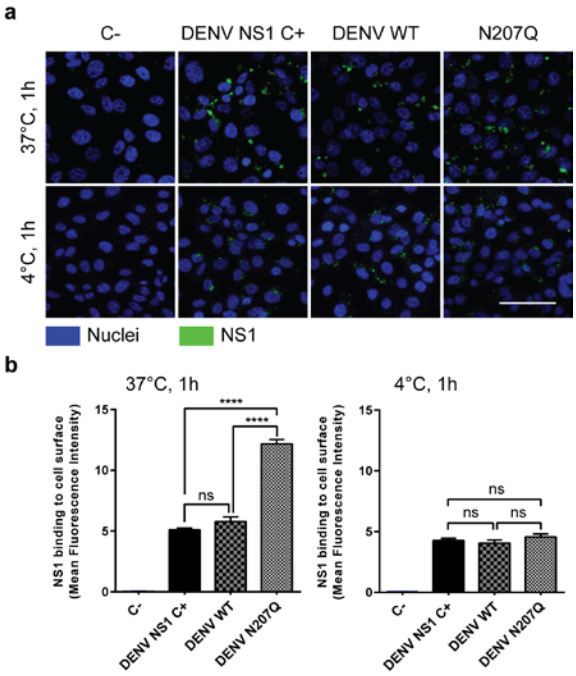

Figure 4.3. Wild-type DENV NS1 and the DENV N207Q NS1 mutant bind at similar levels to HPMEC. **(a)** Binding of NS1 proteins to HPMEC at 4˚C or 37˚C after 1 hpt was visualized via confocal microscopy. Nuclei were stained with Hoechst (blue). Images (20X; scale bars, 50 μm) are representative of 2 independent experiments performed in duplicate. **(b)** Quantification of MFI in **(a)** from two independent experiments. Error bars indicate SD. ns = not significant; ****, P < 0.0001. Confocal microscopy images acquired and analyzed by Dr. Henry Puerta-Guardo.

WT DENV NS1 is internalized by endothelial cells and colocalizes with Rab5, but DENV N207Q NS1 does not

We previously observed that the peak of DENV2 NS1 binding to endothelial cells is 6 hpt, with a noticeable decrease by 12 hpt; binding was hardly detectable at 24 hpt (88). NS1 was previously shown to be endocytosed by hepatocytes (201), and we hypothesized that NS1 needs to be internalized by endothelial cells in order to activate sialidases and the cathepsin L/heparanase pathway. We found that WT DENV NS1 (both commercial and in-house-produced) appeared at higher levels than the N207Q mutant in HPMEC cell lysate at 1 hpt following protease removal of surface-bound NS1, as measured by Western blot, suggesting that the DENV N207Q mutant is not efficiently internalized by

endothelial cells at 37°C **(Figure 4.4a,b)**. To further confirm these findings, we used confocal microscopy to visualize intracellular NS1 and Rab5, a regulatory GTPase associated with early endosomes, in HPMEC at 37°C 1 hour post-treatment. Both WT NS1 and N207Q proteins were detected in HPMEC; however, only WT DENV NS1 colocalized with Rab5 **(Figure 4.4c,d)**. These data suggest that WT DENV NS1 is internalized by endothelial cells and trafficked to the endosome; however, the N207Q mutant does not localize to the same cellular compartment.

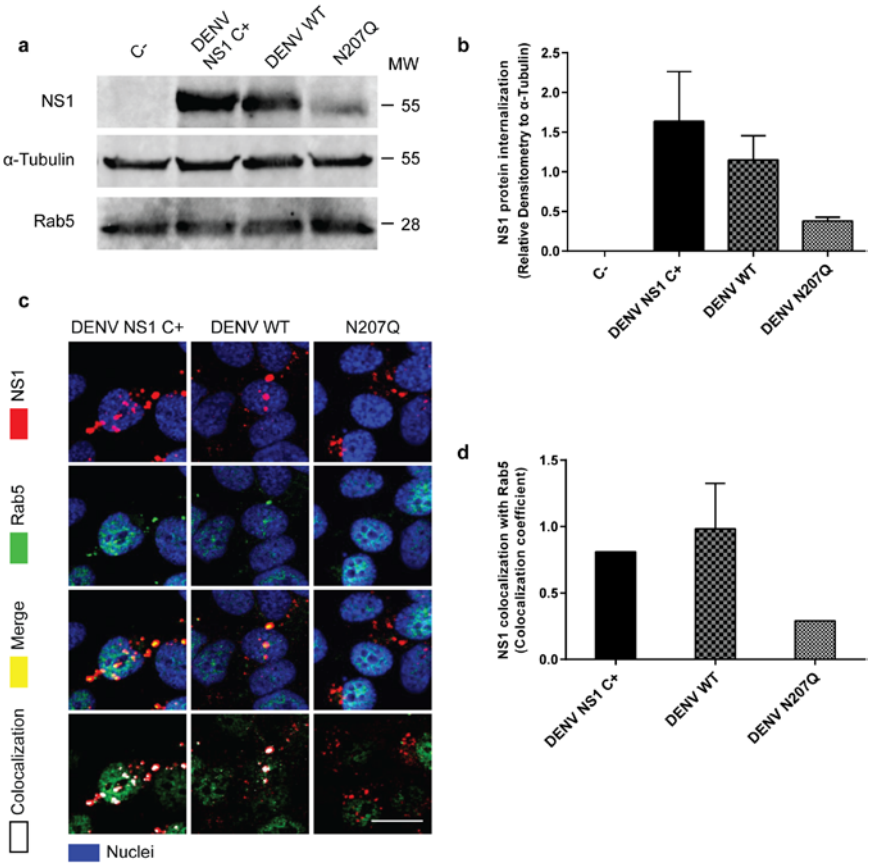

Figure 4.4. Wild-type DENV NS1 is internalized by human endothelial cells but the DENV N207Q NS1 mutant is not.
(a) Confluent HPMEC monolayers were exposed to 10 μg/ml of different NS1 proteins and incubated at 37°C for 1.5 hours. Trypsin was used to remove surface-bound NS1, and protein extracts were collected from cell lysates and analyzed by Western blot. Western blot shows a representative image of detection of the internalized DENV2 NS1 proteins, α-tubulin (loading control), and Rab5, an early endosome marker. **(b)** Relative densitometry quantification of NS1 proteins normalized to α-tubulin in **(a)** from two independent experiments. Error bars indicate SD. **(c)** Colocalization of NS1 proteins (red, first row), as indicated, with early endosome marker Rab5 (green, second row) in HPMEC 1 hpt with NS1. Colocalization is shown in yellow in merge images (third row) or white in colocalization panels (fourth row; JACoP, ImageJ). Nuclei were stained with Hoechst (blue). Images (20X; scale bars, 10 μm) are representative of 2 independent experiments performed in duplicate. **(d)** Quantification of DENV NS1 and Rab5 colocalization in **(c)** was obtained using four different frames from the maximum projections of two RGB images based on the object-based approach (JACoP) and defined by the Manders' Coefficient as previously described (202). The colocalization coefficient was normalized by taking into account the

signal obtained from 300 cells per image. Error bars indicate SD of MFI values in the colocalization analyses obtained from two independent experiments.

DENV NS1 colocalizes with clathrin but not caveolin, and inhibition of CME prevents NS1-induced hyperpermeability and EGL degradation

Endocytosis by endothelial cells can occur via several routes, including CME and caveolin-mediated uptake (CavME) (203). We next sought to determine through which route NS1 was internalized by endothelial cells. Using confocal microscopy, we found that commercial and in-house-produced WT NS1 and N207Q NS1 all colocalized with clathrin in HPMEC at 1 hpt **(Figure 4.5a)**; however, no colocalization with caveolin was observed for any proteins **(Figure 4.5b)**. These results suggest that NS1 activates CME but not CavME for internalization into endothelial cells.

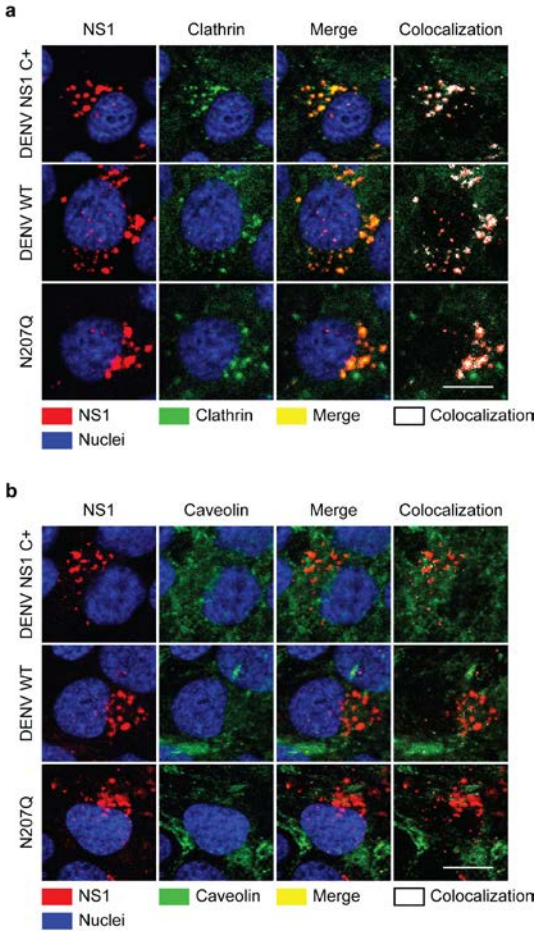

Figure 4.5. Both wild-type and the N207Q mutant NS1 colocalize with clathrin but not with caveolin on the surface of HPMEC *in vitro*.
Confluent HPMEC monolayers were exposed to 10 μg/ml of different NS1 proteins and incubated at 37°C for 30 minutes. Colocalization of NS1 proteins (red, left column), as indicated, with either **(a)** clathrin or **(b)** caveolin (green, second column) in HPMEC. Colocalization is shown in yellow in merge images

(third column) or white in colocalization panels (fourth column; JACoP, ImageJ). Nuclei were stained with Hoechst (blue). Images (20X; scale bars, 5 μm) are representative of 2 independent experiments performed in duplicate.

Because the N207Q mutant colocalizes with clathrin but not with Rab5, indicating that it is not internalized via CME, and also does not trigger downstream pathogenesis, we evaluated whether inhibition of CME could prevent NS1-mediated endothelial hyperpermeability and EGL degradation. We first treated HPMEC with Dynasore, an inhibitor of the GTPase dynamin, which regulates clathrin-coated pit maturation and directs membrane fission (204), and Pitstop 2, a specific inhibitor of CME, and we found that both compounds abrogated WT NS1-induced hyperpermeability as measured by TEER **(Figure 4.6a)**. Because Pitstop 2 is a more specific inhibitor than Dynasore, we next evaluated its effect on cathepsin L activation and heparan sulfate degradation **(Figure 4.6b,c)**. We found that Pitstop 2 prevented both the activation of cathepsin L and the degradation of heparan sulfate by NS1. Finally, we found that Pitstop 2 prevented NS1 colocalization with Rab5 in HPMEC **(Figure 4.6d)**. Taken together, these results suggest that CME is required for both NS1-induced hyperpermeability and EGL degradation as well as endothelial cell internalization of NS1 following binding of the protein to endothelial cells.

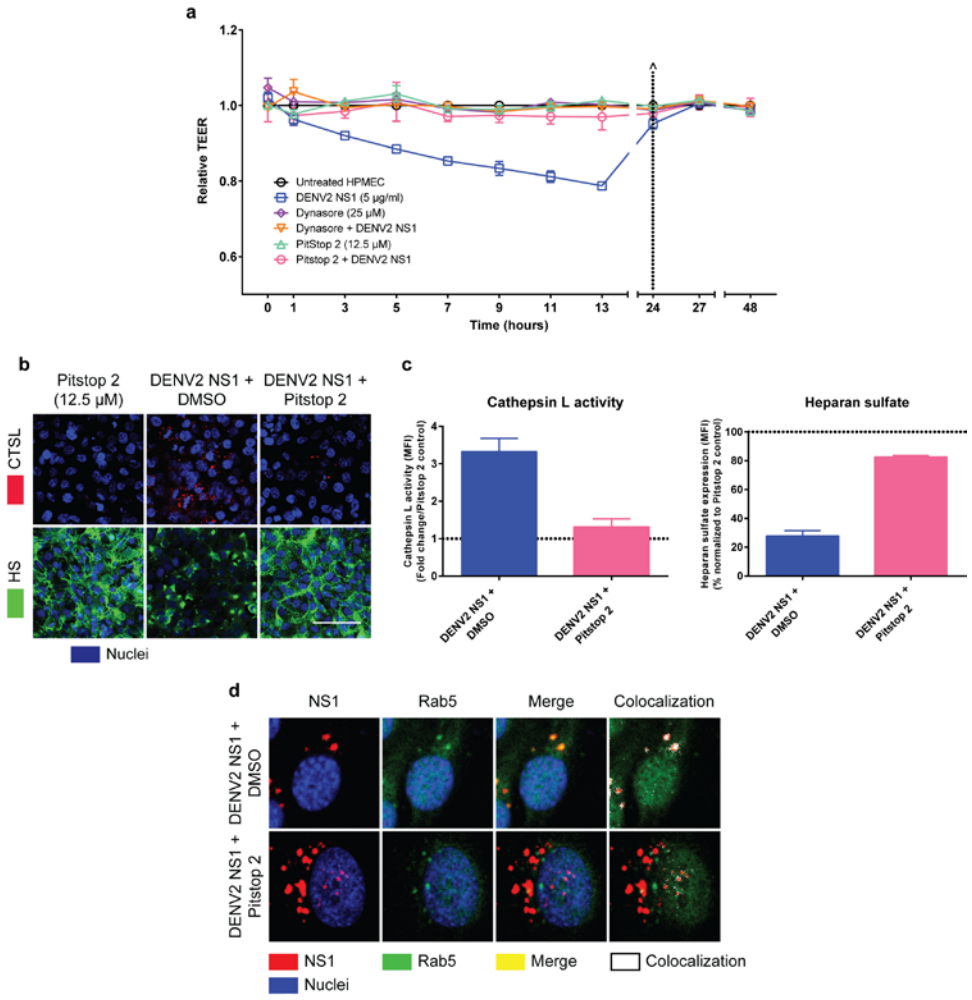

Figure 4.6. Inhibition of CME prevents DENV NS1-induced hyperpermeability, EGL degradation, and internalization by endothelial cells.

(a) HPMEC were grown on Transwell semi-permeable membranes (0.4 µm pore size), and the apical chamber was treated with either DENV2 NS1 (5 µg/ml) alone (blue squares); the dynamin inhibitor Dynasore (25 µM) alone (purple diamonds) or in the presence of NS1 (orange triangles); or the CME inhibitor Pitstop 2 (12.5 µM) alone (light green triangles) or in the presence of NS1 (pink circles). A TEER assay was used to evaluate the effect of NS1 and inhibitors on endothelial permeability at indicated time-points over 48 hours. (^) represents change of medium. Relative TEER values from two independent experiments performed in duplicate are plotted. Error bars indicate standard error of the mean (SEM). **(b)** The integrity of the EGL on HPMEC was assessed by the presence of heparan sulfate (HS) surface expression (green, top row), as well as cathepsin L (CTSL) activity (red, top row), at 6 hpt with DENV2 NS1 (5 µg/ml) in the presence or absence of Pitstop 2 (12.5 µM) at 37°C, as visualized via confocal microscopy. Nuclei were stained with Hoechst (blue). Images (20X; scale bars, 50 µm) are representative of 2 independent experiments performed in duplicate. **(c)** Quantification of MFI in **(b)** from two independent experiments expressed as either fold change of cathepsin L activity from Pitstop 2 control values (left) or normalized percentage of heparan sulfate from Pitstop 2 control values (right). Error bars indicate SEM. **(d)** Colocalization of NS1 proteins (red, first column) on HPMEC treated with either DMSO (top row) or Pitstop 2 (bottom row) with Rab5 (green, second column) 1.5 hpt with NS1. Colocalization is shown in yellow in merge images (third column) or white in colocalization panels (fourth column;

JACoP, ImageJ). Nuclei were stained with Hoechst (blue). Images (20X; scale bars, 5 μm) are representative of 2 independent experiments performed in duplicate.

The role of the N207 glycosylation site of NS1 in endothelial hyperpermeability induction is conserved in other flaviviruses

Given the importance of the N207 glycosylation site for DENV NS1-mediated pathogenesis of HPMEC, we next sought to evaluate whether the N207Q mutation would abrogate hyperpermeability induced by NS1 proteins from Zika virus (ZIKV) and West Nile virus (WNV), two neurotropic flaviviruses, on human brain microvascular endothelial cells (HBMEC). We found that while both commercial and in-house-produced WT ZIKV and WNV NS1 proteins increased the permeability of HBMEC as measured by TEER, the respective N207Q mutants did not induce hyperpermeability **(Figure 4.7a,b)**. Further, given that cases of dengue encephalitis have been reported and that DENV has been found in the brain of dengue shock cases during autopsies (205, 206), we investigated the effect of WT and N207Q mutant DENV NS1 on the permeability of HBMEC. Consistent with our previous results, we found that both WT DENV NS1 proteins but not the N207Q mutant induced endothelial hyperpermeability of HBMEC **(Figure 4.7c)**. Taken together, these data indicate that the N207 glycosylation site is an important molecular determinant of pathogenesis across flaviviruses and tissue sites.

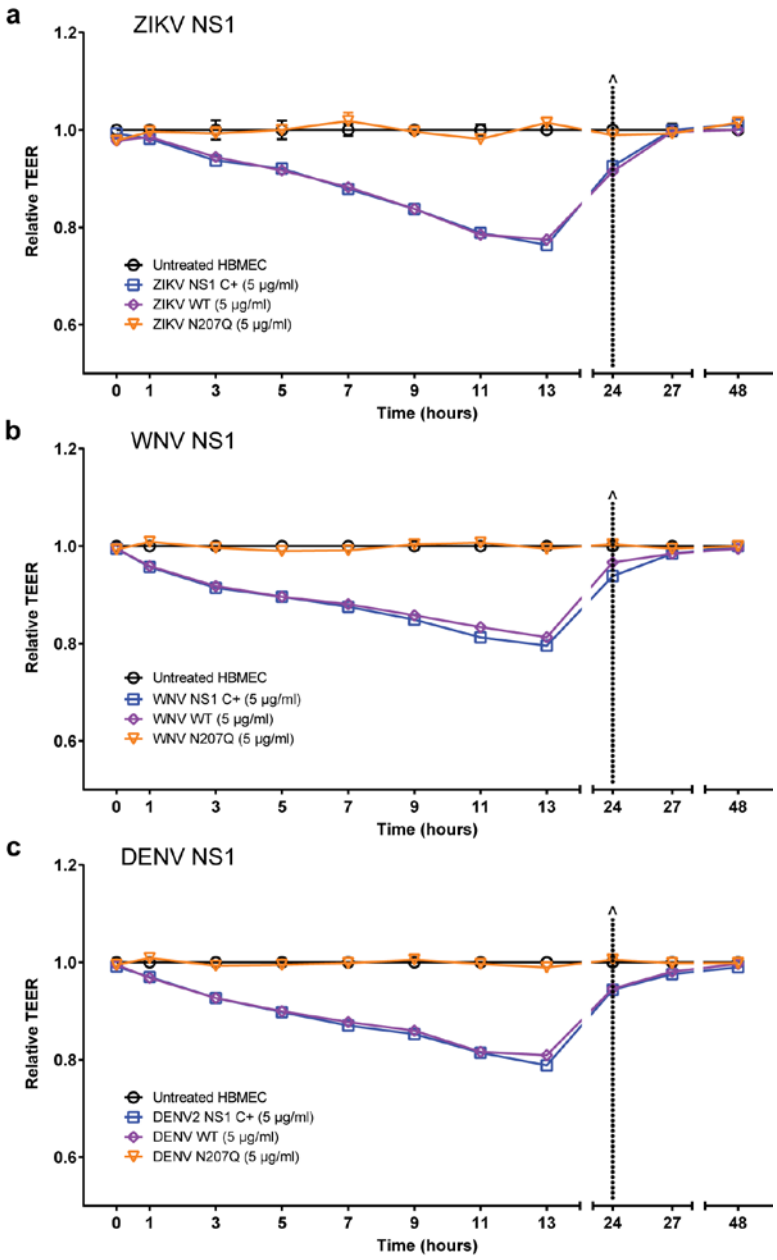

Figure 4.7. Mutation of the N207 glycosylation site abrogates hyperpermeability induced by NS1 proteins from neurotropic flaviviruses.
Human brain microvascular endothelial cells were grown on Transwell semi-permeable membranes (0.4 µm pore size), and **(a)** ZIKV NS1 proteins, **(b)** WNV NS1 proteins, or **(c)** DENV NS1 proteins (5 µg/ml) were added to the apical chamber (WT, commercially purchased, blue squares; WT, produced in-house, purple diamonds; N207Q mutant NS1, orange triangles). A TEER assay was used to evaluate the effect of these NS1 proteins on endothelial permeability at indicated time-points over 48 hours. (^) represents change of medium. Relative TEER values from two independent experiments performed in duplicate are plotted. Error bars indicate (SEM).

Discussion

In this study, we demonstrate that the N207 glycosylation site of DENV2 NS1 is essential for inducing hyperpermeability and EGL degradation of human endothelial cells. The N207Q NS1 mutant binds at similar levels to WT NS1, but it is retained on the cell surface. Consistent with this observation, WT NS1 is rapidly internalized by endothelial cells and colocalizes with Rab5, whereas N207Q NS1 predominantly remains on the cell surface, and what is internalized does not colocalize with Rab5. Further, NS1 colocalizes with clathrin and not caveolin, and inhibiting CME prevents NS1 internalization and NS1-induced hyperpermeability and EGL disruption. Taken together, these results suggest that the N207 glycosylation site is required for endothelial cell internalization via CME and endosomal trafficking of NS1, and this is necessary for the activation of enzymes like cathepsin L that lead to EGL degradation and increased endothelial permeability.

We have previously shown that NS1 leads to activation of key endothelial cell-intrinsic pathways, including the sialidase and cathepsin L/heparanase pathways, and that these contribute to NS1-induced hyperpermeability of human endothelial cells; however, how these enzymes become activated remain unknown. Our results here provide evidence that internalization of NS1 via CME is required for the activation of these pathogenic processes, furthering our understanding of how these pathways interact with NS1.

Because both WT and N207Q NS1 are able to bind HPMEC and colocalize with clathrin, but only WT NS1 colocalizes with Rab5, we hypothesize that NS1 initially binds to endothelial cells via heparan sulfate, an interaction that has been previously described (87), and then interacts with a second, potentially proteinaceous partner, that triggers endocytosis of the protein and trafficking to the endosome, leading to activation of cathepsin L and/or sialidases. Though we observe some N207Q NS1 inside endothelial cells, it is at a lower level than WT NS1 and is not associated with Rab5, suggesting that N207Q NS1 enters through an alternative pathway that does not result in activation of endothelial cell-intrinsic pathogenic processes. This hypothesis is supported by our findings that Pitstop 2, an inhibitor of CME, prevents NS1 internalization, NS1-induced hyperpermeability, and cathepsin L activation and heparan sulfate degradation. Taken together, these results indicate that NS1 must be internalized by endothelial cells and trafficked to the endosome in order to activate cathepsin L, supporting a potential direct interaction between NS1 and cathepsin L or an interaction of heparan sulfate (potentially bound to NS1) with cathepsin L, as heparan sulfate has been shown to activate cathepsin L (207, 208).

In summary, we have identified a single amino acid, N207, at a glycosylation site of DENV2 and WNV NS1 proteins as a key determinant of NS1-mediated endothelial hyperpermeability. Mutation of DENV2 N207 prevents clathrin-mediated endocytosis of NS1 and inhibits activation of the cathepsin L/heparanase and sialidase pathways and subsequent disruption of endothelial barrier function. Thus, this single glycosylation site is required for the endothelial cell-intrinsic pathogenic functions of DENV2 NS1 and is

crucial for understanding DENV pathogenesis, as well as for developing antiviral therapies and NS1-based vaccine approaches.

Experimental Procedures

Cell culture. HPMEC line HPMEC-ST1.6r was kindly donated by Dr. J.C. Kirkpatrick at Johannes Gutenberg University, Germany, and was grown using the EGM-2 bullet kit (Clonetics, Lonza) and maintained as previously described (84). HBMEC was donated by Dr. Ana Rodriguez at New York University and maintained using endothelial cell medium with growth supplement (ScienCell Research Labs). All cells were maintained at 37˚C in humidified air with 5% CO_2.

Recombinant NS1 proteins. Commercially purchased recombinant NS1 proteins used in this study were obtained from the Native Antigen Company (Oxfordshire, United Kingdom). Recombinant DENV2 (Thailand/16681/84), ZIKV (Uganda MR766 and Suriname Z1106033), and WNV (NY99) NS1 proteins were produced in HEK 293 cells with a purity greater than 95%, composed mostly of oligomeric forms and certified by the manufacturer to be free of endotoxin contaminants. NS1 preparations were also tested using the Endpoint Chromogenic Limulus Amebocyte Lysate QCL-1000TM kit (Lonza) and confirmed to be free of bacterial endotoxins. In-house-produced NS1 proteins were produced in 293F suspension cells and purified by batch method using nickel nitrilotriacetic acid resin agarose beads (Thermo Fisher).

Antibodies, recombinant NS1 proteins, and inhibitors. Staining of EGL components and endothelial enzymes including sialic acid, heparan sulfate, human endothelial heparanase, and cathepsin L were performed using previously described antibodies, lectins, and protocols (88). Primary antibodies against clathrin heavy chain (Clathrin Heavy Chain (D3C6) XP Rabbit mAb (4796S), Cell Signaling), caveolin (Anti-Caveolin-2 antibody EPR5471 (ab133484), Abcam), and Rab5 (Anti-Rab5 antibody - Early Endosome Marker (ab18211), Abcam) and a secondary donkey anti-rabbit IgG conjugated to Alexa 568 (ab175470, Abcam) were used in confocal microscopy experiments. An anti 6x-His-tag mAb (HIS.H8) conjugated to DyLight 488 (Thermo Scientific) was used for NS1 protein binding assays. Selective inhibitors of clathrin-mediated endocytosis (Pitstop 2, Abcam) and dynamin (Dynasore, Sigma) were used in TEER assays and confocal microscopy experiments at concentrations that do not affect cell viability. Cell viability was determined using the Promega CellTox Green Cytotoxicity Assay following the manufacturer's instructions.

Western blot. SDS-PAGE gels were transferred semi-dry onto a polyvinylidene difluoride (PVDF) membrane for 7 minutes (min) at 25V. The membrane was blocked and incubated with primary anti-6x-His-tag antibody overnight. After washing, a goat anti-mouse IgG secondary antibody conjugated to Alexa Fluor 680 (Thermo Fisher) was added at a dilution of 1:5,000 for 1 hour, and blots were imaged using the LI-COR Odyssey imaging system.

Transendothelial Electrical Resistance (TEER). To measure the functional effects of the recombinant NS1 proteins, HPMEC and HBMEC were cultured in duplicate wells (80,000 cells in 0.3 ml) in the apical chamber of 24-well Transwell polycarbonate membrane inserts (Transwell permeable support, 0.4 μm, 6.5 mm insert; Corning Inc.)

and incubated with 5 µg/ml NS1 protein (WT or mutants, 1.5 µg total protein). TEER was measured as previously described (84, 88). Resistance values were measured in Ohms (Ω) at sequential 2-hour time-points following the addition of test proteins using an Epithelial Volt Ohm Meter (EVOM) with “chopstick” electrodes (World Precision Instruments). Untreated endothelial cells grown on Transwell inserts were used as negative untreated controls, and inserts with medium alone were used for blank resistance measurements. Relative TEER represents a ratio of resistance values (Ω) as follows: (Ω experimental condition - Ω medium alone)/(Ω non-treated endothelial cells - Ω medium alone). For experiments using inhibitors, compounds were added to the apical compartment of the Transwell 30 minutes before the addition of DENV NS1 protein.

NS1 protein binding assay. Confluent HPMEC monolayers grown on gelatin-coated coverslips (0.2%, Sigma) were exposed to 5 µg/ml of DENV2 WT NS1 from the Native Antigen Company (Oxfordshire, UK) as a positive control, WT NS1, or N207Q mutant NS1 and incubated for 1 hour at 37°C or 4°C or 6 hours at 37°C. An anti-6x-His-tag antibody conjugated to DyLight 488 (TFS) was used to detect NS1 protein bound to the cell surface. Untreated cells were used as a negative control. Images were acquired using a Zeiss LSM 710 AxioObserver-34-channel spectral detector confocal microscope and processed using ImageJ software.

Fluorescent Microscopy. HPMEC were grown and imaged as described above. To assess the effect of flavivirus NS1 on the integrity of EGL components such as Sia and HS, HPMEC monolayers were treated with WT DENV2 NS1 (Native Antigen or produced in-house) or N207Q mutant NS1 proteins (5 µg/ml) and fixed with 2% paraformaldehyde (PFA) at different time-points (1, 6 hpt). A primary antibody against HS (clone F58-10E4, Amsbio) was incubated overnight at 4°C, and detection was performed using a secondary goat anti-mouse IgM antibody conjugated to Alexa 488 (Thermo Fisher). The cell surface expression of Sia was visualized using the lectin wheat germ agglutinin (WGA) conjugated to Alexa 647 (TFS) (88). The proteolytic activity of cathepsin L was evaluated using the Magic Red assay cathepsin L detection kit (ImmunoChemistry Technologies) (88). A primary antibody against clathrin heavy chain (Clathrin Heavy Chain (D3C6) XP Rabbit mAb, Cell Signaling) was incubated overnight at 4°C, and detection was performed using a secondary donkey anti-rabbit IgG conjugated to Alexa 568 (Abcam). A primary antibody against caveolin (Anti-Caveolin-2 antibody EPR5471, Abcam) was incubated overnight at 4°C, and detection was performed using a secondary donkey anti-rabbit IgG conjugated to Alexa 568 (Abcam). For experiments using inhibitors, compounds were added to wells 30 minutes before the addition of DENV NS1 protein. Nuclei were stained with Hoechst (blue). Untreated cells were used as a control for basal Sia and HS expression and cathepsin L activity. Images were acquired using the Zen 2010 software (Zeiss) and analyzed with ImageJ software. For representative pictures, an area of ~1.8 μm^2 (1.25x1.40 µm) containing ~28-30 cells was used. For MFI quantification, the threshold for each individual channel (RGB) was adjusted and converted to grayscale. Then, mean grayscale values and integrated density from selected areas were obtained,

along with adjacent background readings, and plotted as mean fluorescence intensity (MFI).

DENV2 NS1 protein internalization in HPMEC. To evaluate the internalization of DENV NS1 proteins in HPMEC, we used Western blot and immunofluorescence assay (IFA). Briefly, confluent monolayers (pre-chilled 10 min at 4°C) grown on culture plates and/or glass coverslips were exposed to 10 µg/ml of different NS1 proteins (as indicated above) and incubated for 45 min at 4°C to facilitate NS1 protein adsorption but not internalization. Then, plates were transferred to 37°C to allow protein internalization. One hour later, cell supernatants were removed, and cell monolayers were rinsed 3X with PBS and detached with trypsin-EDTA, which also removed any surface-bound, non-internalized NS1 proteins from the outer cell membrane. Cells were pelleted and lysed using radioimmunoprecipitation assay (RIPA) buffer (TFS) supplemented with a protease inhibitor cocktail. Total protein, quantified by BCA (TFS), was separated (15 µg total protein/lane) using an SDS-PAGE gradient gel (4-20%), and visualized by Western blot with primary anti-NS1 mAbs (1G5.3 and 1H7.4) (209) and secondary anti-mouse antibody conjugated to Alexa 750 (Abcam, ab175740). α-Tubulin was used as a protein loading control (anti α-tubulin ab 4074, Abcam), and Rab5 was used as an endosome marker (Abcam, ab18211). Anti-rabbit IgG conjugated to Alexa 680 was used as secondary antibody (Abcam, ab175773). Images were acquired and processed using a LI-COR Odyssey system and ImageJ software, respectively.

Additionally, internalized NS1 (10 µg/ml) was visualized by confocal microscopy by co-staining NS1 and Rab5 (Rab GTPase), a commonly used early endosome marker. Briefly, after 45 min at 4°C (to normalize protein adsorption), plates were transferred to 37°C for 1 hour to facilitate protein internalization. After fixation with 4% PFA, samples were processed by indirect immunofluorescence and confocal microscopy imaging. For experiments using inhibitors, compounds were added to wells 30 minutes before the addition of DENV NS1 protein. Initially, a colocalization plugin analysis in ImageJ software was used to define the colocalizing spots between NS1 and Rab5 in each experimental condition. The amount of spatial overlap between the two signals (NS1, red and Rab5, green) was obtained using four different frames from the maximum projections of two RGB images based on the object-based approach (JACoP) and defined by the Manders' Coefficient as previously described (202).

DENV2 NS1 colocalization with endocytic pathway markers. Confocal microscopy was used to determine whether clathrin-mediated endocytosis or caveolin-mediated uptake contribute to internalization of NS1 by endothelial cells. HPMEC were grown and imaged as described above. Briefly, after 45 min at 4°C (to normalize protein adsorption), plates were transferred to 37°C for 30 minutes to facilitate protein internalization. After fixation with 4% PFA, samples were processed by indirect immunofluorescence and confocal microscopy imaging. Initially, a colocalization plugin analysis in ImageJ software was used to define the colocalizing spots between NS1 and clathrin or caveolin in each experimental condition. The amount of spatial overlap between the two signals (NS1, red

and Rab5, green) was obtained using four different frames from the maximum projections of two RGB images based on the object-based approach (JACoP) and defined by the Manders' Coefficient as previously described (202).

Statistics. Statistical analyses were performed using GraphPad Prism 6 software, and all graphs were generated using Prism 6. For MFI quantification of confocal microscopy images, ordinary one-way ANOVA analyses with multiple comparisons to the WT DENV NS1 from Native Antigen Company and WT DENV NS1 produced in-house using Dunnett’s multiple comparison test was used to determine significance of the effect of DENV NS1 N207Q.

Chapter 5: Flavivirus NS1 triggers tissue-specific vascular endothelial dysfunction reflecting disease tropism

Summary

Flaviviruses cause systemic or neurotropic-encephalitic pathology in humans. The flavivirus non-structural protein 1 (NS1) is a secreted glycoprotein involved in virus replication and immune evasion, as well as vascular leakage during dengue virus (DENV) infection. Here, we demonstrate that NS1 proteins from dengue, Zika (ZIKV), West Nile (WNV), Japanese encephalitis (JEV), and yellow fever (YFV) viruses selectively bind to and alter permeability of human endothelial cell monolayers from lung, dermis, umbilical vein, brain, and liver *in vitro* and cause vascular leakage upon inoculation into mice in a tissue-dependent manner, reflecting the pathophysiology of each flavivirus. Mechanistically, each flavivirus NS1 protein leads to differential disruption of key endothelial glycocalyx components after activation of sialidases, cathepsin L, and heparanase. Our findings reveal a previously unidentified ability of flavivirus NS1 proteins to modulate endothelial barrier function in a tissue-specific manner both *in vitro* and *in vivo*, potentially influencing flavivirus dissemination, pathogenesis and disease.

Introduction

The *Flavivirus* genus consists of enveloped, positive-sense RNA viruses (~11-kb genome) that are transmitted by arthropod vectors, collectively causing hundreds of millions of infections each year. Flaviviruses include medically important mosquito-borne pathogens such as the four dengue virus serotypes (DENV1-4), Zika virus (ZIKV), West Nile virus (WNV), Japanese encephalitis virus (JEV), and yellow fever virus (YFV) (210). In humans, flavivirus infections result in a range of outcomes, from clinically inapparent infections to severe, sometimes fatal disease, characterized by hemorrhagic manifestations and vascular leakage with organ failure (DENV, YFV), meningomyeloencephalitis (JEV, WNV), and congenital Zika syndrome in pregnant women and Guillain-Barré syndrome in adults associated with ZIKV infection (2, 211).

The flavivirus genome encodes three structural proteins (C, prM/M, and E) and seven non-structural (NS) proteins (NS1, NS2A, NS2B, NS3, NS4A, NS4B and NS5). NS1 is a multifunctional viral protein that is secreted as a hexamer by infected cells and circulates in the host bloodstream (146). Inside infected cells, NS1 acts as a cofactor for viral replication and assembly, while the secreted form plays a role in immune evasion by binding and triggering degradation of the complement protein C4 (57, 60, 119) and in dengue pathogenesis via activation of complement (118). Additionally, NS1 has been shown to contribute to dengue pathogenesis by directly triggering endothelial hyperpermeability as well as by inducing the release of vasoactive cytokines from peripheral blood mononuclear cells (PBMCs) via activation of TLR4, both leading to vascular leak (84, 85). Further, DENV NS1 has been shown to directly alter the barrier function of pulmonary endothelial cell monolayers through disruption of the endothelial glycocalyx-like layer (EGL) by triggering the activation of endothelial sialidases, cathepsin L, and heparanase, enzymes responsible for degrading sialic acid and heparan sulfate proteoglycans (88). Importantly, disruption of endothelial glycocalyx components has been shown to correlate with plasma leakage during severe DENV infection (92, 93). More recently, the contribution of these DENV NS1-induced endothelial cell-intrinsic pathways to NS1-mediated vascular leakage was demonstrated to be independent of inflammatory cytokines but dependent on the integrity of endothelial glycocalyx components both *in vitro and in vivo* (89).

NS1 is well-conserved among flaviviruses, exhibiting 20-40% identity and 60-80% similarity (42, 212). During the acute phase of illness in patients with severe dengue disease, DENV NS1 has been shown to circulate at high levels (1-2 μg/ml), correlating with DENV viremia (69). Human studies describing the kinetics of circulating NS1 levels in other flavivirus infections are lacking, although NS1 has been detected in the serum of mice experimentally infected with ZIKV, WNV, JEV, and YFV (140, 213-215). Notably, ZIKV NS1 has been found in placental tissues infected with ZIKV (216). The action of NS1 in relation to vascular leak occurs in capillary beds of tissues, where the cumulative effect of NS1 is likely amplified and/or concentrated.

Here, we demonstrate that NS1 proteins from dengue, Zika, West Nile, Japanese encephalitis, and yellow fever viruses selectively alter the permeability of monolayers of endothelial cell lines derived from distinct human tissues. Additionally, we find that

flavivirus NS1 proteins differentially induce disruption of EGL components, critical determinants of endothelial barrier function (216) and differentially stimulate secretion of inflammatory cytokines from PBMCs. Further, NS1 proteins enhance the extravasation of fluids *in vivo* in a tissue-dependent manner, which correlates with flavivirus pathophysiology. Together, our findings reveal a previously unidentified ability of flavivirus NS1 proteins to modulate endothelial permeability in a tissue-specific manner both *in vitro* and *in vivo*, potentially influencing flavivirus dissemination, pathogenesis, and disease.

Results

Flavivirus NS1 proteins trigger endothelial barrier dysfunction in a tissue-specific manner

Previously, we demonstrated that NS1 proteins from all four DENV serotypes, but not the related WNV, cause a dose-dependent increase in endothelial permeability of human pulmonary microvascular endothelial cells (HPMEC) (84, 88). Further, we showed that DENV2 NS1 alone is able to induce vascular leakage *in vivo* (84, 88, 89). Here, we used a transendothelial electrical resistance (TEER) assay to evaluate the ability of DENV, ZIKV, WNV, JEV, and YFV NS1 proteins to trigger endothelial barrier dysfunction in distinct human endothelial cell monolayers, including pulmonary (HPMEC), dermal (HMEC-1), umbilical vein (HUVEC), brain (HBMEC), and liver (HLSEC) endothelial cells. Recombinant flavivirus NS1 proteins used in all experiments were produced in mammalian cells (HEK 293) and were shown to be >95% pure and oligomeric, as demonstrated by native PAGE followed by silver staining or Western blot analyses. NS1 protein concentrations used in these experiments were based on levels of NS1 circulating in patients with severe dengue disease and on previous studies demonstrating the effect of DENV NS1 on human endothelial cells (84, 88, 89). Interestingly, our results show that the different NS1 proteins trigger hyperpermeability in endothelial cells derived from tissues associated with the viral tropism of each flaviviral disease **(Figure 5.1)**. Specifically, NS1 from DENV, which causes systemic disease, induces endothelial hyperpermeability in all endothelial cells tested, while NS1 from ZIKV, which targets the placenta and developing brain, induces hyperpermeability only in umbilical vein and brain endothelial cells. NS1 from both Uganda and Suriname strains behaved similarly **(Figure 5.S1)**. NS1 from WNV and JEV, which cause encephalitis, induce hyperpermeability only in brain endothelial cells, whereas NS1 from YFV, which is systemic but primarily causes hepatic damage, exerted the strongest effect in liver endothelial cells, with a slight increase of permeability in lung endothelial cells. All endothelial cells demonstrated increased permeability when exposed to the pro-inflammatory cytokine TNF-α as a positive control. However, no increase in permeability was observed with recombinant DENV2 E protein, demonstrating that the hyperpermeability induced is an NS1-specific effect **(Figure 5.1)**. The TEER results were confirmed in a solute flux assay using 70 kDa dextran conjugated to FITC as a tracer in HUVEC monolayers **(Figure 5.S2)**.

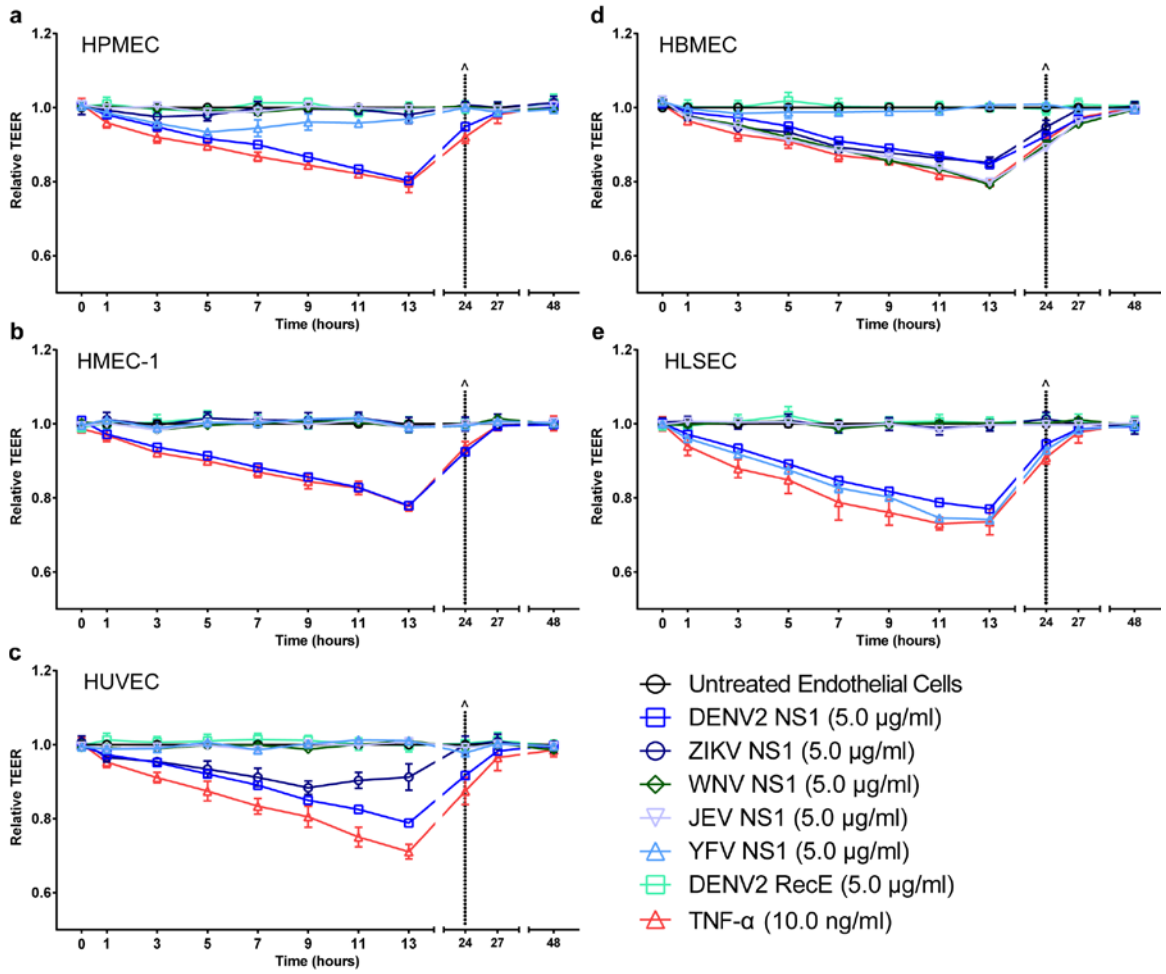

Figure 5.1. Flavivirus NS1 proteins trigger endothelial barrier dysfunction *in vitro* in a tissue-specific manner.
Human endothelial cells from different tissues **(a)** lung, **(b)** skin, **(c)** umbilical vein, **(d)** brain, and **(e)** liver, were grown on Transwell semi-permeable membranes (0.4 µm pore size), and distinct flavivirus NS1 proteins (5 µg/ml) were added to the apical chamber. TNF-α (10 ng/ml) was used as a positive control, and DENV2 recombinant envelope (E) protein (5 µg/ml, 1.5 µg of total protein) was used as a negative control. A TEER assay was used to evaluate the effect of these NS1 proteins on endothelial permeability at indicated time-points over 48 hours. (^) represents change of medium. Relative TEER values from two independent experiments performed in duplicate are plotted. Error bars indicate standard error of the mean (SEM).

In addition to our endothelial permeability assays, we assessed the ability of each flavivirus NS1 protein to interact with the surface of the different human endothelial cells *in vitro* by performing NS1 binding assays. Briefly, NS1 proteins were added to confluent monolayers of human endothelial cells, and the amount of NS1 bound to the surface of the endothelial cell monolayers was determined by immunofluorescence microscopy. At 1 hour post-treatment (hpt), all NS1 proteins showed a binding pattern that reflected their capacity to selectively induce endothelial hyperpermeability as measured by TEER

(Figures 5.2a-e, 5.S3). DENV NS1 bound in a dose-dependent manner to the surface of all endothelial cells, showing maximum binding to pulmonary endothelial cells. ZIKV NS1 showed highest protein binding to the surface of umbilical vein endothelial cells and brain endothelial cells. WNV NS1 and JEV NS1 only exhibited increased binding capacity to the surface of brain endothelial cells. Surprisingly, YFV NS1 bound to all endothelial cells; however, significantly higher amounts were found on the surface of liver endothelial cells **(Figures 5.2, 5.S3, 5.S4)**. These binding patterns were confirmed by Western blot of cell lysates from confluent monolayers of human endothelial cells exposed to 10 µg/ml of individual flavivirus NS1 proteins for 1 hour **(Figures 5.2f-j, 5.S4)**. Furthermore, the specificity of these interactions of NS1 with the surface of human endothelial cells was corroborated by testing the effect of an anti-6x-His-tag monoclonal antibody (mAb) and an NS1-specific mAb (2B7) on DENV NS1-induced barrier dysfunction of HPMEC as measured by TEER **(Figure 5.S5a)** and also NS1 interaction with HPMEC and 293 cells by immunofluorescence microscopy and flow cytometry, respectively **(Figure 5.S5b,c)**. As expected, the anti-6x-His-tag mAb does not prevent either DENV NS1-induced hyperpermeability of HPMEC or NS1 binding to HPMEC and 293 cells. However, the anti-NS1 mAb (2B7) blocked the barrier dysfunction induced by NS1 in HPMEC as well as NS1 binding to 293 cells. These results indicate that the different flavivirus NS1 proteins have the ability to bind to distinct tissue-specific endothelial cells, potentially leading to the endothelial dysfunction and hyperpermeability identified in the TEER assay **(Figure 5.1)**.

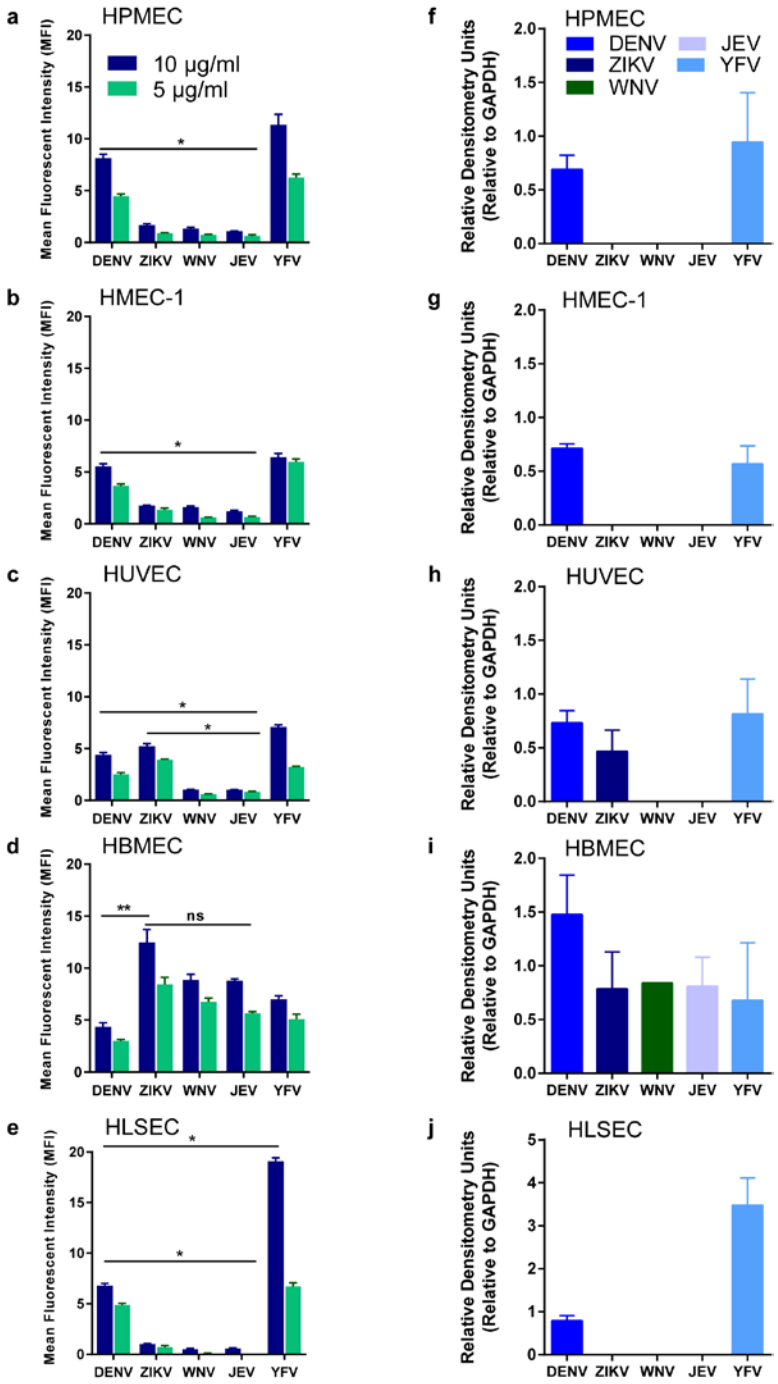

Figure 5.2. Flavivirus NS1 proteins bind differentially to the surface of distinct human endothelial cells.

Binding of flavivirus NS1 proteins to the surface of different human endothelial cell monolayers as measured by **(a-e)** confocal microscopy or **(f-j)** Western blot. **(a)** HPMEC, **(b)** HMEC-1, **(c)** HUVEC, **(d)** HBMEC, and **(e)** HLSEC were grown on cover slips and treated with 5 (1.5 µg of total protein) or 10 µg/ml NS1 (3 µg of total protein) (source confocal microscopy images not shown); binding was evaluated 1 hour post-treatment (hpt). The amount of bound NS1 was quantified and expressed as MFI. Cell lysates from **(f)** HPMEC, **(g)** HMEC-1, **(h)** HUVEC, **(i)** HBMEC, and **(j)** HLSEC treated with 10 µg/ml of flavivirus

NS1 protein were collected 1 hpt and analyzed by Western blot (source Western blot images not shown). All graphs show the average of quantification from two independent experiments run in duplicate. Error bars indicate SEM. In **(a-e)**, statistically significant differences between distinct treatment groups were determined by ANOVA and unpaired t-tests as indicated, with *, $P < 0.05$ and **, $P < 0.01$. **(a-e)** Colors in bars represent protein concentrations as follows: green, 5 µg/ml; and blue, 10 µg/ml.

Flavivirus NS1 proteins induce degradation of EGL components after triggering sialidase and cathepsin L/heparanase activation in human endothelial cells *in vitro*

The EGL is a network of glycosaminoglycans and membrane-bound proteoglycans and glycoproteins expressed on the endothelium that lines the luminal surface of blood vessels and contributes to barrier function critical for vascular homeostasis (36). In previous studies, we demonstrated that DENV but not WNV NS1 activates endothelial cell-intrinsic pathways that lead to barrier dysfunction of HPMEC *in vitro*. NS1 triggered the loss of sialic acid from the cell surface upon activation of endothelial sialidases as well as the shedding of heparan sulfate proteoglycans by activating endothelial cathepsin L and heparanase (88). To establish whether different flavivirus NS1 proteins induce endothelial cell-specific barrier dysfunction via activation of similar mechanisms, polarized monolayers of HPMEC, HMEC-1, HUVEC, HBMEC, and HLSEC were exposed to the different flavivirus NS1 proteins. The integrity of EGL components was evaluated 6 hpt using immunofluorescence staining for sialic acid **(Figure 5.3)**, heparan sulfate **(Figure 5.4)** and syndecan-1, a major heparan sulfate-bearing proteoglycan that supports the integrity of the EGL (180) **(Figure 5.S6)**. DENV NS1 induced disruption of sialic acid on all endothelial cells, with significant reductions in sialic acid expression that ranged from 20% to 80% depending on the endothelial cell type. Reflecting the pattern observed in endothelial permeability **(Figure 5.1)**, we found that ZIKV NS1 disrupted sialic acid in both HUVEC and HBMEC, whereas WNV NS1 and JEV NS1 only disrupted sialic acid on HBMEC. Significant reduction in the expression of sialic acid on HLSEC was only observed in response to YFV NS1 **(Figure 5.3)**. Regarding the expression of heparan sulfate and syndecan-1, degradation of heparan sulfate after treatment with the distinct flavivirus NS1 proteins was detected on the surface of the different human endothelial cells after 6 hpt following a pattern that reflected our observations for sialic acid expression **(Figure 5.4)**. In parallel, accumulation of syndecan-1, whose ectodomain binds back to the surface of endothelial cells after being shed (180), was detected on the surface of the different endothelial cells 6 hpt in a similar pattern **(Figure 5.S6)**. Thus, disruption of EGL components was also determined by the flavivirus NS1 protein and the tissue-specific endothelial cell.

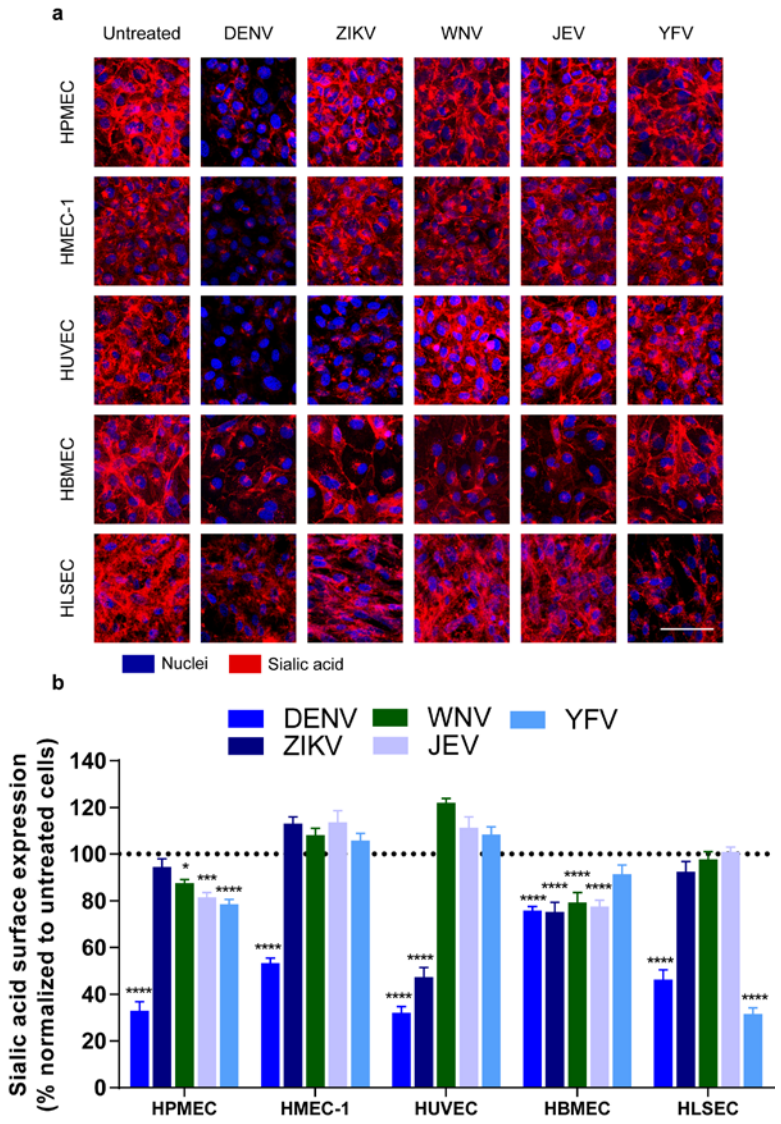

Figure 5.3. Flavivirus NS1 proteins alter the expression of sialic acid on the surface of endothelial cells in a cell type-dependent manner.
(a) Sialic acid expression on human endothelial cell monolayers grown on coverslips 6 hpt with different flavivirus NS1 proteins (5 µg/ml), examined by confocal microscopy. Sialic acid was stained with WGA-A647 (red). Nuclei were stained with Hoechst (blue). Images (20X) are representative of three independent experiments. Scale bar, 10 µm. **(b)** Quantification of MFI in **(a)** from three independent experiments. Error bars indicate SEM. Reduction of sialic acid expression in NS1-treated monolayers was normalized to untreated controls. Statistically significant differences between distinct treatment groups were determined using an ordinary two-way ANOVA with multiple comparisons to untreated cells using Dunnett's multiple comparison test, with *, $P < 0.05$; ***, $P < 0.001$; ****, $P < 0.0001$. Confocal microscopy images acquired and analyzed by Dr. Henry Puerta-Guardo.

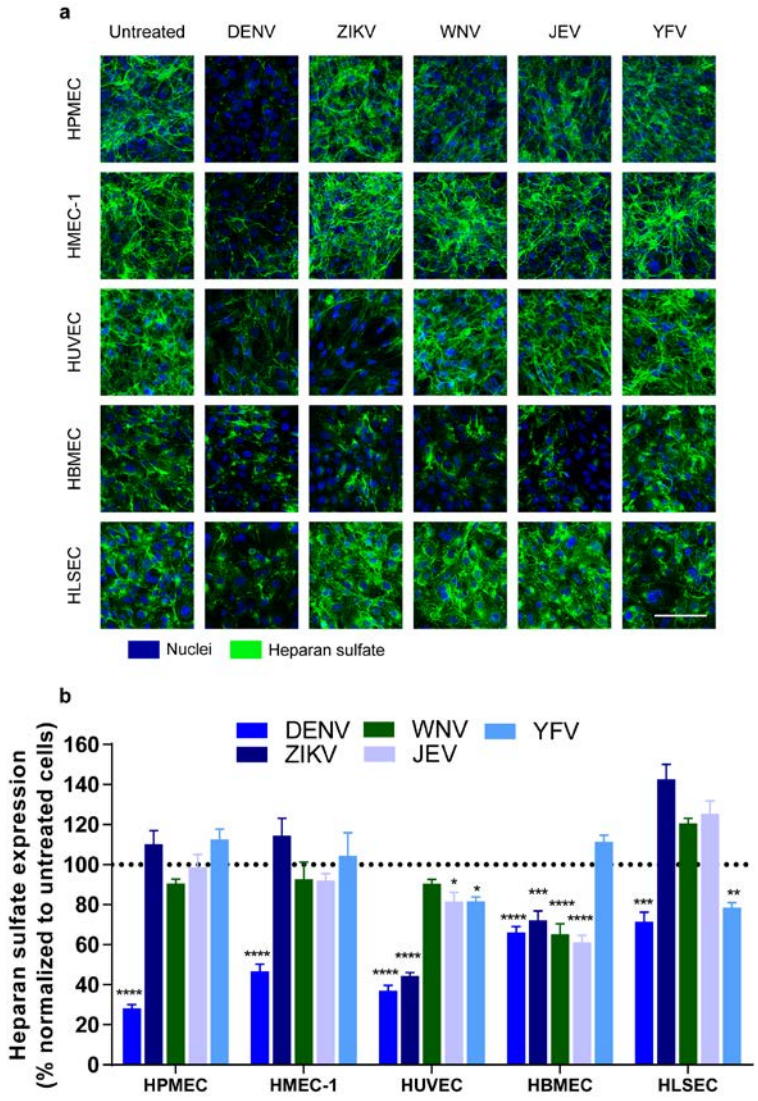

Figure 5.4. Flavivirus NS1 proteins alter the expression of heparan sulfate on the surface of endothelial cells in a cell type-dependent manner.
(a) Heparan sulfate expression on human endothelial cell monolayers grown on coverslips 6 hpt with different flavivirus NS1 proteins (5 µg/ml, 1.5 µg of total protein), examined by confocal microscopy. Heparan sulfate was stained with anti-heparan sulfate mAb (in green). Nuclei were stained with Hoechst (blue). Images (20X) are representative of three independent experiments. Scale bar, 10 µm. **(b)** Quantification of MFI in **(a)** from three independent experiments. Error bars indicate SEM. Reduction of heparan sulfate expression in NS1-treated monolayers was normalized against untreated controls. Statistically significant differences between distinct treatment groups were determined using an ordinary two-way ANOVA with multiple comparisons to untreated cells using Dunnett's multiple comparison test, with *, $P < 0.05$; **, $P < 0.01$; ***, $P < 0.001$; ****, $P < 0.0001$. Confocal microscopy images acquired and analyzed by Dr. Henry Puerta-Guardo.

In addition to the alterations of sialic acid and heparan sulfate expression induced by flavivirus NS1 proteins, we also evaluated the activity and expression of endothelial

cathepsin L and the expression of the endoglycosidase heparanase, enzymes involved in the degradation of EGL components (88, 89). Compared to untreated monolayers, DENV NS1 increased the expression and activity of cathepsin L in all endothelial cells **(Figure 5.5a,b)**. ZIKV NS1 increased levels of cathepsin L expression and proteolytic activity in cultures of umbilical vein endothelial cells and brain endothelial cells. NS1 proteins from DENV, ZIKV, WNV and JEV, but not from YFV, modulated the expression levels of cathepsin L and increased its activity in brain endothelial cells. Finally, YFV NS1 stimulated the proteolytic activity of cathepsin L in liver endothelial cells to levels 25-fold higher than untreated controls, whereas ZIKV NS1, WNV NS1, and JEV NS1 triggered no response **(Figure 5.5a,b)**. We also examined the maturation state of cathepsin L on different endothelial cells exposed to distinct NS1 proteins at 6 hpt. Densitometry analyses of Western blots revealed expression of the pro-cathepsin L form in all the endothelial cells exposed to different NS1 treatments but increased appearance of the active form of cathepsin L **(Figure 5.5c-e)** that reflected the results obtained using the fluorescence proteolytic activity assay **(Figure 5.5a,b)** and correlates with the patterns of hyperpermeability observed in **Figure 5.1**. Because proteolytic activity of cathepsin L is required for the activation of heparanase and subsequent trimming of heparan sulfate from the EGL (164), we also examined the expression of heparanase in endothelial cells after NS1 stimulation using immunofluorescence microscopy. As expected, we observed a similar cell type- and NS1-dependent pattern of heparanase expression compared to the cathepsin L results **(Figure 5.5f)**.

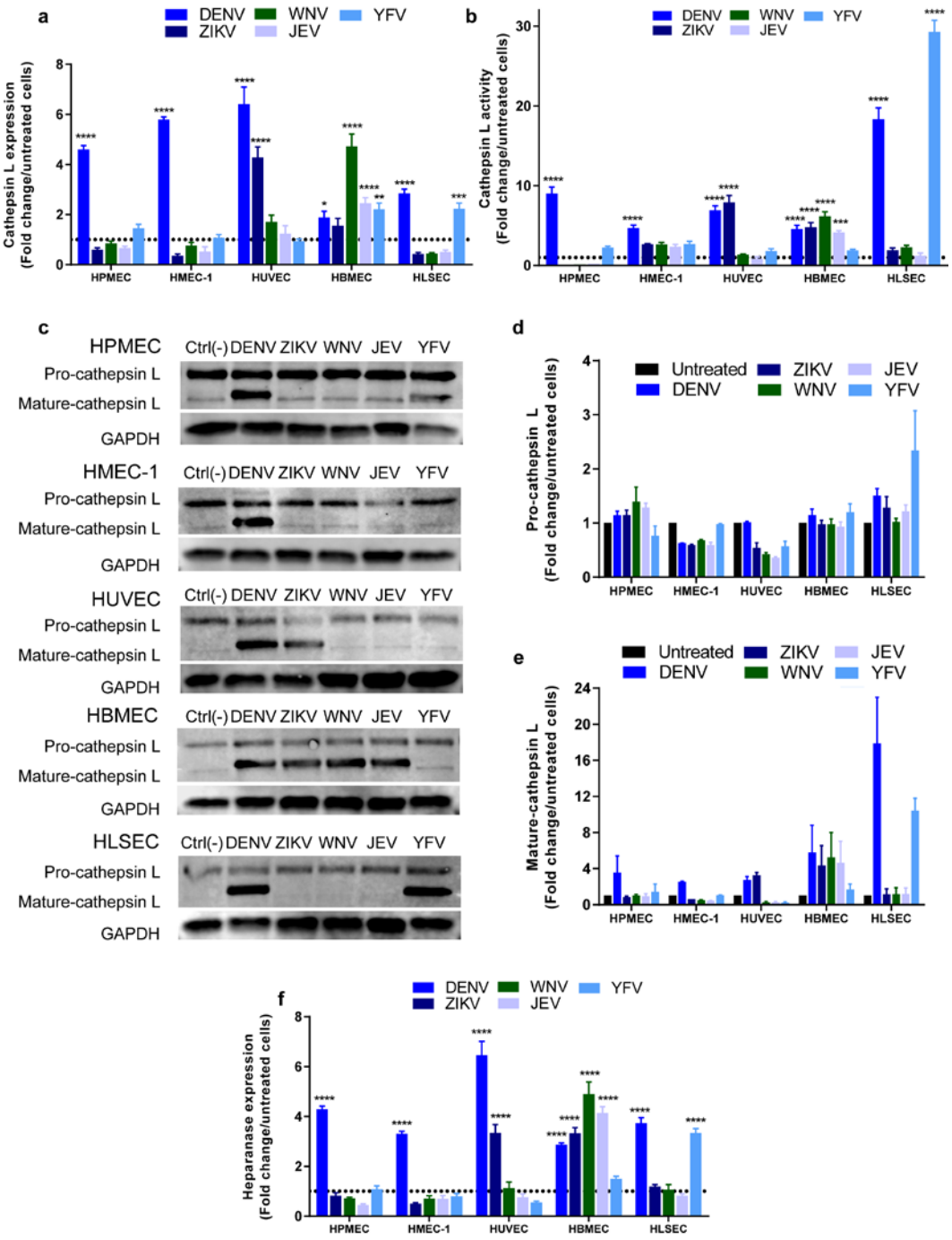

Figure 5.5. Flavivirus NS1 proteins modulate the expression and activity of endothelial cathepsin L and heparanase in a cell type-dependent manner.
(a,b) Fold-change over untreated controls of the quantification of MFI from three independent confocal microscopy experiments examining the **(a)** expression and **(b)** activity of cathepsin L in human endothelial cell monolayers 6 hpt with different flavivirus NS1 proteins (5 μg/ml, 1.5 μg of total protein) (source confocal microscopy images not shown). **(c)** Western blot data of pro-cathepsin L and mature-cathepsin L expression in human endothelial cell monolayers 6 hpt with different flavivirus NS1 proteins (5 μg/ml). **(d,e)** Densitometry of bands in **(c)** for **(d)** pro-cathepsin L and **(e)** mature-cathepsin L with

values normalized to GAPDH and expressed as fold change from untreated monolayers. **(f)** Fold-change over untreated controls of the quantification of MFI from three independent confocal microscopy experiments examining the expression of heparanase in human endothelial cell monolayers 6 hpt with different flavivirus NS1 proteins (5 µg/ml, 1.5 µg of total protein) (source confocal microscopy images not shown). For all graphs, error bars indicate SEM. Statistically significant differences between distinct treatment groups were determined using an ordinary two-way ANOVA with multiple comparisons to untreated cells using Dunnett's multiple comparison test, with *, $P < 0.05$; **, $P < 0.01$; ***, $P < 0.001$; ****, $P < 0.0001$.

Additionally, the expression of endothelial sialidases (Neu1, Neu2, Neu3), glycosidases that catalyze the removal of terminal sialic acids of glycoproteins and glycolipids, was evaluated on endothelial cells treated with the different flavivirus NS1 proteins **(Figure 5.S7)**. Compared to untreated cells, flavivirus NS1 proteins led to increased expression of Neu1, Neu2, and Neu3 in a cell type-dependent manner at 6 hpt. In the case of DENV NS1, which increased the permeability of different endothelial cells, Neu2 was the most upregulated sialidase in all endothelial cells, followed by Neu3 and Neu1. ZIKV NS1 upregulated the expression of Neu2 and Neu3 in HUVEC. Regarding the encephalitic flaviviruses including WNV and JEV NS1 proteins, only HBMEC showed significant changes in the expression of the three sialidases. Finally, for YFV NS1, which significantly increased the permeability of liver endothelial cells, the expression of Neu2 and Neu3 was significantly upregulated only in HLSEC, with some increase in Neu2 in HPMEC, also consistent with the patterns observed above.

Flavivirus NS1 proteins differentially stimulate secretion of inflammatory cytokines from human PBMCs

It was previously reported that DENV2 NS1 triggers production of inflammatory cytokines from human PBMCs via activation of TLR4 (85). To evaluate the effect of different flavivirus NS1 proteins on PBMC production of cytokines, we treated human PBMCs in culture with DENV, ZIKV (from both Uganda and Suriname strains), WNV, JEV, and YFV NS1 proteins; 10 ng/ml of lipopolysaccharide (LPS) was used as a positive control, and untreated PBMCs were used as a baseline for cytokine secretion from cultured cells. 24 hpt, we collected supernatant and performed enzyme-linked immunosorbent assays (ELISAs) for interleukin (IL)-6 **(Figure 5.6a,b)**, IL-8 **(Figure 5.6c,d)**, and TNF-α **(Figure 5.6e,f)**. We found that NS1 from both ZIKV strains and WNV stimulated production of IL-6 and IL-8 at levels comparable to LPS; treatment with ZIKV (Uganda) resulted in high levels of TNF-α secretion, while ZIKV (Suriname) and WNV) were markedly lower. NS1 from DENV and YFV stimulated detectable levels of all three cytokines but were substantially lower than ZIKV and WNV **(Figure 5.6b,d,f)**. Interestingly, JEV NS1 produced an intermediate phenotype. These data suggest that, in addition to NS1- and tissue-specific effects on the vascular endothelium, NS1 from different flaviviruses stimulates production of inflammatory cytokines from human PBMCs at varying levels, potentially contributing to inflammation and disease.

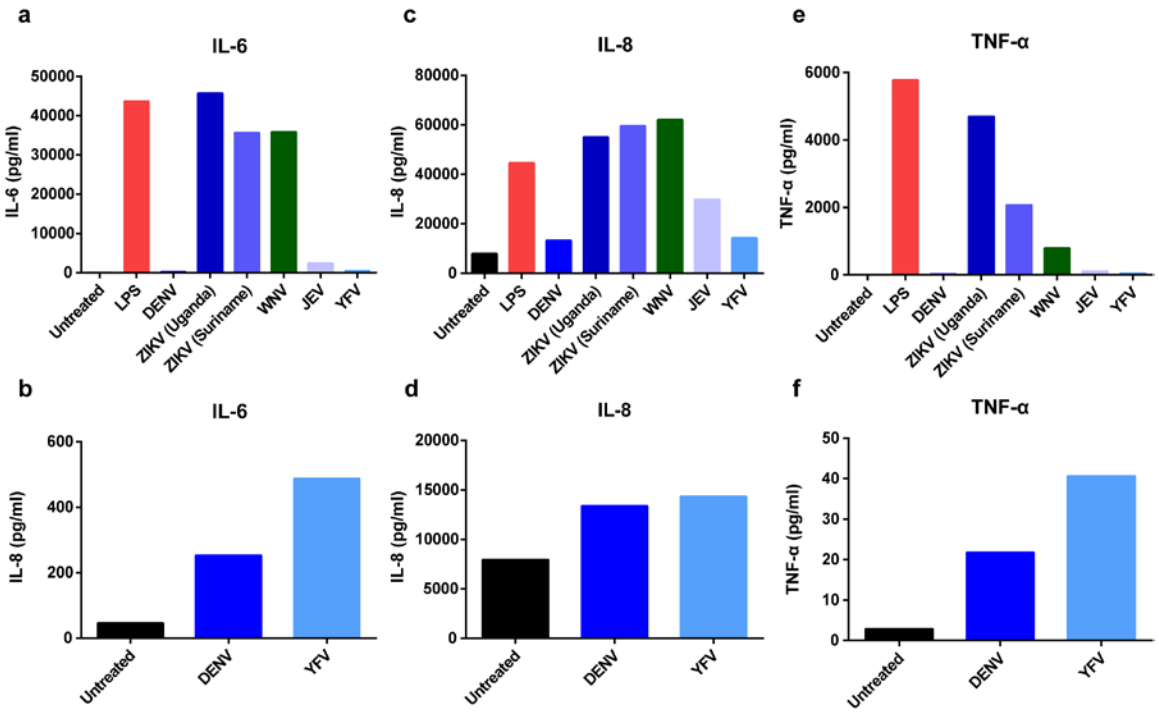

Figure 5.6. Flavivirus NS1 proteins differentially stimulate secretion of inflammatory cytokines from human PBMCs.
Primary human PBMCs were cultured *in vitro* and treated with LPS as a positive control (10 ng/ml; red) or flavivirus NS1 proteins (5 µg/ml: DENV2, blue; ZIKV (Uganda), dark blue; ZIKV (Suriname), cornflower; WNV, green; JEV, lavender; YFV, sky blue). 24 hpt, supernatant was collected and analyzed for **(a,b)** IL-6, **(c,d)** IL-8, or **(e,f)** TNF-α by ELISA. Untreated PBMCs in culture were used as a baseline control. **(b-d)** Data for untreated and DENV- and YFV-treated PBMCs are graphed on a smaller y-axis scale for detail.

Flavivirus NS1 proteins cause increased vascular leakage in a tissue-dependent manner and induce disruption of endothelial glycocalyx components *in vivo*

We next examined the ability of NS1 proteins from different flaviviruses to cause localized dermal or systemic vascular leakage *in vivo* using murine models. To evaluate dermal leak, we performed a fluorescent dextran-adapted Miles assay as previously described (89). Briefly, following intradermal injection of recombinant NS1 proteins, fluorescently-labeled (A680) dextran was delivered intravenously, and two hours later, leakage in the dorsal dermis was visualized using a fluorescence detection system. We found that only DENV NS1, but not ZIKV NS1, WNV NS1, JEV NS1 or YFV NS1, induced a significant increase in vascular leakage in the murine dermis compared to injection of PBS **(Figures 5.6a,b, 5.S8)**. To characterize the systemic effects of flavivirus NS1, we used a traditional Miles assay to evaluate induction of vascular leak in organs including brain, lungs, and liver. Mice were inoculated with 10 mg/kg of flavivirus NS1, an amount that leads to circulating levels of NS1 equivalent to human DHF/DSS cases (69, 84). Three days post-inoculation (dpi), animals were administered Evans Blue dye (EBD) or Alexa Fluor 680-

labeled dextran for downstream tissue extraction or fluorescent imaging, respectively. Following inoculation of DENV NS1, increased amounts of EBD were detected in the lungs and liver **(Figure 5.6c,d)**. However, consistent with previous studies (84), no significant extravasation of EBD was observed in these organs after inoculation of 10 mg/kg of ovalbumin (OVA). YFV NS1 was the only other NS1 protein to induce significantly higher levels of EBD leakage in the liver **(Figure 5.6d)**. In addition to the Miles assay, we also examined vascular leak in the brain and lung by measuring the accumulation of fluorescently-labeled dextran. Intravenous administration of DENV NS1, ZIKV NS1, and WNV NS1 proteins resulted in significant accumulation and extensive leakage of dextran in brain tissue compared to OVA and YFV NS1 treatments **(Figure 5.6e,g)**. In the lungs, accumulation of dextran following inoculation with DENV NS1 resembled the extravasation pattern observed with EBD in the Miles assay, with large areas of increased mean fluorescence intensity (MFI) that result from the accumulation of dextran in tissue **(Figure 5.6f,h)**. In contrast, administration of WNV NS1 and OVA (used as a protein control) resulted in no dextran accumulation **(Figure 5.6f,h)**. Using this assay, mice inoculated with YFV NS1 and ZIKV NS1 proteins showed areas of leakage in the lung with increased MFI for dextran compared to OVA but substantially less than DENV NS1, suggesting a minimal level of vascular leak from the inoculation **(Figure 5.6f,h)**. Finally, to evaluate the impact of flavivirus NS1 proteins on vascular leakage *in vivo*, we investigated the effect of intravenous administration of recombinant NS1 proteins on the circulation of heparan sulfate, a major glycosaminoglycan used as an indirect marker of endothelial glycocalyx integrity *in vivo*. Compared to untreated mice and mice treated with OVA (used as protein control), administration of DENV, YFV, and, to a lesser extent, WNV NS1 proteins led to increased serum levels of heparan sulfate (DENV $P < 0.05$; YFV $P < 0.01$) **(Figure 5.6i)**, suggesting that shedding of heparan sulfate may be a consequence of activation of the Cathepsin L/heparanase pathway by NS1.

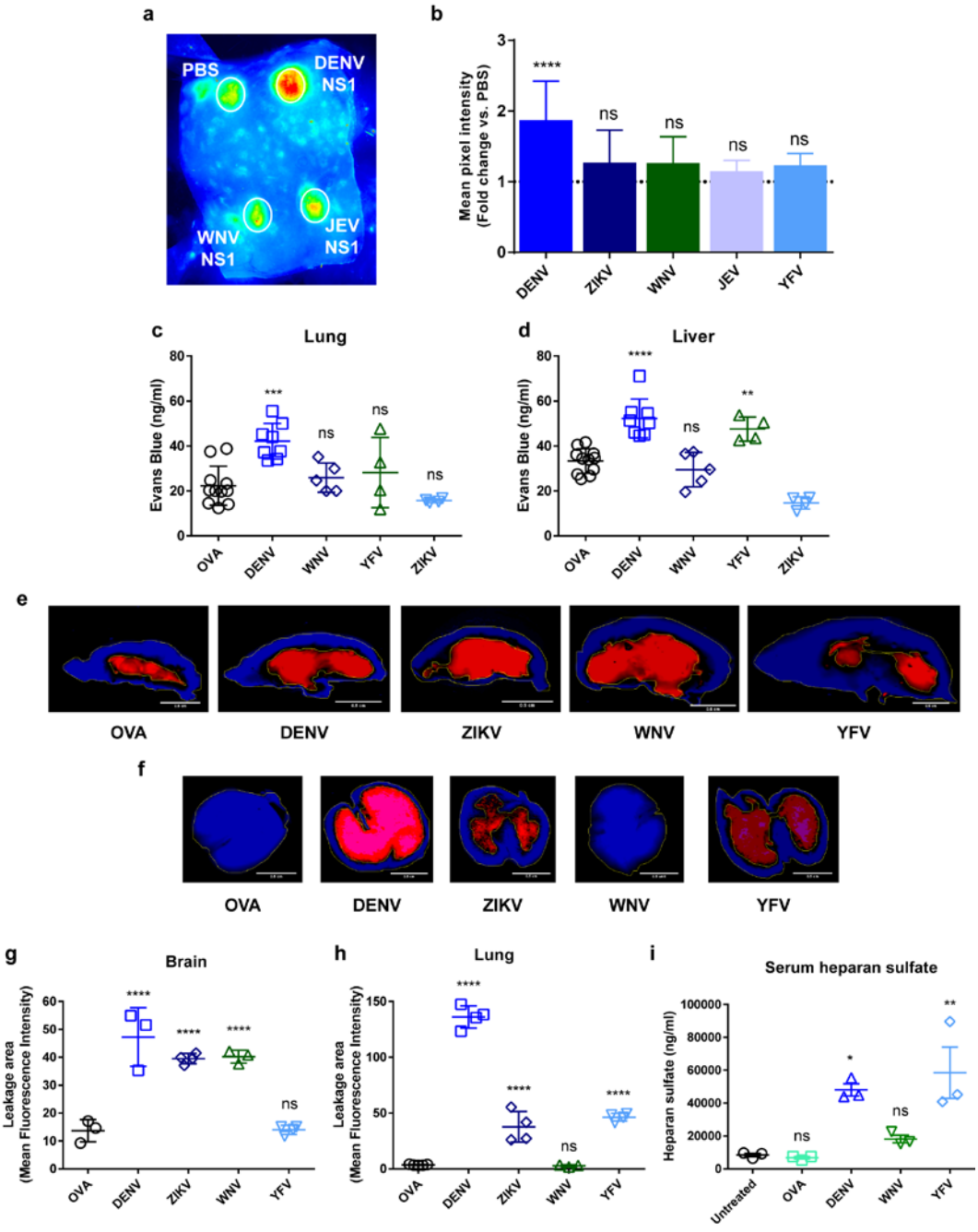

Figure 5.7. Flavivirus NS1 proteins induce differential local and systemic vascular leakage *in vivo*. Wild-type C57BL/6 mice were used to evaluate **(a,b)** local or **(c-h)** systemic vascular leakage induced by flavivirus NS1 proteins injected either **(a,b)** intradermally (dorsal dermis) or **(c-h)** intravenously with 15 µg and 200 µg (10 mg/kg) of total protein concentration, respectively. The magnitude of the vascular leakage induced by these proteins was evaluated by using **(a,b, e-h)** dextran-A680 (10 mg/ml) or **(c,d)** EBD (0.5%) and quantified by **(a,b, e-h)** fluorescent imaging or **(c,d)** spectrophotometric analyses. **(a,e,f)** Images (LI-COR Odyssey) and **(b-d, g,h)** MFI values are representative of two individual experiments (n = 3-6 per group). EBD was extracted from harvested tissues in formamide and quantified by measuring absorbance at OD_{610} against an EBD-standard curve. Ovalbumin (OVA, 10 mg/kg) and PBS were used

as controls for systemic and local vascular leakage experiments, respectively. **(i)** Levels of heparan sulfate detected in serum of mice (n = 3 per group) treated with ovalbumin (OVA, 10 mg/kg), DENV2 NS1 (10 mg/kg), WNV NS1 (10 mg/kg), or YFV NS1 (10 mg/kg) as measured by ELISA. Untreated mice were used as a steady-state control. For dextran-adapted dermal Miles assay, data were derived from three independent experiments and expressed as the fold-change ratio of the MFI obtained in each individual treatment group compared to PBS injection. For the fluorescent systemic leakage assay, MFI was measured inside the leakage area by drawing a standard circular area in each treatment condition using ImageJ tools. Statistically significant differences were determined by nonparametric Mann-Whitney analysis and ordinary one-way ANOVA with multiple comparisons between distinct experimental groups. ns, not significant; *, $P < 0.05$; **, $P < 0.01$; ***, $P < 0.001$; ****, $P < 0.0001$. Error bars indicate SEM. Scale bars, 0.5 cm.

Discussion

In this study, we describe the ability of NS1 proteins from DENV, ZIKV, WNV, JEV, and YFV to cause hyperpermeability of cultured polarized human endothelial cells derived from different tissues including lung, skin, umbilical vein, brain, and liver as measured by TEER. These findings are supported by *in vivo* data collected using both Evans Blue dye (Miles assay) and a fluorescent dye (Dextran-adapted Miles assay), showing that flavivirus NS1 proteins can differentially and selectively induce vascular leakage in distinct organs including lung, skin, brain, and liver, reflecting respective flaviviral pathophysiology. We found that DENV NS1 induced hyperpermeability in all tested human endothelial cells, with maximal effects observed on pulmonary endothelial cells. DENV NS1 also stimulated vascular leak in all evaluated organs upon inoculation into mice. ZIKV NS1 increased the permeability of umbilical vein and brain endothelial cells *in vitro* and caused vascular leakage in the brain *in vivo*, whereas WNV NS1 and JEV NS1 only induced permeability of brain endothelial cells and substantial vascular leakage in the mouse brain. NS1 from YFV significantly increased the permeability of endothelial cells derived from liver and, to a lesser extent, lung, and this same pattern was seen in murine organs *in vivo*. Mechanistically, the observed hyperpermeability *in vitro* is related to disruption of the EGL components sialic acid, heparan sulfate, and syndecan-1 following upregulation of sialidases as well as cathepsin L expression and activity and subsequent expression of heparanase, enzymes known to contribute to the degradation of cellular glycosaminoglycans and proteoglycans in the EGL. Taken together, our results indicate that flavivirus NS1 proteins modulate endothelial permeability in a tissue-specific manner both *in vitro* and *in vivo*, potentially influencing flavivirus dissemination, pathogenesis, and disease **(Figure 5.8)**.

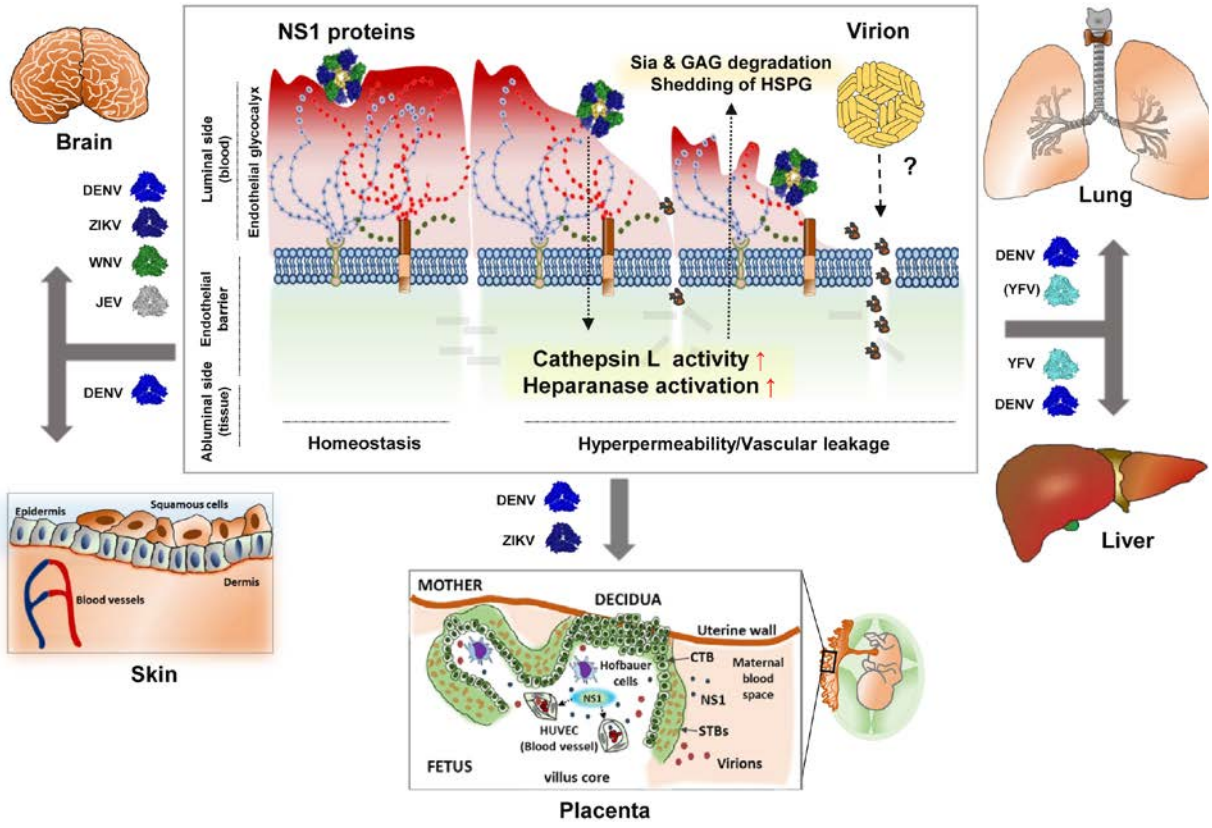

Figure 5.8. Model of flavivirus NS1-induced endothelial cell type-dependent hyperpermeability and tissue-specific vascular leakage and its potential contribution to flavivirus pathogenesis and disease.

Flavivirus infections can affect specific tissues including brain, lung, skin, liver, and also the placenta during pregnancy to cause neurotropic-encephalitic or systemic diseases in humans. Infection with any of the flaviviruses leads to secretion of NS1, a soluble viral protein that directly triggers increased endothelial hyperpermeability and vascular leakage associated with the disruption of key components of the endothelial glycocalyx layer, which lines the luminal surface of endothelial cells in the vasculature. The EGL is composed of monosaccharides, such as sialic acid (Sia), glycosaminoglycans (GAGs), such as heparan sulfate, and heparan sulfate proteoglycans (HSPGs), such as syndecan-1. Here, we describe an endothelial cell type-dependent increase in permeability and vascular leakage induced by different flavivirus NS1 proteins that reflects the disease pathogenesis of distinct flavivirus infections. DENV NS1 increases the permeability of endothelial cells from multiple tissues such as lung, skin, umbilical vein, brain, and liver, consistent with the systemic disease caused by DENV. ZIKV NS1 induces endothelial dysfunction of umbilical vein and brain endothelial cells, reflecting severe congenital and neurological defects associated with Zika, while WNV and JEV NS1 only affect the barrier function of brain endothelial cells, in line with the neurotropic and encephalitic nature of WNV and JEV disease. Finally, YFV NS1 increases the permeability of lung and especially liver endothelial cells, consistent with hepatic and systemic pathology of yellow fever virus. This selective permeability may contribute to the pathogenesis of the different flaviviruses by either inducing extravasation of fluids that results in inflammation of tissues or facilitating virus dissemination into target organs that may lead to enhanced viral infection and disease.

Clinically, severe WNV and JEV infections, as well as fetal ZIKV infections during pregnancy, primarily result in cerebrovascular disease with encephalitis or congenital brain abnormalities with neurological complications (2, 211). In contrast, severe DENV and YFV infections are generally associated with systemic disease, characterized primarily by increased vasculopathy and plasma leakage from blood vessels into tissues, as well as hepatic damage/dysfunction (11). Despite this, there are multiple reports describing DENV-associated neurological complications such as encephalitis and DENV infection in the human brain in autopsies, as well as detection of viral antigens in placental tissues from DENV-infected mothers (205, 217-219). These findings indicate that DENV may also breach the blood-brain barrier as well as reach the placenta during pregnancy. Overall, our data here demonstrate a tissue-specific pattern of interaction between flavivirus NS1 and endothelial cells, where NS1-mediated effects (e.g. binding, induction of hyperpermeability, etc.) mirror the clinical pathophysiology of the corresponding flaviviral disease in humans. Data is lacking regarding levels of flavivirus NS1 in humans (other than DENV), especially in tissues, where vascular leak occurs. Regardless of levels of circulating NS1 antigenemia, the cumulative effect of NS1 is likely amplified and/or concentrated in the capillary beds of tissues, the primary sites of leakage.

Vascular leak is seemingly mediated by the specific interaction of NS1 proteins with the surface of different endothelial cells. Our *in vitro* binding data showed that DENV NS1 binds to the surface of all human endothelial cells included in this study and displayed a greater interaction with lung and liver endothelial cells. This correlates with the pathophysiology of severe DENV disease, in which these tissues are primarily affected (i.e., pleural effusion, liver dysfunction, etc.) (11). ZIKV NS1 was found only on the surface of umbilical vein and brain endothelial cells. Interestingly, ZIKV has been shown to productively infect fetal macrophages (Hofbauer cells) and placental villous fibroblasts, resulting in increased expression/secretion of ZIKV NS1 in placenta villus cores where fetal endothelial cells are present in blood vessels (216, 220). Additionally, ZIKV is able to infect human PBMCs *in vivo* and neural progenitors cells *in vitro,* which suggests that ZIKV NS1 may be circulating in the blood of infected patients and also secreted inside brain tissues (221-223). WNV NS1 and JEV NS1 only interacted with brain endothelial cells, which correlated with their ability to induce hyperpermeability of these human endothelial cells and as well as with their well-known neurotropism and ability to invade the central nervous system, resulting in neurological complications and encephalitis (224). NS1 from YFV, most often associated with severe liver disease and systemic organ failure (225), was unexpectedly found to bind to some degree to all human endothelial cells. However, it bound to liver endothelial cells to the highest level, which was the only cell type that displayed a high degree of YFV NS1-induced hyperpermeability. These results suggest that NS1 binding specificity may rely on the tissue-specific expression of surface molecules on different endothelial cells that may facilitate the early stages of NS1 binding via protein-protein or protein-glycan interactions. Although these interactions may explain NS1-endothelial cell specificity, they do not explain why YFV NS1 only induces endothelial hyperpermeability of liver endothelial cells despite evidence of binding to other endothelial cells. These data suggest that in addition to the initial binding, NS1 may interact with a second cell type-specific component that is responsible for internalization and/or downstream signaling and activation of pathogenic mechanisms. Thus, a higher “threshold” may exist for YFV NS1 in HLSEC to trigger functional consequences leading

to disruption of the glycocalyx and subsequent increased hyperpermeability. Studies are ongoing to elucidate the cellular factors as well as the molecular basis in the different flavivirus NS1 proteins that mediate their binding to the different endothelial cells and the ensuing endothelial dysfunction.

The vascular endothelium is composed of a single layer of endothelial cells that form blood vessels and modulate vascular homeostasis. On the endothelium, the negative charge provided by EGL components, including glycoproteins containing sialic acid residues and glycosaminoglycans, such as heparan sulfate (more than 50% of the total glycosaminoglycan pool), chondroitin sulfate, and hyaluronic acid, contribute to the maintenance of endothelial barrier function (36). Degradation of the EGL has been linked to disease severity in several viral hemorrhagic fever diseases (226), including dengue, where increased levels of heparan sulfate, hyaluronic acid, and syndecan have been found in the blood of patients with severe dengue disease, as compared to controls with milder forms of dengue (39, 92, 93). However, the importance of vascular permeability and the role of EGL components in the pathogenesis of other flavivirus infections is still unknown. Here, we found that NS1-induced endothelial hyperpermeability correlates with increased disruption of key EGL components, regardless of the tissue origin of the human endothelial cells. The interaction of distinct flavivirus NS1 proteins with the surface of different human endothelial cells led to significantly decreased expression of sialic acid and heparan sulfate, suggesting degradation of these components. This interaction also resulted in increased deposition and accumulation of syndecan-1, which, after being shed, can bind back to the endothelial surface, inducing endothelial dysfunction (88, 180). Importantly, inoculation of these recombinant NS1 proteins in a mouse model, particularly DENV, YFV, and WNV, led to a systemic increase in the levels of heparan sulfate, confirming the role of NS1 in remodeling the integrity of EGL components in endothelial beds *in vivo* and consistent with increased heparan sulfate circulation in severe human dengue cases with vascular leak (93). Notably, NS1-induced EGL alterations *in vitro* were associated with increased expression and activation of the cysteine protease cathepsin L, endothelial sialidases (Neu1, Neu2, and Neu3), and the endoglycosidase heparanase, which have been implicated in the degradation of the extracellular matrix as well as cleavage of proteoglycans mainly expressed on the luminal surface of endothelial cells (36, 164, 180). The pattern revealed is consistent with the flavivirus NS1- and tissue-specific profiles reported above. However, the molecular mechanisms leading to the upregulation and activation of the mammalian sialidases still remain elusive. In turn, Cathepsin L is known to activate heparanase after proteolytic processing of the non-active precursor (65 kDa) into an active protein (50 kDa). We previously showed that inhibitors of sialidases, heparanase and cathepsin L prevent NS1-induced disruption of the EGL *in vitro* and vascular leak *in vivo* (88, 89). Thus, we found that the cell type-dependent pattern of endothelial hyperpermeability observed following flavivirus NS1 treatment of human cell monolayers is also reflected in endothelial cell-intrinsic mechanisms implicated in NS1 pathogenesis *in vitro* and putative disruption of the endothelial glycocalyx in a mouse model.

In addition to the glycocalyx layer, the hemostasis of the endothelium is maintained by the presence of intercellular junctional complex composed of protein-protein interactions that help to preserve the cell-to-cell contacts (33). Disruption of the glycocalyx and/or

intercellular junctional complex may condition the increased passage of fluids, small molecules or plasma proteins of different molecular weights (MW), such as human albumin (~65 kDa), high-density lipoproteins (HDL, 175-500 kDa), and low-density lipoproteins (LDL, ~3,000 kDa). Although we have implicated the endothelial glycocalyx as an important mediator of hyperpermeability following stimulus with flavivirus NS1 proteins, it will be important for future work to determine the role of tight and adherens junctions in NS1-induced pathogenesis. Very recently, the potential role of the adherens junction protein VE-cadherin in DENV NS1-induced vascular leakage was reported (95). Additionally, the association of circulating levels of tight and adherens junction proteins with severe dengue disease has been described (92).

The assessment of vascular permeability is complicated because it is affected by multiple factors including the type of microvessels, endothelial cells, the size and charge of extravasating molecules, and the pathway that molecules take to traverse the endothelium. In these studies, we utilized five distinct measures of endothelial permeability and vascular leak: TEER and a dextran flux assay *in vitro*; and Evans blue dye and fluorescently-labeled dextran in a systemic Miles assay and fluorescently-labeled dextran in a modified local Miles assay *in vivo*. These assays all assess endothelial permeability, but because of the nature of the assays, potentially measure different pathways. *In vitro*, TEER measures the ohmic resistance of a barrier, whereas flux assays measure the direct passage of a macromolecule from the apical to the basolateral chamber. Both of these methods represent a composite of both paracellular and transcellular pathways. *In vivo*, Evans blue binds to albumin, which does not cross the endothelium in the absence of inflammation or stimulus that disrupts normal barrier function. On the other hand, 10 kDa dextran should extravasate from the blood into tissue, even during basal conditions (227). As with the *in vitro* models, these assays most likely measure a composite of paracellular and transcellular pathways. The results from each of these models support our overarching hypothesis that NS1 exerts a virus- and tissue-specific effect on the human endothelium, leading to barrier dysfunction and hyperpermeability, but the amount of leakage due to transcellular versus paracellular pathways remains unknown, and further studies are needed to elucidate the molecular mechanisms driving this phenomenon. As the primary determinant of paracellular permeability, intercellular junctions are important regulators of endothelial barrier function, though it is likely that both the glycocalyx and intercellular junctions are involved in NS1-induced barrier dysfunction and that multiple factors work in synergy resulting in endothelial hyperpermeability. Discerning the relative contributions of the glycocalyx and intercellular junctions will undoubtedly prove to be challenging, but a more complete understanding of the dynamics and kinetics involved in disruption of the endothelial barrier by NS1 may inform clinical management and treatment protocols for flavivirus disease.

Flavivirus infection has been shown to compromise the integrity of many biological barriers, including the pulmonary microvascular endothelium and the blood-brain barrier, which are usually able to protect against virus infection (228-231). So far, this process has been primarily attributed to exacerbated host immune responses that lead to increased permeability of endothelial cells in the different microvascular beds. However, other than DENV NS1, the role of secreted NS1 proteins in the pathophysiology of

endothelial cells has not been reported. Despite the mounting evidence suggesting that high levels of NS1 antigenemia during the acute phase of DENV infection correlate with increased risk of developing severe dengue disease, including vascular leakage (42), little is known about circulating levels of NS1 from other flavivirus infections including ZIKV, WNV, JEV, and YFV. Here, our data suggest a potential role for flavivirus NS1 proteins in causing tissue-specific pathology associated with endothelial dysfunction. We hypothesize that NS1 may induce selective hyperpermeability of different microvascular beds as a means of facilitating virus dissemination into target organs where permissive cells critical for local replication are found, resulting in virus amplification. Numerous studies of flavivirus infection in different animal models as well as human autopsies have shown a selective tropism of distinct groups of flavivirus that target different tissues, leading to systemic versus neurotropic/encephalitic pathology (2). Despite studies describing the potential infection of endothelial cells by flaviviruses *in vitro*, flavivirus infection of endothelial cells *in vivo* is still controversial. In this study, infection of endothelial cells by DENV and ZIKV does not occur during the time frame of the experiment (12-24 hours) (data not shown). Thus, we posit that NS1 is a virulence factor that, in addition to facilitating virus replication and immune evasion, may also facilitate virus dissemination from the bloodstream into tissues, influencing virus tissue tropism and disease manifestations.

Modhiran et al. previously demonstrated that DENV NS1 triggers the production of inflammatory cytokines from PBMCs (85), and inflammatory cytokines such as TNF-α have been implicated in flavivirus pathogenesis, including during WNV crossing of the blood-brain barrier and development of ZIKV-related neurological abnormalities (229, 232). Here, we show that NS1 proteins from different flaviviruses differentially stimulate the secretion of IL-6, IL-8, and TNF-α from human PBMCs, with WNV and ZIKV NS1 proteins having the most potent effect. Because cytokines are known to increase the permeability of the blood-brain barrier (233, 234), we hypothesize that cytokines produced by PBMCs following stimulation by NS1 from neurotropic flaviviruses, such as WNV, may further contribute to virus dissemination during infection, potentially leading to more severe disease.

Taken together, we report a previously undescribed function of different flavivirus NS1 proteins in modulating endothelial barrier function *in vitro* and *in vivo* in a tissue-dependent manner. Mechanistically, we found that all NS1 proteins were able to alter the integrity of EGL components on the surface of endothelial cells, leading to endothelial hyperpermeability. This new evidence strongly suggests that distinct flavivirus NS1 proteins may modulate virus dissemination and thus influence viral pathogenesis and disease. These findings provide novel insights into the biology of NS1 and contribute to a better understanding of flavivirus pathogenesis, supporting the inclusion of NS1 protein in flavivirus vaccine development and generating new targets for future therapies against flavivirus infections.

Experimental Procedures

Cell culture. Human pulmonary microvascular endothelial cells (HPMEC) (line HPMEC-ST1.6r) were kindly donated by Dr. J.C. Kirkpatrick at Johannes Gutenberg University, Germany; human umbilical vein endothelial cells (HUVEC) were a kind gift from Melissa Lodoen at the University of California, Irvine. Both of these cell lines were grown using the EGM-2 bullet kit (Clonetics, Lonza) and maintained as previously described (84). The human dermal microvascular endothelial cell line HMEC-1, kindly donated by Dr. Matthew Welch, University of California, Berkeley, was propagated and maintained as previously described (89). The human brain microvascular endothelial cell (HBMEC) was donated by Ana Rodriguez at New York University and maintained using endothelial cell medium with endothelial cell growth supplement (ScienCell Research Labs). Primary human liver sinusoidal microvascular endothelial cells (HLSEC) were acquired from Cell Biologics and maintained using complete human endothelial cell medium supplemented with an endothelial cell medium supplement kit (Cell Biologics) according to the manufacturer's recommendations. Human PBMCs were isolated from a Trima Residual blood pack (Blood Centers of the Pacific, San Francisco, CA) and cultured in RPMI 1640 supplemented with 10% human serum (MP Biomedicals), 2 mM glutamine (Life Technologies), and 1% penicillin/streptomycin (Life Technologies). All cells were maintained at 37˚C in humidified air with 5% CO_2.

Mice and ethical approvals. Five- to eight-week old wild-type C57BL/6 mice were purchased from the Jackson Laboratory (Sacramento, CA) or bred and maintained under specific pathogen-free conditions at the University of California, Berkeley, Animal Facility. All experimental procedures involving animals were pre-approved by the Animal Care and Use Committee (ACUC) of the University of California, Berkeley.

Antibodies and recombinant NS1 proteins. Staining of EGL components and endothelial enzymes including sialic acid, syndecan-1, heparan sulfate, human endothelial heparanase, sialidases (Neu1, Neu2, and Neu3), and cathepsin L were performed using previously described antibodies, lectins, and protocols (88). An anti 6x-His-tag mAb (HIS.H8) conjugated to DyLight 488 (Thermo Scientific) was used for NS1 protein binding assays. All recombinant NS1 proteins used in this study were obtained from the Native Antigen Company (Oxfordshire, United Kingdom). Recombinant DENV2 (Thailand/16681/84), ZIKV (Uganda MR766 and Suriname Z1106033), WNV (NY99), JEV (SA-14), and YFV (17D) NS1 proteins were produced in HEK 293 cells with a purity greater than 95%, composed mostly of oligomeric forms and certified by the manufacturer to be free of endotoxin contaminants. NS1 preparations were also tested using the Endpoint Chromogenic Limulus Amebocyte Lysate QCL-1000TM kit (Lonza) and confirmed to be free of bacterial endotoxins.

Transendothelial electrical resistance (TEER). The effect of recombinant flavivirus NS1 proteins on endothelial permeability was evaluated by measuring TEER of endothelial cell (EC) monolayers grown on a 24-well Transwell polycarbonate membrane system (Transwell permeable support, 0.4 μm, 6.5 mm insert; Corning Inc.) as previously described (88, 89). Briefly, TEER was measured in Ohms (Ω) at sequential 2-hour time-points following the addition of test proteins (5 μg/ml, 1.5 μg of total protein) to the apical

chamber (top chamber, 300 µl) of a Transwell system using an Epithelial Volt Ohm Meter (EVOM) with “chopstick” electrodes (World Precision Instruments). Untreated endothelial cells grown on Transwell inserts were used as negative untreated controls, and inserts with medium alone were used for blank resistance measurements. Relative TEER represents a ratio of resistance values (Ω) as follows: (Ω experimental condition - Ω medium alone)/(Ω non-treated endothelial cells - Ω medium alone). After 24 hours of treatment, 50% of upper and lower chamber media were replaced by fresh endothelial cell medium.

Solute flux assay. To evaluate the effect of different flavivirus NS1 proteins on the passage of macromolecules through a polarized monolayer of human endothelial cells, HUVEC were grown on collagen-coated Transwell insert (Corning Transwell-COL collagen-coated membrane inserts, 24-well, 0.4 µm, 6.5 mm insert; Corning Inc.). After three days of culture using complete endothelial cell media (Lonza), 50% of upper and lower chamber media were replaced with fresh Endothelial Cell Growth Media-2 (PromoCell) for 24 hours before beginning the experiment. Test proteins (10 µg/ml, 3 µg total protein) were added to the apical chamber of the Transwell inserts and incubated for 6 hours at 37˚C. At 6 hpt, 70 kDa dextran conjugated to FITC (Sigma) was added to the apical chamber of the Transwell inserts at a final concentration of 1 mg/ml and allowed to circulate for one hour at 37°C. Transwell inserts were removed, and 100 µl from each well was collected in duplicate wells in a 96-well flat-bottom plate. Fluorescence was measured on a plate reader, and the concentration of dextran-FITC that passed from the apical to and accumulated in the basolateral chamber was determined using a standard curve (0.488 – 1000 µg/ml). TNF-α (100 ng/ml) was used as a positive control, and untreated cell monolayers were used as a baseline control.

Flavivirus NS1 protein binding assay. To assess the ability of each flavivirus NS1 protein to interact with the surface of human endothelial cells, we used two different approaches: an immunofluorescence assay (IFA) to visualize the extracellular NS1 protein (5 and 10 µg/ml; 1.5 and 3 µg total protein, respectively) on non-permeabilized monolayers of endothelial cells grown on gelatin-coated coverslips (0.2%, Sigma) and a Western blot assay using total protein extracts collected from confluent endothelial cell monolayers exposed to 10 µg/ml (3 µg) of each NS1 protein. All individual flavivirus NS1 proteins were incubated for one hour at 37°C as previously described (88). All flavivirus NS1 proteins used in this study contain a C-terminal 6x-His-tag. NS1 protein bound to the cell surface was detected by IFA using an anti-6x-His-tag mAb (HIS.H8) conjugated to DyLight 488 (Thermo Scientific) followed by confocal microscopy analyses. Alternatively, a combination of anti-6x-His-tag mAb with an anti-mouse IgG (H+L) conjugated to Alexa 680 was used to detect the presence of NS1 protein in total protein extracts by Western blot using an infrared detection system (LICOR). Untreated monolayers were used for background subtraction in both assays. For Western blots, GAPDH was used as protein loading control to normalize the relative amount of NS1 protein bound to the surface of each endothelial cell. Densitometry analyses was performed using Image Studio Lite software v 5.2.

Fluorescence microscopy. For imaging experiments, all human endothelial cells were grown on sterile coverslips coated with 0.2% gelatin (Sigma) and imaged on a Zeiss LSM

710 Axio Observer inverted fluorescence microscope equipped with a 34-channel spectral detector. To visualize the effect of all flavivirus NS1 proteins on the expression of EGL components such as sialic acid, heparan sulfate, endothelial sialidases (Neu1, Neu2, and Neu3), and syndecan-1, as well as cathepsin L expression and activity and heparanase expression, confluent endothelial cell monolayers were treated with 5 µg/ml of each flavivirus NS1 proteins and were fixed with 4% of cold paraformaldehyde (PFA) 6 hpt. Untreated monolayers were used as a control for normal expression/distribution of all EGL components and endothelial enzymes mentioned above. Indirect immunofluorescence was performed using primary mAbs incubated overnight at 4°C, and detection was performed with secondary species-specific anti-IgG or anti-IgM antibodies conjugated to Alexa fluorophores (488, 568 and 647) as previously described (89). Images acquired (20x) using Zeiss Zen 2010 software were processed and analyzed with ImageJ software. All RGB images were converted to grayscale. Then, mean grayscale values and integrated density from selected areas were taken, along with adjacent background readings, and plotted as mean fluorescence intensity (MFI). For MFI quantification, individual images (708.48 x 708.48 µm) were obtained as RGB composite and split into 4-channel to adjust the threshold for each individual channel. Then, each channel was converted into a grayscale format and equally divided into four framed non-overlapping areas (341.9 x 353.8 µm, ~45-50 nuclei/frame). Minimum and maximum gray values, expressed here as MFI, were measured using an ImageJ plugin. All different experimental conditions were run in duplicate in two individual experiments. Representative images (125.73 x 138.96 µm).

Cytokine secretion assay. To evaluate the stimulation of cytokine production from PBMCs by flavivirus NS1 proteins, primary human PBMCs were cultured in 24-well plates. After thawing cells from cryo-preservation, 250,000 cells were plated in 500 µl in each well and allowed to settle for 3 hours. 5 µg/ml of flavivirus NS1 protein was then added to each well; 10 ng/ml was used as a positive control. At 24 hpt, cells were spun down at 1500 RPM for 5 minutes at 4˚C, and supernatant was collected and frozen down at -80˚C. ELISA analyses were later performed to determine levels of cytokine production.

***In vivo* vascular leakage assays.** To evaluate the *in vivo* effect of flavivirus NS1 proteins in vascular hemostasis, we used a conventional Miles assay using Evans Blue dye (EBD), as well as a modified version using fluorescently-labeled dextran. Briefly, wild-type C57BL/6 mice were initially injected with either 10 mg/kg of ovalbumin or each individual flavivirus NS1 protein. Three days post-injection, mice were intravenously administrated 100 µl of 0.5% EBD in PBS and 200 µl of 10 kDa dextran conjugated to Alexa Fluor 680 (dextran-A680; 1 mg/ml). Both compounds were allowed to circulate for 3 or 2 hours, respectively, before euthanizing animals and perfusing tissues with 20 ml of PBS and 10 ml of formalin solution (Sigma) for tissue fixation. To quantify the levels of vascular leakage into the extravascular space of tissue using dextran-A680, tissues were analyzed using the LI-COR Odyssey CLx Imaging System. Images were evaluated using Image Studio Lite software, and the leakage area was quantified from a standard-scanned area selected for each tissue to obtain a mean fluorescence intensity value. For EBD extraction, tissues were vacuum dried, snap-frozen in liquid nitrogen, and pre-weighed before incubation in formamide (1 ml/g of tissue; Sigma) at 65°C for 48 hours (231). The absorbance of the extravasated dye was measured at 620 nm using a spectrophotometer.

EBD concentration was calculated using a standard curve (3.9 to 250 ng/ml) using linear regression analysis (R^2=0.998). To determine the effect of flavivirus NS1 proteins at a local microvascular level, we used the Dextran-adapted dermal Miles assay based on a previously described protocol (89). Briefly, flavivirus NS1 proteins were intradermally injected (15 µg in 50 µl PBS) into the dorsal dermis of previously shaved mice (3-4 days prior injection). PBS (50 µl) was used as an injection control, and VEGF (200 ng in 50 µl PBS) was used as positive control for inducing vascular leakage. Following intradermal injections, 200 µl of dextran-A680 (5 mg/ml) was delivered by retro-orbital injection. Two hours post-injection, mice were euthanized, and the dorsal dermis was removed and placed in Petri dishes. Tissues were then scanned using the LI-COR Odyssey CLx Imaging System and analyzed as previously described (89).

Western blots. Confluent cell monolayers (~3x10^5 cells/well, 24-well tissue culture-treated plates) of human endothelial cells from lung (HPMEC), skin (HMEC-1), umbilical vein (HUVEC), brain (HBMEC) and liver (HSLEC) were treated with 5 µg/ml of individual flavivirus NS1 proteins (DENV, ZIKV, WNV, JEV and YFV) and at 6 hpt, cells were lysed using RIPA lysis buffer (50 mM Tris [pH 7.4], 150 mM NaCl, 1% [v/v] Nonidet-P40, 2 mM EDTA, 0.1% [w/v] SDS, 0.5% Na-deoxycholate, and 50 mM NaF) supplemented with complete protease inhibitor cocktail (Roche). Ten to twenty µg of total protein per sample was diluted using reducing Laemmeli buffer and separated by 4-20% gradient SDS-PAGE. For subsequent analyses, proteins were transferred onto PDVF membranes using a Western blotting transfer system (Trans-Blot Turbo™ Transfer System, BioRad) and detected using primary antibodies for NS1 proteins (anti-6x-His-tag mAb, Thermo Scientific), human cathepsin L (eBiosciences), and GAPDH (Santa Cruz Biotech) (used as a housekeeping protein control) and secondary species-specific anti-IgG antibody conjugated to Alexa 680 or Alexa 750. Protein detection and quantification was performed using the Odyssey CLx Infrared Imaging System (LI-COR). Relative densitometry represents a ratio of the values obtained from each experimental protein band over the values obtained from loading controls (GAPDH) after subtracting background from both using Image Studio Lite V 5.2 (LI-COR Biosciences).

ELISAs. TNF-α, IL-6, and IL-8 levels were measured using ELISA assays following the manufacturer's instructions (Abcam). Circulating levels of heparan sulfate (LSBio, Inc) in the bloodstream of mice (n=3 per group) treated with different recombinant NS1 proteins (10 mg/kg) were measured in serum samples collected three days post-treatment as indirect markers of endothelial glycocalyx integrity *in vivo,* as has been previously described (93)**.** Ovalbumin was used as a protein control. Quantification of each analyte was done using standards provided and following manufacturer's recommendations.

Statistical analysis. All statistical analyses and graphs were performed and generated using GraphPad Prism 6 software. For binding experiments, statistically significant differences between distinct treatment groups were determined by ANOVA and unpaired t-tests. For microscopy analyses, comparisons between the mean fluorescence intensities obtained from three individual experiments, run in duplicate and using untreated cells as baseline controls, was conducted using an ordinary two-way ANOVA with multiple comparisons to untreated cells using Dunnett's multiple comparison test. For all *in vivo* experiments (murine dermal leak, systemic vascular leak, serum heparan

sulfate), an ordinary one-way ANOVA with multiple comparisons to control groups (untreated, PBS, or OVA) using Dunnett's multiple comparison tests was used to determine significance of different flavivirus NS1 proteins. For TEER experiments, statistical significance was determined using an ordinary two-way ANOVA. For solute flux assays, statistical significance was determined using an ordinary two-way ANOVA with multiple comparisons to untreated cells using Dunnett's multiple comparison test. For all analyses, differences were considered significant for P values <0.05.

Supplementary Material

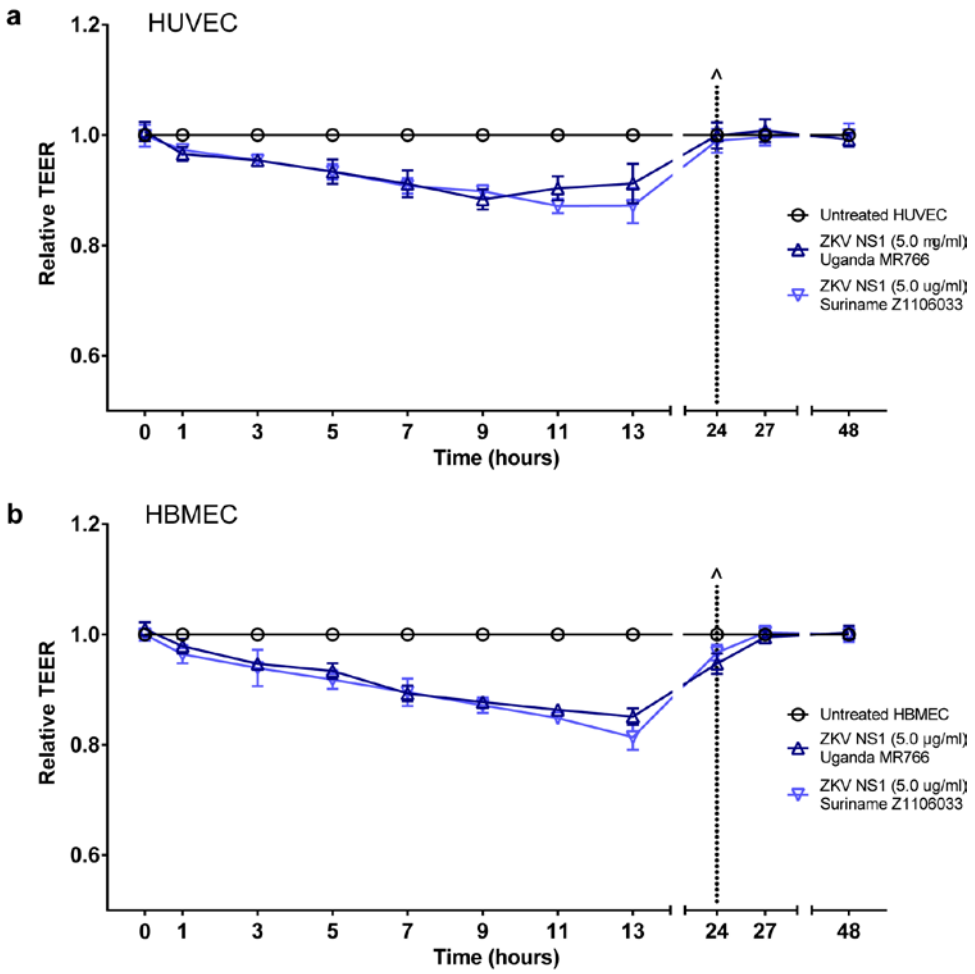

Figure 5.S1. Related to Figure 5.1. NS1 from two different ZIKV lineages induces similar levels of hyperpermeability of human brain and umbilical vein endothelial cells.
Human endothelial cells from the **(a)** umbilical vein (HUVEC) and **(b)** brain (HBMEC) were grown on Transwell semi-permeable membrane inserts (0.4 µm pore size), and NS1 (5 µg/ml, 1.5 µg of total protein) from two different ZIKV strains, Uganda (MR766) and Suriname (Z1106033), was added to the apical chamber. A TEER assay was used to evaluate the effect of these proteins on endothelial permeability at indicated time-points over 48 hours. (^) represents change of medium. Relative TEER values from two independent experiments performed in duplicate are plotted. Error bars indicate standard error of the mean (SEM).

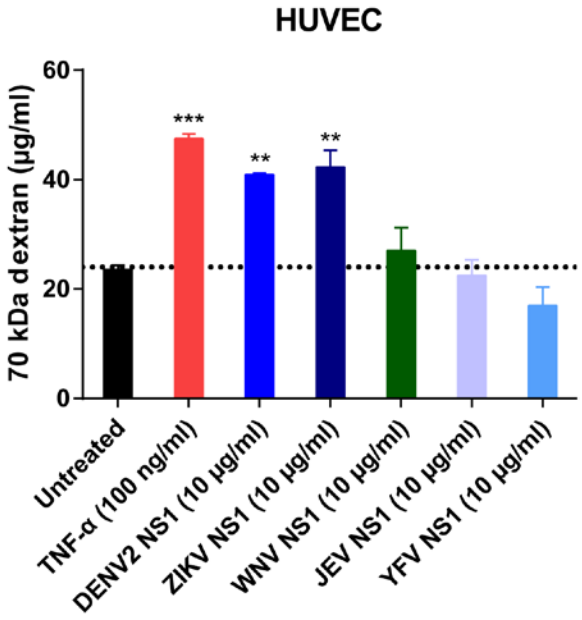

Figure 5.S2. Related to Figure 5.1. Flavivirus NS1 proteins differentially increase endothelial permeability in HUVEC as measured by dextran flux *in vitro*.
HUVEC were grown on collagen-treated Transwell semi-permeable membrane inserts (0.4 µm pore size), and distinct flavivirus NS1 proteins (5 µg/ml, 1.5 µg of total protein) were added to the apical chamber. At 6 hpt, 70 kDa dextran conjugated to FITC (1 mg/ml) was added to the apical chamber and allowed to circulate for one hour, after which 100 µl of supernatant from the basolateral chamber was collected and analyzed on a plate reader in duplicate wells. Data from two independent experiments performed in duplicate are plotted. Error bars indicate SEM. Statistically significant differences were determined using an ordinary one-way ANOVA with multiple comparisons to untreated cells using Dunnett's multiple comparison tests, with **, $P < 0.01$; ***, $P < 0.001$.

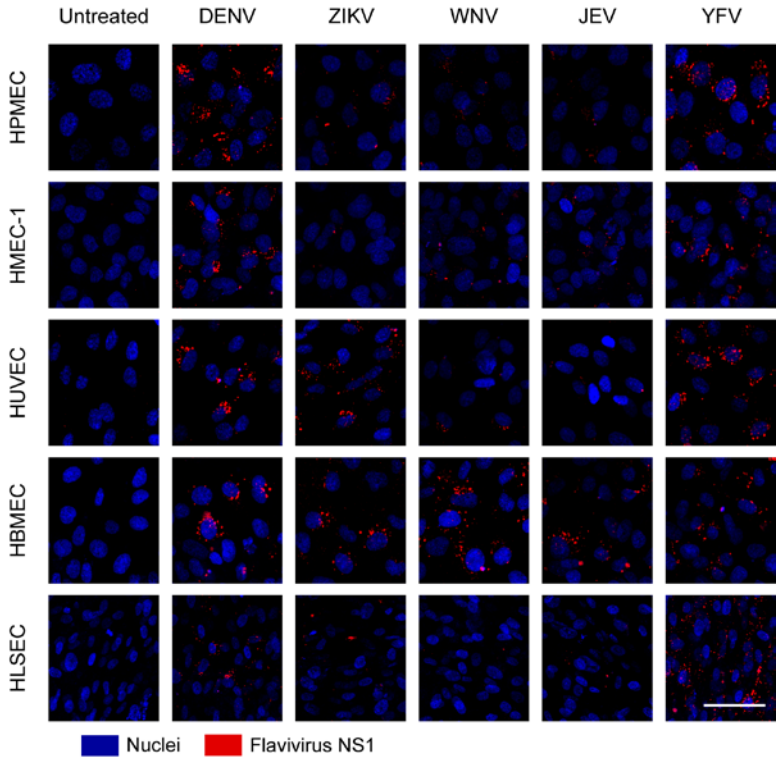

Figure 5.S3. Related to Figure 5.2. Flavivirus NS1 proteins bind differentially to the surface of human endothelial cells as measured by confocal microscopy.
Binding of flavivirus NS1 proteins to the surface of different human endothelial cells grown on coverslips was examined by confocal microscopy. The amount of NS1 bound to different human endothelial cell monolayers (red) was quantified 1 hpt at 37°C using an anti-6x-His-tag mAb conjugated to Alexa 647 and expressed as MFI **(Figure 5.2a-e)**. Nuclei were stained with Hoechst (blue). Images (20X) are representative of two individual experiments run in duplicate. Scale bar, 10 μm. MFI values are quantified in **Figure 5.2a-e**. Confocal microscopy images acquired and analyzed by Dr. Henry Puerta-Guardo.

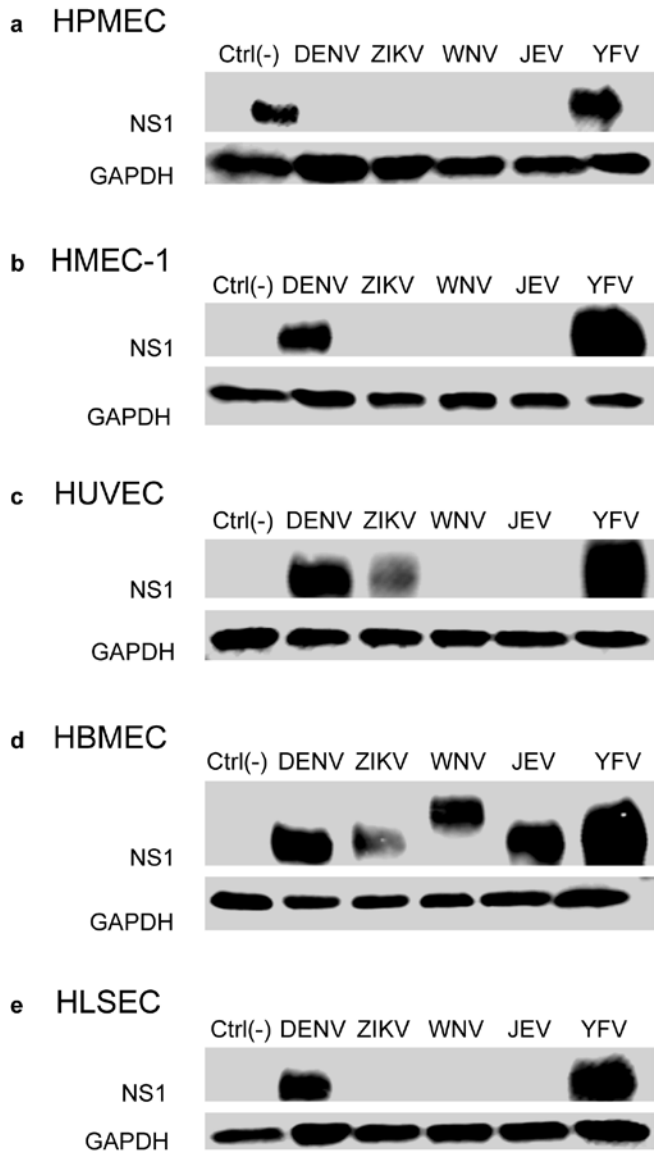

Figure 5.S4. Related to Figure 5.2. Flavivirus NS1 proteins bind differentially to the surface of human endothelial cells as measured by Western blot.
(a-e) Cell lysates from monolayers of **(a)** HPMEC, **(b)** HMEC-1, **(c)** HUVEC, **(d)** HBMEC, and **(e)** HLSEC treated with different flavivirus NS1 proteins (10 µg/ml, 3 µg of total protein) were collected 1 hpt and were analyzed by Western blot. Representative images of Western blots from two independent experiments. Densitometry values are quantified in **Figure 5.2f-j**.

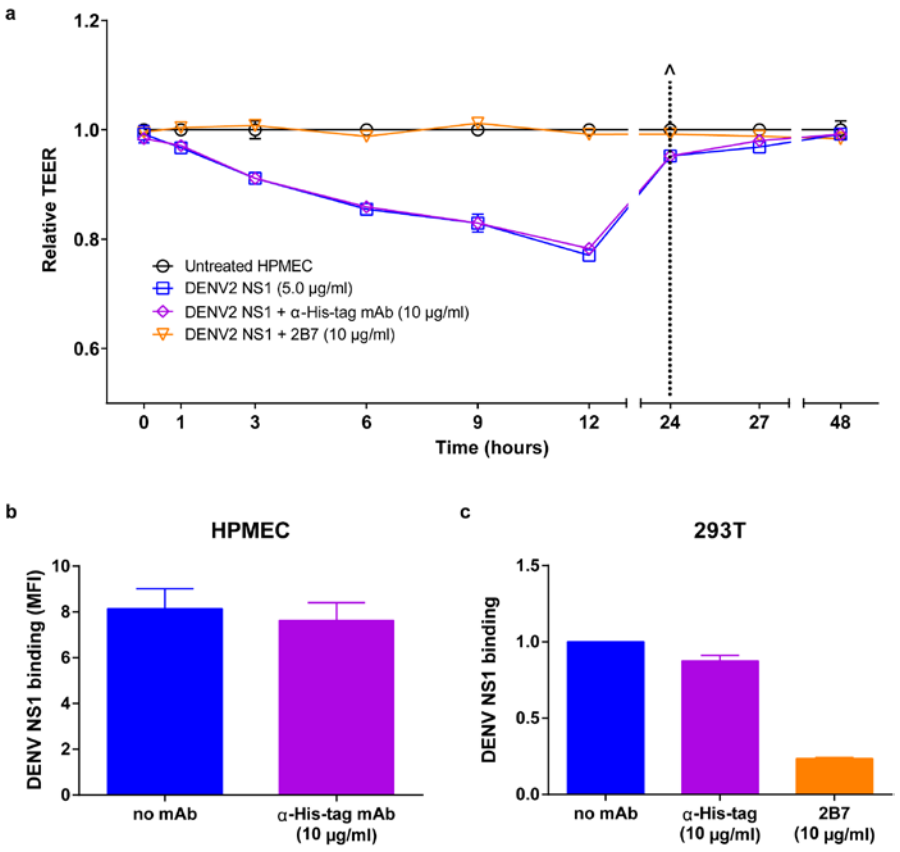

Figure 5.S5. Related to Figure 5.2. An anti-6x-His-tag mAb does not prevent NS1-induced hyperpermeability of human endothelial cells or NS1 binding to the cell surface.
(a) HPMEC were cultured on Transwell semi-permeable membrane inserts (0.4 µm pore size) until confluent and treated with DENV2 NS1 (5 µg/ml, blue squares), DENV2 NS1 and an anti-6x-His-tag mAb (10 µg/ml, purple diamonds), or DENV2 NS1 and 2B7, an anti-NS1 mAb (10 µg/ml, orange triangles). A TEER assay was used to evaluate the effect of these treatments on endothelial permeability at indicated time-points over 48 hours. (^) represents change of medium. Relative TEER values from one experiment performed in duplicate are plotted. Error bars indicate standard error of the mean (SEM). NS1 binding assay on HPMEC **(b)** and 293T cells **(c)** evaluated by confocal microscopy and flow cytometry, respectively. **(b)** Quantification of MFI from confocal microscopy images of DENV2 NS1 (5 µg/ml) binding to HPMEC in the presence or absence of an anti-6x-His-tag mAb (10 µg/ml). **(c)** Relative NS1 binding to the surface of 293 cells in the presence or absence of an anti-6x-His-tag mAb (10 µg/ml) and an anti-NS1 mAb (2B7). The relative binding of NS1 to 293 cells was determined using the percentage of NS1-positive cells (treated with NS1 in the absence of mAbs) and the negative control (cells not treated with NS1 but stained using an anti-NS1 mAb). Error bars indicate SEM.

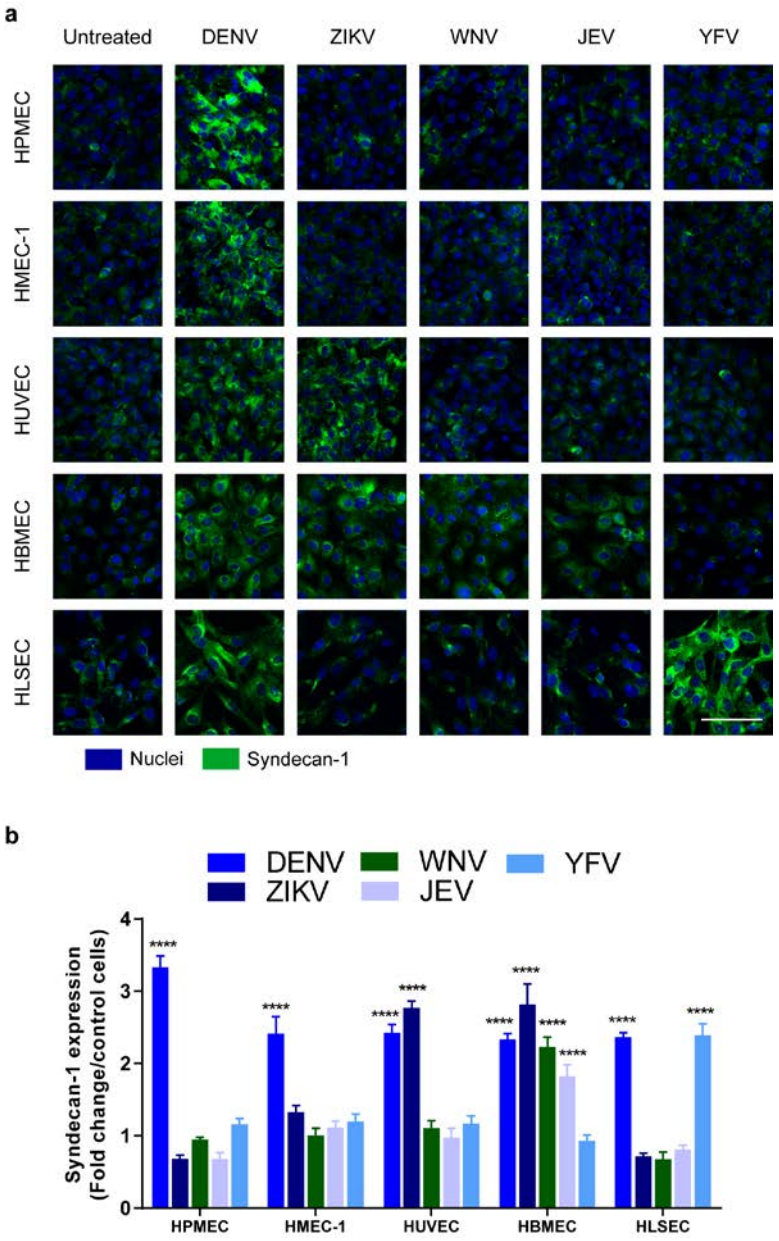

Figure 5.S6. Related to Figure 5.4. Flavivirus NS1 proteins alter the expression of syndecan-1 in a cell type-dependent manner.
(a) Syndecan-1 expression on human endothelial cell monolayers grown on coverslips 6 hpt with different flavivirus NS1 proteins (5 µg/ml) and examined by confocal microscopy. Syndecan-1 was stained with anti-syndecan-1 mAb (green). Nuclei were stained with Hoechst (blue). Images (20X) and MFI values are representative of three independent experiments. Scale bar, 10 µm. **(b)** Quantification of MFI in **(a)** from three independent experiments. Error bars indicate SEM. Fold-change in MFI for syndecan-1 expression in NS1-treated monolayers was normalized to untreated controls. Statistically significant differences between distinct treatment groups were determined using an ordinary two-way ANOVA with multiple comparisons to untreated cells using Dunnett's multiple comparison test, with ****, $P < 0.0001$. Confocal microscopy images acquired and analyzed by Dr. Henry Puerta-Guardo.

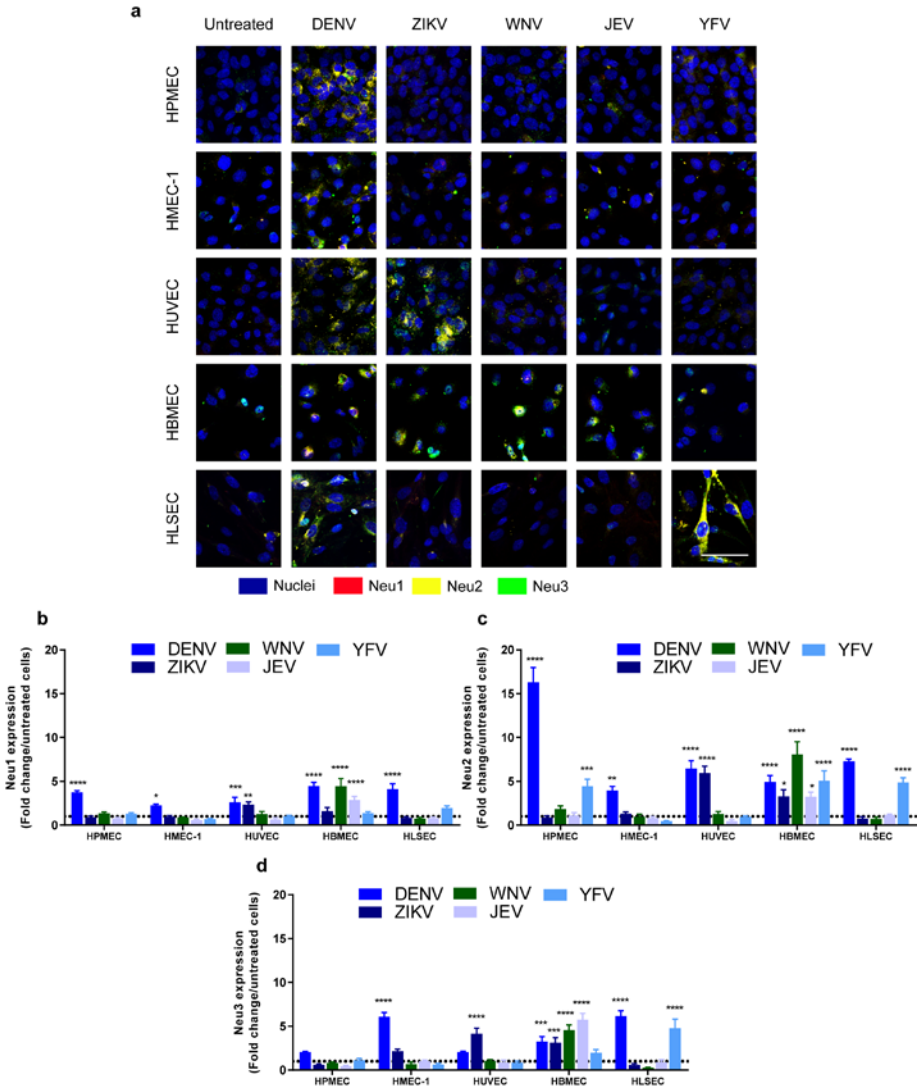

Figure 5.S7. Related to Figure 5.3. Flavivirus NS1 proteins increase the expression of human endothelial sialidases in a cell type-dependent manner.
(a) Neu1, Neu2, and Neu3 expression in human endothelial cell monolayers grown on coverslips 6 hpt with different flavivirus NS1 proteins (5 µg/ml, 1.5 µg of total protein) and examined by confocal microscopy. Neu1, Neu2, and Neu3 were stained with Neu1 antibody H-300 (Santa Cruz Biotech, red), Neu2 polyclonal antibody (PA5-35114, Thermo Scientific, yellow) and Ganglioside sialidase antibody N-18 (Santa Cruz Biotech, green), respectively. The merged image is shown for each condition. Nuclei were stained with Hoechst (blue). Images (20X) are representative of two independent experiments. Scale bar, 10 µm. **(b-d)** Quantification of MFI in **(a)** from two independent experiments. Error bars indicate SEM. Fold-change in MFI for **(b)** Neu1, **(c)** Neu2, and **(d)** Neu3 expression in NS1-treated monolayers was normalized to untreated controls. Statistically significant differences between distinct treatment groups were determined using an ordinary two-way ANOVA with multiple comparisons to untreated cells using Dunnett's multiple comparison test, with *, $P < 0.05$; **, $P < 0.01$; ***, $P < 0.001$; ****, $P < 0.0001$. Confocal microscopy images acquired and analyzed by Dr. Henry Puerta-Guardo.

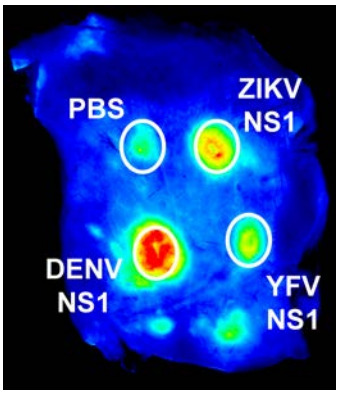

Figure 5.S8. Related to Figure 5.7. Flavivirus NS1 proteins induce differential local vascular leakage *in vivo*.
Representative image of data from **Figure 5.7b**. Briefly, wild-type C57BL/6 mice were injected intradermally with 15 µg of different flavivirus NS1 proteins (pictured: DENV2, ZIKV, YFV), and the magnitude of the local vascular leakage induced by these proteins was evaluated by using dextran-A680 (10 mg/ml). PBS was used as a vehicle control. Fluorescence was quantified using the LI-COR Odyssey.

Chapter 6: Functionality of the NS1-specific antibody response elicited by Takeda's Tetravalent Dengue Vaccine Candidate

Summary

Dengue virus (DENV) is the most medically important arbovirus, affecting 40% of people worldwide and infecting ~390 million individuals annually. Cases range from dengue fever to life-threatening dengue hemorrhagic fever/dengue shock syndrome, which is characterized by endothelial dysfunction and vascular leakage. Previously, we demonstrated that DENV non-structural protein 1 (NS1) can induce endothelial hyperpermeability in both cultured human cells and mouse models and that vaccination with NS1 confers antibody-mediated protective immunity. Takeda's live attenuated tetravalent dengue vaccine (TDV) candidate has four components with structural proteins from each serotype on the DENV2 genomic backbone. Here, we evaluated the functionality of the DENV NS1-specific antibody response. Using an *in vitro* model of endothelial permeability, we found that DENV2 NS1-induced endothelial hyperpermeability in human pulmonary microvascular endothelial cell monolayers, as measured by transendothelial electrical resistance, was not inhibited by pre-vaccination day 0 serum from subjects who had not been previously exposed to DENV infection (DENV-naïve subjects). Pre-existing NS1-specific antibodies in day 0 pre-vaccination serum from previously DENV exposed (DENV-pre-immune) subjects inhibited NS1-induced hyperpermeability to varying levels. All post-TDV vaccination samples from both naïve and pre-immune vaccine recipients completely abrogated NS1-induced hyperpermeability. These effects correlated with anti-NS1 antibody concentrations as measured by ELISA. Post-vaccination sera also prevented NS1-induced degradation of endothelial glycocalyx components as visualized by confocal microscopy. Finally, post-TDV vaccination sera inhibited hyperpermeability induced by DENV1, DENV3, and DENV4 NS1, and inhibition correlated with cross-reactive IgG concentration against NS1. Taken together, this is the first indication of functional NS1-specific antibody responses elicited by a candidate dengue vaccine.

Introduction

Dengue virus (DENV) is the most prevalent arbovirus worldwide, with half of the world's population at risk of infection from one of the four serotypes of the virus (DENV1-4) (1). DENV is a member of the flavivirus family and is transmitted by the bites of infected female *Aedes aegypti* mosquitoes. There are an estimated ~390 million infections annually (1), and infection can lead to a range of outcomes, from inapparent infection to dengue fever (DF) to dengue hemorrhagic fever/dengue shock syndrome (DHF/DSS), the most severe manifestations of disease (12). The first dengue vaccine, Dengvaxia®, was produced by Sanofi Pasteur and licensed for use in 11 countries in 2016; however, substantial concerns exist surrounding the potential of the vaccine to lead to antibody-dependent enhancement, resulting in more severe infection post-vaccination (20, 235, 236). As such, research and clinical trials of other dengue vaccine candidates continues unabated.

Takeda's live attenuated tetravalent dengue vaccine candidate (TDV) is comprised of an attenuated DENV2 strain with structural proteins from DENV1, DENV3, and DENV4 on the DENV2 backbone (237). During Phase 2 clinical trials, TDV was well-tolerated and immunogenic, regardless of the patient's immune status to DENV (238, 239). Because the vaccine elicits a neutralizing antibody response, we can assume that the vaccine virus infects and replicates in target cells and possesses functional versions of all proteins, including the 7 non-structural proteins.

Non-structural protein 1 (NS1) is the only protein secreted from DENV-infected cells, and it plays a variety of roles in the viral lifecycle, including replication and immune evasion (146). We and others have previously shown that NS1 can act as a viral toxin and that it contributes to pathogenesis via at least two mechanisms: an endothelial cell-intrinsic pathway, where NS1 directly interacts with endothelial cells to induce degradation of the glycocalyx via activation of sialidases and the cathepsin L/heparanase pathway (88, 89); and a cytokine-dependent route, where NS1 stimulates production of inflammatory cytokines from immune cells (85). We have also demonstrated that vaccination with adjuvanted NS1 protein protects mice from lethal vascular leak disease, and passive transfer of anti-NS1 serum abrogates NS1-induced lethality *in vivo* (84).

A substantial proportion of the antibody response to DENV after infection is directed against NS1, and anti-NS1 antibodies have been found in convalescent sera after primary DENV infection, during the acute and convalescent phases of secondary DENV infection, and in DF and DHF/DSS patients (52, 240-243). Although no differences have been found in the levels of total anti-NS1 antibodies measured in patients with DF versus DHF (52, 240-242), antibodies to particular NS1 epitopes have been shown to be present at higher levels in DF compared with DHF patients (244). It is not yet clear what precise role these antibodies play in resolving infection or preventing reinfection, as no studies have compared levels of anti-NS1 antibody prior to asymptomatic vs. symptomatic DENV infection.

Though the post-TDV vaccination neutralizing and binding antibody response against DENV prM/E has previously been analyzed (245), the response against NS1 has not.

And because a full complement of functional non-structural proteins, including NS1, is required for viral replication, we assume that NS1 is secreted by vaccine virus-infected cells. In this study, we sought to determine the magnitude and functionality of the anti-NS1 IgG response elicited by Takeda's TDV. We found that vaccination stimulates a strong anti-NS1 antibody response that protects against DENV2 NS1-induced endothelial hyperpermeability and endothelial glycocalyx-like layer degradation (EGL) *in vitro*. This level of activity correlated with antibody concentration measured by ELISA, and this activity was cross-reactive against DENV1, DENV3, and DENV4 NS1-induced barrier dysfunction and correlated with the respective antibody concentrations as well. Taken together, these results suggest that Takeda's TDV elicits an anti-NS1 response that blocks a key pathogenic mechanism of NS1 and may be beneficial for protection against NS1-mediated complications of severe dengue disease.

Results

Subjects vaccinated with Takeda TDV develop anti-DENV2 NS1 IgG responses that abrogate NS1-induced hyperpermeability *in vitro*

We have previously shown that NS1 from all four DENV serotypes can induce endothelial hyperpermeability of human pulmonary microvascular endothelial cells (HPMEC) as measured by transendothelial electrical resistance (TEER) (88), and that this effect can be blocked using immune serum from NS1-immunized mice (84). Here, we demonstrate that sera from subjects vaccinated with Takeda's TDV develop antibody responses that prevent DENV2 NS1-induced hyperpermeability. First, researchers at Takeda determined anti-NS1 antibody concentrations against NS1 from all 4 DENV serotypes **(Table 6.1)** in samples that were collected during the Phase 1b INV-DEN-203 clinical trial (ClinicalTrials.gov identifier: NCT01511250). Briefly, healthy participants were enrolled in the study and received two doses of TDV (at day 0 and day 90), and serum samples were collected at day 0 before vaccination and day 120 post-vaccination. Subjects were grouped into DENV-naïve and pre-immune categories based on their micro-neutralization test results for DENV2 (246). Next, we evaluated sera from 12 subjects (6 DENV-naïve and 6 DENV-pre-immune) at day 0 before vaccination and day 120 post-vaccination. We found that day 0 serum samples from DENV-naïve subjects did not protect against NS1-mediated barrier dysfunction, but day 120 post-vaccination samples from all naïve subjects blocked decreases in TEER values **(Figures 6.1a, 6.S1)**. Day 0 samples from pre-immune subjects produced varying levels of protection, and all day 120 post-vaccination samples completely abrogated NS1-induced hyperpermeability **(Figures 6.1b, 6.S2)**. Pooled serum from DENV-pre-immune individuals, used as a positive control, also completely prevented DENV2 NS1-induced hyperpermeability, while negative control serum from DENV-naïve individuals did not **(Figure 6.S3b)**. We then analyzed the reduction in NS1-mediated hyperpermeability generated by TDV sera (measured as area under the curve (AUC) from each TEER analysis) and performed a correlation analysis against NS1-specific antibody concentration from each serum sample as measured by ELISA and found that protection strongly correlated with anti-NS1 antibody levels ($r = 0.8826$; $P < 0.0001$) **(Figure 6.1c)**. Taken together, these results suggest that Takeda's TDV stimulates protective anti-DENV2 NS1 antibody responses following vaccination.

DENV-naïve subjects Anti-NS1 antibody concentration (RU/ml)								
	DENV1		DENV2		DENV3		DENV4	
Subject ID	d0	d120	d0	d120	d0	d120	d0	d120
1023014	13.5	602.6	16.2	2570.4	10.0	489.8	28.2	302.0
1025011	66.1	173.8	35.5	794.3	67.6	117.5	42.7	85.1
1025013	5.6	380.2	24.6	2454.7	17.0	316.2	10.0	186.2
1035002	34.7	177.8	31.6	977.2	17.8	114.8	19.1	44.7
1035005	50.1	467.7	20.4	1659.6	104.7	309.0	66.1	288.4
1035001	40.7	186.2	52.5	489.8	44.7	169.8	51.3	177.8

DENV-pre-immune subjects Anti-NS1 antibody concentration (RU/ml)								
	DENV1		DENV2		DENV3		DENV4	
Subject ID	d0	d120	d0	d120	d0	d120	d0	d120
1052010	691.8	11481.5	309.0	12022.6	436.5	7585.8	245.5	4677.4
1052014	758.6	1445.4	407.4	891.3	758.6	1122.0	724.4	708.0
1052015	3890.5	3467.4	2570.4	2344.2	3235.9	2818.4	660.7	708.0
1071007	478.6	851.1	239.9	478.6	660.7	1202.3	871.0	1258.9
1071012	691.8	776.3	724.4	676.1	776.3	812.8	346.7	446.7
1082009	5888.4	5370.3	7413.1	6309.6	5248.1	4897.8	891.3	794.3

Table 6.1. Magnitude of anti-NS1 antibody response elicited by Takeda TDV vaccination. Researchers at Takeda determined the anti-NS1 antibody concentrations (RU/ml) of day 0 pre-vaccination and day 120 post-vaccination serum samples against NS1 from DENV1-4. Top: DENV-naïve subjects; bottom: DENV-pre-immune subjects.

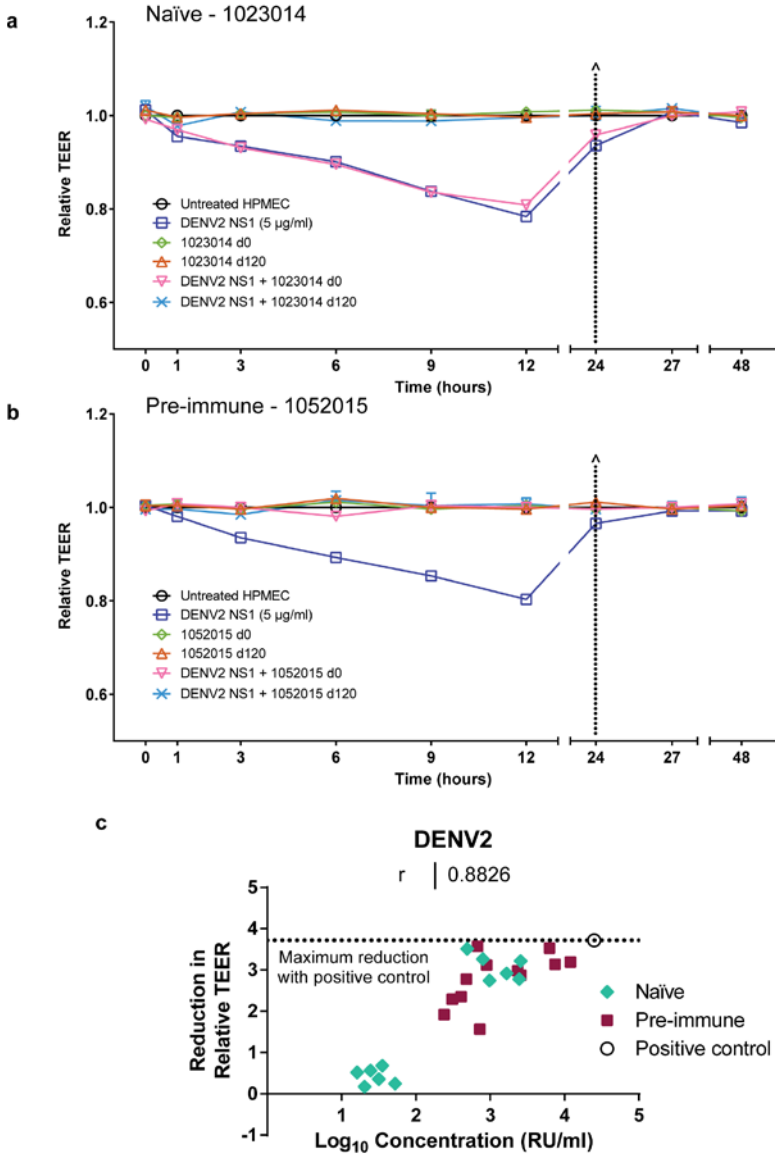

Figure 6.1. Post-TDV vaccination sera protects against DENV2 NS1-induced hyperpermeability, and protection correlates with antibody concentration.
Researchers at Takeda collected serum from either **(a)** DENV-naïve or **(b)** DENV-pre-immune subjects at day 0 before vaccination and day 120 post-vaccination with Takeda's TDV as previously described (246). **(a,b)** The effect of sera on DENV2 NS1-induced endothelial hyperpermeability was evaluated by TEER. Graphs are shown for representative **(a)** naïve (1023014) and **(b)** pre-immune (1052010) samples. HPMEC were grown on Transwell semi-permeable membranes (0.4 µm pore size), and serum samples (30 µl) were added to the apical chamber at a final dilution of 1:10 in the presence or absence of DENV2 NS1 (5 µg/ml) (DENV2 NS1, blue squares; day 0 serum alone, green diamonds; day 120 serum alone, orange triangles; day 0 serum + DENV2 NS1, red triangles; day 120 serum + DENV2 NS1, light blue X's). Endothelial permeability was measured at indicated time-points over 48 hours. (^) represents change of medium. Relative TEER values from one independent experiment performed in duplicate are plotted. Error bars indicate standard error of the mean (SEM). **(c)** Correlation analysis of 6 naïve and 6 pre-immune samples from both day 0 and day 120 (24 total samples). Area under the curve (AUC) values were calculated for each curve in each TEER experiment. The absolute reduction in

relative TEER for each serum sample **(a,b; 6.S1, 6.S2)** was calculated by subtracting the AUC of NS1 + serum from the AUC of NS1 alone. Reduction was plotted against the $\log_{10}$ of antibody concentrations for each sample, and a correlation analysis was performed. The dotted line represents the reduction of TEER by positive control serum. Naïve subjects, red circles; pre-immune subjects, light blue squares; positive control serum, blue circle. r = 0.8826; < 0.0001.

Post-TDV vaccination sera prevents NS1-induced glycocalyx-like layer (EGL) degradation *in vitro*

The endothelial glycocalyx is a major determinant of endothelial barrier function, and we previously demonstrated that NS1 from all 4 DENV serotypes triggers degradation of glycocalyx components on the surface of endothelial cells *in vitro* (88, 89). Using a subset of serum samples evaluated by TEER **(Figures 6.1, 6.S1, 6.S2)**, we next used confocal microscopy to visualize the effect of pre- and post-vaccination sera from DENV-naïve and pre-immune subjects on NS1-induced disruption of sialic acid and heparan sulfate, two key components of the EGL. Reflecting the endothelial permeability results, we found that day 0 sera from naïve subjects had no substantial protective effect, while day 120 post-vaccination sera from naïve subjects completely blocked degradation of both sialic acid and heparan sulfate **(Figures 6.2a,c,d, 6.S4a)**. Day 0 samples from pre-immune subjects exhibited varying levels of protection, while sera from pre-immune subjects at day 120 post vaccination were completely protective **(Figures 6.2b-d, 6.S4b)**. Positive control serum was used as a baseline for protection, and negative control serum represented maximum NS1-mediated disruption. Taken together, these results suggest that the anti-NS1 antibody response stimulated by TDV can protect against NS1-induced hyperpermeability by preventing the degradation of key EGL components.

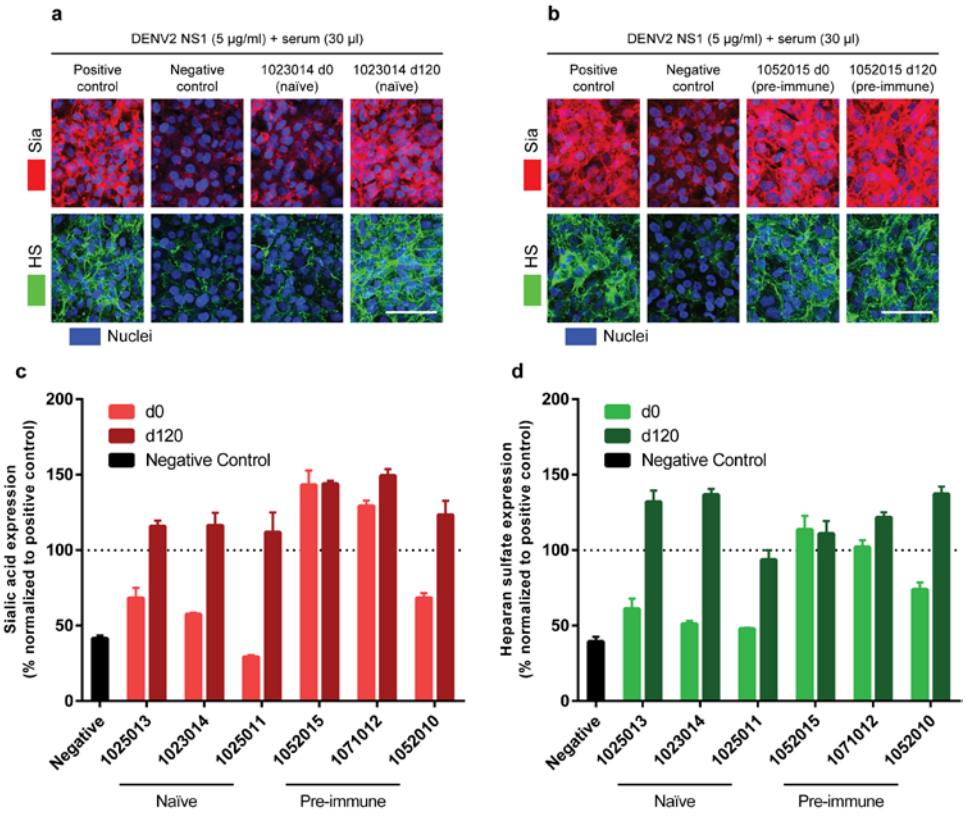

Figure 6.2. Sera from TDV-vaccinated subjects prevents DENV2 NS1-induced sialic acid and heparan sulfate degradation on HPMEC.
The effect of representative **(a)** DENV-naïve (1023014) and **(b)** pre-immune (1052010) sera on DENV2 NS1-induced disruption of sialic acid (Sia) and heparan sulfate (HS). **(a,b)** The integrity of the EGL on HPMEC was assessed by the presence of sialic acid surface expression, stained with WGA-A647 (red, top row), and heparan sulfate surface expression (green, bottom row) at 6 hours post-treatment (hpt) with serum (as indicated) + DENV2 NS1 (5 µg/ml) at 37°C, as visualized via confocal microscopy. Nuclei were stained with Hoechst (blue). Images (20X; scale bars, 50 µm) are representative of 1 independent experiment performed in duplicate. **(c,d)** Quantification of mean fluorescence intensity (MFI) of **(c)** sialic acid and **(d)** heparan sulfate expression from **(a,b)** and **Figure 6.S4** from one independent experiment. Values normalized to MFI from the NS1 + positive control serum group (represented by dotted line at 100%) and expressed as percentage of control. Error bars indicate SEM. Confocal microscopy images acquired and analyzed by Dr. Henry Puerta-Guardo.

Anti-NS1 IgG responses elicited by Takeda's TDV are cross-reactive against NS1 from other DENV serotypes, and protection correlates with antibody concentration

DENV infection in humans results in the production of serotype-specific NS1 antibodies as well as cross-reactive antibodies to at least one if not all three other serotypes (52, 240, 247). In addition, we previously demonstrated that vaccination with recombinant DENV1, DENV3, or DENV4 NS1 combined with adjuvant provided partial protection against lethal DENV2 infection in mice (84). Because Takeda's TDV is constructed on an

attenuated DENV2 backbone, only DENV2 NS1 is produced by the vaccine virus. Therefore, we next evaluated whether the TDV-elicited anti-DENV2 NS1 antibody response was cross-protective against DENV1, DENV3, and DENV4 NS1-induced hyperpermeability. We analyzed a subset of DENV-naïve and pre-immune day 0 and day 120 post-vaccination samples against recombinant DENV1, DENV3, and DENV4 NS1 proteins using TEER and found that sera could cross-protect against NS1 from other DENV serotypes **(Figures 6.3a,b, 6.S5, 6.S6, 6.S7)**. The positive control serum fully blocked hyperpermeability induced by all four DENV serotypes while the negative control serum did not **(Figure 6.S3)**. As we observed with the DENV2 results, the ability to prevent DENV1, DENV3, and DENV4 NS1-induced hyperpermeability correlated with the magnitude of cross-reactive NS1-specific antibodies in each sample **(Figure 6.3c)**. Taken together, these results suggest that vaccination with TDV elicits a protective, cross-reactive, NS1-specific antibody response capable of blocking NS1-mediated barrier dysfunction.

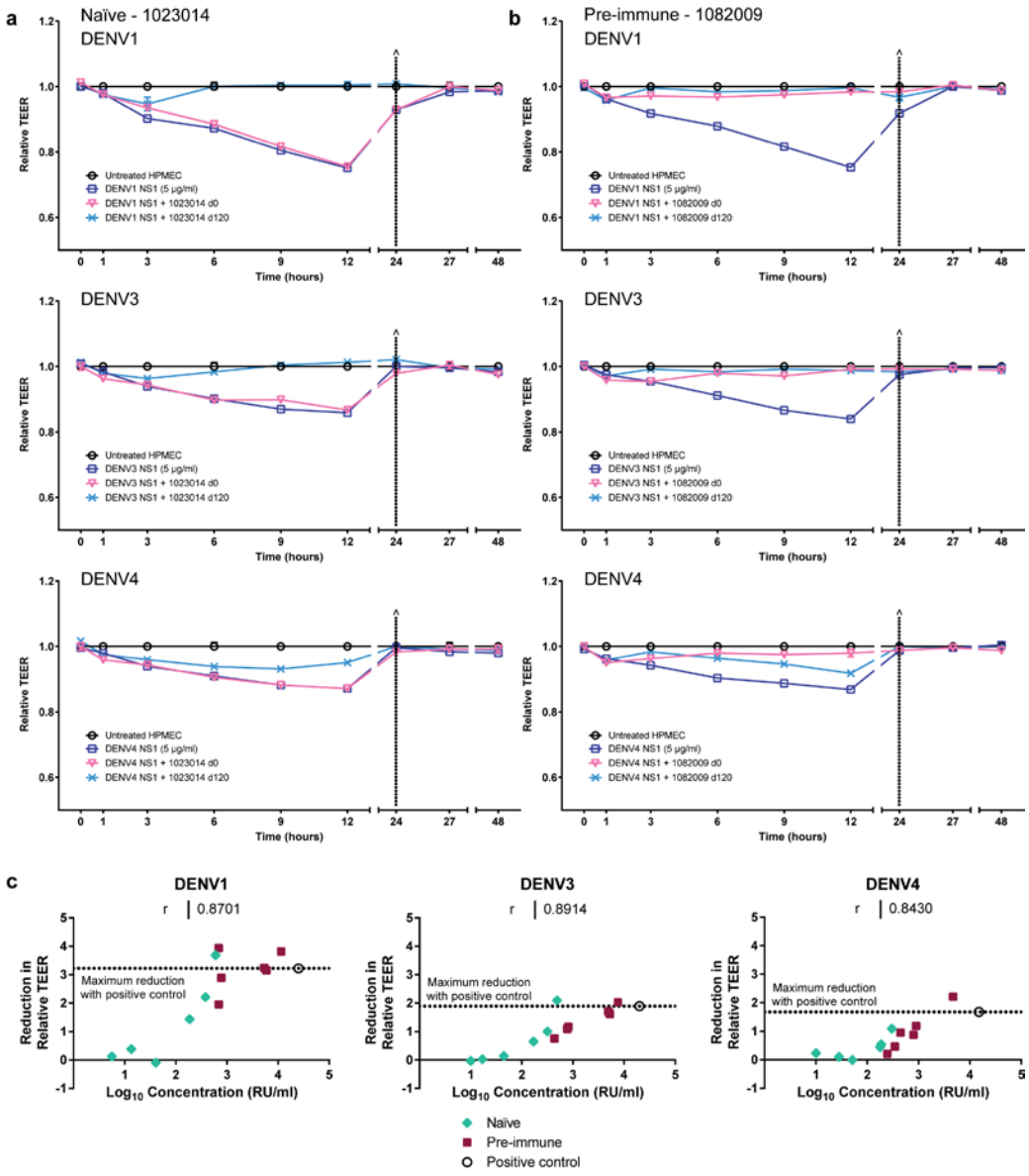

Figure 6.3. Anti-DENV2 NS1 serum from TDV-immunized subjects provides cross-reactive responses that protect against DENV1, DENV3, and DENV4 NS1-induced hyperpermeability.
(a,b) The effect of serum on DENV1 **(top)**, DENV3 **(middle)**, and DENV4 **(bottom)** NS1-induced endothelial hyperpermeability was evaluated by TEER. Representative graphs are shown for **(a)** DENV-naïve (1023014) and **(b)** pre-immune (1052010) samples. HPMEC were grown on Transwell semi-permeable membranes (0.4 µm pore size), and serum samples (30 µl) were added to the apical chamber at a dilution of 1:10 in the presence of DENV NS1 (5 µg/ml) (DENV NS1, blue squares; day 0 serum + DENV NS1, red triangles; day 120 serum + DENV NS1, light blue X's). Endothelial permeability was measured at indicated time-points over 48 hours. (^) represents change of medium. Relative TEER values from one independent experiment performed in duplicate are plotted. Error bars indicate SEM. **(c)** Correlation analysis of 3 DENV-naïve and 3 pre-immune samples from both day 0 and day 120 (12 total samples) for DENV1 **(left)**, DENV3 **(middle)**, DENV4 **(right)**. AUC values were calculated for each curve in each TEER experiment. The absolute reduction in relative TEER for each serum sample **(a,b; 6.S5, 6.S6, 6.S7)** was calculated by subtracting the AUC of NS1 + serum from the AUC of NS1 alone.

Reduction was plotted against the $\log_{10}$ of antibody concentrations for each sample, and a correlation analysis was performed. The dotted line represents the reduction of TEER by positive control serum. Naïve subjects, red circles; pre-immune subjects, light blue squares; positive control serum, blue circle. DENV1: $r = 0.8826$, $P < 0.0001$; DENV3: $r = 0.8914$, $P < 0.0001$; DENV4: $r = 0.8430$, $P = 0.0006$.

Discussion

Over the past 5 years, substantial progress has been made towards understanding the role of NS1 in viral pathogenesis, and evidence suggests that NS1 plays a key role in mediating vascular leak during DENV infection. However, the inclusion of NS1 in a DENV vaccine or other flavivirus vaccines remains under discussion. The approved CYD vaccine (Dengvaxia®) for dengue from Sanofi Pasteur does not include DENV NS1 (248), whereas other live-attenuated DENV vaccines in development, including TDV, include the DENV NS1 sequence.

It has previously been shown that candidate NS1 recombinant protein and DNA vaccines are highly immunogenic and protective in mouse models (84, 116, 249-251). Several studies have shown that immunization with adjuvanted recombinant NS1 or passive transfer of polyclonal antibodies from NS1-immunized mice or of certain anti-NS1 mAbs to naïve mice were shown to protect against DENV vascular leak disease, presumably by triggering lysis of infected cells and/or blocking the pathogenic effects of secreted NS1 (84, 139, 252).

Chu et al. previously demonstrated that vaccination with TDV elicits an NS1-specific CD8+ T cell response that cross-reacts with NS1 from all 4 DENV serotypes (253). Further, in human trials, the NIH TV-003 DENV vaccine elicited NS1-specific CD4+ T cell and CD8+ T cell responses similar in magnitude and breadth to those found after natural infection (254, 255). An NS1 DNA vaccine study in mice used depletion and transfer studies to demonstrate that CD4+ T cells were critical for NS1-specific immune protection from virus challenge (256). Additionally, investigators identified several immunodominant B cell NS1 epitopes in DENV-infected mice that are conserved across all four DENV serotypes (54), suggesting that vaccination with an NS1 subunit or live vaccine could potentially provide protection against other DENV serotypes. Taken together, these studies suggest that immune responses to NS1 may contribute to protection against DENV infection and therefore may be important to elicit with dengue vaccines.

In the Takeda TDV study, we evaluated the functionality of the anti-DENV2 NS1 antibody response elicited by the Takeda's TDV and found that vaccination with TDV stimulates an IgG response that protects against DENV2 NS1-induced hyperpermeability and EGL disruption, and this response correlates with antibody concentration. Post-vaccination sera also provide cross-reactive protection against DENV1, DENV3, and DENV4 NS1-induced hyperpermeability that also correlates with antibody concentrations as well. Taken together, these results demonstrate that vaccination with TDV can induce IgG responses that may protect against NS1-mediated pathogenesis during DENV infection.

Our data here, combined with previous studies, support the inclusion of NS1 in future DENV vaccines, either as a separate protein component or as protein secreted by vaccine virus-infected cells. In light of the recent controversy surrounding the Sanofi Pasteur DENV vaccine, particularly the potential to trigger ADE during secondary DENV infection post-vaccination (20, 235, 236), it is perhaps more pertinent than ever to explore the importance of NS1 antibodies, which do not induce ADE, in future DENV vaccine candidates.

With regard to the Takeda TDV, further work is required to evaluate the protective effect of post-TDV vaccination sera, particularly in an animal model of local (89) or, ideally, systemic vascular leakage (84) induced by DENV NS1. As NS1 is known to play a variety of roles in pathogenesis, including activation of immune cells leading to production of inflammatory cytokines (85) and interactions with complement (118, 123), it will be important to evaluate the effects of TDV vaccination sera in the larger context of NS1 pathogenesis *in vivo* in addition to the endothelial-intrinsic context we have explored here. It would also be interesting to compare the anti-NS1 antibody repertoire elicited by vaccination compared with natural infection (52), including both quality and quantity of the response. Efforts are ongoing to conduct these studies.

This is the first study to show that a candidate DENV vaccine can induce functional anti-NS1 antibody responses that could protect against NS1-mediated pathogenesis, and our work here provides further evidence supporting inclusion of NS1 in DENV vaccines. In this study, we demonstrated that vaccination with the Takeda TDV elicits an anti-NS1 antibody response that protects against DENV2 NS1-induced endothelial hyperpermeability, and the level of protection correlates with antibody concentrations. We further showed that post-TDV sera abrogate degradation of key endothelial glycocalyx components by NS1. Finally, we determined that the post-vaccination anti-NS1 antibody response is cross-protective against NS1 from DENV1, DENV3, and DENV4 NS1, and protection also correlates with antibody concentrations. Taken together, our results suggest that the Takeda TDV stimulates a protective anti-NS1 antibody response that may contribute to protection against severe dengue disease.

Experimental Procedures

Cell culture. The human pulmonary microvascular endothelial cell line HPMEC-ST1.6r (HPMEC) was kindly donated by Dr. J.C. Kirkpatrick (Institute of Pathology, Johannes Gutenberg University, Germany) and grown as previously described (88).

Recombinant NS1 proteins. Recombinant DENV1 (Nauru/Western Pacific/1974), DENV2 (Thailand/16681/84), DENV3 (Sri Lanka D3/H/IMTSSA-SRI/2000/1266), and DENV4 (Dominica/814669/1981) NS1 proteins, greater than 95% purity and certified to be free of endotoxin contaminants, were produced by the Native Antigen Company (Oxfordshire, United Kingdom) in HEK293 cells at their facility and used in all experiments. NS1 preparations were also tested using the Endpoint Chromogenic Limulus Amebocyte Lysate (LAL) QCL-1000TM kit (Lonza) and confirmed to be free of bacterial endotoxins (88).

Serum samples. Serum samples were collected by researchers at Takeda from 6 DENV-naïve and 6 DENV-pre-immune subjects on day 0 before vaccination and day 120 post-vaccination with the Takeda TDV (246). Antibody concentrations were determined by ELISA. Aliquots were then sent to UC Berkeley for functional analysis. Positive control serum (DLS pool, from DENV-immune individuals) and negative control serum (BioIVT, Westbury, NY) were also provided by Takeda for experiments performed at UC Berkeley.

Monoclonal antibodies. For staining of EGL components, the following monoclonal antibodies (mAbs) and lectins were used: Wheat germ agglutinin (WGA) lectin conjugated to Alexa Fluor 647 (WGA-A647, Molecular Probes) to stain N-acetyl neuraminic acid (sialic acid); Heparan Sulfate monoclonal antibody, purified (clone F58-10E4, Amsbio). Donkey anti-mouse IgM conjugated to Alexa Fluor 488 (Jackson) was used as a secondary detection antibody in confocal microscopy experiments.

Transendothelial electrical resistance (TEER). The effect of recombinant DENV1, DENV2, DENV3, and DENV4 NS1 proteins and Takeda TDV sera on endothelial permeability was evaluated by measuring TEER of HPMEC grown on a 24-well Transwell polycarbonate membrane system (Transwell permeable support, 0.4 μm, 6.5 mm insert; Corning Inc.) as previously described (84, 88). Briefly, TEER was measured in Ohms (Ω) at sequential 2-hour time-points following the addition of test proteins using an Epithelial Volt Ohm Meter (EVOM) with “chopstick” electrodes (World Precision Instruments). Untreated endothelial cells grown on Transwell inserts were used as negative untreated controls, and inserts with medium alone were used for blank resistance measurements. Relative TEER represents a ratio of resistance values (Ω) as follows: (Ω experimental condition - Ω medium alone) / (Ω non-treated endothelial cells - Ω medium alone). After 24 hours of treatment, 50% of upper and lower chamber media were replaced by fresh endothelial cell medium. For experiments using sera, 30 μl of culture supernatant was removed from the apical chamber and replaced with 30 μl of serum sample immediately before the addition of DENV NS1.

Fluorescence microscopy. Microscopy was performed as previously described (88). For imaging experiments, HPMEC were grown on coverslips coated with 0.2% gelatin

(Sigma) and imaged on a Zeiss LSM 710 Axio Observer inverted fluorescence microscope equipped with a 34-channel spectral detector. Images acquired using the Zen 2010 software (Zeiss) were processed and analyzed with ImageJ software (188). All RGB images were converted to grayscale, then mean grayscale values and integrated density from selected areas were taken, along with adjacent background readings, and plotted as mean fluorescence intensity (MFI). To assess the effect of Takeda TDV sera on DENV2 NS1-induced EGL disruption, the distribution of sialic acid and heparan sulfate was examined on confluent HPMEC monolayers treated with DENV2 NS1 (5 µg/ml) + negative control serum (30 µl), NS1 + positive control serum (30 µl), or NS1 + TDV serum (30 µl) and fixed with 4% paraformaldehyde (PFA) at 6 hours post-treatment. Primary antibodies were incubated overnight at 4°C, and detection was performed using secondary species-specific anti-IgG or anti-IgM antibodies conjugated to Alexa fluorophores (488 and 647).

Statistics. Statistical analyses were performed using GraphPad Prism 6 software, and all graphs were generated using Prism 6. For correlation analyses, the area under the curve (AUC) was taken from all curves in all TEER experiments using a baseline of Y = 1 and also considering troughs that go below the set baseline (because TEER values decrease below Y = 1). The net area was then used. For each experiment, the AUC of NS1 + serum was subtracted from the AUC of NS1 alone, providing a reduction in relative TEER for each serum sample. The reduction in relative TEER was then plotted against the $\log_{10}$ antibody concentration for each sample, and a correlation analysis was performed. The Pearson correlation coefficient and two-tailed p-value are reported.

Supplementary Material

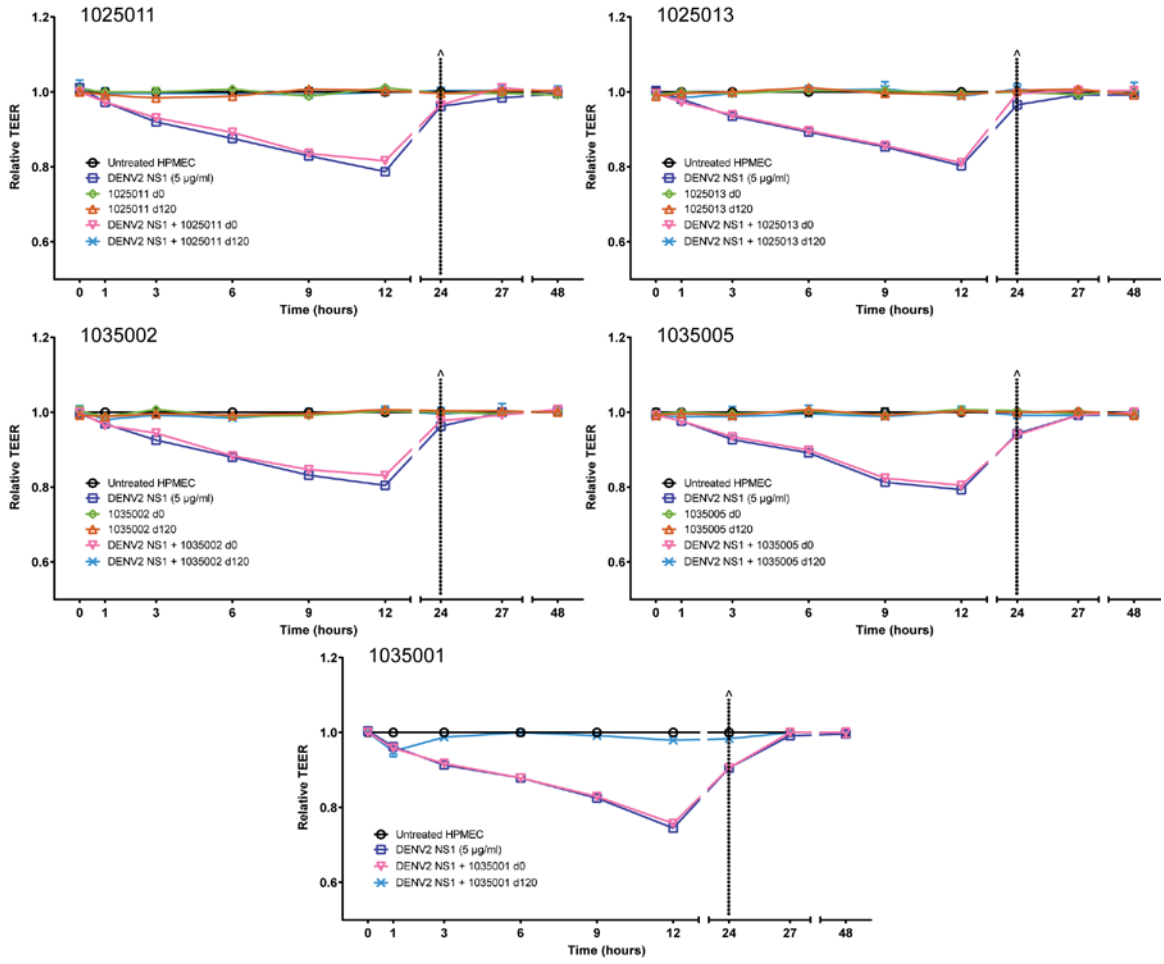

Figure 6.S1. Related to Figure 6.1. Serum from DENV-naïve subjects vaccinated with Takeda TDV protects against DENV2 NS1-induced hyperpermeability.
The effect of DENV-naïve serum on DENV2 NS1-induced endothelial hyperpermeability was evaluated by TEER. HPMEC were grown on Transwell semi-permeable membranes (0.4 µm pore size), and serum samples (30 µl) were added to the apical chamber in the presence or absence of DENV2 NS1 (5 µg/ml) (DENV2 NS1, blue squares; day 0 serum alone, green diamonds; day 120 serum alone, orange triangles; day 0 serum + DENV2 NS1, red triangles; day 120 serum + DENV2 NS1, light blue X's). Endothelial permeability was measured at indicated time-points over 48 hours. (^) represents change of medium. Relative TEER values from one independent experiment performed in duplicate are plotted. Error bars indicate SEM.

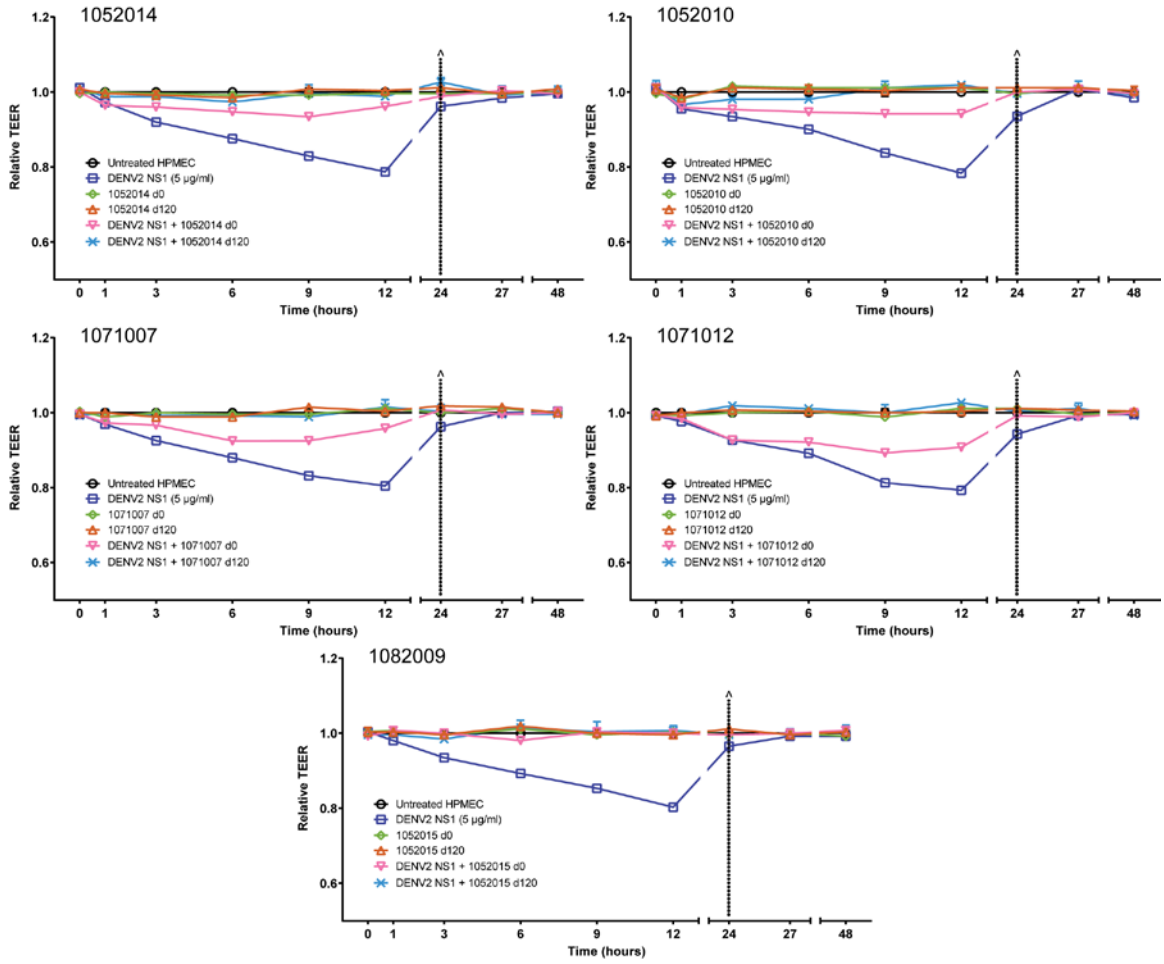

Figure 6.S2. Related to Figure 6.1. Serum from DENV-pre-immune subjects vaccinated with Takeda TDV protects against DENV2 NS1-induced hyperpermeability.
The effect of DENV-pre-immune serum on DENV2 NS1-induced endothelial hyperpermeability was evaluated by TEER. HPMEC were grown on Transwell semi-permeable membranes (0.4 µm pore size), and serum samples (30 µl) were added to the apical chamber in the presence or absence of DENV2 NS1 (5 µg/ml) (DENV2 NS1, blue squares; day 0 serum alone, green diamonds; day 120 serum alone, orange triangles; day 0 serum + DENV2 NS1, red triangles; day 120 serum + DENV2 NS1, light blue X's). Endothelial permeability was measured at indicated time-points over 48 hours. (^) represents change of medium. Relative TEER values from one independent experiment performed in duplicate are plotted. Error bars indicate SEM.

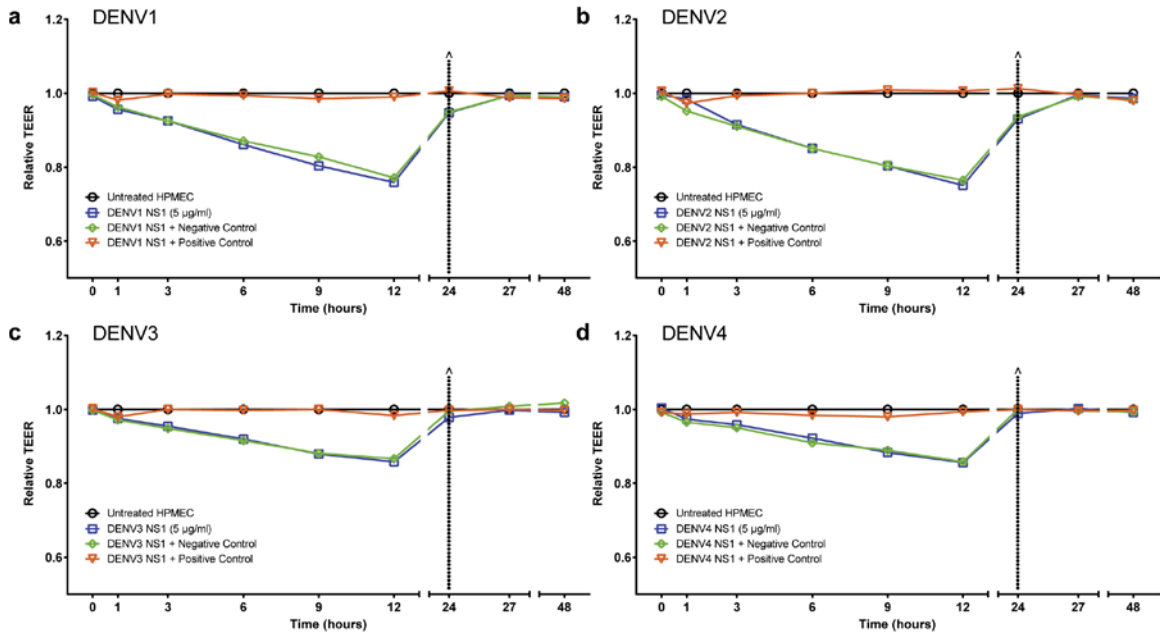

Figure 6.S3. Related to Figures 6.1, 6.3. Positive control serum protects against hyperpermeability induced by NS1 from DENV1-4, but negative control serum does not.
The effects of positive and negative control sera on **(a)** DENV1, **(b)** DENV2, **(c)** DENV3, and **(d)** DENV4 NS1-induced endothelial hyperpermeability were evaluated by TEER. HPMEC were grown on Transwell semi-permeable membranes (0.4 µm pore size), and serum samples (30 µl) were added to the apical chamber in the presence or absence of DENV NS1 (5 µg/ml) (DENV NS1, blue squares; negative control serum + DENV NS1, pink diamonds; positive control serum + DENV NS1, purple triangles). Endothelial permeability was measured at indicated time-points over 48 hours. (^) represents change of medium. Relative TEER values from two independent experiments performed in duplicate are plotted. Error bars indicate SEM.

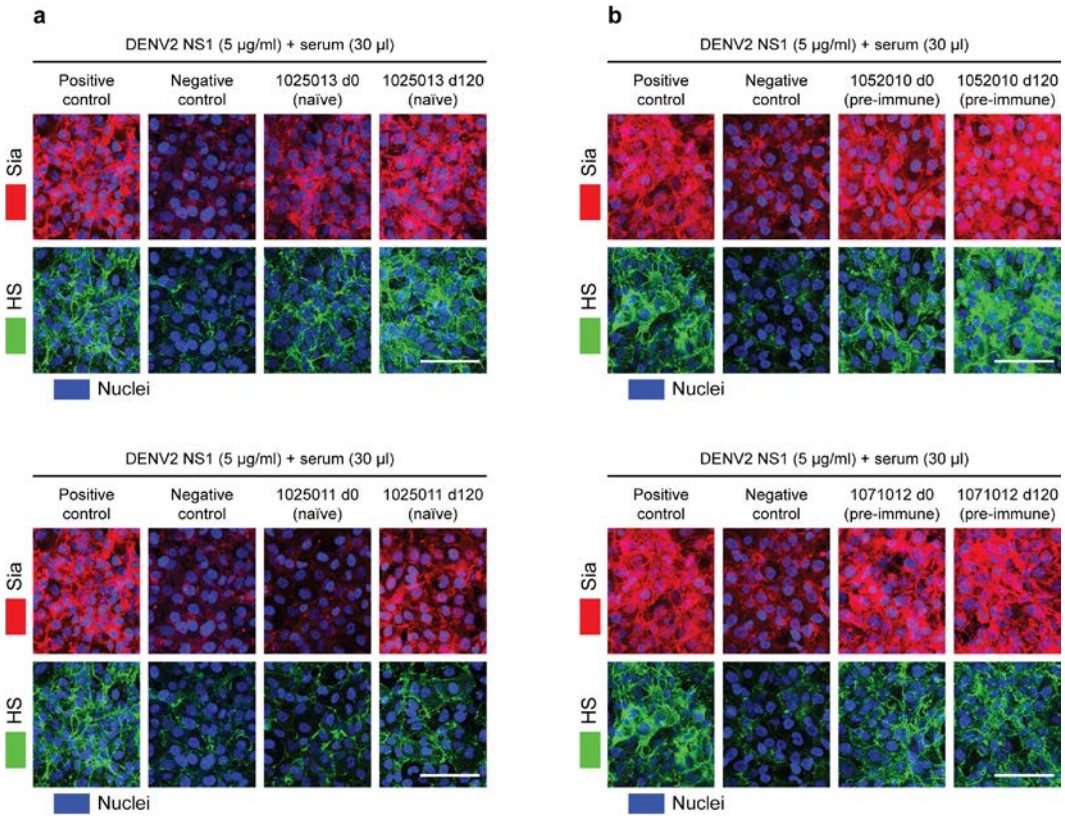

Figure 6.S4. Related to Figure 6.2. TDV serum prevents DENV2 NS1-induced sialic acid and heparan sulfate degradation on HPMEC.
The effect of **(a)** DENV-naïve (1025013, top; 1025011, bottom) and **(b)** pre-immune (1052015, top; 1071012, bottom) sera on DENV2 NS1-induced disruption of sialic acid (Sia) and heparan sulfate (HS). **(a,b)** The integrity of the EGL on HPMEC was assessed by the presence of sialic acid surface expression, stained with WGA-A647 (red, top row), and heparan sulfate surface expression (green, bottom row) at 6 hpt with serum (as indicated) + DENV2 NS1 (5 µg/ml) at 37°C, as visualized via confocal microscopy. Nuclei were stained with Hoechst (blue). Images (20X; scale bars, 50 µm) are representative of 1 independent experiment performed in duplicate. Confocal microscopy images acquired and analyzed by Dr. Henry Puerta-Guardo.

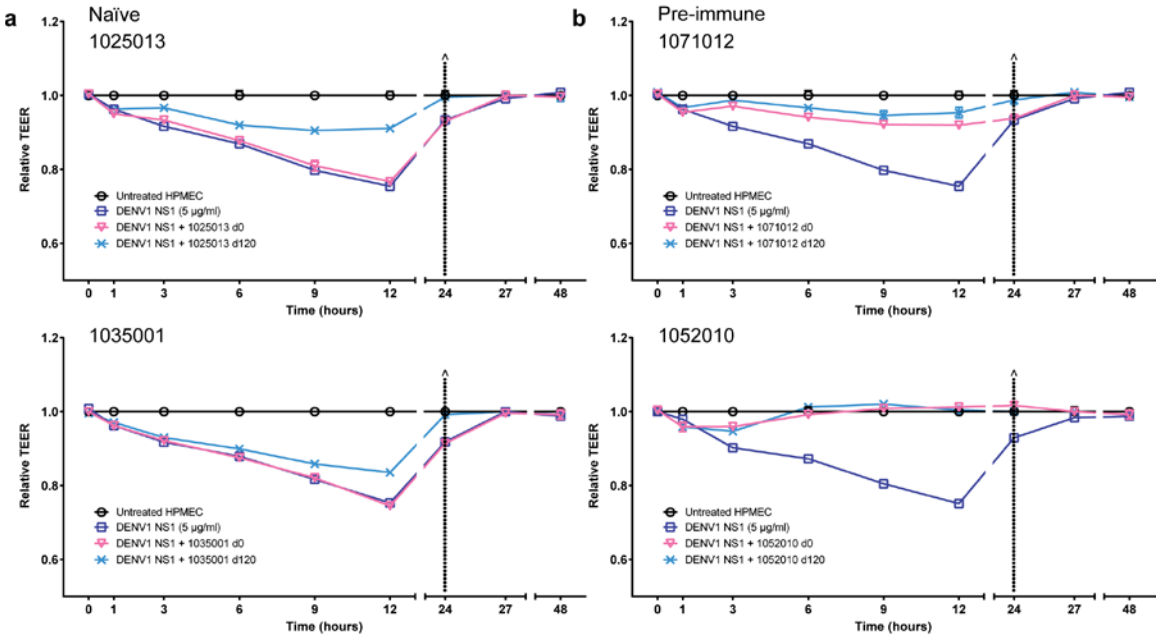

Figure 6.S5. Related to Figure 6.3. TDV anti-NS1 serum provides cross-reactive protection against DENV1 NS1-induced hyperpermeability.
The effect of **(a)** DENV-naïve or **(b)** pre-immune sera on DENV1 NS1-induced endothelial hyperpermeability was evaluated by TEER. HPMEC were grown on Transwell semi-permeable membranes (0.4 µm pore size), and serum samples (30 µl) were added to the apical chamber in the presence or absence of DENV1 NS1 (5 µg/ml) (DENV1 NS1, blue squares; day 0 serum + DENV1 NS1, red triangles; day 120 serum + DENV1 NS1, light blue X's). Endothelial permeability was measured at indicated time-points over 48 hours. (^) represents change of medium. Relative TEER values from one independent experiment performed in duplicate are plotted. Error bars indicate SEM.

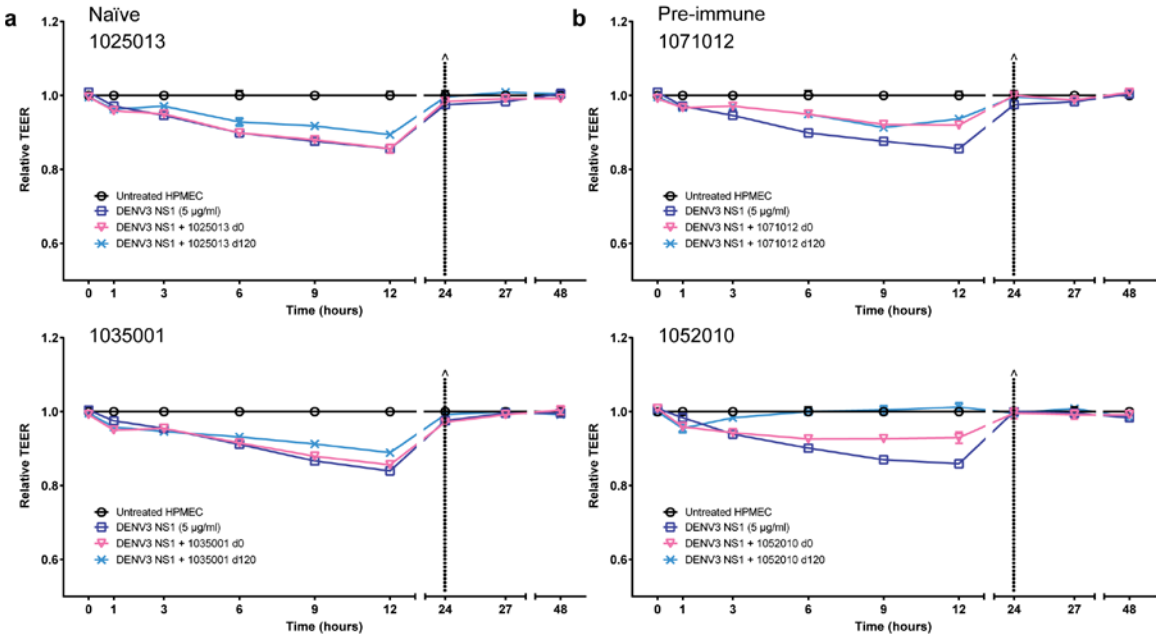

Figure 6.S6. Related to Figure 6.3. TDV anti-NS1 serum provides cross-reactive protection against DENV3 NS1-induced hyperpermeability.
The effect of **(a)** DENV-naïve or **(b)** pre-immune sera on DENV3 NS1-induced endothelial hyperpermeability was evaluated by TEER. HPMEC were grown on Transwell semi-permeable membranes (0.4 µm pore size), and serum samples (30 µl) were added to the apical chamber in the presence or absence of DENV3 NS1 (5 µg/ml) (DENV1 NS1, blue squares; day 0 serum + DENV3 NS1, red triangles; day 120 serum + DENV3 NS1, light blue X's). Endothelial permeability was measured at indicated time-points over 48 hours. (^) represents change of medium. Relative TEER values from one independent experiment performed in duplicate are plotted. Error bars indicate SEM.

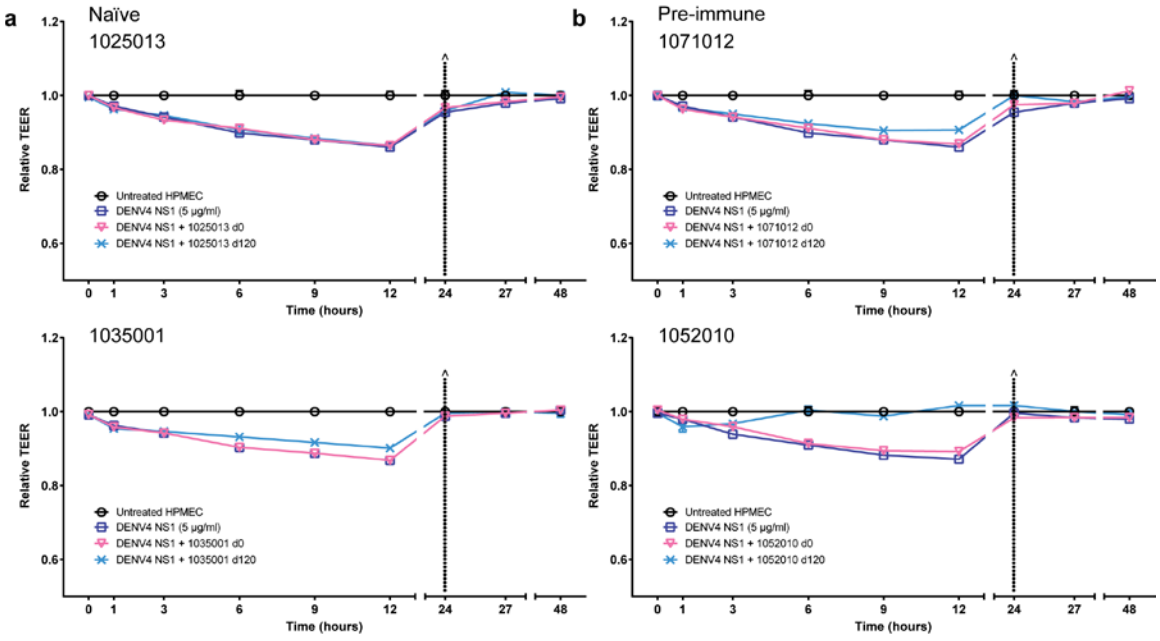

Figure 6.S7. Related to Figure 6.3. TDV anti-NS1 serum provides cross-reactive protection against DENV4 NS1-induced hyperpermeability.
The effect of **(a)** DENV-naïve or **(b)** pre-immune sera on DENV4 NS1-induced endothelial hyperpermeability was evaluated by TEER. HPMEC were grown on Transwell semi-permeable membranes (0.4 µm pore size), and serum samples (30 µl) were added to the apical chamber in the presence or absence of DENV4 NS1 (5 µg/ml) (DENV1 NS1, blue squares; day 0 serum + DENV4 NS1, red triangles; day 120 serum + DENV4 NS1, light blue X's). Endothelial permeability was measured at indicated time-points over 48 hours. (^) represents change of medium. Relative TEER values from one independent experiment performed in duplicate are plotted. Error bars indicate SEM.

Chapter 7: Concluding thoughts and future directions

Summary

Since we initially identified a novel role for DENV NS1 in viral pathogenesis, substantial work has been undertaken to better understand the mechanisms underlying NS1-induced endothelial barrier dysfunction. We first identified enzymes in endothelial cells that are activated upon NS1 stimulation, including sialidases, cathepsin L, and heparanase, leading to the disruption of the EGL. Second, we showed that NS1 induces vascular leak in the dermis of wild-type mice in the absence of viral infection and that this effect is dependent on the activity of sialidases, cathepsin L, and heparanase but independent of TLR4 and TNF-α signaling. Third, we determined that glycosylation at Asn-207 is a key molecular determinant of NS1-mediated pathogenesis and showed that the N207Q NS1 mutation results in loss of NS1-induced endothelial hyperpermeability and EGL disruption. Additionally, we demonstrated that endothelial cells internalize NS1 via clathrin-mediated endocytosis and that this internalization is required for downstream pathogenic functions. Fourth, we investigated whether NS1 from other flaviviruses, including ZIKV, WNV, JEV, and YFV, could induce barrier dysfunction of endothelial cells from distinct tissue sites, including the dermis, umbilical vein, brain, and liver. We found that NS1 triggered endothelial hyperpermeability and EGL disruption in an NS1- and tissue-specific manner that reflected viral tropism. Finally, we evaluated whether vaccination with Takeda's live-attenuated Tetravalent Dengue Vaccine candidate could elicit protective anti-NS1 antibody responses and found that the vaccine induced antibody responses that abrogated NS1-induced endothelial hyperpermeability and EGL degradation. These responses provided cross-reactive protection against DENV1, DENV3, and DENV4 NS1 and correlated with the titer of anti-NS1 antibodies in patient sera. Taken together, this body of work represents an extensive advancement in our understanding of the NS1 protein and its contributions to disease.

Future Directions

Because of its many roles in DENV replication and infection, NS1 is one of the most fascinating viral proteins, and with key functions in viral replication, immune evasion, and pathogenesis (146), it is arguably the most important protein in the flavivirus life cycle. Although major advances have been made over the past decade to better understand the complex roles of NS1 during DENV and other flavivirus infections, important questions still remain, particularly regarding pathogenesis and the mechanisms – and evolutionary benefit – of induction of endothelial hyperpermeability.

The most obvious open question is the identity of the cognate receptor for NS1. Though DENV NS1 has been previously described to attach to cells, including microvascular endothelial cells, via heparan sulfate and chondroitin sulfate (87), our results show that binding alone is not sufficient to induce endothelial hyperpermeability and downstream mechanisms driving pathogenesis. Preliminary data support a role for glycans on the cell surface as a binding partner and suggest that sulfation levels of these glycans may contribute to the NS1- and tissue-specific binding patterns observed in Chapter 5. Extensive glycobiology studies are currently being performed to better understand these interactions. Beyond this initial binding step, our data comparing wild-type NS1 to the N207Q NS1 mutant suggest that clathrin-mediated endocytosis of the protein is required

for cathepsin L activation and induction of endothelial barrier dysfunction, and binding is required but not sufficient to induce endocytosis. As such, we believe that there is a proteinaceous receptor that drives internalization of NS1 working in conjunction with heparan sulfate and chondroitin sulfate as co-receptors or binding partners.

Though we have identified several key enzymes, including cathepsin L and sialidases, that contribute to NS1-induced endothelial glycocalyx degradation and hyperpermeability, the precise mechanisms leading to their activation remain unclear. One of our leading hypotheses is that endocytosis of NS1 leads to internalization of heparan sulfate, which has been previously shown to activate cathepsin L (207, 208), leading to cleavage of pro-cathepsin L to its activate form in the endolysosome. Given our data that show that endothelial cells internalize NS1 via clathrin-mediated endocytosis, and that this internalization is required for downstream pathogenesis, this hypothesis is well within the realm of possibility; however, it is also possible that NS1 directly interacts with and activates cathepsin L and/or endothelial sialidases, specifically Neu1, upon its internalization into the endolysosome or that a signaling cascade leads to activation of these enzymes. Further study is required to better elucidate the steps that occur immediately following NS1 binding to endothelial cells.

Relatedly, there are two structural biology questions that may be particularly interesting to address. First, it is unknown whether NS1 is internalized as a hexamer and, if it is, whether it remains as a hexamer while inside the cell. Second, it is unclear whether NS1 is degraded inside endothelial cells after triggering downstream pathogenic mechanisms or if is eventually trafficked out of the cell, leading to accumulation in the tissue. The answers to these questions may provide insight into the ultimate fate of NS1 during human disease and contribute to our overall understanding of its role during infection.

We have strongly implicated the endothelial glycocalyx as an important target of DENV NS1-mediated pathogenesis. Our *in vitro* studies demonstrate that NS1 leads to the loss of sialic acid, heparan sulfate, and syndecan-1, key glycocalyx components, from the surface of endothelial cells via the activity of cathepsin L, heparanase, and sialidases, and inhibition of these enzymes prevents loss of components following NS1 treatment. *In vivo*, we have shown that inhibiting cathepsin L, heparanase, and sialidases prevents DENV NS1-induced vascular leakage in the dermis of mice, and injection with NS1 or DENV leads to higher circulating levels of heparan sulfate and sialic acid (D.A. Espinosa & E. Harris, unpublished data) in the serum of treated mice. However, we have yet to directly demonstrate that the glycocalyx is disrupted by NS1 *in vivo*. Because cultured endothelial cells lack a true glycocalyx layer (257, 258), visualization of the glycocalyx *in vivo* will be required to definitively show that it is disrupted by NS1. This would require use of intravital microscopy, two-photon microscopy, and electron microscopy (151, 192-194), challenging techniques that take specific expertise to perform. It would also be interesting to study the glycocalyx *in vivo* in the context of DENV infection in addition to administration of NS1 alone. Importantly, circulating levels of hyaluronic acid and heparan sulfate in serum have been shown to be increased in dengue patients (93), and levels of chondroitin sulfate and syndecan-1 correlate with dengue plasma leakage (92), providing evidence that glycocalyx degradation occurs during dengue disease in humans.

NS1 has been shown to play a variety of roles in DENV pathogenesis, and the relative contributions of each role are difficult to dissect from each other. These roles include activation of complement (118-120), degradation of the endothelial glycocalyx (88, 89), activation of immune cells leading to inflammatory cytokine production (85), and disruption of tight and adherens junctions (95, 259). Though several of these observations have been substantiated in animal models, much of the work was conducted in reductionist cell culture models *in vitro*. As such, it is difficult to ascertain if any one phenomenon contributes more than another to vascular leak in animal models or, more interestingly, during infection in humans. Most likely, NS1-mediated disruption of the endothelial glycocalyx and intercellular junctions as well as production of inflammatory cytokines all occur throughout the course of severe dengue disease with varied kinetics and magnitude, though peaking during the critical period, leading to a complex synergy of viral- and host-specific factors that all contribute to endothelial barrier dysfunction and vascular leak.

Perhaps more important than the relative contributions of specific mechanisms to NS1-mediated pathogenesis is the pathogenic role and contributions of NS1 in the greater context of DENV infection. In addition to NS1, DENV infection of immune cells can lead to dysregulated production of cytokines and other inflammatory mediators that contribute to vascular leakage (27-31), and cytotoxic T cells have previously been implicated in pathogenesis as well (22, 24-26). Additionally, antibody-dependent enhancement is hypothesized to result in increased viremia and activation of target immune cells, leading to more severe secondary infection with a heterologous serotype (15-20). The growing body of literature about NS1 and its roles in pathogenesis adds multiple layers of complexity to an already complex disease, and a more complete understanding of the dynamics that occur during infection may lead to better management strategies, novel therapeutics, and/or vaccine candidates.

A fascinating but ultimately difficult question to answer is what the evolutionary role of flavivirus NS1-induced barrier dysfunction is in the context of viral infection and disease. Though we demonstrated a striking pattern of NS1- and tissue-specific hyperpermeability and vascular leak, it is unclear what the importance of this effect is during human infection. Zika, West Nile, and Japanese encephalitis are not diseases characterized by vascular leak, and little is known about the levels of secreted NS1 in humans during non-DENV flavivirus infections. However, we hypothesize that vascular leak in target organs facilitates virus entry into tissues from the vasculature, thereby leading to more infection of target cells at specific sites in the body and contributing to the viral tropism associated with these infections. Researchers have also reported that NS1 directly interacts with the structural DENV proteins Envelope and pre-Membrane, modulating the production of infectious particles (60). Thus, it is possible that NS1 can interact with the virus outside of the cell, and NS1 could potentially serve as a binding partner for the virus on the surface of endothelial cells, contributing to viral entry, passage across the endothelium, and dissemination into tissues. This same NS1-to-particle binding may also occur on non-endothelial cell types, contributing to viral infection of target cells. Work is ongoing in the Harris Laboratory to further address this hypothesis, and the results could substantially alter our current understanding of flavivirus infection.

Mosquitoes acquire NS1 when feeding on DENV-infected humans, and researchers have shown that NS1 helps the virus overcome barriers to infection in the arthropod host (140). Additionally, Thiemmeca et al. found that NS1 is detectable in the saliva of DENV-infected mosquitoes and that mosquito-derived NS1 binds to mannose-binding lectin, potentially protecting DENV from complement-mediated neutralization at the site of infection (122). However, it is unclear if saliva-delivered NS1 plays other roles during transmission and dissemination of the virus. I have previously shown that salivary gland extract (SGE) from uninfected female *Aedes aegypti* mosquitoes can induce endothelial hyperpermeability in human dermal microvascular endothelial cells and vascular leak in the dermis of mouse ears, and SGE increased morbidity and mortality during antibody-enhanced DENV infection (143). Further, proteins in mosquito saliva have been shown to impact viral replication and pathogenesis (141-143). It is, therefore, conceivable that NS1 plays a role immediately after inoculation into the dermis by infected mosquitoes, perhaps altering the dermal microenvironment at the site of infection and aiding in virus dissemination and/or the establishment of infection.

DENV NS1 and NS1-mediated pathogenesis represent a potential target for drug and vaccine development. Because of the effect of NS1 on the glycocalyx (88, 89), currently licensed sialidase inhibitors for treatment of influenza (260) and heparanase inhibitors used in cancer therapy (261, 262) may prevent NS1-induced degradation of the glycocalyx and subsequent vascular leak. We have already shown that a cocktail of sialidase, cathepsin L, and heparanase inhibitors can prevent NS1-induced vascular leak in mice; however, studies have not yet been conducted to assess a protective effect of these inhibitors during DENV infection. In addition to its effects on the endothelial glycocalyx, NS1 also mediates disruption of endothelial intercellular junctions and release of inflammatory cytokines from PBMCs, and these pathways offer further targets for drug development. Beyond its involvement in vascular leak, NS1 also helps facilitate the spread of DENV from humans into the mosquito vector, and it may also play an important role locally immediately after inoculation from the mosquito into the host dermis. These phenomena may be potential targets for vaccines and therapeutics designed to decrease transmission or halt the establishment of infection in hosts.

Perspectives and Concluding Thoughts

Over the past four years, major research advances have reshaped our understanding of DENV NS1 as an inextricable component of viral pathogenesis. This growing body of literature, including the work described here, suggests that NS1 acts as a viral toxin during DENV infection, leading to glycocalyx degradation, intercellular junction disruption, and cytokine production, all of which contribute to endothelial hyperpermeability and barrier function. Interestingly, NS1 is not the first viral protein described to act as a toxin. Rotavirus non-structural protein 4 (NSP4) is considered the first viral protein shown to mimic the effects of classic bacterial enterotoxins, and a role for NSP4 as a pathogen-associated molecular pattern during rotavirus infection has been proposed (263). NSP4 is actively secreted in oligomeric forms by infected epithelial cells and binds to glycosaminoglycans on uninfected cells (264), and it acts as an ER-localized viroporin that can form ion channels, disrupt cellular calcium homeostasis, and inhibit sodium adsorption, leading to the characteristic diarrhea during rotavirus infection (265).

In a similar vein to DENV, infection with Ebola virus (EBOV), a single-stranded negative-sense RNA virus in the family *Filoviridae*, can lead to vascular leak and hemorrhagic manifestations. The EBOV glycoprotein (GP) is a trimeric viral surface protein involved in virus attachment to host cells and membrane fusion (266, 267). Following infection, soluble GP is secreted by infected cells, and a truncated surface GP (shed GP) is cleaved from the cell surface by cellular metalloproteases. Both GP forms are found in the blood of patients and experimentally infected animals (268, 269). EBOV shed GP has been implicated in triggering vascular leak by activating immune cells to produce inflammatory cytokines and by acting directly on endothelial cells (270, 271). When added directly to human umbilical vein endothelial cells, shed GP triggers changes in relative permeability, and the same effects were observed after treatment with supernatants collected from shed GP-treated macrophages. The effects of shed GP were diminished with anti-TLR4 antibodies or the deglycosylation of shed GP (270). These findings are strikingly similar to the effects of DENV NS1 on the endothelium, including direct and indirect pathogenesis on endothelial cells as well as a potential role for TLR4 signaling (84, 85).

The work included in this dissertation represents a substantial proportion of the published material on NS1-mediated pathogenesis to this point in time; however, as more research groups begin working in this area of study, new findings will undoubtedly be uncovered by others. Moving forward, NS1 represents not only a fascinating topic of molecular virology but also a potential target for the development of novel therapeutics and vaccine candidates. With that said, NS1 is only a single player in DENV infection and pathogenesis, and it is important to keep the broader context in mind when studying NS1. Until now, studying NS1 in simple *in vitro* systems has allowed us to identify key mechanistic aspects of NS1-mediated pathogenesis. But as we continue to learn more about NS1 and its role in disease, it will be increasingly important to consider NS1 in the framework of DENV infection as a whole, particularly as more work is performed in animal models. Because of the many interesting but challenging questions that remain regarding NS1, it is likely that we have only scratched the surface of knowledge that is to be gleaned about this multi-functional viral protein, and it is reasonable to expect even more fascinating studies to be published in the coming years.

References

1. Bhatt S, Gething PW, Brady OJ, Messina JP, Farlow AW, et al. 2013. The global distribution and burden of dengue. *Nature* 496: 504-7

2. Gould EA, Solomon T. 2008. Pathogenic flaviviruses. *Lancet* 371: 500-9

3. Shepard DS, Undurraga EA, Halasa YA, Stanaway JD. 2016. The global economic burden of dengue: a systematic analysis. *Lancet Infect Dis* 16: 935-41

4. World Health Organization. 2012. Global Strategy for dengue prevention and control, 2012–2020. Geneva: World Health Organization

5. Selck FW, Adalja AA, Boddie CR. 2014. An estimate of the global health care and lost productivity costs of dengue. *Vector Borne Zoonotic Dis* 14: 824-6

6. Pierson TS, Diamond MS. 2013. Flaviviruses. In *Fields Virology, 6th Edition*, pp. 747-94. Philadelphia: Wolters Kluwer Health/Lippincott Williams & Wilkins

7. Durbin AP, Vargas MJ, Wanionek K, Hammond SN, Gordon A, et al. 2008. Phenotyping of peripheral blood mononuclear cells during acute dengue illness demonstrates infection and increased activation of monocytes in severe cases compared to classic dengue fever. *Virology* 376: 429-35

8. Kyle JL, Beatty PR, Harris E. 2007. Dengue virus infects macrophages and dendritic cells in a mouse model of infection. *J Infect Dis* 195: 1808-17

9. Aye KS, Charngkaew K, Win N, Wai KZ, Moe K, et al. 2014. Pathologic highlights of dengue hemorrhagic fever in 13 autopsy cases from Myanmar. *Hum Pathol* 45: 1221-33

10. Chambers TJ, Hahn CS, Galler R, Rice CM. 1990. Flavivirus genome organization, expression, and replication. *Annu Rev Microbiol* 44: 649-88

11. World Health Organization. 1997. *Dengue haemorrhagic fever : diagnosis, treatment, prevention, and control*. Geneva: World Health Organization

12. World Health Organization. 2009. *Dengue: guidelines for diagnosis, treatment, prevention, and control*. Geneva: World Health Organization

13. Sangkawibha N, Rojanasuphot S, Ahandrik S, Viriyapongse S, Jatanasen S, et al. 1984. Risk factors in dengue shock syndrome: a prospective epidemiologic study in Rayong, Thailand. I. The 1980 outbreak. *Am J Epidemiol* 120: 653-69

14. Guzman MG, Kouri G, Valdes L, Bravo J, Vazquez S, Halstead SB. 2002. Enhanced severity of secondary dengue-2 infections: death rates in 1981 and 1997 Cuban outbreaks. *Rev Panam Salud Publica* 11: 223-7

15. Halstead SB, O'Rourke EJ. 1977. Dengue viruses and mononuclear phagocytes. I. Infection enhancement by non-neutralizing antibody. *J Exp Med* 146: 201-17

16. Kliks SC, Nisalak A, Brandt WE, Wahl L, Burke DS. 1989. Antibody-dependent enhancement of dengue virus growth in human monocytes as a risk factor for dengue hemorrhagic fever. *Am J Trop Med Hyg* 40: 444-51

17. Halstead SB. 1979. In vivo enhancement of dengue virus infection in rhesus monkeys by passively transferred antibody. *J Infect Dis* 140: 527-33

18. Balsitis SJ, Williams KL, Lachica R, Flores D, Kyle JL, et al. 2010. Lethal antibody enhancement of dengue disease in mice is prevented by Fc modification. *PLoS Pathog* 6: e1000790

19. Zellweger RM, Prestwood TR, Shresta S. 2010. Enhanced infection of liver sinusoidal endothelial cells in a mouse model of antibody-induced severe dengue disease. *Cell Host Microbe* 7: 128-39

20. Katzelnick LC, Gresh L, Halloran ME, Mercado JC, Kuan G, et al. 2017. Antibody-dependent enhancement of severe dengue disease in humans. *Science* 358: 929-32

21. Weiskopf D, Sette A. 2014. T-cell immunity to infection with dengue virus in humans. *Front Immunol* 5: 93

22. Malavige GN, Ogg GS. 2013. T cell responses in dengue viral infections. *J Clin Virol* 58: 605-11

23. Hatch S, Endy TP, Thomas S, Mathew A, Potts J, et al. 2011. Intracellular cytokine production by dengue virus-specific T cells correlates with subclinical secondary infection. *J Infect Dis* 203: 1282-91

24. Chandele A, Sewatanon J, Gunisetty S, Singla M, Onlamoon N, et al. 2016. Characterization of Human CD8 T Cell Responses in Dengue Virus-Infected Patients from India. *J Virol* 90: 11259-78

25. Kurane I, Rothman AL, Livingston PG, Green S, Gagnon SJ, et al. 1994. Immunopathologic mechanisms of dengue hemorrhagic fever and dengue shock syndrome. *Arch Virol Suppl* 9: 59-64

26. Kurane I, Ennis FA. 1994. Cytotoxic T lymphocytes in dengue virus infection. *Curr Top Microbiol Immunol* 189: 93-108

27. Iyngkaran N, Yadav M, Sinniah M. 1995. Augmented inflammatory cytokines in primary dengue infection progressing to shock. *Singapore Med J* 36: 218-21

28. Pang T, Cardosa MJ, Guzman MG. 2007. Of cascades and perfect storms: the immunopathogenesis of dengue haemorrhagic fever-dengue shock syndrome (DHF/DSS). *Immunol Cell Biol* 85: 43-5

29. Tuchinda M, Dhorranintra B, Tuchinda P. 1977. Histamine content in 24-hour urine in patients with dengue haemorrhagic fever. *Southeast Asian J Trop Med Public Health* 8: 80-3

30. Jeewandara C, Gomes L, Wickramasinghe N, Gutowska-Owsiak D, Waithe D, et al. 2015. Platelet activating factor contributes to vascular leak in acute dengue infection. *PLoS Negl Trop Dis* 9: e0003459

31. St John AL, Rathore AP, Raghavan B, Ng ML, Abraham SN. 2013. Contributions of mast cells and vasoactive products, leukotrienes and chymase, to dengue virus-induced vascular leakage. *Elife* 2: e00481

32. Reitsma S, Slaaf DW, Vink H, van Zandvoort MA, oude Egbrink MG. 2007. The endothelial glycocalyx: composition, functions, and visualization. *Pflugers Arch* 454: 345-59

33. Dejana E. 2004. Endothelial cell-cell junctions: happy together. *Nat Rev Mol Cell Biol* 5: 261-70

34. Yuan SY, Rigor RR. 2010. *Regulation of Endothelial Barrier Function*. San Rafael, CA: Morgan & Claypool Life Sciences

35. Dudek SM, Garcia JG. 2001. Cytoskeletal regulation of pulmonary vascular permeability. *J Appl Physiol (1985)* 91: 1487-500

36. Weinbaum S, Tarbell JM, Damiano ER. 2007. The structure and function of the endothelial glycocalyx layer. *Annu Rev Biomed Eng* 9: 121-67

37. Mehta D, Malik AB. 2006. Signaling mechanisms regulating endothelial permeability. *Physiol Rev* 86: 279-367

38. Tsukita S, Furuse M, Itoh M. 2001. Multifunctional strands in tight junctions. *Nat Rev Mol Cell Biol* 2: 285-93

39. Trung DT, Wills B. 2010. Systemic vascular leakage associated with dengue infections - the clinical perspective. *Curr Top Microbiol Immunol* 338: 57-66

40. Muylaert IR, Chambers TJ, Galler R, Rice CM. 1996. Mutagenesis of the N-linked glycosylation sites of the yellow fever virus NS1 protein: effects on virus replication and mouse neurovirulence. *Virology* 222: 159-68

41. Flamand M, Megret F, Mathieu M, Lepault J, Rey FA, Deubel V. 1999. Dengue virus type 1 nonstructural glycoprotein NS1 is secreted from mammalian cells as a soluble hexamer in a glycosylation-dependent fashion. *J Virol* 73: 6104-10

42. Song H, Qi J, Haywood J, Shi Y, Gao GF. 2016. Zika virus NS1 structure reveals diversity of electrostatic surfaces among flaviviruses. *Nat Struct Mol Biol* 23: 456-8

43. Xu X, Song H, Qi J, Liu Y, Wang H, et al. 2016. Contribution of intertwined loop to membrane association revealed by Zika virus full-length NS1 structure. *EMBO J* 35: 2170-78

44. Pryor MJ, Wright PJ. 1994. Glycosylation mutants of dengue virus NS1 protein. *J Gen Virol* 75 (Pt 5): 1183-7

45. Mandl CW, Heinz FX, Stockl E, Kunz C. 1989. Genome sequence of tick-borne encephalitis virus (Western subtype) and comparative analysis of nonstructural proteins with other flaviviruses. *Virology* 173: 291-301

46. Mason PW. 1989. Maturation of Japanese encephalitis virus glycoproteins produced by infected mammalian and mosquito cells. *Virology* 169: 354-64

47. Somnuke P, Hauhart RE, Atkinson JP, Diamond MS, Avirutnan P. 2011. N-linked glycosylation of dengue virus NS1 protein modulates secretion, cell-surface expression, hexamer stability, and interactions with human complement. *Virology* 413: 253-64

48. Gutsche I, Coulibaly F, Voss JE, Salmon J, d'Alayer J, et al. 2011. Secreted dengue virus nonstructural protein NS1 is an atypical barrel-shaped high-density lipoprotein. *Proc Natl Acad Sci U S A* 108: 8003-8

49. Muller DA, Landsberg MJ, Bletchly C, Rothnagel R, Waddington L, et al. 2012. Structure of the dengue virus glycoprotein non-structural protein 1 by electron microscopy and single-particle analysis. *J Gen Virol* 93: 771-9

50. Akey DL, Brown WC, Dutta S, Konwerski J, Jose J, et al. 2014. Flavivirus NS1 structures reveal surfaces for associations with membranes and the immune system. *Science* 343: 881-5

51. Edeling MA, Diamond MS, Fremont DH. 2014. Structural basis of Flavivirus NS1 assembly and antibody recognition. *Proc Natl Acad Sci U S A* 111: 4285-90

52. Hertz T, Beatty PR, MacMillen Z, Killingbeck SS, Wang C, Harris E. 2017. Antibody Epitopes Identified in Critical Regions of Dengue Virus Nonstructural 1 Protein in Mouse Vaccination and Natural Human Infections. *J Immunol* 198: 4025-35

53. Falconar AK, Young PR, Miles MA. 1994. Precise location of sequential dengue virus subcomplex and complex B cell epitopes on the nonstructural-1 glycoprotein. *Arch Virol* 137: 315-26

54. Chen Y, Pan Y, Guo Y, Qiu L, Ding X, Che X. 2010. Comprehensive mapping of immunodominant and conserved serotype- and group-specific B-cell epitopes of nonstructural protein 1 from dengue virus type 1. *Virology* 398: 290-8

55. Youn S, Li T, McCune BT, Edeling MA, Fremont DH, et al. 2012. Evidence for a genetic and physical interaction between nonstructural proteins NS1 and NS4B that modulates replication of West Nile virus. *J Virol* 86: 7360-71

56. Welsch S, Miller S, Romero-Brey I, Merz A, Bleck CK, et al. 2009. Composition and three-dimensional architecture of the dengue virus replication and assembly sites. *Cell Host Microbe* 5: 365-75

57. Mackenzie JM, Jones MK, Young PR. 1996. Immunolocalization of the dengue virus nonstructural glycoprotein NS1 suggests a role in viral RNA replication. *Virology* 220: 232-40

58. Lindenbach BD, Rice CM. 1997. trans-Complementation of yellow fever virus NS1 reveals a role in early RNA replication. *J Virol* 71: 9608-17

59. Lindenbach BD, Rice CM. 1999. Genetic interaction of flavivirus nonstructural proteins NS1 and NS4A as a determinant of replicase function. *J Virol* 73: 4611-21

60. Scaturro P, Cortese M, Chatel-Chaix L, Fischl W, Bartenschlager R. 2015. Dengue Virus Non-structural Protein 1 Modulates Infectious Particle Production via Interaction with the Structural Proteins. *PLoS Pathog* 11: e1005277

61. Crabtree MB, Kinney RM, Miller BR. 2005. Deglycosylation of the NS1 protein of dengue 2 virus, strain 16681: construction and characterization of mutant viruses. *Arch Virol* 150: 771-86

62. Hafirassou ML, Meertens L, Umana-Diaz C, Labeau A, Dejarnac O, et al. 2017. A Global Interactome Map of the Dengue Virus NS1 Identifies Virus Restriction and Dependency Host Factors. *Cell Rep* 21: 3900-13

63. Heaton NS, Randall G. 2010. Dengue virus-induced autophagy regulates lipid metabolism. *Cell Host Microbe* 8: 422-32

64. Perera R, Riley C, Isaac G, Hopf-Jannasch AS, Moore RJ, et al. 2012. Dengue virus infection perturbs lipid homeostasis in infected mosquito cells. *PLoS Pathog* 8: e1002584

65. Noisakran S, Dechtawewat T, Avirutnan P, Kinoshita T, Siripanyaphinyo U, et al. 2008. Association of dengue virus NS1 protein with lipid rafts. *J Gen Virol* 89: 2492-500

66. Fry SR, Meyer M, Semple MG, Simmons CP, Sekaran SD, et al. 2011. The diagnostic sensitivity of dengue rapid test assays is significantly enhanced by using a combined antigen and antibody testing approach. *PLoS Negl Trop Dis* 5: e1199

67. Hunsperger EA, Yoksan S, Buchy P, Nguyen VC, Sekaran SD, et al. 2014. Evaluation of commercially available diagnostic tests for the detection of dengue virus NS1 antigen and anti-dengue virus IgM antibody. *PLoS Negl Trop Dis* 8: e3171

68. Duyen HT, Ngoc TV, Ha do T, Hang VT, Kieu NT, et al. 2011. Kinetics of plasma viremia and soluble nonstructural protein 1 concentrations in dengue: differential effects according to serotype and immune status. *J Infect Dis* 203: 1292-300

69. Libraty DH, Young PR, Pickering D, Endy TP, Kalayanarooj S, et al. 2002. High circulating levels of the dengue virus nonstructural protein NS1 early in dengue illness correlate with the development of dengue hemorrhagic fever. *J Infect Dis* 186: 1165-8

70. Paranavitane SA, Gomes L, Kamaladasa A, Adikari TN, Wickramasinghe N, et al. 2014. Dengue NS1 antigen as a marker of severe clinical disease. *BMC Infect Dis* 14: 570

71. Young PR, Hilditch PA, Bletchly C, Halloran W. 2000. An antigen capture enzyme-linked immunosorbent assay reveals high levels of the dengue virus protein NS1 in the sera of infected patients. *J Clin Microbiol* 38: 1053-7

72. Alcon S, Talarmin A, Debruyne M, Falconar A, Deubel V, Flamand M. 2002. Enzyme-linked immunosorbent assay specific to Dengue virus type 1 nonstructural protein NS1 reveals circulation of the antigen in the blood during the acute phase of disease in patients experiencing primary or secondary infections. *J Clin Microbiol* 40: 376-81

73. Xu H, Di B, Pan YX, Qiu LW, Wang YD, et al. 2006. Serotype 1-specific monoclonal antibody-based antigen capture immunoassay for detection of circulating nonstructural protein NS1: Implications for early diagnosis and serotyping of dengue virus infections. *J Clin Microbiol* 44: 2872-8

74. Dussart P, Labeau B, Lagathu G, Louis P, Nunes MR, et al. 2006. Evaluation of an enzyme immunoassay for detection of dengue virus NS1 antigen in human serum. *Clin Vaccine Immunol* 13: 1185-9

75. Tricou V, Minh NN, Farrar J, Tran HT, Simmons CP. 2011. Kinetics of viremia and NS1 antigenemia are shaped by immune status and virus serotype in adults with dengue. *PLoS Negl Trop Dis* 5: e1309

76. Metsky HC, Matranga CB, Wohl S, Schaffner SF, Freije CA, et al. 2017. Zika virus evolution and spread in the Americas. *Nature* 546: 411-15

77. Paules CI, Fauci AS. 2017. Yellow Fever - Once Again on the Radar Screen in the Americas. *N Engl J Med* 376: 1397-99

78. Lanciotti RS, Kosoy OL, Laven JJ, Velez JO, Lambert AJ, et al. 2008. Genetic and serologic properties of Zika virus associated with an epidemic, Yap State, Micronesia, 2007. *Emerg Infect Dis* 14: 1232-9

79. Priyamvada L, Quicke KM, Hudson WH, Onlamoon N, Sewatanon J, et al. 2016. Human antibody responses after dengue virus infection are highly cross-reactive to Zika virus. *Proc Natl Acad Sci U S A* 113: 7852-7

80. Balmaseda A, Stettler K, Medialdea-Carrera R, Collado D, Jin X, et al. 2017. Antibody-based assay discriminates Zika virus infection from other flaviviruses. *Proc Natl Acad Sci U S A* 114: 8384-89

81. Bosch I, de Puig H, Hiley M, Carre-Camps M, Perdomo-Celis F, et al. 2017. Rapid antigen tests for dengue virus serotypes and Zika virus in patient serum. *Sci Transl Med* 9

82. Balmaseda A, Zambrana JV, Collado D, Garcia N, Saborio S, et al. 2018. Comparison of four serological methods and two RT-PCR assays for diagnosis and surveillance of Zika. *J Clin Microbiol*

83. World Health Organization. 2017. Updated Questions and Answers related to the dengue vaccine Dengvaxia® and its use. Geneva: World Health Organization

84. Beatty PR, Puerta-Guardo H, Killingbeck SS, Glasner DR, Hopkins K, Harris E. 2015. Dengue virus NS1 triggers endothelial permeability and vascular leak that is prevented by NS1 vaccination. *Sci Transl Med* 7: 304ra141

85. Modhiran N, Watterson D, Muller DA, Panetta AK, Sester DP, et al. 2015. Dengue virus NS1 protein activates cells via Toll-like receptor 4 and disrupts endothelial cell monolayer integrity. *Sci Transl Med* 7: 304ra142

86. Chisenhall DM, Christofferson RC, McCracken MK, Johnson AM, Londono-Renteria B, Mores CN. 2014. Infection with dengue-2 virus alters proteins in naturally expectorated saliva of Aedes aegypti mosquitoes. *Parasit Vectors* 7: 252

87. Avirutnan P, Zhang L, Punyadee N, Manuyakorn A, Puttikhunt C, et al. 2007. Secreted NS1 of dengue virus attaches to the surface of cells via interactions with heparan sulfate and chondroitin sulfate E. *PLoS Pathog* 3: e183

88. Puerta-Guardo H, Glasner DR, Harris E. 2016. Dengue Virus NS1 Disrupts the Endothelial Glycocalyx, Leading to Hyperpermeability. *PLoS Pathog* 12: e1005738

89. Glasner DR, Ratnasiri K, Puerta-Guardo H, Espinosa DA, Beatty PR, Harris E. 2017. Dengue virus NS1 cytokine-independent vascular leak is dependent on endothelial glycocalyx components. *PLoS Pathog* 13: e1006673

90. Wills BA, Oragui EE, Dung NM, Loan HT, Chau NV, et al. 2004. Size and charge characteristics of the protein leak in dengue shock syndrome. *J Infect Dis* 190: 810-8

91. Nguyen-Pouplin J, Pouplin T, Van TP, The TD, Thi DN, et al. 2011. Dextran fractional clearance studies in acute dengue infection. *PLoS Negl Trop Dis* 5: e1282

92. Suwarto S, Sasmono RT, Sinto R, Ibrahim E, Suryamin M. 2017. Association of Endothelial Glycocalyx and Tight and Adherens Junctions With Severity of Plasma Leakage in Dengue Infection. *J Infect Dis* 215: 992-99

93. Tang TH, Alonso S, Ng LF, Thein TL, Pang VJ, et al. 2017. Increased Serum Hyaluronic Acid and Heparan Sulfate in Dengue Fever: Association with Plasma Leakage and Disease Severity. *Sci Rep* 7: 46191

94. Sahaphong S, Riengrojpitak S, Bhamarapravati N, Chirachariyavej T. 1980. Electron microscopic study of the vascular endothelial cell in dengue hemorrhagic fever. *Southeast Asian J Trop Med Public Health* 11: 194-204

95. Chen HR, Chuang YC, Lin YS, Liu HS, Liu CC, et al. 2016. Dengue Virus Nonstructural Protein 1 Induces Vascular Leakage through Macrophage Migration Inhibitory Factor and Autophagy. *PLoS Negl Trop Dis* 10: e0004828

96. Chakravarti A, Kumaria R. 2006. Circulating levels of tumour necrosis factor-alpha & interferon-gamma in patients with dengue & dengue haemorrhagic fever during an outbreak. *Indian J Med Res* 123: 25-30

97. Braga EL, Moura P, Pinto LM, Ignacio SR, Oliveira MJ, et al. 2001. Detection of circulant tumor necrosis factor-alpha, soluble tumor necrosis factor p75 and interferon-gamma in Brazilian patients with dengue fever and dengue hemorrhagic fever. *Mem Inst Oswaldo Cruz* 96: 229-32

98. Bozza FA, Cruz OG, Zagne SM, Azeredo EL, Nogueira RM, et al. 2008. Multiplex cytokine profile from dengue patients: MIP-1beta and IFN-gamma as predictive factors for severity. *BMC Infect Dis* 8: 86

99. Malavige GN, Gomes L, Alles L, Chang T, Salimi M, et al. 2013. Serum IL-10 as a marker of severe dengue infection. *BMC Infect Dis* 13: 341

100. Azeredo EL, Zagne SM, Santiago MA, Gouvea AS, Santana AA, et al. 2001. Characterisation of lymphocyte response and cytokine patterns in patients with dengue fever. *Immunobiology* 204: 494-507

101. Suharti C, van Gorp EC, Dolmans WM, Setiati TE, Hack CE, et al. 2003. Cytokine patterns during dengue shock syndrome. *Eur Cytokine Netw* 14: 172-7

102. Chen LC, Lei HY, Liu CC, Shiesh SC, Chen SH, et al. 2006. Correlation of serum levels of macrophage migration inhibitory factor with disease severity and clinical outcome in dengue patients. *Am J Trop Med Hyg* 74: 142-7

103. Chen J, Ng MM, Chu JJ. 2015. Activation of TLR2 and TLR6 by Dengue NS1 Protein and Its Implications in the Immunopathogenesis of Dengue Virus Infection. *PLoS Pathog* 11: e1005053

104. Modhiran N, Watterson D, Blumenthal A, Baxter AG, Young PR, Stacey KJ. 2017. Dengue virus NS1 protein activates immune cells via TLR4 but not TLR2 or TLR6. *Immunol Cell Biol* 95: 491-95

105. Alayli F, Scholle F. 2016. Dengue virus NS1 enhances viral replication and pro-inflammatory cytokine production in human dendritic cells. *Virology* 496: 227-36

106. Ferreira RA, de Oliveira SA, Gandini M, Ferreira Lda C, Correa G, et al. 2015. Circulating cytokines and chemokines associated with plasma leakage and hepatic dysfunction in Brazilian children with dengue fever. *Acta Trop* 149: 138-47

107. Flores-Mendoza LK, Estrada-Jimenez T, Sedeno-Monge V, Moreno M, Manjarrez MDC, et al. 2017. IL-10 and socs3 Are Predictive Biomarkers of Dengue Hemorrhagic Fever. *Mediators Inflamm* 2017: 5197592

108. Adikari TN, Gomes L, Wickramasinghe N, Salimi M, Wijesiriwardana N, et al. 2016. Dengue NS1 antigen contributes to disease severity by inducing interleukin (IL)-10 by monocytes. *Clin Exp Immunol* 184: 90-100

109. King CA, Anderson R, Marshall JS. 2002. Dengue virus selectively induces human mast cell chemokine production. *J Virol* 76: 8408-19

110. Syenina A, Jagaraj CJ, Aman SA, Sridharan A, St John AL. 2015. Dengue vascular leakage is augmented by mast cell degranulation mediated by immunoglobulin Fcgamma receptors. *Elife* 4

111. Simon AY, Sutherland MR, Pryzdial EL. 2015. Dengue virus binding and replication by platelets. *Blood* 126: 378-85

112. Ojha A, Nandi D, Batra H, Singhal R, Annarapu GK, et al. 2017. Platelet activation determines the severity of thrombocytopenia in dengue infection. *Sci Rep* 7: 41697

113. Brandt WE, Chiewslip D, Harris DL, Russell PK. 1970. Partial purification and characterization of a dengue virus soluble complement-fixing antigen. *J Immunol* 105: 1565-8

114. McCloud TG, Brandt WE, Russell PK. 1970. Molecular size and charge relationships of the soluble complement-fixing antigens of dengue viruses. *Virology* 41: 569-72

115. Falkler WA, Jr., Diwan AR, Halstead SB. 1973. Human antibody to dengue soluble complement-fixing (SCF) antigens. *J Immunol* 111: 1804-9

116. Schlesinger JJ, Brandriss MW, Walsh EE. 1987. Protection of mice against dengue 2 virus encephalitis by immunization with the dengue 2 virus non-structural glycoprotein NS1. *J Gen Virol* 68 (Pt 3): 853-7

117. Wan SW, Chen PW, Chen CY, Lai YC, Chu YT, et al. 2017. Therapeutic Effects of Monoclonal Antibody against Dengue Virus NS1 in a STAT1 Knockout Mouse Model of Dengue Infection. *J Immunol* 199: 2834-44

118. Avirutnan P, Punyadee N, Noisakran S, Komoltri C, Thiemmeca S, et al. 2006. Vascular leakage in severe dengue virus infections: a potential role for the nonstructural viral protein NS1 and complement. *J Infect Dis* 193: 1078-88

119. Avirutnan P, Fuchs A, Hauhart RE, Somnuke P, Youn S, et al. 2010. Antagonism of the complement component C4 by flavivirus nonstructural protein NS1. *J Exp Med* 207: 793-806

120. Avirutnan P, Hauhart RE, Somnuke P, Blom AM, Diamond MS, Atkinson JP. 2011. Binding of flavivirus nonstructural protein NS1 to C4b binding protein modulates complement activation. *J Immunol* 187: 424-33

121. Conde JN, da Silva EM, Allonso D, Coelho DR, Andrade ID, et al. 2016. Inhibition of the Membrane Attack Complex by Dengue Virus NS1 through Interaction with Vitronectin and Terminal Complement Proteins. *J Virol* 90: 9570-81

122. Thiemmeca S, Tamdet C, Punyadee N, Prommool T, Songjaeng A, et al. 2016. Secreted NS1 Protects Dengue Virus from Mannose-Binding Lectin-Mediated Neutralization. *J Immunol* 197: 4053-65

123. Nascimento EJ, Silva AM, Cordeiro MT, Brito CA, Gil LH, et al. 2009. Alternative complement pathway deregulation is correlated with dengue severity. *PLoS One* 4: e6782

124. Falconar AK. 1997. The dengue virus nonstructural-1 protein (NS1) generates antibodies to common epitopes on human blood clotting, integrin/adhesin proteins and binds to human endothelial cells: potential implications in haemorrhagic fever pathogenesis. *Arch Virol* 142: 897-916

125. Lin CF, Wan SW, Chen MC, Lin SC, Cheng CC, et al. 2008. Liver injury caused by antibodies against dengue virus nonstructural protein 1 in a murine model. *Lab Invest* 88: 1079-89

126. Lin YS, Yeh TM, Lin CF, Wan SW, Chuang YC, et al. 2011. Molecular mimicry between virus and host and its implications for dengue disease pathogenesis. *Exp Biol Med* 236: 515-23

127. Falconar AK. 1999. Identification of an epitope on the dengue virus membrane (M) proten defined by cross-protective monoclonal antibodies: design of an improved epitope sequence based on common determinants present in both envelope (E and M) proteins. *Arch. Virol.* 144: 2313-31

128. Lin CF, Chiu SC, Hsiao YL, Wan SW, Lei HY, et al. 2005. Expression of cytokine, chemokine, and adhesion molecules during endothelial cell activation induced by antibodies against dengue virus nonstructural protein 1. *J Immunol* 174: 395-403

129. Chu YT, Wan SW, Chang YC, Lee CK, Wu-Hsieh BA, et al. 2017. Antibodies against nonstructural protein 1 protect mice from dengue virus-induced mast cell activation. *Lab Invest* 97: 602-14

130. Falconar AK, Martinez F. 2011. The NS1 glycoprotein can generate dramatic antibody-enhanced dengue viral replication in normal out-bred mice resulting in lethal multi-organ disease. *PLoS One* 6: e21024

131. Sun DS, King CC, Huang HS, Shih YL, Lee CC, et al. 2007. Antiplatelet autoantibodies elicited by dengue virus non-structural protein 1 cause thrombocytopenia and mortality in mice. *J Thromb Haemost* 5: 2291-99

132. Lin CF, Lei HY, Shiau AL, Liu HS, Yeh TM, et al. 2002. Endothelial cell apoptosis induced by antibodies against dengue virus nonstructural protein 1 via production of nitric oxide. *Journal of Immunology* 169: 657-64

133. Lin CF, Lei HY, Shiau AL, Liu CC, Liu HS, et al. 2003. Antibodies from dengue patient sera cross-react with endothelial cells and induce damage. *Journal of Medical Virology* 69: 82-90

134. Chuang YC, Lei HY, Lin YS, Liu HS, Wu HL, Yeh TM. 2011. Dengue virus-induced autoantibodies bind to plasminogen and enhance its activation. *J Immunol* 187: 6483-90

135. Chen CL, Lin CF, Wan SW, Wei LS, Chen MC, et al. 2013. Anti-dengue virus nonstructural protein 1 antibodies cause NO-mediated endothelial cell apoptosis via ceramide-regulated glycogen synthase kinase-3beta and NF-kappaB activation. *J Immunol* 191: 1744-52

136. Wan SW, Lin CF, Chen MC, Lei HY, Liu HS, et al. 2008. C-terminal region of dengue virus nonstructural protein 1 is involved in endothelial cell cross-reactivity via molecular mimicry. *Am J Infect Dis* 4: 85-91

137. Chen MC, Lin CF, Lei HY, Lin SC, Liu HS, et al. 2009. Deletion of the C-terminal region of dengue virus nonstructural protein 1 (NS1) abolishes anti-NS1-mediated platelet dysfunction and bleeding tendency. *J Immunol* 183: 1797-803

138. Cheng HJ, Lei HY, Lin CF, Luo YH, Wan SW, et al. 2009. Anti-dengue virus nonstructural protein 1 antibodies recognize protein disulfide isomerase on platelets and inhibit platelet aggregation. *Mol Immunol* 47: 398-406

139. Wan SW, Lu YT, Huang CH, Lin CF, Anderson R, et al. 2014. Protection against dengue virus infection in mice by administration of antibodies against modified nonstructural protein 1. *PLoS One* 9: e92495

140. Liu J, Liu Y, Nie K, Du S, Qiu J, et al. 2016. Flavivirus NS1 protein in infected host sera enhances viral acquisition by mosquitoes. *Nat Microbiol* 1: 16087

141. Schneider BS, Higgs S. 2008. The enhancement of arbovirus transmission and disease by mosquito saliva is associated with modulation of the host immune response. *Trans R Soc Trop Med Hyg* 102: 400-8

142. Conway MJ, Watson AM, Colpitts TM, Dragovic SM, Li Z, et al. 2014. Mosquito saliva serine protease enhances dissemination of dengue virus into the mammalian host. *J Virol* 88: 164-75

143. Schmid MA, Glasner DR, Shah S, Michlmayr D, Kramer LD, Harris E. 2016. Mosquito Saliva Increases Endothelial Permeability in the Skin, Immune Cell Migration, and Dengue Pathogenesis during Antibody-Dependent Enhancement. *PLoS Pathog* 12: e1005676

144. Srikiatkhachorn A, Krautrachue A, Ratanaprakarn W, Wongtapradit L, Nithipanya N, et al. 2007. Natural history of plasma leakage in dengue hemorrhagic fever: a serial ultrasonographic study. *Pediatr Infect Dis J* 26: 283-90; discussion 91-2

145. Green S, Rothman A. 2006. Immunopathological mechanisms in dengue and dengue hemorrhagic fever. *Curr Opin Infect Dis* 19: 429-36

146. Muller DA, Young PR. 2013. The flavivirus NS1 protein: molecular and structural biology, immunology, role in pathogenesis and application as a diagnostic biomarker. *Antiviral Res* 98: 192-208

147. Miserocchi G. 1997. Physiology and pathophysiology of pleural fluid turnover. *Eur Respir J* 10: 219-25

148. Wiesinger A, Peters W, Chappell D, Kentrup D, Reuter S, et al. 2013. Nanomechanics of the endothelial glycocalyx in experimental sepsis. *PLoS One* 8: e80905

149. Varki A, Schauer R. 2009. Sialic Acids. In *Essentials of Glycobiology*, ed. A Varki, RD Cummings, JD Esko, HH Freeze, P Stanley, et al. Cold Spring Harbor (NY)

150. Singh A, Satchell SC, Neal CR, McKenzie EA, Tooke JE, Mathieson PW. 2007. Glomerular endothelial glycocalyx constitutes a barrier to protein permeability. *J Am Soc Nephrol* 18: 2885-93

151. Reitsma S, oude Egbrink MG, Vink H, van den Berg BM, Passos VL, et al. 2011. Endothelial glycocalyx structure in the intact carotid artery: a two-photon laser scanning microscopy study. *J Vasc Res* 48: 297-306

152. Hata K, Koseki K, Yamaguchi K, Moriya S, Suzuki Y, et al. 2008. Limited inhibitory effects of oseltamivir and zanamivir on human sialidases. *Antimicrob Agents Chemother* 52: 3484-91

153. Cairo CW. 2014. Inhibitors of the human neuraminidase enzymes. *MedChemComm* 5: 1067

154. Pries AR, Secomb TW, Gaehtgens P. 2000. The endothelial surface layer. *Pflugers Arch* 440: 653-66

155. Sarrazin S, Lamanna WC, Esko JD. 2011. Heparan sulfate proteoglycans. *Cold Spring Harb Perspect Biol* 3: a004952

156. Bernfield M, Gotte M, Park PW, Reizes O, Fitzgerald ML, et al. 1999. Functions of cell surface heparan sulfate proteoglycans. *Annu Rev Biochem* 68: 729-77

157. Alexopoulou AN, Multhaupt HA, Couchman JR. 2007. Syndecans in wound healing, inflammation and vascular biology. *Int J Biochem Cell Biol* 39: 505-28

158. Kolarova H, Ambruzova B, Svihalkova Sindlerova L, Klinke A, Kubala L. 2014. Modulation of endothelial glycocalyx structure under inflammatory conditions. *Mediators Inflamm* 2014: 694312

159. Bame KJ. 2001. Heparanases: endoglycosidases that degrade heparan sulfate proteoglycans. *Glycobiology* 11: 91R-98R

160. Fux L, Ilan N, Sanderson RD, Vlodavsky I. 2009. Heparanase: busy at the cell surface. *Trends Biochem Sci* 34: 511-9

161. Nardella C, Lahm A, Pallaoro M, Brunetti M, Vannini A, Steinkuhler C. 2004. Mechanism of activation of human heparanase investigated by protein engineering. *Biochemistry* 43: 1862-73

162. Yang Y, Macleod V, Miao HQ, Theus A, Zhan F, et al. 2007. Heparanase enhances syndecan-1 shedding: a novel mechanism for stimulation of tumor growth and metastasis. *J Biol Chem* 282: 13326-33

163. Purushothaman A, Uyama T, Kobayashi F, Yamada S, Sugahara K, et al. 2010. Heparanase-enhanced shedding of syndecan-1 by myeloma cells promotes endothelial invasion and angiogenesis. *Blood* 115: 2449-57

164. Abboud-Jarrous G, Atzmon R, Peretz T, Palermo C, Gadea BB, et al. 2008. Cathepsin L is responsible for processing and activation of proheparanase through multiple cleavages of a linker segment. *J Biol Chem* 283: 18167-76

165. Turk V, Stoka V, Vasiljeva O, Renko M, Sun T, et al. 2012. Cysteine cathepsins: from structure, function and regulation to new frontiers. *Biochim Biophys Acta* 1824: 68-88

166. McKenzie EA. 2007. Heparanase: a target for drug discovery in cancer and inflammation. *Br J Pharmacol* 151: 1-14

167. Halstead SB. 2007. Dengue. *Lancet* 370: 1644-52

168. Feletou M. 2011. In *The Endothelium: Part 1: Multiple Functions of the Endothelial Cells-Focus on Endothelium-Derived Vasoactive Mediators*. San Rafael (CA)

169. Schauer R. 2009. Sialic acids as regulators of molecular and cellular interactions. *Curr Opin Struct Biol* 19: 507-14

170. Pahakis MY, Kosky JR, Dull RO, Tarbell JM. 2007. The role of endothelial glycocalyx components in mechanotransduction of fluid shear stress. *Biochem Biophys Res Commun* 355: 228-33

171. Crocker PR, Varki A. 2001. Siglecs, sialic acids and innate immunity. *Trends Immunol* 22: 337-42

172. Monti E, Bonten E, D'Azzo A, Bresciani R, Venerando B, et al. 2010. Sialidases in vertebrates: a family of enzymes tailored for several cell functions. *Adv Carbohydr Chem Biochem* 64: 403-79

173. Varki A, Gagneux P. 2012. Multifarious roles of sialic acids in immunity. *Ann N Y Acad Sci* 1253: 16-36

174. Tringali C, Papini N, Fusi P, Croci G, Borsani G, et al. 2004. Properties of recombinant human cytosolic sialidase HsNEU2. The enzyme hydrolyzes monomerically dispersed GM1 ganglioside molecules. *J Biol Chem* 279: 3169-79

175. Abdulkhalek S, Amith SR, Franchuk SL, Jayanth P, Guo M, et al. 2011. Neu1 sialidase and matrix metalloproteinase-9 cross-talk is essential for Toll-like receptor activation and cellular signaling. *J Biol Chem* 286: 36532-49

176. Amith SR, Jayanth P, Franchuk S, Finlay T, Seyrantepe V, et al. 2010. Neu1 desialylation of sialyl alpha-2,3-linked beta-galactosyl residues of TOLL-like receptor 4 is essential for receptor activation and cellular signaling. *Cell Signal* 22: 314-24

177. Chen GY, Brown NK, Wu W, Khedri Z, Yu H, et al. 2014. Broad and direct interaction between TLR and Siglec families of pattern recognition receptors and its regulation by Neu1. *Elife* 3: e04066

178. Feng C, Stamatos NM, Dragan AI, Medvedev A, Whitford M, et al. 2012. Sialyl residues modulate LPS-mediated signaling through the Toll-like receptor 4 complex. *PLoS One* 7: e32359

179. Amith SR, Jayanth P, Franchuk S, Siddiqui S, Seyrantepe V, et al. 2009. Dependence of pathogen molecule-induced toll-like receptor activation and cell function on Neu1 sialidase. *Glycoconj J* 26: 1197-212

180. Choi Y, Chung H, Jung H, Couchman JR, Oh ES. 2011. Syndecans as cell surface receptors: Unique structure equates with functional diversity. *Matrix Biol* 30: 93-9

181. Fitzgerald ML, Wang Z, Park PW, Murphy G, Bernfield M. 2000. Shedding of syndecan-1 and -4 ectodomains is regulated by multiple signaling pathways and mediated by a TIMP-3-sensitive metalloproteinase. *J Cell Biol* 148: 811-24

182. Lambaerts K, Wilcox-Adelman SA, Zimmermann P. 2009. The signaling mechanisms of syndecan heparan sulfate proteoglycans. *Curr Opin Cell Biol* 21: 662-9

183. Ramani VC, Pruett PS, Thompson CA, DeLucas LD, Sanderson RD. 2012. Heparan sulfate chains of syndecan-1 regulate ectodomain shedding. *J Biol Chem* 287: 9952-61

184. Goldberg R, Meirovitz A, Hirshoren N, Bulvik R, Binder A, et al. 2013. Versatile role of heparanase in inflammation. *Matrix Biol* 32: 234-40

185. Esko JD, Kimata K, Lindahl U. 2009. Proteoglycans and Sulfated Glycosaminoglycans. In *Essentials of Glycobiology*, ed. A Varki, RD Cummings, JD Esko, HH Freeze, P Stanley, et al. Cold Spring Harbor (NY)

186. Rothman AL. 2011. Immunity to dengue virus: a tale of original antigenic sin and tropical cytokine storms. *Nat Rev Immunol* 11: 532-43

187. Chung KM, Nybakken GE, Thompson BS, Engle MJ, Marri A, et al. 2006. Antibodies against West Nile Virus nonstructural protein NS1 prevent lethal infection through Fc gamma receptor-dependent and -independent mechanisms. *J Virol* 80: 1340-51

188. Schneider CA, Rasband WS, Eliceiri KW. 2012. NIH Image to ImageJ: 25 years of image analysis. *Nat Methods* 9: 671-5

189. Ranta V, Orpana A, Carpen O, Turpeinen U, Ylikorkala O, Viinikka L. 1999. Human vascular endothelial cells produce tumor necrosis factor-alpha in response to proinflammatory cytokine stimulation. *Crit Care Med* 27: 2184-7

190. de Andino RM, Botet MV, Gubler DJ, Garcia C, Laboy E, et al. 1985. The absence of dengue virus in the skin lesions of dengue fever. *Int J Dermatol* 24: 48-51

191. Boonpucknavig S, Boonpucknavig V, Bhamarapravati N, Nimmannitya S. 1979. Immunofluorescence study of skin rash in patients with dengue hemorrhagic fever. *Arch Pathol Lab Med* 103: 463-6

192. Kataoka H, Ushiyama A, Kawakami H, Akimoto Y, Matsubara S, Iijima T. 2016. Fluorescent imaging of endothelial glycocalyx layer with wheat germ agglutinin using intravital microscopy. *Microsc Res Tech* 79: 31-7

193. Yoon JH, Lee ES, Jeong Y. 2017. In vivo Imaging of the Cerebral Endothelial Glycocalyx in Mice. *J Vasc Res* 54: 59-67

194. Hegermann J, Lunsdorf H, Ochs M, Haller H. 2016. Visualization of the glomerular endothelial glycocalyx by electron microscopy using cationic colloidal thorium dioxide. *Histochem Cell Biol* 145: 41-51

195. Bonten E, van der Spoel A, Fornerod M, Grosveld G, d'Azzo A. 1996. Characterization of human lysosomal neuraminidase defines the molecular basis of the metabolic storage disorder sialidosis. *Genes Dev* 10: 3156-69

196. Monti E, Bassi MT, Papini N, Riboni M, Manzoni M, et al. 2000. Identification and expression of NEU3, a novel human sialidase associated to the plasma membrane. *Biochem J* 349: 343-51

197. Shresta S, Sharar KL, Prigozhin DM, Beatty PR, Harris E. 2006. Murine model for dengue virus-induced lethal disease with increased vascular permeability. *J Virol* 80: 10208-17

198. Claffey KP, Brown LF, del Aguila LF, Tognazzi K, Yeo KT, et al. 1996. Expression of vascular permeability factor/vascular endothelial growth factor by melanoma cells increases tumor growth, angiogenesis, and experimental metastasis. *Cancer Res* 56: 172-81

199. Orozco S, Schmid MA, Parameswaran P, Lachica R, Henn MR, et al. 2012. Characterization of a model of lethal dengue virus 2 infection in C57BL/6 mice deficient in the alpha/beta interferon receptor. *J Gen Virol* 93: 2152-7

200. Gubler DJ. 1998. Dengue and dengue hemorrhagic fever. *Clin Microbiol Rev* 11: 480-96

201. Alcon-LePoder S, Drouet MT, Roux P, Frenkiel MP, Arborio M, et al. 2005. The secreted form of dengue virus nonstructural protein NS1 is endocytosed by hepatocytes and accumulates in late endosomes: implications for viral infectivity. *J Virol* 79: 11403-11

202. Bolte S, Cordelieres FP. 2006. A guided tour into subcellular colocalization analysis in light microscopy. *J Microsc* 224: 213-32

203. Stan RV. 2006. Endocytosis pathways in endothelium: how many? *Am J Physiol Lung Cell Mol Physiol* 290: L806-8

204. Mettlen M, Pucadyil T, Ramachandran R, Schmid SL. 2009. Dissecting dynamin's role in clathrin-mediated endocytosis. *Biochem Soc Trans* 37: 1022-6

205. Balsitis SJ, Coloma J, Castro G, Alava A, Flores D, et al. 2009. Tropism of dengue virus in mice and humans defined by viral nonstructural protein 3-specific immunostaining. *Am J Trop Med Hyg* 80: 416-24

206. Ng DHL, Sadarangani SP. 2017. "Locked in a cage"-A case of dengue virus 4 encephalitis. *PLoS Negl Trop Dis* 11: e0005369

207. Ishidoh K, Kominami E. 1995. Procathepsin L degrades extracellular matrix proteins in the presence of glycosaminoglycans in vitro. *Biochem Biophys Res Commun* 217: 624-31

208. Mason RW, Massey SD. 1992. Surface activation of pro-cathepsin L. *Biochem Biophys Res Commun* 189: 1659-66

209. Falconar AK, Young PR. 1991. Production of dimer-specific and dengue virus group cross-reactive mouse monoclonal antibodies to the dengue 2 virus non-structural glycoprotein NS1. *J Gen Virol* 72 (Pt 4): 961-5

210. Calisher CH, Gould EA. 2003. Taxonomy of the virus family Flaviviridae. *Adv Virus Res* 59: 1-19

211. Krauer F, Riesen M, Reveiz L, Oladapo OT, Martinez-Vega R, et al. 2017. Zika Virus Infection as a Cause of Congenital Brain Abnormalities and Guillain-Barre Syndrome: Systematic Review. *PLoS Med* 14: e1002203

212. Xu X, Vaughan K, Weiskopf D, Grifoni A, Diamond MS, et al. 2016. Identifying Candidate Targets of Immune Responses in Zika Virus Based on Homology to Epitopes in Other Flavivirus Species. *PLoS Curr* 8

213. Chung KM, Diamond MS. 2008. Defining the levels of secreted non-structural protein NS1 after West Nile virus infection in cell culture and mice. *J Med Virol* 80: 547-56

214. Macdonald J, Tonry J, Hall RA, Williams B, Palacios G, et al. 2005. NS1 protein secretion during the acute phase of West Nile virus infection. *J Virol* 79: 13924-33

215. Liu Y, Liu J, Du S, Shan C, Nie K, et al. 2017. Evolutionary enhancement of Zika virus infectivity in Aedes aegypti mosquitoes. *Nature* 545: 482-86

216. Jurado KA, Simoni MK, Tang Z, Uraki R, Hwang J, et al. 2016. Zika virus productively infects primary human placenta-specific macrophages. *JCI Insight* 1

217. Kumar R, Tripathi S, Tambe JJ, Arora V, Srivastava A, Nag VL. 2008. Dengue encephalopathy in children in Northern India: clinical features and comparison with non dengue. *J Neurol Sci* 269: 41-8

218. Ribeiro CF, Lopes VG, Brasil P, Pires AR, Rohloff R, Nogueira RM. 2017. Dengue infection in pregnancy and its impact on the placenta. *Int J Infect Dis* 55: 109-12

219. Soni BK, Das DSR, George RA, Aggarwal R, Sivasankar R. 2017. MRI features in dengue encephalitis: A case series in South Indian tertiary care hospital. *Indian J Radiol Imaging* 27: 125-28

220. Tabata T, Petitt M, Puerta-Guardo H, Michlmayr D, Wang C, et al. 2016. Zika Virus Targets Different Primary Human Placental Cells, Suggesting Two Routes for Vertical Transmission. *Cell Host Microbe* 20: 155-66

221. Michlmayr D, Andrade P, Gonzalez K, Balmaseda A, Harris E. 2017. CD14(+)CD16(+) monocytes are the main target of Zika virus infection in peripheral blood mononuclear cells in a paediatric study in Nicaragua. *Nat Microbiol* 2: 1462-70

222. Tang H, Hammack C, Ogden SC, Wen Z, Qian X, et al. 2016. Zika Virus Infects Human Cortical Neural Progenitors and Attenuates Their Growth. *Cell Stem Cell* 18: 587-90

223. Mlakar J, Korva M, Tul N, Popovic M, Poljsak-Prijatelj M, et al. 2016. Zika Virus Associated with Microcephaly. *N Engl J Med* 374: 951-8

224. Diamond MS, Klein RS. 2004. West Nile virus: crossing the blood-brain barrier. *Nat Med* 10: 1294-5

225. Monath TP, Barrett AD. 2003. Pathogenesis and pathophysiology of yellow fever. *Adv Virus Res* 60: 343-95

226. Connolly-Andersen AM, Thunberg T, Ahlm C. 2014. Endothelial activation and repair during hantavirus infection: association with disease outcome. *Open Forum Infect Dis* 1: ofu027

227. Egawa G, Nakamizo S, Natsuaki Y, Doi H, Miyachi Y, Kabashima K. 2013. Intravital analysis of vascular permeability in mice using two-photon microscopy. *Sci Rep* 3: 1932

228. Spindler KR, Hsu TH. 2012. Viral disruption of the blood-brain barrier. *Trends Microbiol* 20: 282-90

229. Wang T, Town T, Alexopoulou L, Anderson JF, Fikrig E, Flavell RA. 2004. Toll-like receptor 3 mediates West Nile virus entry into the brain causing lethal encephalitis. *Nat Med* 10: 1366-73

230. Li F, Wang Y, Yu L, Cao S, Wang K, et al. 2015. Viral Infection of the Central Nervous System and Neuroinflammation Precede Blood-Brain Barrier Disruption during Japanese Encephalitis Virus Infection. *J Virol* 89: 5602-14

231. Puerta-Guardo H, Raya-Sandino A, Gonzalez-Mariscal L, Rosales VH, Ayala-Davila J, et al. 2013. The cytokine response of U937-derived macrophages infected through antibody-dependent enhancement of dengue virus disrupts cell apical-junction complexes and increases vascular permeability. *J Virol* 87: 7486-501

232. Nem de Oliveira Souza I, Frost PS, Franca JV, Nascimento-Viana JB, Neris RLS, et al. 2018. Acute and chronic neurological consequences of early-life Zika virus infection in mice. *Sci Transl Med* 10

233. Tsao N, Hsu HP, Wu CM, Liu CC, Lei HY. 2001. Tumour necrosis factor-alpha causes an increase in blood-brain barrier permeability during sepsis. *J Med Microbiol* 50: 812-21

234. de Vries HE, Blom-Roosemalen MC, van Oosten M, de Boer AG, van Berkel TJ, et al. 1996. The influence of cytokines on the integrity of the blood-brain barrier in vitro. *J Neuroimmunol* 64: 37-43

235. Halstead SB. 2016. Licensed Dengue Vaccine: Public Health Conundrum and Scientific Challenge. *Am J Trop Med Hyg* 95: 741-45

236. Hadinegoro SR, Arredondo-Garcia JL, Capeding MR, Deseda C, Chotpitayasunondh T, et al. 2015. Efficacy and Long-Term Safety of a Dengue Vaccine in Regions of Endemic Disease. *N Engl J Med* 373: 1195-206

237. Osorio JE, Wallace D, Stinchcomb DT. 2016. A recombinant, chimeric tetravalent dengue vaccine candidate based on a dengue virus serotype 2 backbone. *Expert Rev Vaccines* 15: 497-508

238. Saez-Llorens X, Tricou V, Yu D, Rivera L, Jimeno J, et al. 2018. Immunogenicity and safety of one versus two doses of tetravalent dengue vaccine in healthy children aged 2-17 years in Asia and Latin America: 18-month interim data from a phase 2, randomised, placebo-controlled study. *Lancet Infect Dis* 18: 162-70

239. Saez-Llorens X, Tricou V, Yu D, Rivera L, Tuboi S, et al. 2017. Safety and immunogenicity of one versus two doses of Takeda's tetravalent dengue vaccine in children in Asia and Latin America: interim results from a phase 2, randomised, placebo-controlled study. *Lancet Infect Dis* 17: 615-25

240. Shu PY, Chen LK, Chang SF, Yueh YY, Chow L, et al. 2000. Dengue NS1-specific antibody responses: isotype distribution and serotyping in patients with Dengue fever and Dengue hemorrhagic fever. *J Med Virol* 62: 224-32

241. Kuno G, Vorndam AV, Gubler DJ, Gomez I. 1990. Study of anti-dengue NS1 antibody by western blot. *J Med Virol* 32: 102-8

242. Churdboonchart V, Bhamarapravati N, Peampramprecha S, Sirinavin S. 1991. Antibodies against dengue viral proteins in primary and secondary dengue hemorrhagic fever. *Am J Trop Med Hyg* 44: 481-93

243. Valdes K, Alvarez M, Pupo M, Vazquez S, Rodriguez R, Guzman MG. 2000. Human Dengue antibodies against structural and nonstructural proteins. *Clin Diagn Lab Immunol* 7: 856-7

244. Lai YC, Chuang YC, Liu CC, Ho TS, Lin YS, et al. 2017. Antibodies Against Modified NS1 Wing Domain Peptide Protect Against Dengue Virus Infection. *Sci Rep* 7: 6975

245. Swanstrom JA, Henein S, Plante JA, Yount BL, Widman DG, et al. 2018. Analyzing the Human Serum Antibody Responses to a Live Attenuated Tetravalent Dengue Vaccine Candidate. *J Infect Dis* 217: 1932-41

246. Rupp R, Luckasen GJ, Kirstein JL, Osorio JE, Santangelo JD, et al. 2015. Safety and immunogenicity of different doses and schedules of a live attenuated tetravalent dengue vaccine (TDV) in healthy adults: A Phase 1b randomized study. *Vaccine* 33: 6351-9

247. Shu PY, Chen LK, Chang SF, Yueh YY, Chow L, et al. 2002. Potential application of nonstructural protein NS1 serotype-specific immunoglobulin G enzyme-linked immunosorbent assay in the seroepidemiologic study of dengue virus infection: correlation of results with those of the plaque reduction neutralization test. *J Clin Microbiol* 40: 1840-4

248. Guy B, Barrere B, Malinowski C, Saville M, Teyssou R, Lang J. 2011. From research to phase III: preclinical, industrial and clinical development of the Sanofi Pasteur tetravalent dengue vaccine. *Vaccine* 29: 7229-41

249. Falgout B, Bray M, Schlesinger JJ, Lai CJ. 1990. Immunization of mice with recombinant vaccinia virus expressing authentic dengue virus nonstructural protein NS1 protects against lethal dengue virus encephalitis. *J Virol* 64: 4356-63

250. Amorim JH, Diniz MO, Cariri FA, Rodrigues JF, Bizerra RS, et al. 2012. Protective immunity to DENV2 after immunization with a recombinant NS1 protein using a genetically detoxified heat-labile toxin as an adjuvant. *Vaccine* 30: 837-45

251. Lu H, Xu XF, Gao N, Fan DY, Wang J, An J. 2013. Preliminary evaluation of DNA vaccine candidates encoding dengue-2 prM/E and NS1: their immunity and protective efficacy in mice. *Mol Immunol* 54: 109-14

252. Henchal EA, Henchal LS, Schlesinger JJ. 1988. Synergistic interactions of anti-NS1 monoclonal antibodies protect passively immunized mice from lethal challenge with dengue 2 virus. *J Gen Virol* 69 (Pt 8): 2101-7

253. Chu H, George SL, Stinchcomb DT, Osorio JE, Partidos CD. 2015. CD8+ T-cell Responses in Flavivirus-Naive Individuals Following Immunization with a Live-Attenuated Tetravalent Dengue Vaccine Candidate. *J Infect Dis* 212: 1618-28

254. Weiskopf D, Angelo MA, Bangs DJ, Sidney J, Paul S, et al. 2015. The human CD8+ T cell responses induced by a live attenuated tetravalent dengue vaccine are directed against highly conserved epitopes. *J Virol* 89: 120-8

255. Angelo MA, Grifoni A, O'Rourke PH, Sidney J, Paul S, et al. 2017. Human CD4(+) T Cell Responses to an Attenuated Tetravalent Dengue Vaccine Parallel Those Induced by Natural Infection in Magnitude, HLA Restriction, and Antigen Specificity. *J Virol* 91

256. Goncalves AJ, Oliveira ER, Costa SM, Paes MV, Silva JF, et al. 2015. Cooperation between CD4+ T Cells and Humoral Immunity Is Critical for Protection against Dengue Using a DNA Vaccine Based on the NS1 Antigen. *PLoS Negl Trop Dis* 9: e0004277

257. Chappell D, Jacob M, Paul O, Rehm M, Welsch U, et al. 2009. The glycocalyx of the human umbilical vein endothelial cell: an impressive structure ex vivo but not in culture. *Circ Res* 104: 1313-7

258. Potter DR, Damiano ER. 2008. The hydrodynamically relevant endothelial cell glycocalyx observed in vivo is absent in vitro. *Circ Res* 102: 770-6

259. Glasner DR, Puerta-Guardo H, Beatty PR, Harris E. 2018. The Good, the Bad, and the Shocking: The Multiple Roles of Dengue Virus Nonstructural Protein 1 in Protection and Pathogenesis. *Annu Rev Virol*

260. Kawai N, Ikematsu H, Iwaki N, Maeda T, Kawashima T, et al. 2009. Comparison of the effectiveness of Zanamivir and Oseltamivir against influenza A/H1N1, A/H3N2, and B. *Clin Infect Dis* 48: 996-7

261. Dredge K, Hammond E, Handley P, Gonda TJ, Smith MT, et al. 2011. PG545, a dual heparanase and angiogenesis inhibitor, induces potent anti-tumour and anti-metastatic efficacy in preclinical models. *Br J Cancer* 104: 635-42

262. Ritchie JP, Ramani VC, Ren Y, Naggi A, Torri G, et al. 2011. SST0001, a chemically modified heparin, inhibits myeloma growth and angiogenesis via disruption of the heparanase/syndecan-1 axis. *Clin Cancer Res* 17: 1382-93

263. Ge Y, Mansell A, Ussher JE, Brooks AE, Manning K, et al. 2013. Rotavirus NSP4 Triggers Secretion of Proinflammatory Cytokines from Macrophages via Toll-Like Receptor 2. *J Virol* 87: 11160-7

264. Didsbury A, Wang C, Verdon D, Sewell MA, McIntosh JD, Taylor JA. 2011. Rotavirus NSP4 is secreted from infected cells as an oligomeric lipoprotein and binds to glycosaminoglycans on the surface of non-infected cells. *Virol J* 8: 551

265. Ousingsawat J, Mirza M, Tian Y, Roussa E, Schreiber R, et al. 2011. Rotavirus toxin NSP4 induces diarrhea by activation of TMEM16A and inhibition of Na+ absorption. *Pflugers Arch* 461: 579-89

266. Jeffers SA, Sanders DA, Sanchez A. 2002. Covalent modifications of the ebola virus glycoprotein. *J Virol* 76: 12463-72

267. Volchkov VE. 1999. Processing of the Ebola virus glycoprotein. *Curr Top Microbiol Immunol* 235: 35-47

268. Dolnik O, Volchkova V, Garten W, Carbonnelle C, Becker S, et al. 2004. Ectodomain shedding of the glycoprotein GP of Ebola virus. *EMBO J* 23: 2175-84

269. Falzarano D, Krokhin O, Wahl-Jensen V, Seebach J, Wolf K, et al. 2006. Structure-function analysis of the soluble glycoprotein, sGP, of Ebola virus. *Chembiochem* 7: 1605-11

270. Escudero-Perez B, Volchkova VA, Dolnik O, Lawrence P, Volchkov VE. 2014. Shed GP of Ebola virus triggers immune activation and increased vascular permeability. *PLoS Pathog* 10: e1004509

271. Yang ZY, Duckers HJ, Sullivan NJ, Sanchez A, Nabel EG, Nabel GJ. 2000. Identification of the Ebola virus glycoprotein as the main viral determinant of vascular cell cytotoxicity and injury. *Nat Med* 6: 886-9